A Fast Method for Out-of-Step Protection Using State Plane Trajectories Analysis

A Thesis Submitted
to the College of Graduate Studies and Research
in Partial Fulfillment of the Requirements
for the M.Sc. Degree
in the Department of Electrical and Computer Engineering
University of Saskatchewan

by

Binod Shrestha

Saskatoon, Saskatchewan, Canada

Permission to Use

In presenting this thesis in partial fulfillment of the requirements for a Postgraduate degree from the University of Saskatchewan, it is agreed that the Libraries of this University may make it freely available for inspection. Permission for copying of this thesis in any manner, in whole or in part, for scholarly purposes may be granted by the professors who supervised this thesis work or, in their absence, by the Head of the Department of Electrical and Computer Engineering or the Dean of the College of Graduate Studies and Research at the University of Saskatchewan. Any copying, publication, or use of this thesis, or parts thereof, for financial gain without the written permission of the author is strictly prohibited. Proper recognition shall be given to the author and to the University of Saskatchewan in any scholarly use which may be made of any material in this thesis.

Request for permission to copy or to make any other use of material in this thesis in whole or in part should be addressed to:

Head of the Department of Electrical and Computer Engineering
57 Campus Drive
University of Saskatchewan
Saskatoon, Saskatchewan, Canada
S7N 5A9

Acknowledgments

I would like to take an opportunity to thank and acknowledge those who made this thesis possible. Firstly, I would like to express my sincere gratitude to my supervisors Dr. Rama Gokaraju and Dr. Mohindar Singh Sachdev for giving me an opportunity to pursue M.Sc. study under their supervision. Their wide knowledge, guidance, thoughtful suggestions and support throughout my M.Sc. program were invaluable to me. I am grateful for their constructive technical discussions and suggestions which have always motivated and inspired me throughout the research and helped me on successful completion of the thesis. I would also like to thank my advisory committee members and external examiner for their comments and suggestions on my research work and thesis.

My heartfelt thanks to all the faculty at Department of Electrical and Computer Engineering who helped me to build understanding in different courses. I am also thankful to Dr. Dharshana Muthumuni and PSCAD Support Team for their continuous support during modeling power systems in PSCAD-EMTDC. I am very thankful to Mr. Eli Pajuelo and Mr. Dipendra Rai for their helpful ideas during the research work. I am also grateful to staffs and fellow students at University for their direct and indirect help during the research.

It is my honour to thank Natural Sciences and Engineering Research Council (NSERC) of Canada and University of Saskatchewan for providing financial support throughout my study.

Finally, I would like thank my parents Mr. Surya Kumar Shrestha and Ms. Indra Laxmi Shrestha, and my family members for their wonderful encouragement, love and support through-out my educational journey. This thesis is dedicated to all of them who helped to make it successful.

−Binod Shrestha

Abstract

This thesis proposes a novel out-of-step protection technique using the state-plane representation of the generator speed and power angle. The critical clearing angle is computed using the principle that the total energy of the system at the instant the fault is cleared should be equal to the maximum potential energy of the system. The critical clearing time corresponding to this value of critical clearing angle is obtained directly using the time calibration of the relative speed versus power angle solution curve. The simultaneous calculation of the critical clearing angle and the time makes the proposed state plane approach much faster than the two-blinder scheme, Equal Area Criterion (EAC) method, rate of change of impedance method, the Swing Center Voltage (SCV) technique, transient energy calculation method, and the frequency deviation calculation from voltage signal method discussed in the literature.

The proposed state plane prediction scheme is used to detect the first swing out-of-step condition in single machine infinite bus (SMIB) system as well as larger power system configurations (two-area and IEEE 39-bus test systems) using system wide information. A coherency analysis is performed in a multi-machine system to find out the two critical groups of generators. The critical generator groups are then represented with a SMIB equivalent system, and the state plane algorithm is applied to the reduced equivalent. Electromagnetic transient simulations are carried out using PSCAD/EMTDC^{TM} to test the proposed algorithm in the above discussed test systems. The simulation studies show that the proposed method is computationally efficient, and accurate even for the larger power systems. The technique also does not require any offline studies.

This thesis also proposes another out-of-step protection technique using generator state deviations to detect multi-swing instability conditions in power system. It uses wide-area measurements of generator electrical power and speed deviations as inputs to the proposed scheme to detect instability. This technique is not as fast as the state plane approach but can predict multi-swing instability conditions in power system. The state plane method and state deviation method are used together to find first swing and multi-swing instability

conditions. Two-area power system configuration is used to demonstrate multi-swing instability prediction. Different power swing conditions such as stable, first swing unstable and multi-swing unstable scenarios are created and the proposed techniques are tested to verify their performance. The proposed techniques are also compared with the conventional two blinder technique.

A facility for hardware-in-the-loop testing of the relays using a digital simulator is available in the Power System Laboratory at the University of Saskatchewan. An out-of-step relay module is developed in a digital signal processing board (ADSP − BF533$^{\text{TM}}$ from Analog Devices Inc.) and a closed loop test is performed using the real time digital simulator (RTDS$^{\text{TM}}$). The simulator mimics the power system behaviour in real time, and the analog time signals from simulator can be communicated to the relay module. The relay can also feed back the signals to the simulator which can be used to operate the circuit breaker elements in the power system. The SMIB and two area systems are used to test the relay in real time. The relay prototypes for both of the proposed techniques are developed in this thesis. The hardware-in-the-loop implementation and testing show that the calculation times required for the proposed methods are small, and the state plane method especially can predict instability condition much faster than all other methods in current literature.

Table of Contents

List of Tables

List of Figures

List of Symbols and Abbreviations

δ	Power angle
δ_t	Power angle at generator bus
δ_{cr}	Critical clearing angle
ω	Speed of the machine with respect to synchronous speed
ω_1	Speed of the machine during fault
ω_2	Speed of the machine for post-fault condition
ω_{2cl}	Speed of the machine at the moment when the fault is cleared
M	Inertia constant
P_1	Ratio of mechanical input power and maximum power for during-fault condition
P_2	Ratio of mechanical input power and maximum power for post-fault condition
P_e	Electrical power
P_m	Mechanical input Power
P_{eaf}	Electrical power transfer after fault
P_{edf}	Electrical power transfer during fault
P_{maxaf}	Maximum possible power transfer for the post fault condition
P_{maxdf}	Maximum possible power transfer during fault
P_{max}	Maximum electrical power transfer

t_{cl}	Fault clearing time
t_{cr}	Critical clearing time
3PC	Triple Processor Card
AM	Amplitude Modulation
CCA	Critical clearing angle
CCT	Critical clearing time
COA	Center of angle
CTs	Current transformers
DSB-SC	Double Side Band-Suppressed Carrier
DYP	dynamic saddle point
EAC	Equal area criteria
GPC	GIGA Processor Card
GTWIF	Gigabit Transceiver Workstation Interface Card
IEEE	Institute of Electrical and Electronics Engineers
LRI	Left resistance element (inner)
LRO	Left resistance element (outer)
PSBD	Power swing blocking time delay
PTs	Potential Transformers
RAM	Random access memory
ROM	Read only memory
RRI	Right resistance element (inner)

RRO	Right resistance element (outer)
SCV	Swing center voltage
SMIB	Single machine infinite bus

Chapter 1

Introduction

1.1 Background

Electricity became an ever-increasing demand after the industrial revolution during the 18^{th} and 19^{th} century. Electricity generation, as a result, is increasing day by day all over the world. The recent data from 2008 shows that the world's total generation is 20261 TWh per year, which includes multiple sources of generation such as fossil fuel, renewable, biomass and others. The generations and loads, which are often located far apart, are interconnected through a transmission network, where the distant generating units operate in parallel to continuously supply the loads. The interconnections between multiple generators, networks and loads have multiplied the complexity to solve the engineering problems in a power system. An electric power system is therefore a complex network of electrical components which are designed to supply reliable, reasonably priced and quality energy to the consumers. A power system mainly consist of generation, transmission and distribution units. The generation units generates electrical energy from other forms of energy such as coal, hydro, or fossil fuel, which are interconnected through networks of transmission lines called an electric grid. The transmission unit transmits the bulk amount of generated energy from one location to other location at higher voltage levels. The distribution unit finally distributes the energy to the consumers at lower voltage levels [1–3].

The electrical energy balance between generation and consumption is important for power system operation. However, the consumption or the demand of electricity is usually random and the system has no control over it. To accommodate these changes, a power system is equipped with power generation and flow control devices throughout the transmission

and generation units (such as an excitation system, governor, regulating transformers etc.). These devices help to achieve the required operation of the power system by maintaining voltage, frequency and other system variables within the values defined by standards [1].

Disturbances such as faults, load changes, line trip-outs etc. in a power system cause system variables to deviate from the normal values. The deviations due to small disturbances can be handled by control devices which bring them back to a normal condition. However, the control devices cannot handle changes due to large disturbances which lead the system to an abnormal condition. A protection system design is necessary to safeguard the power systems from such abnormal conditions, which will be discussed in detail in Section 1.3.

An abnormal condition may lead a power systems into an unstable situation. An imbalance between the input mechanical power and the output electrical power because of the disturbance causes generators in a region to run faster than the generators in another region. This results in angular separation between these two regions, which keeps on increasing if the system cannot absorb the kinetic energy corresponding to the rotor speed differences. If the angular separation exceeds beyond 180 degrees, the two regions lose synchronism. This condition in a power system is called a out-of-step condition. For such a condition, out-of-step tripping needs to be initiated for selected breakers in the system. Out-of-step tripping was not widely used in power system over many years. However, it is receiving more attention because of very large generating units connected to extra high voltage and ultra high voltage circuits. The lower inertias and the higher reactances of the generators have reduced the stability limit of the system [4]. If the out-of-step condition is not identified in time, it initiates undesired tripping of transmission line relays, cascade outage of generators, and a wide area blackout, resulting in severe technical, economical and social impacts [5]. A number of system blackouts have been experienced in the past decades. The largest disturbances had occurred in Northeast U.S. and Southeast of Canada on August 14, 2003, causing the loss of 61.8 GW of generation in a matter of 1-2 hours, and disconnecting approximately 50 millions of customers from supply. The outage started with the tripping of a generator in Ohio, caused by overloaded excitation, and several 345 kV lines tripping. It caused a power swing in other lines and tripped many other lines and loads, which finally

led to loss of synchronism among multiple regions in the Northeastern and Southeastern interconnected network. A similar disturbance happened in the Western US in July 2, 1996, affecting millions of customers [6, 7]. In such circumstances, the control center operators have to deal with a very complex situation and rely on heuristic solutions to take remedial actions. Heuristics solutions need not be the most appropriate all the time.

For the events discussed above, local protection systems applied to protect equipment are not going to be sufficient to solve large scale power system problems that are caused by system level disturbances. A wide area effective protection system design is therefore necessary to handle such cases, and needs a wide area measurement system (WAMS). The data collected from various locations are used to monitor and estimate the system conditions and to design protection systems [5, 8, 9].

This research is focused on developing and testing a new fast scheme for out-of-step protection in a power system using the wide area measurements discussed above. Moreover, electromagnetic transient (EMT) type time domain simulations (i.e., PSCAD/EMTDC$^{\text{TM}}$ and RTDS$^{\text{TM}}$) have been used in this research to get an accurate behaviour of a power system under faulted conditions, instead of the normally used stability programming tools. Such stability programs rely on phasor type solutions and simplified models and do not provide an accurate representation of the behaviour for the out-of-step transient conditions. The EMT simulations described in this thesis use detailed transient models of the various power system components, and therefore give an accurate representation of the oscillations. They produce the responses of the components in time time domain which closely resembles actual component behaviours.

The following sections in this chapter explain the power system stability and protection in brief, and the current research trends in the power industry in this area. The past and present practices in out-of-step relaying are discussed in the literature review section. The contributions of this thesis and the thesis outline are also discussed.

1.2 Power System Stability

The stability of a dynamic system means the ability of the system to absorb the excess energy developed due to disturbances, and bring the system back to the previous state or to a new operating state. A power system is a complex dynamic system with multiple generators, loads, motors and other fast-acting power electronic units forming a highly nonlinear system, where each unit has different characteristics and responses. All the dynamic units have to be steady state stable in order to ensure the steady operation of the whole power system. When a disturbance happens, a power system might suffer from different forms of stability issues. The power system stability is hence classified into three major areas: rotor angle stability, frequency stability and voltage stability. Further classification of power system stability is based on the strength of the disturbance and the time duration to be considered for the stability studies. The classifications are shown in diagram 1.1 [10]. This research is focused on the rotor angle transient stability of the power system.

The power system disturbances are an abnormal situation that causes the system state to move from its steady state equilibrium. Small disturbances such as continuous load changes result in small shift in the system states from which the system can easily recover. The large disturbances, such as faults, major line tripping, loss of generation or huge load changes, result in large shift in the states of the system. They result in high oscillations in voltage and current throughout the system. The power output from a synchronous machine starts

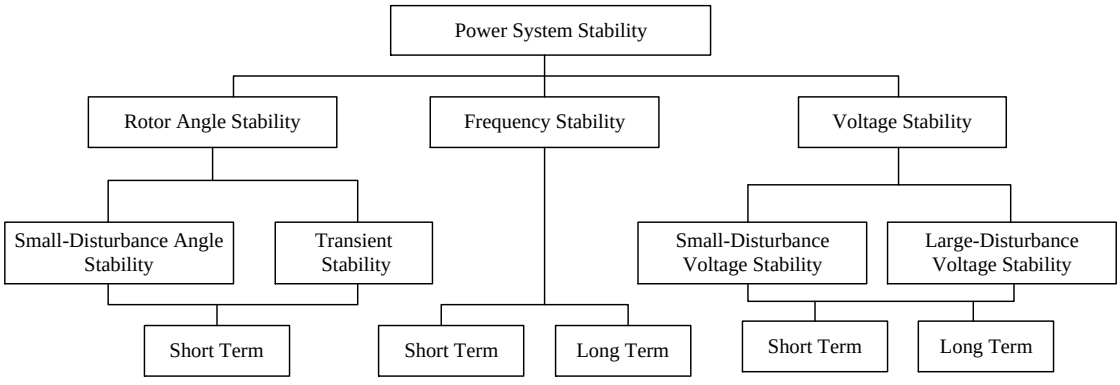

Figure 1.1: Classification of power system stability

fluctuating, which causes the rotor of the machine to accelerate and decelerate with respect to the stator circuit. As a result, the synchronous generator starts oscillating with other synchronous machines in the system [11]. If the system has sufficient synchronizing and damping energy, the oscillations damp out and settle to an equilibrium state in a finite time. This implies stable operation of the system. In case of the system not being able to dampen the oscillations, an unstable situation arises from which the system cannot return to a steady state and the generator rotor angles keep separating from each other. This is called an out-of-step condition. It is also referred to as loss of synchronism or rotor angle instability. If the out-of-step condition is not detected quickly, it can have a cascading effect, such as unnecessary tripping of other major lines, generator tripping and so on. Major loss of system generation and loads due to the out-of-step conditions can be learned from the past decade blackout experience. [10, 12]. The situation, therefore, demands a fast out-of-step protection strategy to be designed and implemented in power systems.

1.3 Power System Protection

Installing a complete power system is a huge investment. Disturbances in power systems cannot be avoided no matter how robust the system design is, and they always put the system at risk. A proper protection system is therefore necessary for a secure and reliable power system operation [13].

Power system protection is a system of entities that protects the power system components such as generators, transformers, transmission lines, and the devices at the consumer level from the high system currents and voltages during or after the disturbances. The main function of the protection system is to ensure the prompt isolation of the power system elements that might cause damage or otherwise interfere in the effective operation of the rest of the system. The entities of protection (i.e., protective devices) mainly consists of instrument transformers(Current Transformers (CTs), Potential Transformers (PTs)), relays, breakers and communication devices. Instrument transformers acts as sensors which sense current and voltage and feed them to the relays. Protective relays are like a brain for the protection

system which detects dangerous and intolerable situations in power system via sensors and make decisions using operating principles or past experiences to perform corrective action as soon as possible. A relaying system is usually designed to protect only a certain portion of the power system. The communication system helps to establish a continuous communication between two or more relaying systems to ensure a coordinated operation of the whole protection system [7, 11, 13].

A relay designed to protect a certain region should not operate for a fault outside the region. However, there should be no region in a power system which is left unprotected. The requirement is achieved by dividing the power system into various overlapping sections called zones of protection. Each section represents a region to be protected by a relay. A protection zone is normally defined for a generator, transformer, substation, transmission line, distribution line or a motor. An edge of a zone of protection is defined by the CTs through which the associated relay sees the system inside the zone of protection. Figure 1.2 gives an overview on how the protection zones are defined for different power system elements in the power system.

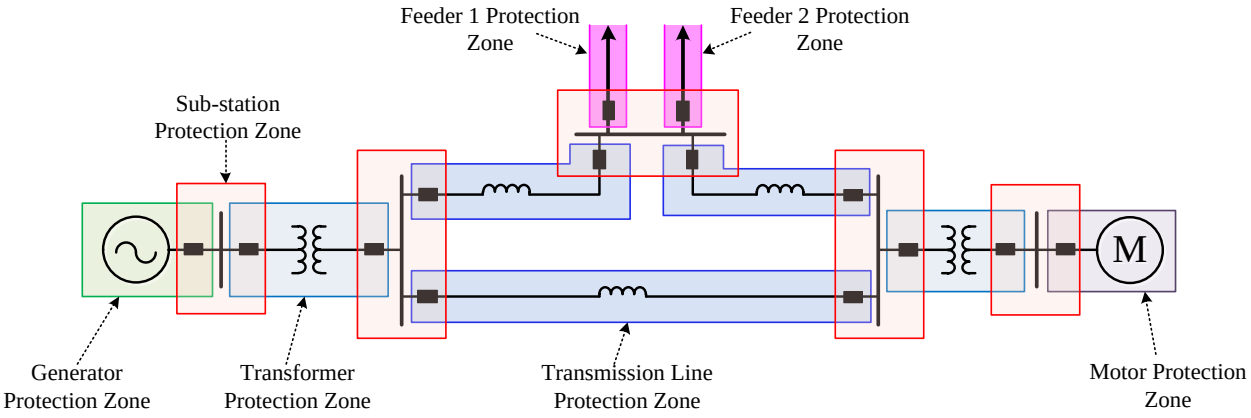

Figure 1.2: A power system showing overlapping protection zones

Conventionally, protection systems in the power industry are designed to address local problems which are not adequate to handle system-wide disturbances. Due to the increased interconnections, the modern power system now requires system-wide protection schemes with modern relays and communications. The advent of computer based relays with communication capabilities has made the solution possible and has brought the protection design

practices to the next level. The wide area monitoring, protection and control (WAMPAC), and the synchronized phasor measurement technology (SPMT) are being explored and implemented in the power industry around the world [9]. The WAMPAC collects data using phasor measurement units (PMUs) located at various locations of the power systems. The PMUs measure and send the data to the control center and the data are synchronized in time using a GPS clock. The IEEE Power System Relaying Committee (PERC) has reported a scheme called System Integrity Protection Scheme (SIPS) [12], which is intended to protect the integrity of a power system, or some portion thereof via incorporating various protection schemes in a package. It includes Special Protection Schemes (SPS), Remedial Action Schemes (RAS), and other additional schemes such as underfrequency, undervoltage, out-of-step, etc., and requires multiple detection and actuation units with communication facilities . The SPS and RAS are the event-based systems which are specially designed to directly detect the selected disturbances that would lead to instability using a binary signal and perform predetermined corrective action [12].

1.4 Digital and Numerical Relays

As discussed in Section 1.3, modern protection schemes require multifunction relays with communication capabilities. Digital and numerical relays are developed to fulfil these requirements of modern protection systems. A digital relay consists of an analog to digital (A/D) converter, microprocessor or microcontrollers, random access memory (RAM) , read only memory (ROM) and software programs to implement a protection logic. It provides low cost, fast performance, flexibility, wider range of settings and greater accuracy than mechanical relays. However, the limited computational power of the microprocessors used in digital relays results in longer operation time and also limits the number of protection functions that can be included in a relay. Numerical relays overcome such limitation by the use of specialized digital signal processors and dedicated microprocessors as computational hardware. Numerical relays are a one-box solution for power system protection and automation [13]. The SEL 421 relay, manufactured by Schweitzer Engineering Laboratories, Inc., is

one example of a numerical relay which encompasses 26 protection functions, auto-reclosing, synchronism check, communication interfaces, synchrophasor capabilities, etc. in a single unit [14].

1.5 Literature Review

Several methods are proposed in the literature to predict out-of-step conditions in a power system. The methods are briefly summarized next, and followed by their advantages and disadvantages.

During a power swing, electrical quantities such as voltage, current and frequency change. Because of the change in voltages and currents, impedance values seen at various location of the power system also change. One of the conventional techniques reported in references [6, 15] is based on the rate of change of impedance. The scheme continuously monitors the change in impedance at the relay location. The power swing detection is based on the time taken by impedance to travel between pre-set impedance elements called blinders. The time taken by the impedance is compared with the pre-set timer to differentiate between a power swing and a fault. The scheme is called a Blinder Scheme. Setting the blinders and determining a pre-set delay are two of the major tasks in this technique. References [15, 16] describe some techniques to set these blinders where the settings are system specific, depend on system loading conditions and are only applicable up to a two-machine system. Setting blinders requires extensive system stability studies, and a relay design using blinders to work for all possible system conditions is impossible. The settings are therefore made with certain assumptions on expected load conditions and oscillations following the major disturbances. The settings perform well for the assumed system conditions, whereas the system continuously goes through changes in its structure and loading patterns. It needs continuous updating of the settings to cope with the changing system conditions. However, this is not done in most of the power systems because of the scheduling difficulties and lack of manpower [8]. Moreover, the time delay setting for the relay depends on the slip frequency. Relays set for low slip frequencies will not work for high slip frequencies [6].

An out-of-step relaying scheme with rate of change of apparent resistance augmentation is proposed in [17]. The relay was installed at Malin substation on the Pacific AC Intertie and Western North American Power System in February 1983. The relay characteristic is a modified version of the blinder scheme where the rate of change of apparent impedance is replaced with the apparent resistance augmented with the rate of change of apparent resistance and relay characteristic is defined in an R-Rdot plane. The technique involve setting a piecewise linear resistive element on an R-Rdot plane. The scheme also requires extensive simulation studies under various contingency conditions to set the relay characteristics and has similar types of demerits as the blinder scheme.

The swing center voltage (SCV) technique discussed in [6] is also an option for out-of-step protection. The SCV is a point of zero voltage between two source equivalent system when angular separation becomes 180 degrees. The point of zero voltage is also called the electrical center. The SCV technique estimates the rate of change of voltage, which will be maximum at the electrical center. The detection is usually made at a voltage angle separation close to 180 degrees. If tripping is initiated under this condition, it causes twice the rated stress for the circuit breaking device. Hence the operation of the circuit breaker is deferred to a later instant when the voltage angle separation is less. Also, the estimate of the SCV using local measurements of voltage phasor will only be valid when the impedance angle is 90 degrees.

Out-of-step detection schemes using transient energy calculation are also proposed in the literature. Reference [18] implements Lapunov's direct method to predict the out-of-step condition of a generator using local substation measurements. For a particular fault scenario mentioned in [18], the detection angle is 136.7 degrees, which results nearly in twice (1.9 times) the stress for out-of-step breakers. The technique is only limited to local generator protection and does not cover wide-area instability issues. Moreover, the technique does not provide critical clearing time (CCT) information, which is an important piece of information for relaying and stability study purposes.

The Equal Area Criterion (EAC) is popularly used as a transient stability analysis tool. The stability study using EAC is based on calculation of accelerating and decelerating area using power-angle characteristic curves. During a transient condition, if the accelerating area

is less than the decelerating area available, the system will be stable and if the accelerating area is greater than the decelerating area, the system will become unstable. The approach is directly applicable to a single machine infinite bus system [3]. The technique has been extended to a multi-machine system by Pavella et al. [19]. The scheme was investigated in a large system configuration when it separates into two oscillating groups during transient condition. The technique is called an Extended EAC (EEAC). Based on the EEAC, an adaptive out-of-step relay was developed by Phadke et al. [20]. The relay was implemented on the intertie between the states of Georgia and Florida in US in October 1993 and was operational until January of 1995. The behaviour of the system during power swings is approximated by two machine equivalent, one of which represents the generators in Florida and the other represents the generators in the southeastern US. The generator group in the southeastern US is a very large system and is assumed as an infinite bus to the Florida system. The relay estimates input mechanical power using the electrical power and angular separation between these two regions and uses EEAC for out of step detection. Reference [21] uses an autoregressive model to predict electrical power and phase angle of single machine infinite bus system, and uses EAC to detect an out-of-step condition. The out-of-step detection using EAC is simple and well established; however, EAC-based techniques cannot provide the critical clearing angle (CCA) and CCT for the fault simultaneously. It requires step-by-step integration techniques to calculate CCT. Moreover, the system's dynamic behaviour for different initial states cannot be visualised using EAC .

Fuzzy logic and neural networks are based on the principle of creating an artificially intelligent system which is able to perform tasks in future which they are trained for. Such an approach is applied for out-of-step detection by training the fuzzy and neural system for a number of possible power swing scenarios. Reference [22] proposed an out-of-step protection scheme using fuzzy logic and reference [23] proposed a technique using a neural network. Rajapakse et al. [24] proposed a rotor angle instability prediction technique using fuzzy C-means clustering algorithm and support vector machine. Fuzzy C-means clustering needed a large offline simulation study database to identify the variation in voltage at generator buses. The support vector machine also uses the same data base to build a trajectory template,

which is used to compare the actual voltage oscillations. These approaches require a large number of offline simulations for training their algorithms. The algorithms work well only if they are sufficiently trained and the training signals are appropriately identified. However, the method becomes cumbersome with increased interconnections and tends to fail for the unforeseen conditions in a power system.

Reference [25] proposed an out-of-step detection technique using frequency deviation of voltage method. The technique estimates the frequency using voltage angle calculated at the local bus. Further the angular acceleration is calculated using the calculated frequency. The instability is detected when the frequency measured at the point, where acceleration changes its sign from negative to positive, is greater than zero. Otherwise, the system will be stable. One of the major benefits of this technique is that it can detect not only the first swing instability but also the multi-swing instability. However, the detection is based on electrical voltage signal which can change very rapidly and may result in false tripping during switching transients. The method is based on local measurements, and a system-wide protection using the technique has not been reported so far.

1.6 Objective of the Thesis

Out-of-step relaying involves two steps. Firstly, it involves identifying the type of swing from which the system will recover (stable swing) or will not recover (unstable swing). Secondly, it involves relay blocking in the case of a stable swing, or performing selective tripping to separate power systems into islands in the case of an unstable swing. The first task is more difficult than the latter one. There are some established techniques, discussed in Section 1.5, to differentiate between stable and unstable power swings. A technique based on the rate of change of impedance has been used in most of the power industries to date. Some of the inaccuracies involved in setting the impedance relays can lead to false detection and undesired tripping. In addition, the technique uses local measurements, which may not be adequate to detect out-of-step conditions for large power systems [26]. Reference [8] has reported that new investigations are currently in progress at VirginiaTech,

using a transient energy function and parallel processing for an early detection of out-of-step conditions. With the modern computing and communication technologies available, a system-wide measurement and communication to the relay is a very practical and a feasible solution. This has provided the main motivation for carrying out further research in out-of-step protection. This thesis proposes a fast, simple, and accurate technique using a "state plane" analysis to find first swing instability and a "state deviation" technique to find the first swing and multi-swing instability conditions in a large power system configurations. The objectives of this thesis are summarized below.

1. Develop a fast algorithm for predicting first swing instability conditions using "state plane" trajectory analysis.

2. Detect the multi-swing instability conditions by studying the "state deviation".

3. Test the proposed scheme in small and large power system configurations and compare its performance with the conventional blinder scheme.

4. Develop a digital prototype of the relay and test the relay using hardware-in-the-loop simulations with real time digital simulator (RTDS^{TM}).

1.7 Organization of the Thesis

The thesis includes six chapters. Chapter 1 explains the concept of power system stability and protection. The importance and necessity of out-of-step protection in power systems are highlighted. Some of the current practices of out-of-step protection and those mentioned in the literature are briefly discussed, and their merits and demerits are also pointed out. The motivation behind the thesis and the thesis objectives are also discussed in Chapter 1.

Chapter 2 discusses power swing phenomena and their impact on the existing protection elements. The necessity of out-of-step protection and some of the major schemes to detect power swings are also discussed. The advantages and disadvantages of the existing methods

for out-of-step detection are also briefly described. Chapter 2 also introduces a new approach using generator "state deviation" to predict the out-of-step condition in the power systems.

Chapter 3 describes the "state plane" analysis by explaining first the transient behaviour of power systems in a state plane. A proposed out-of-step relay algorithm using the state plane analysis is also explained in this chapter. The results are given using the proposed algorithm on a SMIB and two area test systems using an electromagnetic transient simulation tool (i.e., PSCAD^{TM}). The technique is compared with the state deviation technique and conventional two blinder based technique. Further, a multi-swing instability condition in a power system is discussed, and a scheme combining state plane analysis and state deviation is proposed to detect the multi-swing instability conditions. The test cases for the multi-swing instability detection in a two area system are also reported in this chapter.

In Chapter 4, a hardware implementation of the proposed out-of-step detection techniques is reported. The test results from closed loop testing, using a real-time digital simulator, are presented for a SMIB and two area test systems.

In Chapter 5, out-of-step conditions are studied for a large power system configuration. The algorithm based on state plane analysis, state deviation technique and time domain energy equilibrium is extended to the multi-machine system using the SMIB equivalent, and are used to detect instability conditions in a large power system configuration. An IEEE 39-bus test system is used to evaluate the performance of the methods.

In Chapter 6, the research contributions are summarised and the future extensions of the work are outlined.

Some of the additional information is included in five appendices. Appendix A gives the test system data and information used in this research. In Appendix B, power system models developed in PSCAD^{TM} and RSCAD^{TM} are shown. Appendix C explains basic concepts of stability in the state plane. The guidelines for blinder settings to detect the out-of-step condition are discussed in Appendix D. Appendix E explains the network admittance matrix reduction. Appendix F discusses a time domain energy equilibrium method for out-of-step protection.

Chapter 2

Out-of-Step Prediction/Detection in Power Systems

2.1 Introduction

Out-of-step conditions in power systems have been a problem as far back as the 1920s. A typical power system at that time consisted of a generating station feeding a load center over long distances, and the instability was usually caused by lack of synchronising torque [27]. The power systems in the present scenario consist of groups of such generating stations interconnected with each other, where one or more generating stations may lose synchronism with the other generating stations. This chapter explains the concept of power swing phenomena in a power system. The swing locus in an impedance plane is discussed first and the effect of a power swing on different types of protection such as a distance relay, an overcurrent relay etc. are discussed. The usefulness of out-of-step relaying and the current state-of-the-art in this area are also discussed. The strengths and limitations of each of the techniques are also discussed.

2.2 Power Swing Phenomena and Rotor Angle Instability

During the steady state (normal operating condition), the generators connected to the power system deliver constant power, maintaining a balance between the mechanical input and the electrical output of the machines. Similarly, there is a balance between the electrical

power output of the machines and the consumed load. The interconnected generators also run at synchronous speed with a constant relative rotor angle separation between them and the frequency of the system remains close to nominal frequency (50 or 60 Hz) [1, 6]. Figure 2.1a shows a typical current and voltage waveform during the steady state operation of a power system.

However, as we know, the power systems are continuously subjected to various types of disturbances (large changes in loads, power system configuration changes, line switching, loss of generation, etc.), which cause oscillations in the rotating units. During these disturbances, a sudden change in the electrical power output of the generator occurs. Since the mechanical input to the generators is relatively constant during this short interval, the generator rotor starts accelerating resulting in electromechanical oscillations in the system. These oscillations cause fluctuation in the magnitude and phase of the voltages and currents throughout the system [28]. As a result, the power flow between the various parts of the system also starts oscillating. Such a power system phenomena is known as a power swing [6]. The oscillations of current and voltage during a power swing condition are portrayed in Figure 2.1b.

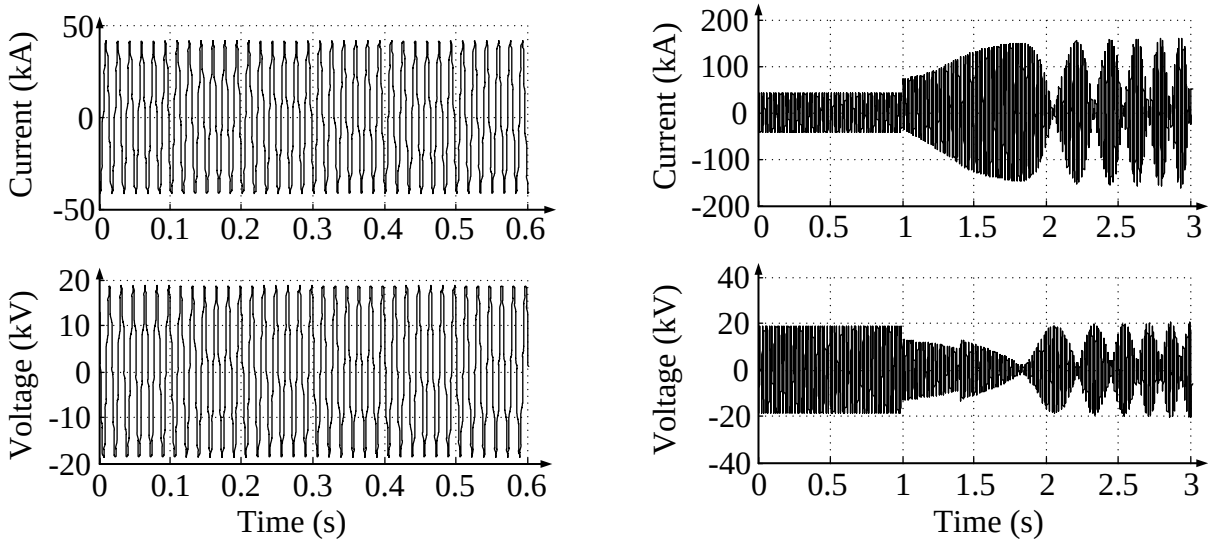

(a) During steady state

(b) During power swing

Figure 2.1: Instantaneous current and voltage waveforms

The system is designed to withstand variations in current, voltage, power and frequency

as long as it is within certain desired limits (maximum 5% for voltage, 1% for frequency and so on). The standards for these operating limits are laid out in the Power System Reliability Committee (PERC) report [6]. When the voltage angle separation between the tie line buses in an interconnected system goes beyond 180 degrees, it leads to an asynchronous operation of the generators in the system (the generators start slipping poles), leading to sustained oscillations of power. Therefore, the system state after the disturbance depends upon various factors such as the initial operating point, severity of a disturbance, action of the control equipment and the existence of synchronizing and damping torques in each machine [10].

The power swings are classified into two categories: stable swings and unstable swings. Whenever the swing damps out and converges to a new steady state point, it is referred to as a stable swing. If the swing goes through a sustained oscillation, it is referred to as an unstable swing. This condition is also referred to as an out-of-step condition or is also referred to as a rotor angle instability [6, 10].

The power swing can be detected directly using voltage and current fluctuations but it may take several slip cycles to detect. Power engineers instead found a more convenient method for visualizing and detecting a power swing by looking at the apparent impedance at the relay location [29]. The apparent impedance seen by the relay changes during a power swing and is discussed in Section 2.3.

2.3 Swing Locus in Impedance Plane

A distance relay in a power system measures impedance and uses the impedance characteristics to detect faults in the system. The impedance characteristic of a relay is defined in such a way that the impedance enters inside the characteristic only when the fault is within the zone of protection of the relay. During a power swing, impedance seen by the relay changes, and it might enter inside the relay characteristic. It causes unwanted operation of the distance relay. Consider a simplified system diagram, as shown in Figure 2.2, where the generator voltage E_A leads another generator voltage E_B by angle δ. Z_A and Z_B are system impedances and Z_L is the line impedance which connects the two generators. R indicates

the relay location at which the relay measures voltage V_R and current I_R.

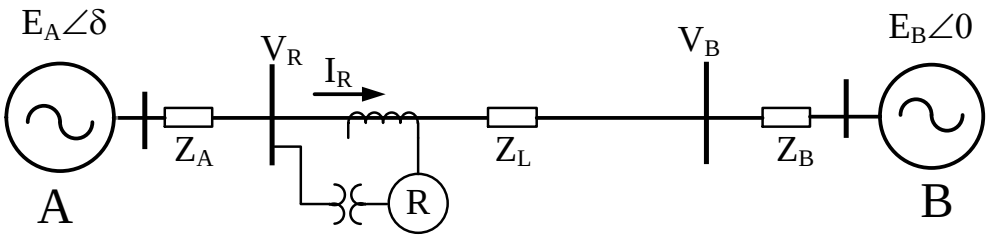

Figure 2.2: Two machine system used to illustrate impedance trajectory

In Figure 2.2, current and voltage measured by the relay is given by Equation (2.1) and (2.2), respectively.

$$I_R = \frac{E_A\angle\delta - E_B\angle 0}{(Z_A + Z_L + Z_B)} \tag{2.1}$$

$$V_R = E_A\angle\delta - I_R * Z_A \tag{2.2}$$

The impedance measured at the relay location is,

$$Z_R = \frac{V_R}{I_R} = \frac{E_A\angle\delta - I_R * Z_A}{I_R} = \frac{E_A\angle\delta}{I_R} - Z_A \tag{2.3}$$

$$= \frac{E_A\angle\delta((Z_A + Z_L + Z_B))}{E_A\angle\delta - E_B} - Z_A \tag{2.4}$$

Let $Z_T = Z_A + Z_L + Z_B$ and the ratio of two voltage magnitudes $\frac{E_A}{E_B}$ is n, then Z_R can be written as

$$Z_R = n\frac{(n - \cos\delta) - j\sin\delta}{(n - \cos\delta)^2 + \sin^2\delta} Z_T - Z_A \tag{2.5}$$

Assume n=1,then

$$Z_R = \frac{Z_T}{2}(1 - j\cot\frac{\delta}{2}) - Z_A \tag{2.6}$$

The Equation (2.6) gives the impedance value seen by the relay during power swing which depends on the phase angle between the sources. The geometrical interpretation of the trajectory can be seen in Figure 2.3. For n=1, the impedance locus becomes a straight line which passes perpendicularly through the midpoint of the system impedance between A and B. If n is greater or less than 1, the trajectory becomes a circle with the center on the extensions of the total impedance line AB [29].

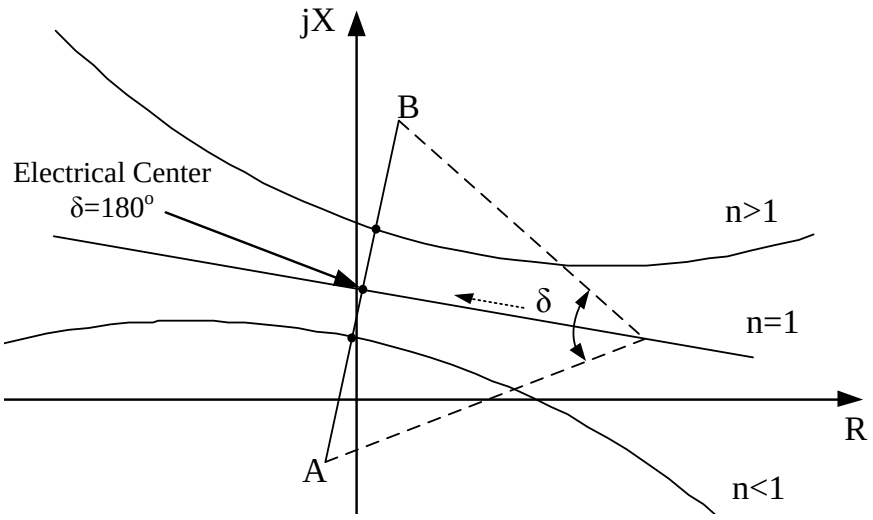

Figure 2.3: Impedance trajectory during a power swing for different values of n

2.4 Effect of Power Swing in Relaying

As discussed before, during a power swing, the voltage angle between two interconnected systems might reach 180 degrees and the voltages down to a minimum and the currents to a maximum. Such an electrical condition appears like a fault to the relay. The relays which operate during the fault may operate during a power swing. The current differential relay used to protect generators, transformers, buses and lines does not respond, as the swing appears as an external fault condition to them, but the other types of relays such as an overcurrent, directional overcurrent, undervoltage, distance relays may operate during a power swing [6, 11, 29].

During an unstable swing (out-of-step condition), the current magnitudes can be greater than the pick up setting of the overcurrent relay when the V_A leads V_B by 180 degrees. A stable swing also results in higher current magnitudes than the normal current but is much less than that during an unstable swing and hence does not reach the pick up setting value of the overcurrent relay [11].

Distance relays measure positive sequence impedance and are meant to operate when the impedance lies within the relay characteristics. Figure 2.4 shows a typical relay character-

istics of the distance relay. From the previous derivation it can be seen that the positive sequence impedance at the relay location varies as a function of δ. The swing locus during stable and out-of-step conditions is represented by swing locus c_1, c_2, and c_3 respectively. The unstable swing c_3 enters the operating zone of the the relay and causes it to trip. For stable swing, impedance locus c_2 does not enter the relay characteristics but in some cases even the stable swing as shown by impedance locus c_1 might enter the relay characteristics.

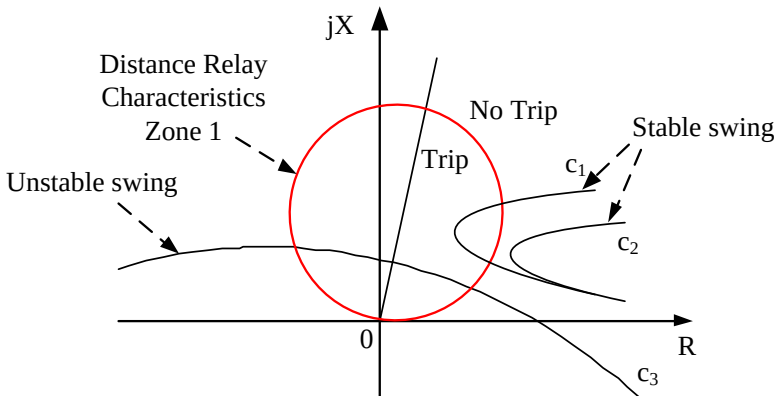

Figure 2.4: Distance relay characteristics and power swing locii

Undesired operation of the protection elements due to both stable or unstable power swing may have severe impact on the system stability, security and reliability. Further, the relay tripping at random locations because of the power swings weakens the system and creates imbalance between demand and supply and may lead to cascading conditions – outages, loss of generations and loads.

The system can be protected from such an event using out-of-step protection which is the subject of the next sections.

2.5 Out-of-Step Protection

The relays, as discussed in the previous section, might operate during some stable conditions from which the system can recover by itself and during an out-of-step condition. An additional protective function is therefore required to distinguish between a faulted condi-

tion and a power swing condition. This protective function has to block the breaker during a stable swing and has to send the trip signal to selected breakers during an out-of-step condition [6, 11, 28, 29].

Therefore the two major functions for an out-of-step relay are:

- Power swing blocking (PSB): This function allows the breakers to operate during fault and blocks all the relay elements that tend to operate during stable or unstable swing.
- Out-of-step tripping (OST) function: It trips selected breakers for an out-of-step condition. The tripping is done to disconnect a generator or a large power system area in order to ensure that the stability is achieved for rest of the generators or areas.

In addition, the out-of-step relay has to be fast enough so that the tripping can be initiated before 120 degrees of voltage angle separation in order to minimize the voltage stress on the breakers [11]. The fast detection also gives enough time to coordinate between many other protective elements in the system.

As discussed before, during an instability, the voltage angle difference increases from the pre-fault value and reaches 180 degrees and starts slipping pole. The voltage values experienced by the breaker for different angles can be seen in Figure 2.5. If the breaker operates at a lower voltage angle of separation for an imminent out-of-step condition, the life of the breaker can be extended. However, with most of the current out-of-step relaying technologies, the breakers operate at angle values closer to 180 degrees (when the voltage reaches as much as twice the normal value).

In Figure 2.5, V_S is sending end voltage, V_R is the receiving voltage and, V_B is the voltage experienced by the breaker during a power swing. From the figure we can see clearly that the voltage while opening the breaker may reach up to two times the rated voltage. Another useful point to make here is about the restriking voltage. The voltage which appears across the breaker immediately after the breaker operation is called a restriking voltage.

Consider a power system as shown in Figure 2.6. At an instant of the breaker operation, the input voltage source can be represented by a step voltage V_m. The inductance L and

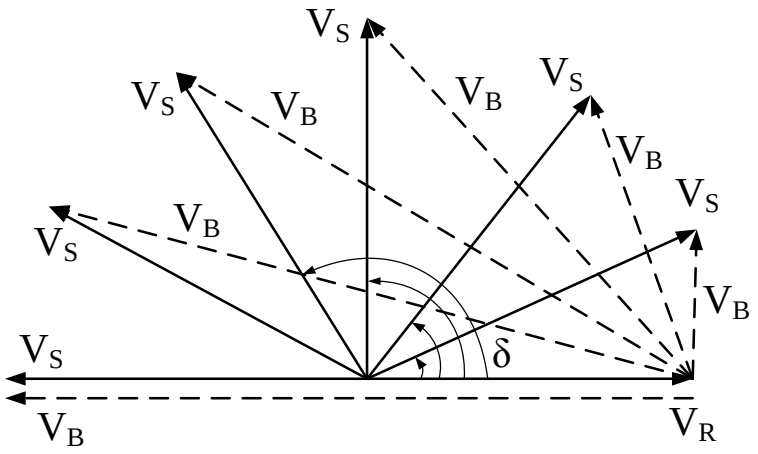

Figure 2.5: Voltage across the breaker during power swing for different values of δ

capacitance C represents the equivalent network parameters. If the circuit breaker (CB) is

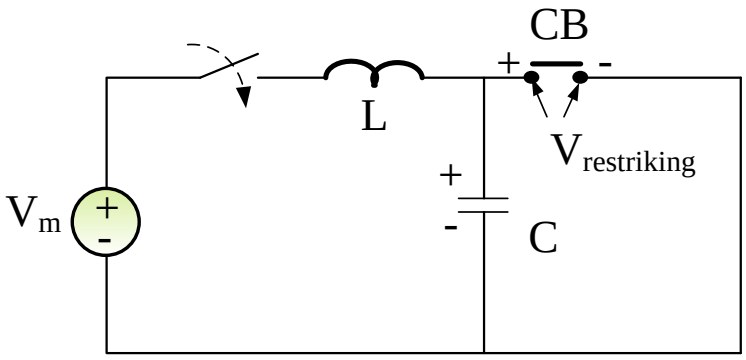

Figure 2.6: Equivalent circuit of a power system at the instant of breaker operation

interrupted at current zero position, the breaker will experiences a step voltage of V_m. The restriking voltage for a step input of V_m is given by the Equation (2.7) below.

$$V_{restriking} = V_m(1 - \cos \omega_n t) \tag{2.7}$$

where, ω_n is the natural frequency of the transmission circuit, which depends on the inductance and capacitance parameter values of the circuit. Equation 2.7 shows that the restriking voltage is proportional to the voltage across the breaker at the time of breaking and the natural frequency of the transmission circuit. From this equation we can clearly see that if the tripping is initiated at an angle close to 180 degrees, the step voltage experienced by the breaker at the moment of breaking is 2 times the rated value. The restriking voltage is going to be larger and obviously will lead to more wear and tear of the breaker contacts.

2.6 Out-of-Step Detection Techniques

Various techniques have been reported in literature for out-of-step relaying. One of the conventional and most widely implemented ones is the rate of change of impedance or resistance method. Some other methods include SCV technique, R-dot scheme, fuzzy logic method, neural network and artificial intelligence-based methods, synchronized phasor measurement based techniques, equal area criterion-based methods and a method based on frequency deviation of voltage measurement. There are also techniques which use wide area measurements to detect out-of -step condition in power system.

The methods are discussed briefly below.

2.6.1 Rate of Change of Impedance Methods (Blinder Technique)

The PSB and OST schemes have been implemented mostly so far with the rate of change of impedance scheme. It is basically a distance relay with different shapes of impedance elements (i.e., blinders) which measures the positive sequence impedance at the relay location. The scheme is also called as a Blinder Scheme. The relay schemes can be divided into the following types based on the different shapes used:

- One blinder scheme
- Two blinder scheme
- Concentric Characteristics schemes (Mho, Lenticular, Polygon)

Figure 2.7 shows the concentric scheme and the two blinder scheme. The choice of the scheme depends on the loading conditions, power system parameters and the desired performance but the operating principle is the same for all. All the methods measure apparent impedance and time between the two measuring elements [15]. The method uses the fact that the rate of change of impedance is different during a fault and a power swing condition. The change is very fast when there is a fault and is slow when the system is experiencing a power swing condition.

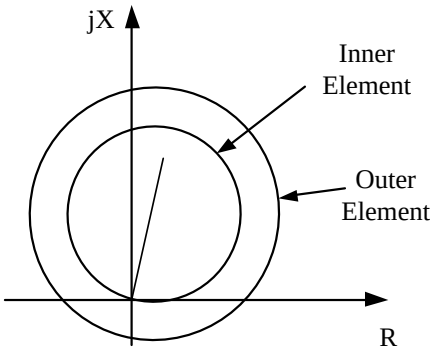

(a) Concentric Mho

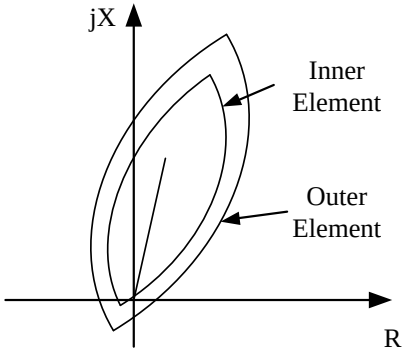

(b) Concentric Lenticulars

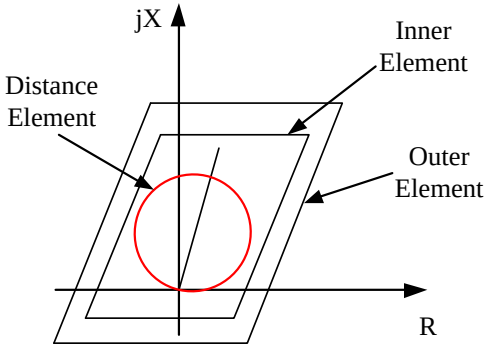

(c) Concentric Polygons

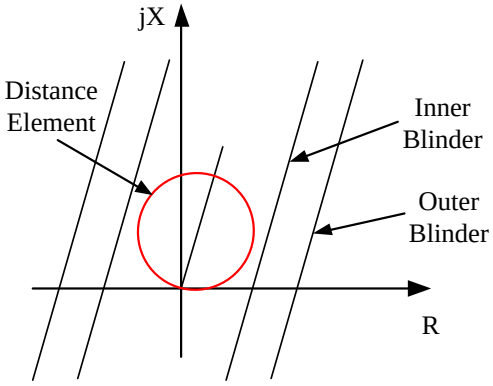

(d) Two Blinders

Figure 2.7: Various types of out-of-step relay characteristics

To understand the operating principle of these relays, let us consider the two blinder scheme as shown in Figure 2.7d. The inner and outer blinders are set according to the guidelines explained in Appendix D. The relay measures the time taken by the impedance locus to travel between the two blinders. If the time exceeds the pre-set value of time delay, the relay detects the case to be a power swing and the PSB elements is operated to block the selected distance elements. An out-of-step condition is detected when the impedance locus passes through both the blinders. The OST element can trip the distance element anytime after this point. If the voltage angle at the moment of detection is close to 180 degrees, out-of-step breaker is going to experience twice the rated voltage. The tripping is therefore delayed until the voltage reaches a favourable value to minimize the stress on the breakers.

The principle of operation of the scheme is simple and straightforward, but the implementation of the scheme involves extensive and time-consuming stability studies [15]. The inner blinder should be outside the distance relay characteristics under consideration and the outer blinder should be set inside all the possible loading conditions. Setting the separation between the two elements is a tedious and time consuming task. It depends on the slip frequency during the transient and the slip depends on the accelerating torque and machine inertia. Setting the blinders is quite difficult for heavily loaded long transmission lines where the load region lies very close to the operating characteristics of distance relay. The method is prone to false detection when there is significant change in system and transfer impedance values [6, 15].

2.6.2 Rdot Scheme

The Rdot scheme is similar to a blinder scheme. In this scheme, apparent resistance and rate of change of apparent resistance is used instead of using the apparent impedance. The Rdot scheme is given by Equation (2.8) [17].

$$P_1 = (R - R_1) + T_1 \frac{dR}{dt} \leq 0 \tag{2.8}$$

where, P_1 is the control output, R is the apparent resistance measured by the relay and R_1, T_1 are the relay-setting parameters. Figure 2.8 shows the rate of change of resistance versus the resistance and the relay characteristic. The relay characteristic is a straight line having a slope of T_1 which passes through (R_1,0) in R-Rdot plane. In Figure 2.8, the slope T_1 is equal to (-$\Delta\dot{R}/\Delta R$). If the control output P_1 during swing is negative, relay trips the breakers to separate the lines [30]. Since the technique again involves the setting of relay parameters(R_1 and T_1) using transient stability studies, it faces similar issues as that of the rate of change of impedance method.

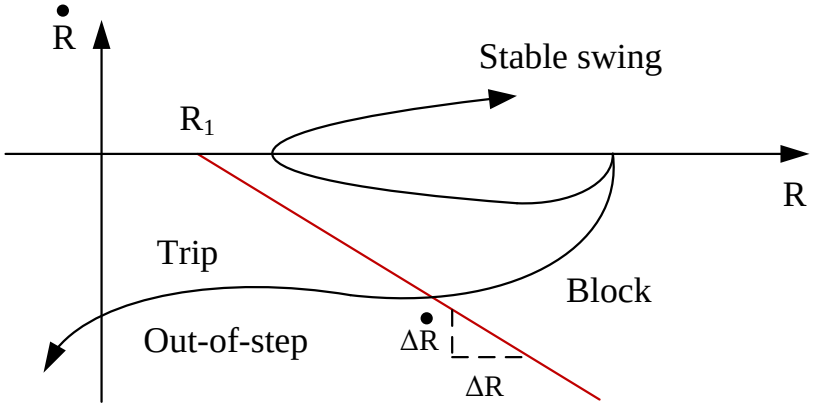

Figure 2.8: Illustration of Rdot method

2.6.3 Swing Center Voltage (SCV) technique

Consider the two machine system examples as shown in Figure 2.2. During a power swing, whenever the voltage angle separation between the two equivalent sources becomes 180 degrees, the voltage at a point between the two sources becomes zero. The voltage at that point is called SCV . Figure 2.9 shows the voltage phasor diagram of the system where the vector OO' represents the SCV [6]. Assuming the equivalent source voltage magnitude

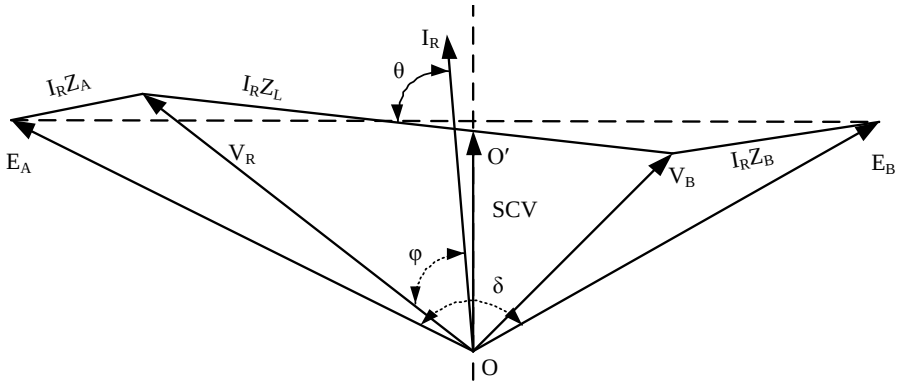

Figure 2.9: Swing Center Voltage (SCV) phasor diagram for a two machine system

as E, the SCV is given by Equation (2.9) [31].

$$SCV(t) = \sqrt{2}E\sin(\omega t + \frac{\delta(t)}{2})\cos(\frac{\delta(t)}{2}) \tag{2.9}$$

The SCV does not lie exactly at relay location (i.e., R) where the measurements are taken, but can be approximated from the voltage phasor V_R available at the relay location.

The approximation of SCV using V_R is given by Equation (2.10).

$$SCV \approx |V_R| \cos \varphi \tag{2.10}$$

where φ is the phase angle between V_R and I_R. The quantity $|V_R| \cos \varphi$ approximates the magnitude of SCV for a homogeneous system with system impedance angle(θ) close to 90 degrees. Figure 2.10 shows the approximate calculation of SCV which is the projection of V_R on the axis of I_R.

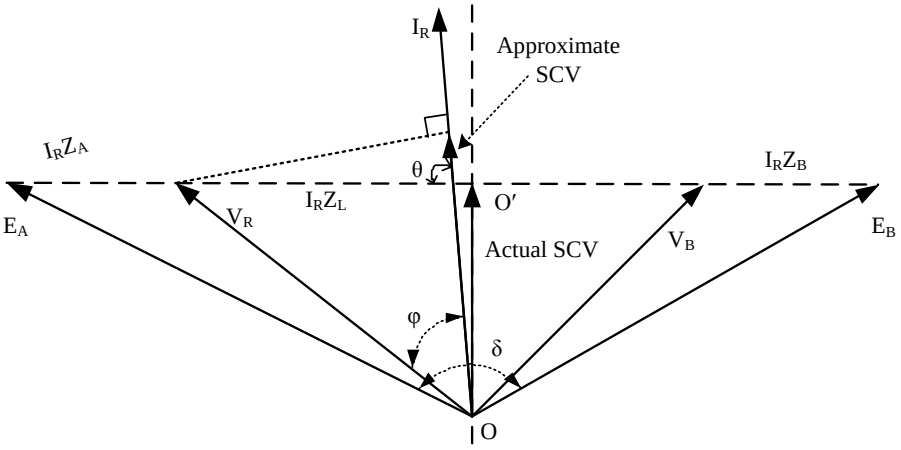

Figure 2.10: Estimating SCV using local measurements

Equation (2.10) can be written in a simplified form using the phase angle difference δ as,

$$SCV \approx |V_R| \cos \frac{\delta}{2} \tag{2.11}$$

The rate of change of SCV is used for detecting the power swing.

$$\frac{d(SCV)}{dt} \approx \frac{|V_R|}{2} \frac{\delta}{dt} \cos \frac{\delta}{2} \tag{2.12}$$

The rate of change of SCV is zero when δ is 0 or 360 degrees and will be maximum when δ is 180 degrees. The method has an advantage that it is independent of source and line parameters and requires no settings. However, the estimate is based on the local measurement available at substation and is close to actual SCV only when impedance angle of the line is 90 degrees. Moreover, the local estimate of the SCV has a sign change when δ goes through 0 degree which causes discontinuity in the estimated SCV whereas the system SCV does not have such a discontinuity [31]. In addition, the method also requires extensive stability

studies to set a threshold for the rate of change of SCV to differentiate between stable and out-of-step-conditions.

2.6.4 Fuzzy Logic and Neural Network based Out-of-Step Detection

Fuzzy logic and neural network (NN)-based out-of-step detection techniques have been reported in literatures [22, 23]. The detection procedure explained in literature [22] uses a set of input signals to train the fuzzy inference system (FIS). The output of the FIS is then compared with some threshold value to make a decision. Figure 2.11 shows the block diagram of FIS based out-of-step detection procedure.

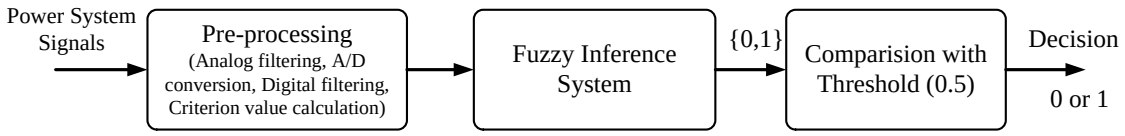

Figure 2.11: Block diagram of FIS based out-of-step detection

With the machine angular frequency deviation and impedance angle at machine terminal as input signals, the FIS was trained for over 108 fault cases. The FIS produces output equal to 0 for stable cases, and 1 for unstable cases. A threshold value of 0.5 was used to compare the output of FIS. The output lower than 0.5 is classified as stable swing and that greater than 0.5 is classified as out-of-step.

Reference [23] uses a feed-forward model of neural network based on stochastic back propagation training algorithm to predict an out-of-step condition in a power system. The schematic diagram of NN used for out-of-step detection is shown in Figure 2.12 For training purposes, three input signals – mechanical input power, kinetic energy deviation and average kinetic energy deviation – were chosen. A nine bus test system was used with three machines and three randomly distributed loads. The NN was trained using 162 simulation runs with the fault applied at six different locations and three different initial loading conditions for different fault durations. A test case was identified as out-of-step, if the rotor angle of the

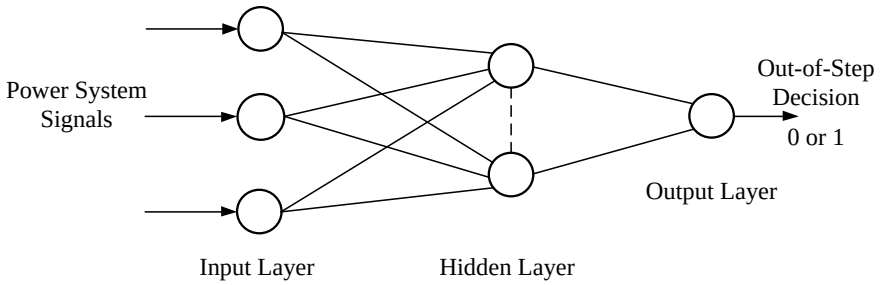

Figure 2.12: NN for out-of-step detection

generator approached 180 degrees within 1 second and was given a stability index of 0; otherwise, the case was classified as a stable swing and was given a stability index of 1. One of the advantages of this method is that all the required signals are locally measured at the generator to be protected.

The above discussed methods make correct decisions only when the new test cases have close resemblance to the trained cases. The methods need training for a wide variety of operating conditions and require a huge computer memory for the storage of their databases.

2.6.5 Frequency Deviation of Voltage Method

Reference [25] explains a method using frequency deviation of voltage to detect an out-of-step condition. The voltage is measured at the local bus, and the frequency is estimated from the voltage signal using the Discrete Fourier Transform (DFT). The angular velocity and acceleration of the voltage are then calculated. Instability detection is done by observing the angular velocity of the voltage when the acceleration goes from negative to positive. If the angular velocity at this point is greater than the nominal angular frequency, then the instability is detected. The method detects a generator out-of-step condition using the voltage signal at the generator substation. The voltage signal rapidly fluctuates during a transient condition, and hence the algorithm is suceptible to an incorrect operation during the switching transients. In addition, this technique is localized as it relies on localized measurements only. However, for modern interconnected power networks, an algorithm which is suitable for detecting instability at the system level is needed.

A modified method is therefore proposed as one of the research contributions of this thesis and is discussed in the following Section 2.6.6. It uses a more stable quantity, i.e., the generator speed deviation, to detect instability in an interconnected system.

2.6.6 State Deviation Approach

An approach based on the online measurement of the generator speed ("state") at the "equilibrium points" is proposed in this section. Figure 2.13a shows the power-angle characteristics for a typical pre-fault, during fault and post fault conditions. If we analyze this curve; following the disturbance, the generator accelerates, first causing an increase in the generator speed, and then starts decelerating after clearing the fault. The pre-fault operat-

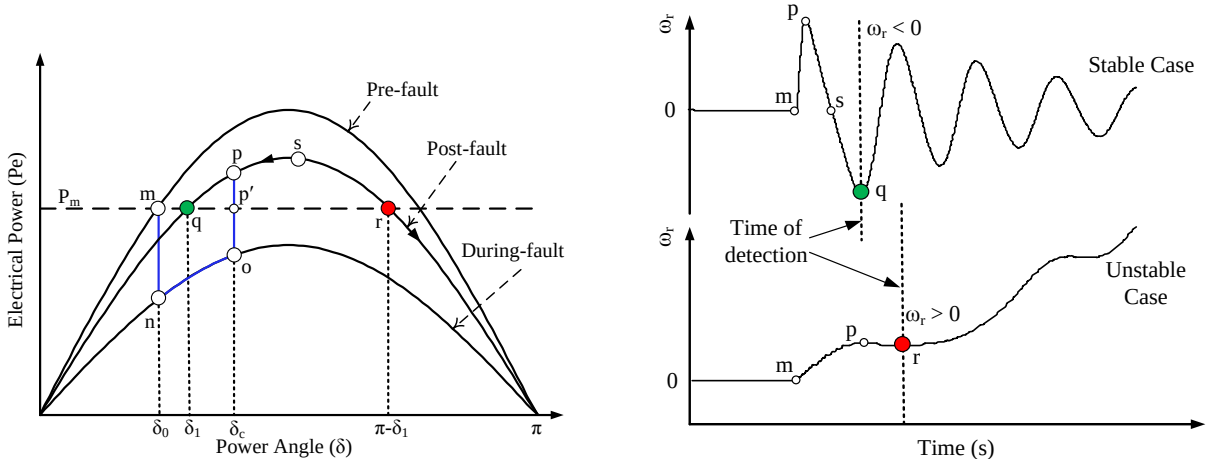

(a) Power-angle characteristics

(b) Generator relative speed versus time

Figure 2.13: Illustration of the state deviation technique

ing point is shown by point m. When fault occurs in the system, the machine accelerates in the region marked by m-n-o-p′. At p, machine speed is greater than the synchronous speed, the rotor angle separation (δ) keeps increasing while the machine starts decelerating. If the machine regains its synchronous speed at point s, it starts swinging backward. At point q, machine state changes from deceleration to acceleration. But since the relative speed of the machine at q is less than 0, the machine becomes stable and settles at equilibrium point q. Suppose the machine oscillates beyond point s and reaches point r across which machine

state changes from deceleration to acceleration. If the relative speed of the machine is greater than 0 at the point r, instability is detected. Figure 2.13b shows the generator state (i.e., relative speed, ω_r) for stable and unstable conditions.

The proposed method uses online measurement of electrical power and the generator speed as inputs. The equilibrium point is obtained using electrical power signal; i.e., the point where $(P_m - P_e)$ goes from negative to positive assuming that the P_m is constant. The main advantage of this technique is that the parameters used by the relay are readily available and easy to measure. One of the advantages of this method is that it does not require network admittance matrix reduction and any dynamic model approximations. In addition, it is not affected by any switching transients, as the generator speed, due to the machine inertia, have a smoother change even during the transient conditions. The method is sound and performs well with various generator controls such as exciter, governor and turbine dynamics included. The technique has been tested for different power system configurations and is discussed in detail in Chapters 3, 4 and 5.

2.7 Summary

This chapter explained the power swing phenomena in power system and the importance of out-of-step protection. The study of the impedance trajectory during a power swing condition was explained: how a power swing affects the various protection elements such as distance relays, overcurrent relays in power system. The chapter also discussed the out-of-step protection functions (OSB and OST) that are implemented in out-of-step relay. Different techniques such as the rate of change of impedance method, SCV technique, fuzzy logic and neural network methods, rate of change of frequency from voltage method, state deviation method were discussed along with their advantages and shortcomings. The next chapter explains the proposed state plane method to predict an out-of-step condition.

Chapter 3

Out-of-Step Protection Using State Plane Analysis

3.1 Introduction

A power system's transient stability behaviour can be represented by a mathematical model using nonlinear ordinary differential equations. As we know, there are no methods to find an exact analytical solution of non-linear differential equation [32]. A number of numerical methods have been described in the literature for solving non-linear differential equations. State plane analysis (SPA) methods [32] are one of the most elegant and efficient methods for solving differential equations of dynamic systems in general. It represents the dynamic behaviour of the system in the form of state plane trajectories. This chapter proposes a new fast state plane method for out-of-step relaying, which uses the trajectories to analyse dynamic behaviour at different system conditions. It has the unique capability to calculate CCA and CCT simultaneously, unlike the EAC which calculates the CCA first followed by the iterative calculation of the CCT. The proposed method is also simple, computationally fast compared to EAC and is able to predict the transient instability condition faster. The proposed approach has been tested in a single machine infinite bus (SMIB) and two area system configurations to predict the first swing instability. The approach has been also compared with a two blinder scheme and the state deviation technique, and the results are presented in this chapter. Unlike a first swing instability, a power system may experience instability beyond first swing. This chapter proposes a new approach to predict multi-swing instability, where the first swing instability is found using the state plane ap-

proach and the instability in subsequent swings is found using the state deviation technique. The multi-swing scenarios are created and tested in the two area test system.

3.2 State Plane Analysis

3.2.1 Mathematical Formulation

Consider that a power system is described with the following second order differential equation

$$\ddot{y} = f(y, \dot{y}) \tag{3.1}$$

Let us define the state variables as

$$\begin{aligned} x_1 &= y \\ x_2 &= \dot{y} \end{aligned} \tag{3.2}$$

Equation (3.1) can now be represented with a set of first order differential equations

$$\begin{aligned} \dot{x_1} &= x_2 \\ \dot{x_2} &= f(x_1, x_2) \end{aligned} \tag{3.3}$$

The plane, with coordinates x_1 and x_2 is called state plane. The solution of Equation (3.3) with respect to time could be represented as a curve in state plane (state plane trajectory). If one knows the initial states of the system, the dynamics followed by the power system during faults could be easily predicted using the state plane trajectory. Also, the state plane trajectories for different initial states could be represented in a graphical fashion to analyse the power system behaviour for various types of contingencies in power system.

3.2.2 Singular Points

Eliminating time from Equation (3.3)gives,

$$\frac{dx_2}{dx_1} = \frac{f(x_1, x_2)}{x_2} \tag{3.4}$$

Equation (3.4)can be written as,

$$\frac{dx_2}{dx_1} = \frac{Q(x_1, x_2)}{P(x_1, x_2)} \tag{3.5}$$

The point for which the system is going to be at rest, i.e., $P(x_{1s}, x_{2s}) = 0$ and $Q(x_{1s}, x_{2s}) = 0$, is a singular point. The system will continuously stay at a singular point if it is left undisturbed. Singular points hence represents points of equilibrium. Determination of singular points represent an essential step in the process of plotting the state plane trajectories. Most of the linear systems consist only of one singular point, whereas the highly nonlinear power systems have many singular points corresponding to many equilibria. In particular, it is important to determine the stability status of the power system at these points. These points can either represent stable or unstable equilibrium. The stability around the singular points is found by linearising the system at the singular points. The determination of stability around the singular points is discussed in Appendix C. State plane trajectories in general converge towards the stable equilibrium point and will diverge away from the unstable equilibrium point. The stable and unstable equilibrium points are called vortex and saddle point, respectively.

3.2.3 Determining Time from Trajectories

A state plane trajectory contains time information implicitly. The time information can be extracted from the trajectory by using a simple procedure as explained below. State variable x_1 can be evenly or unevenly divided into small intervals. For each small increment of x_1, average increment in x_2 can be calculated and hence the corresponding small increment in time can be calculated using Equation (3.6a). In Figure 3.1, x_1 is evenly divided into small intervals Δx_1. The small increment in time Δt for Δx_1 and $x_{2,avg}$ corresponding to the i^{th} interval is given by Equation (3.6b).

$$dt = \frac{dx_1}{x_2} \tag{3.6a}$$

$$\Delta t_i = \frac{\Delta x_1}{x_{2,avgi}} \tag{3.6b}$$

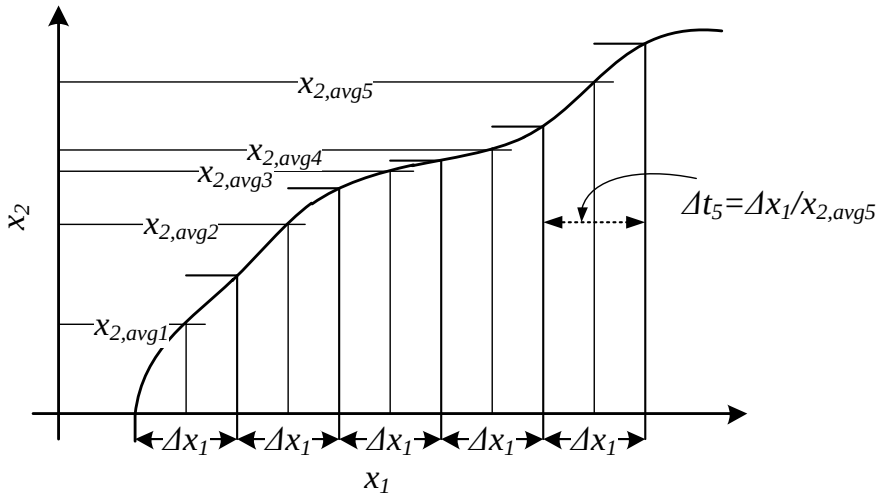

Figure 3.1: Time calculation from state plane trajectory

Time for each point of intervals is now calculated by cumulatively adding the incremental time for each interval.

$$t(i) = t(i-1) + \Delta t_i \tag{3.7}$$

3.3 Analysis of System Stability in State Plane

As explained before, the loss of synchronism in an interconnected system happens due to the separation of rotor angle of machines with each other. This happens because of the inability of each generator to restore equilibrium between electromagnetic torque and mechanical torque [7]. The stability behaviour of the power system has been analysed using a new SPA procedure and the method is explained in detail in the following sections.

3.3.1 Representing Machine Dynamics: Swing Equation

Transient stability analysis of the power system involves solving of the classical swing Equation (3.8).

$$M\frac{d^2\delta}{dt^2} = P_m - P_e(\delta) \tag{3.8}$$

where, M is the inertia constant, δ is the rotor angle of generator, P_m is the mechanical input power and P_e is the electrical output power. For a single machine connected to a large system through a purely inductive transmission line, as shown in Figure 3.2, electrical power output is given by Equation (3.9a).

$$P_e(\delta) = \frac{E_s * E_r}{X} \sin\delta \tag{3.9a}$$

$$= P_{max} \sin\delta \tag{3.9b}$$

where X is the total impedance between the generator and the receiving ends and P_{max} is the maximum possible electrical power power transfer. The solution of the swing equation

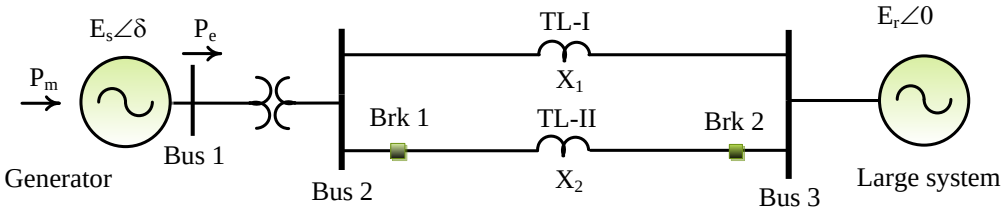

Figure 3.2: Single machine connected to a large system

gives the dynamic behaviour of the system during transient condition. Under a steady state condition, there is an equilibrium between input mechanical power and output electrical power, and hence the speed remains constant. Whenever the system is perturbed, the equilibrium condition is violated and hence machine accelerates or decelerates according to the swing equation. Consider a three phase fault on the transmission line TL-II of the power system shown in Figure 3.2. Because of the fault, the transfer reactance of the faulted network increases, which decreases the electrical power transfer between the generator and infinite bus (i.e., bus 3). As a result, the generator starts accelerating. The dynamic motion of the generator for during-fault condition is given by Equation (3.10).

$$M\frac{d^2\delta}{dt^2} = P_m - P_{edf}(\delta) \tag{3.10}$$

where, P_{edf} is the electrical power output during disturbance.

When the fault is cleared by opening the breakers Brk1 and Brk2, the electrical power transfer increases as the transfer reactance is reduced from that of the during-fault condition.

If the electrical power transfer for post-fault condition is greater than the mechanical power, the generator starts decelerating. The dynamic motion of the system for post-fault condition is given by Equation (3.11).

$$M\frac{d^2\delta}{dt^2} = P_m - P_{eaf}(\delta) \tag{3.11}$$

where, P_{eaf} is the electrical power output after the disturbance is cleared.

This project uses state plane analysis as a technique to determine the solution of swing equation. The solution procedure is explained next.

3.3.2 State Plane Representation of Swing Equation

Substituting Equation (3.9b) in the swing Equation (3.8,

$$M\frac{d^2\delta}{dt^2} = P_m - P_{max}\sin\delta \tag{3.12}$$

Equation (3.12) could be modified as,

$$\frac{d^2\delta}{dT^2} = P - \sin\delta \tag{3.13}$$

where $P = \dfrac{P_m}{P_{max}}$, $T = t\sqrt{\dfrac{\pi * P_{max}}{180 * M}}$ and P_{max} is the maximum electrical power value that could flow through the lines. State space representation of the Equation (3.13) is given by,

$$\dot{\delta} = \omega \tag{3.14a}$$

$$\dot{\omega} = P - \sin\delta \tag{3.14b}$$

where δ and ω are two state variables and ω represents the speed of the machine with respect to the synchronous speed. The two state variables give the current dynamic state of the machine. During transient condition, machine starts oscillating because of the change in P in Equation (3.13). As a result, the state variables exhibit an oscillatory behavior. The dynamic motion of the machine is hence represented by the change in state variables of the system, which can be demonstrated by plotting state variables ω versus δ in a state plane. The path followed by state variable ω in state plane with respect to δ gives important

information about stability of the synchronous machines. Angle δ gives the position of the rotor and the speed ω represents the energy associated with the machine. Increase in ω represents increase in kinetic energy or decrease in potential energy and vice versa. The variation in states in state plane during disturbed condition therefore mimics the variation in machine energy. Equation (3.14) can also be written as,

$$\frac{d\omega}{d\delta} = \frac{P - \sin\delta}{\omega} \tag{3.15}$$

The singular points of the system could be found out by equating numerator and denominator of right hand side of Equation (3.15) to zero, i.e., $P - \sin\delta = 0$ and $\omega = 0$. The singular points will be $(\sin^{-1} P, 0)$ and $(\pi - \sin^{-1} P, 0)$. Stability of the system around these points could be obtained by analyzing the eigenvalues of the system (Lyapunov's indirect method), which is briefly explained in Appendix C. Using this analysis, the first point is found to be a stable equilibrium point and the second point is obtained as an unstable equilibrium point. Equation (3.15) can be rearranged so that the same variables appear on one side,

$$\omega d\omega = (P - \sin\delta)d\delta \tag{3.16}$$

Integrating both sides of Equation (3.16) gives,

$$\underbrace{\frac{\omega^2}{2}} + \underbrace{\int_0^{\delta} (\sin\delta - P)d\delta} = 0 \tag{3.17}$$

where the first term in the left hand side of Equation (3.17) represents kinetic energy, and the second term represents potential energy of the machine. Since the kinetic energy is zero at the singular point, it gives maxima or minima of potential energy.

3.3.3 State Plane Trajectories Obtained from the Swing Equation for Different Types of Disturbances

As explained in Chapter 1, following a disturbance, the power system could continue to remain stable or become unstable. Sustained faults, if not cleared quickly, result in an unstable condition in the system. To understand machine dynamics in state plane under different fault conditions, consider a single machine connected to a large system as shown

in Figure 3.2. The system parameters are given in Appendix A. Under normal condition, the system operates at a stable equilibrium point, delivering constant power output. Faults, such as single phase to ground fault, double phase to ground fault, and three phase fault, are applied at the middle of transmission line II and are cleared by opening the breakers Brk1 and Brk2 at the two ends of the line. The operating conditions are named as pre-fault condition, during-fault condition and post-fault condition. With the SMIB parameters as given in Appendix A.1 and the initial state of generator $(0.738\,rad, 0\,rad/s)$, the state plane trajectories are plotted for the above conditions with randomly selected initial points. They are shown in Figures 3.3, 3.4, 3.5, 3.6 and 3.7 respectively. In the figures, the three different lines denote the following,

- Solid blue lines are isoclines plotted for different values of slopes varying from -5 to 5 with an equal interval of 0.5. All isoclines go through the singular points and hence the intersections of them give the singular points.
- Solid black lines are the state plane trajectories.
- Dotted red line is critical trajectory known as separatrix.

The shaded area inside the separatrix is a stable region and the region outside the separatrix is an unstable region.

1. Pre-fault Condition

   For the pre-fault system, the value of P is 0.673 pu (P_{max} for pre-fault condition is 1.3370 pu). Figure 3.3 shows the various possible paths that the machine can follow during pre-fault condition. Since the machine is operating at $(0.738\,rad, 0\,rad/s)$, which is the vortex of the system, the machine stays stable. The trajectories near the vortex are bounded around it and the region is a stable region. The trajectories around the saddle are unbounded (where ω increases as δ increases) and the region is called an unstable region. These two regions are separated by a separatrix.

2. During-fault condition

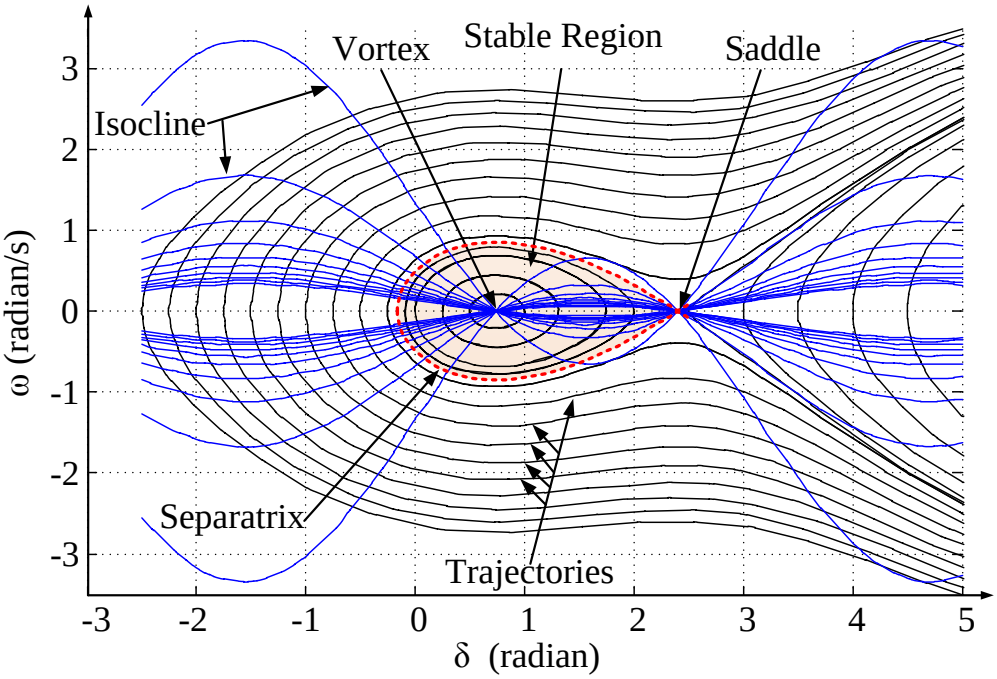

Figure 3.3: State plane trajectories of a SMIB for a pre-fault condition

a) Single phase to ground fault

The value of P for single line to ground fault at the middle of the transmission line (TL-II) is 0.7 pu (P_{max}=1.2866 pu). The state plane trajectories for the fault is shown in Figure 3.4. It is apparent from the trajectories that it has a stable and an unstable region. Because of the fault, machine starts oscillating along the trajectory from its initial state. The initial state decides which path the trajectory will follow during fault, and the fault duration will determine the new state of the machine at the moment when the fault is cleared. Looking at the figures for pre-fault condition (Figure 3.3) and during-fault condition (Figure 3.4), it can be seen that the stable region for during-fault condition is smaller than that for the pre-fault condition.

b) Double phase to ground fault

For the double phase to ground fault, the value of P is 0.79 pu (P_{max}=1.1395 pu). Figure 3.5 shows the state plane trajectories for a double phase to ground fault. The trajectories seems similar to that for single phase to ground fault, but the stable region in this case is much smaller than that for the single phase to ground

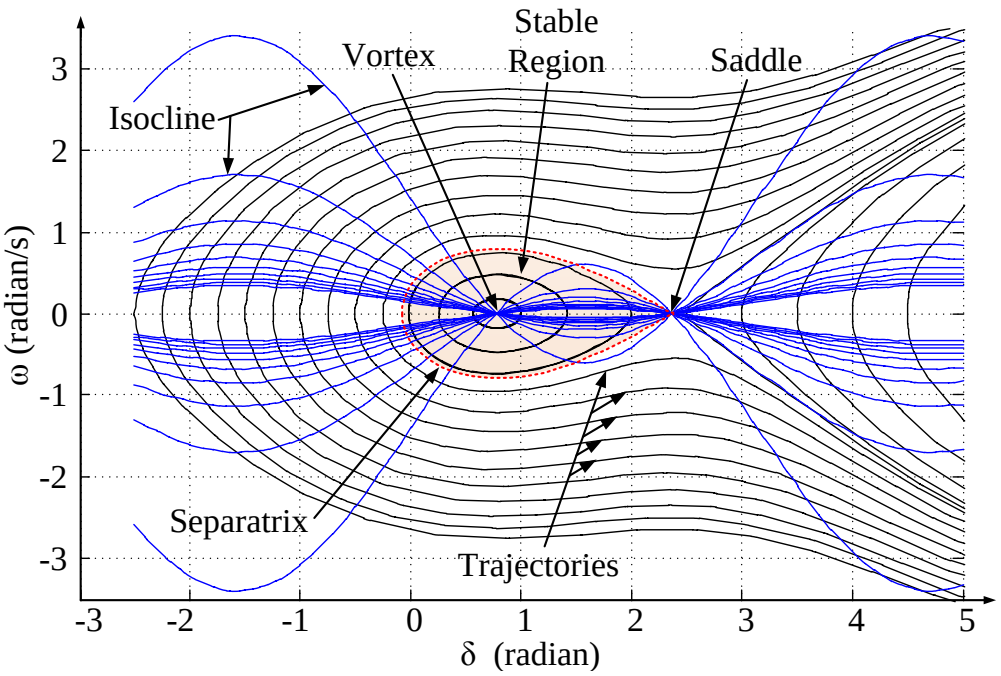

Figure 3.4: State plane trajectories of a SMIB for a during-fault condition (single phase to ground fault)

fault scenario. If the initial pre-fault state of the machine lies inside the stable region, the machine oscillations will be stable. If the initial pre-fault state of the machine lies in the unstable region, the trajectories becomes unbounded and the machine will become unstable.

c) Three phase fault

For the three phase fault, the value of P is 1.20 pu (P_{max}=0.7480 pu). Figure 3.6 shows the state plane trajectories for a three phase fault. As can be seen from the trajectories, there are no singular points. This means that there is no stable region throughout the state plane and all the trajectories are unbounded. It suggests that the fault must be cleared to prevent an unstable operation.

3. Post-fault condition

The fault is cleared by removing the faulted line from the system (Figure 3.2). The P value becomes 0.95 pu (P_{max}=1.1024 pu)and the post fault trajectories are shown in Figure 3.7. The post-fault figure has a smaller stable region as compared to the

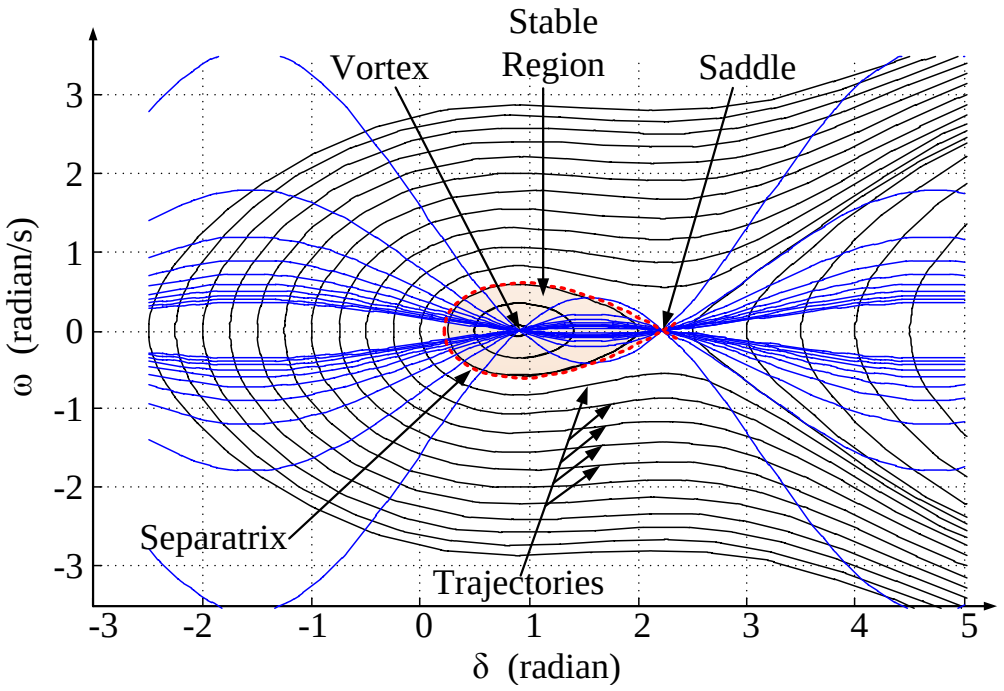

Figure 3.5: State plane trajectories of a SMIB for a during-fault condition (double phase to ground fault)

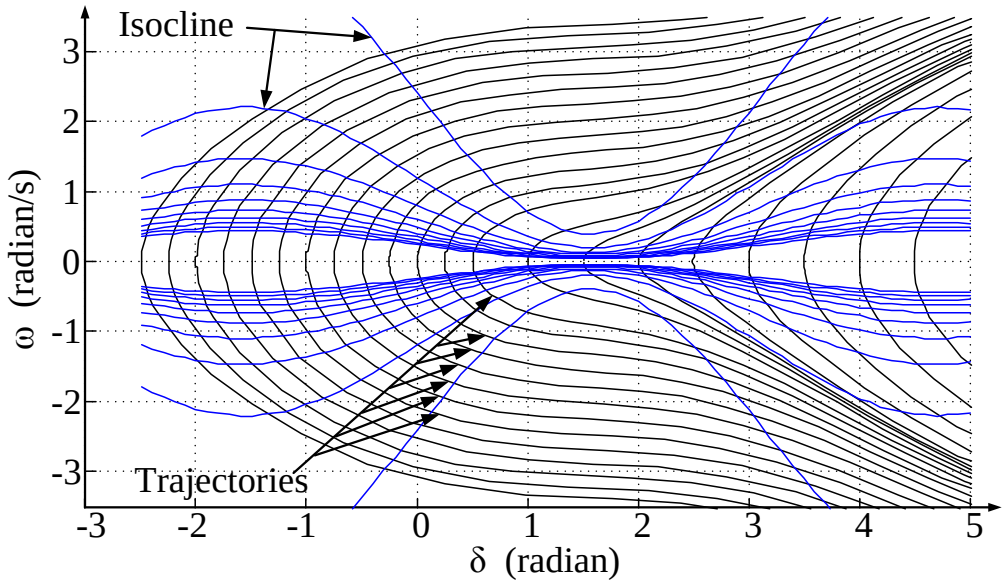

Figure 3.6: State plane trajectories of a SMIB for a during-fault condition (three phase fault)

pre-fault figure. If the states at the moment of clearing the fault lie inside the stable region, the machine remains stable. If the states at the instant of clearing the fault have reached a value beyond the separatrix, the machine is going to become unstable.

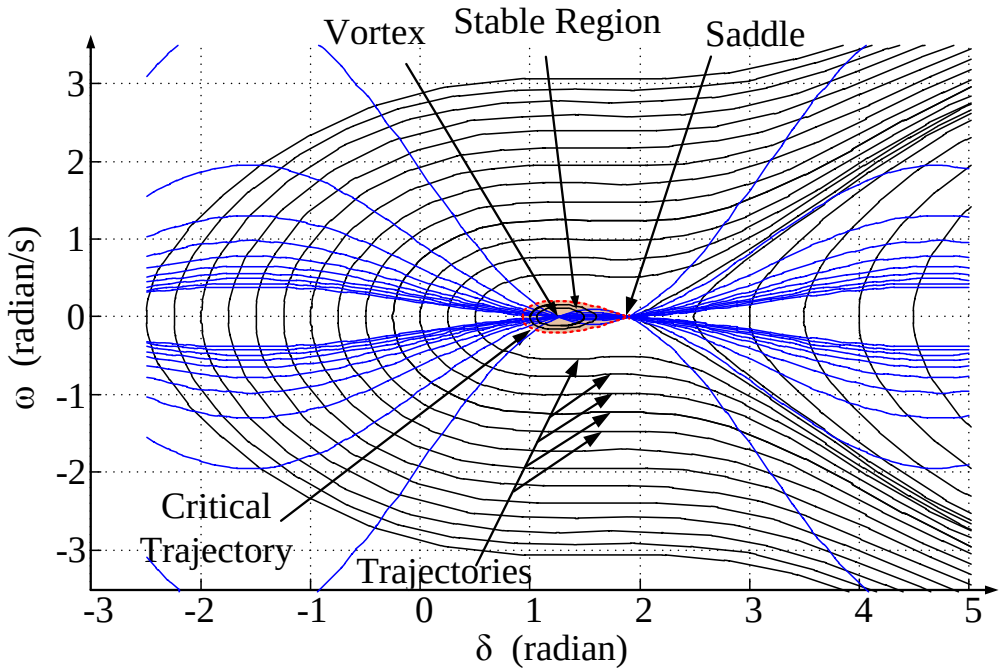

Figure 3.7: State plane trajectories of a SMIB for a post-fault condition

3.3.4 Out-of-Step Detection Using Equal Area Criterion (EAC)

The power-angle curve for the pre-fault, during-fault, and post-fault condition are shown in Figure 3.8. The well known EAC uses the power-angle curve. It calculates the accelerating area(A_1) during the fault, and the decelerating area (A_2) after the fault. The area A_1 depends on fault clearing time. The longer the fault clearing time, greater will be the area A_1. According to EAC, whatever accelerating energy added to the system during fault must be removed after the fault to restore the synchronous speed. The EAC hence determines the stability of a system as follows,

a. If $A_1 < A_2$ Stable swing

b. If $A_1 = A_2$ Critical condition

c. If $A_1 > A_2$ Unstable swing or out-of-step condition

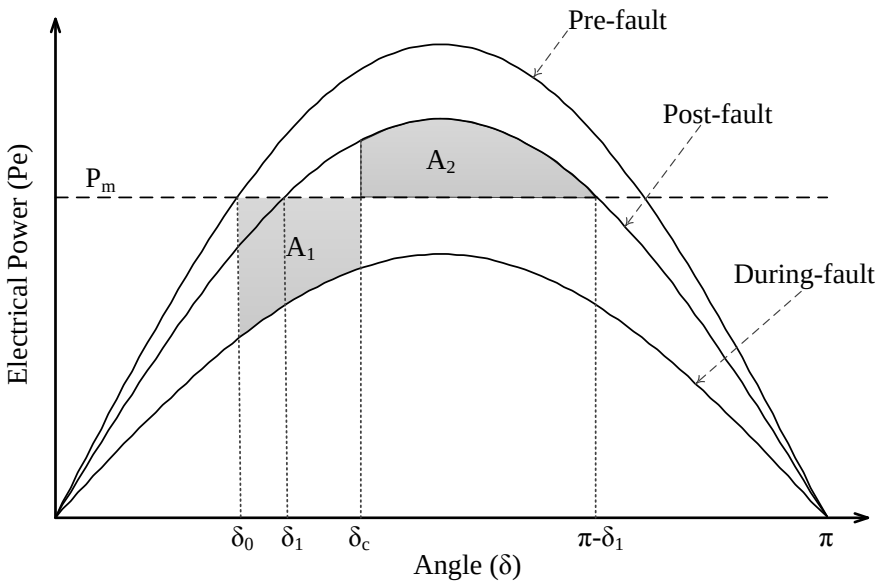

Figure 3.8: Power-angle characteristics

3.4 Out-of-Step Prediction Using State Plane Analysis

The state plane trajectory analysis technique explained in Section 3.3.3 for assessing transient stability along with the time calculation technique from the state plane trajectory discussed in Section 3.2.3 are used to develop an algorithm to predict an out-of-step condition in power system. The algorithm calculates the system's critical clearing angle(δ_{cr}) and the critical clearing time (t_{cr}) simultaneously using the state plane plot of during-fault and post-fault condition. The t_{cr} calculated is compared with the fault clearing time(t_{cl}) to make the decision. The algorithm consists of four distinct steps:

Step - I ***Finding state plane plot during disturbance:***

Suppose the initial state is $(\delta_0, 0)$, Equation (3.15) can be used to calculate ω for incremental values of δ. The derived expression for ω_1 is given by Equation (3.18). It gives the values of ω_1 *vs* δ during disturbance.

$$\omega_1 = \pm\sqrt{2(P_1(\delta - \delta_0) + \cos\delta - \cos\delta_0)} \tag{3.18}$$

where, $\omega_1 = d\delta/dT_1$ is the speed of the machine, and P_1 is the value of P for the during-fault condition.

Step - II ***Calculating time scale values:*** The time scale values for (Step - I) are calculated using the method explained in Section 3.2.3. The calculated time would be the time T_1 from which the exact time is calculated using Equation (3.19).

$$t(i) = T_1(i) \times TF_1 \tag{3.19}$$

where,

$$TF_1 = \sqrt{\frac{180 * M}{\pi * P_{maxdf}}} \tag{3.20}$$

where, P_{maxdf} refers to maximum power that can be transferred for during-fault condition.

To illustrate the algorithm, a three phase fault is applied on TL-II at $(1/4)^{th}$ distance from the bus 2 for the system shown in Figure 3.2. The test case is named as 'E'. The initial generator bus voltage angle (δ_t) is 30^o and the initial voltage angle behind transient reactance is 44.1803 degrees (0.7711 radian). The mechanical input power is 0.9486 pu. For the faulted network condition, the power-angle characteristic is obtained using the standard Y_{BUS} network reduction technique (which is discussed in Appendix E). The $P_e - \delta$ curve obtained is $0.5661 \sin \delta$. The ω_1 and time (t) values calculated for the during-fault condition are given in Table 3.1.

Step - III ***Finding of critical trajectory (separatrix) for post fault condition:*** The post-fault power-angle characteristic is predicted using the post-fault network condition. The power-angle characteristic for the test case E is $1.1024 \sin \delta$. The post-fault swing equation is therefore given by Equation (3.21).

$$\frac{d^2\delta}{dT_2^2} = P_2 - \sin \delta \tag{3.21}$$

$$\frac{d^2\delta}{dT_2^2} = 0.8604 - \sin \delta \tag{3.22}$$

The above equation can be put in the form,

$$\frac{d\omega_2}{d\delta} = \frac{0.8604 - \sin \delta}{\omega_2} \tag{3.23}$$

where, $\omega_2 = d\delta/dT_2$ and P_2 is the value of P for post-fault condition.

Table 3.1: Calculation of during-fault trajectory and time scale

δ (radian)	ω_1 (radian/s)	$\Delta\delta$ (radian)	ω_{1avg} (radian/s)	ΔT (s)	Δt (s)	t (s)
0.7711	0.0000					0.00
0.8025	0.2466	0.0314	0.1233	0.2548	0.0462	0.0462
0.8339	0.3467	0.0314	0.2966	0.1059	0.0192	0.0653
0.8653	0.4223	0.0314	0.3845	0.0817	0.0148	0.0801
0.8968	0.4849	0.0314	0.4536	0.0693	0.0125	0.0927
0.9282	0.5392	0.0314	0.5121	0.0614	0.0111	0.1038
0.9596	0.5875	0.0314	0.5633	0.0558	0.0101	0.1139
0.9910	0.6312	0.0314	0.6093	0.0516	0.0093	0.1232
1.0224	0.6713	0.0314	0.6512	0.0482	0.0087	0.1320
1.0538	0.7083	0.0314	0.6898	0.0455	0.0082	0.1402
1.0853	0.7429	0.0314	0.7256	0.0433	0.0078	0.1480
1.1167	0.7754	0.0314	0.7591	0.0414	0.0075	0.1555
1.1481	0.8060	0.0314	0.7907	0.0397	0.0072	0.1627
1.1795	0.8350	0.0314	0.8205	0.0383	0.0069	0.1697
1.2109	0.8626	0.0314	0.8488	0.0370	0.0067	0.1764
1.2423	0.8889	0.0314	0.8757	0.0359	0.0065	0.1829
1.2737	0.9142	0.0314	0.9015	0.0348	0.0063	0.1892
1.3052	0.9384	0.0314	0.9263	0.0339	0.0061	0.1953

The singularities for Equation (3.23) are obtained by equating the numerator and denominator to zero. The singular points are located at $(1.036, 0)$ and $(2.105, 0)$. To identify the type of singularities at these points, the method discussed in Appendix C is adopted. For the first singular point $(1.036, 0)$, define translated states as $\widetilde{\delta}$= $\delta - 1.036$ and $\widetilde{\omega_2}$= ω_2. The corresponding state equation becomes,

$$\frac{d\widetilde{\omega_2}}{d\widetilde{\delta}} = \frac{0.8604 - \sin(\widetilde{\delta} + 1.036)}{\omega_2} \tag{3.24}$$

which could also be written as,

$$\begin{bmatrix} \dot{\widetilde{\delta}} \\ \dot{\widetilde{\omega_2}} \end{bmatrix} = \begin{bmatrix} \omega_2 \\ 0.8604 - \sin(\widetilde{\delta} + 1.036) \end{bmatrix} \tag{3.25}$$

Equation (3.25) is linearised around (0,0). The linearised system is given by Equation (3.26),

$$\begin{bmatrix} \dot{\widetilde{\delta}} \\ \dot{\widetilde{\omega_2}} \end{bmatrix} = \begin{bmatrix} 0 & 1 \\ -0.51 & 0 \end{bmatrix} \begin{bmatrix} \widetilde{\delta} \\ \omega_2 \end{bmatrix} \tag{3.26}$$

The eigenvalues of the system are $\pm 0.712i$, which results in an oscillatory system with zero damping. This singular point corresponds to a Vortex point. Following a similar procedure for the singular point $(2.105, 0)$, eigenvalues obtained are ± 0.712. This will result in an unstable system and hence the singular point is a saddle point.

Equation (3.17) for post-fault condition can be written as,

$$\frac{\omega_2^2}{2} + \int_0^{\delta} (\sin\delta - P_2)\, d\delta = 0 \tag{3.27}$$

Equation (3.27) can be written as,

$$\frac{\omega_{2cl}^2}{2} + \int_0^{\delta_{cl}} (\sin\delta - P_2)\, d\delta = 0 \tag{3.28}$$

where, δ_{cl} is the value of δ and ω_{2cl} is the speed of the machine, when the fault is cleared. The ω_{2cl} is given by Equation (3.29).

$$\omega_{2cl} = \left(\frac{d\delta}{dT_2}\right)_{T_2=0} = \frac{dT_1}{dT_2}\frac{d\delta}{dT_1} = \left(\frac{TF_1}{TF_2}\right)\omega_1 \tag{3.29}$$

where, TF_1 is given by equation (3.20) and

$$TF_2 = \sqrt{\frac{180 * M}{\pi * P_{maxaf}}} \tag{3.30}$$

where, P_{maxaf} is the maximum possible power transfer for the post-fault condition. As discussed in Section 3.3.2, the potential energy ($V(\delta) = \int_0^{\delta}(\sin\delta - P_2)\, d\delta$) of the machine will have a maximum and a minimum at the singular points. It can be seen by setting the first derivative of potential energy $\left(\frac{dV}{d\delta}\right)$ to zero which means

$(\sin\delta - P_2 = 0)$. The second derivative of $V(\delta)$ is $\cos\delta$. For singular point $(\sin^{-1} P_2, 0)$, the second derivative is positive and therefore it results in a minimum, and for singular point $(\pi - \sin^{-1} P_2, 0)$ it is negative, resulting in a maximum. Figure 3.9 shows the plot of potential energy for the test case E.

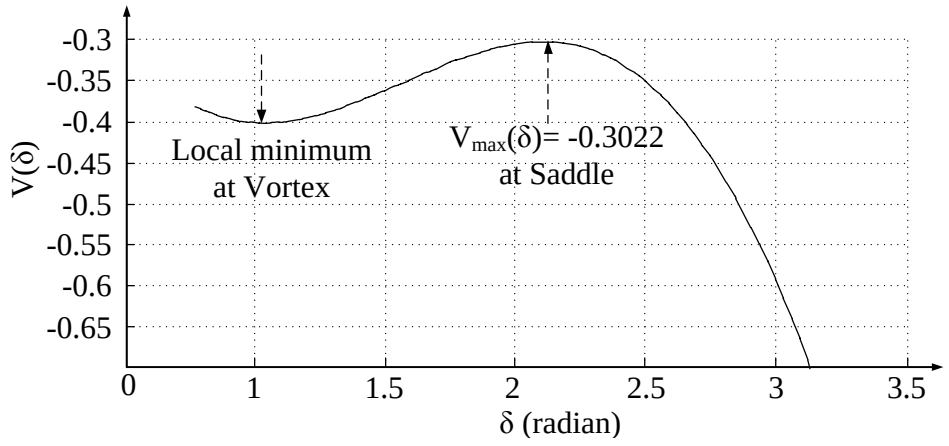

Figure 3.9: Potential energy plot for test case E

The minimum potential energy occurs at vortex point and the maximum potential energy (V_{max}) occurs at the saddle point. If the total energy (i.e., sum of kinetic energy gained during the fault condition and potential energy gained for the post-fault condition) of the machine is less than V_{max} at the moment when the disturbance is cleared, the machine becomes stable. Otherwise, it becomes unstable.

The Equation (3.27) can be written in the form given by the Equation (3.31). From the Equation (3.31), the state ω_2 can be calculated, which is given by Equation (3.32).

$$\frac{\omega_2^2}{2} + V(\delta) = E \tag{3.31}$$

$$\omega_2 = \sqrt{2(E - V(\delta))} \tag{3.32}$$

For different values of total energy E_i (where i=1,2,...,7), state plane plots for ω_2 are shown in Figure 3.10. When the value of E becomes equal to V_{max}, the corresponding trajectory gives the separatrix. For (i=1,2,...,5), E_i is less than V_{max}, which means the system is stable, and the total energy E_7 is greater than V_{max}, which indicates that the system becomes unstable.

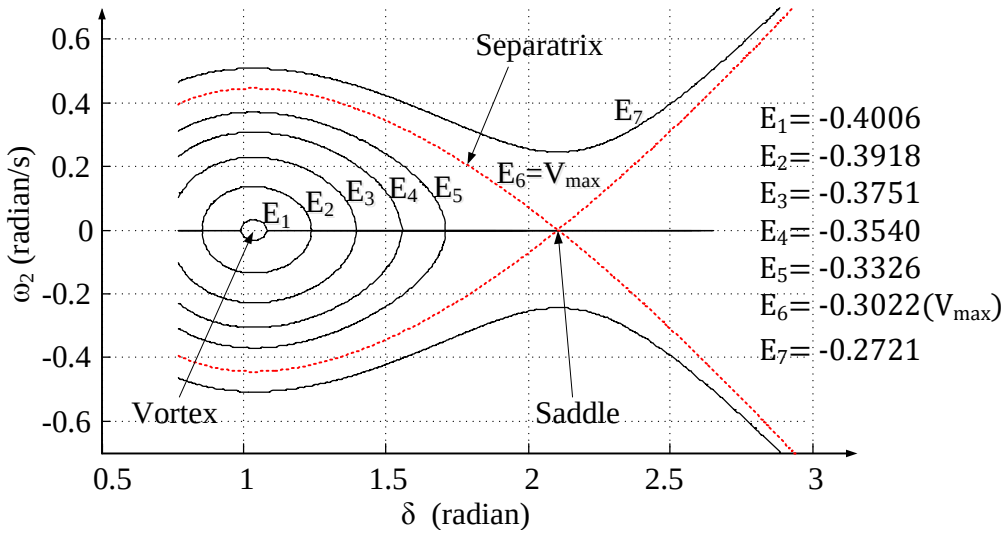

Figure 3.10: State plane trajectories of SMIB for post-fault condition for different values of E

Step - IV ***Finding CCA (δ_{cr}) and CCT (t_{cr}):*** Two approaches could be used for calculating the critical clearing angle of the system and are explained below:

1. When the sum of the kinetic energy gained by the machine during fault condition and the potential energy that can be gained by the machine for the after fault condition is equal to the maximum potential energy (V_{max}), it gives the CCA (δ_{cr}).

$$E = \frac{\omega_{2cl}^2}{2} + \int_0^{\delta_{cr}} (\sin\delta - P_2)\, d\delta = V_{max} \tag{3.33}$$

2. In state plane plot shown in Figure 3.11, starting from δ_0, the ω_{2cl} represents the kinetic energy gained by the machine at the moment when the fault is cleared and the ω_2 is the separatrix which represents the gain in potential energy by the machine after the fault condition. If the fault is cleared at angle δ_1, post-fault speed will follow C_1 curve, which shows the stable operation. At the point of intersection of these two plots, the sum of the gain in kinetic energy gained during fault and the potential energy for after fault condition will be equal. The point of intersection gives the critical clearing point and the corresponding angle will be the CCA (δ_{cr}) as shown in Figure 3.11. If the fault is cleared at angle

δ_2, post-fault speed will follow C_2 curve (since the speed keeps on increasing the machine becomes unstable). If the fault is not cleared from the system due to breaker failure, speed will follow the during-fault trajectory (ω_1) and the machine becomes unstable.

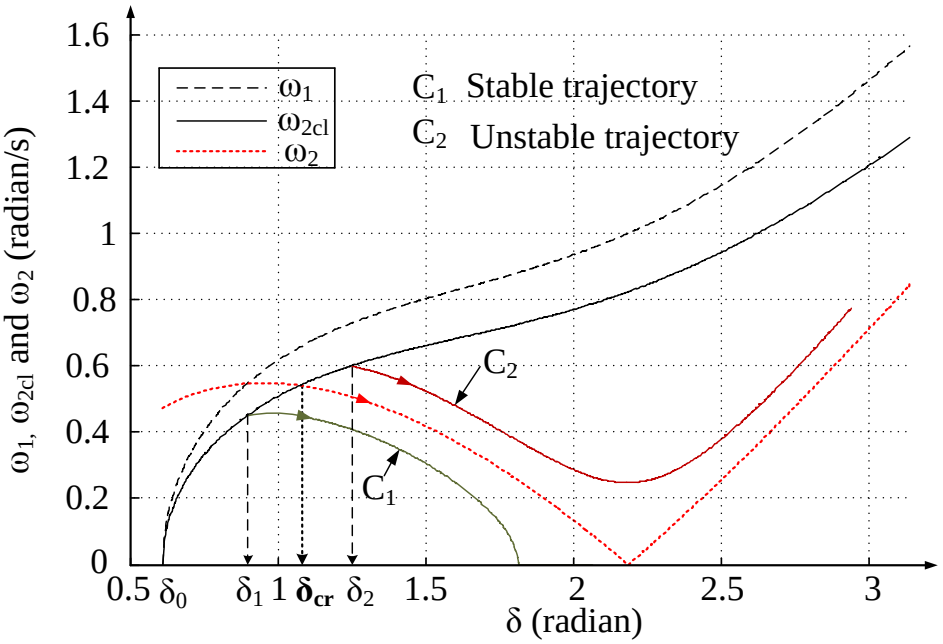

Figure 3.11: Finding critical clearing angle

The second approach has been adopted here to calculate the CCA. The angle δ, time scale (t), ω_{2cl} and ω_2 calculated for the test case E are shown in Table 3.2. The point of intersection of ω_{2cl} and ω_2 is found by calculating absolute difference between ω_{2cl} and ω_2. The minimum difference gives the point of intersection. The critical clearing time (t_{cr}) can now be calculated using the time scale given in Step II. From the Table 3.2, the CCA determined is 0.9910 radian and the CCT observed is 0.1232 s. Figure 3.12 demonstrates the procedure just explained pictorially.

A decision is made based on the following logic.

* If $t_{cr} < t_{cl}$:**Stable swing**
* If $t_{cr} = t_{cl}$:**Critical condition**
* If $t_{cr} > t_{cl}$:**Unstable swing**

Table 3.2: Calculation of CCA and CCT

Index	δ (radian)	t (s)	ω_{2cl} (radian/s)	ω_2 (radian/s)	abs(ω_{2cl}-ω_2) (radian/s)
1	0.7711	0.0000	0.0000	0.3961	0.3961
2	0.8025	0.0462	0.1767	0.4080	0.2313
3	0.8339	0.0653	0.2485	0.4179	0.1695
4	0.8653	0.0801	0.3026	0.4261	0.1235
5	0.8968	0.0927	0.3475	0.4326	0.0851
6	0.9282	0.1038	0.3864	0.4376	0.0512
7	0.9596	0.1139	0.4210	0.4412	0.0203
8	0.9910	0.1232	0.4523	0.4436	0.0088
9	1.0224	0.1320	0.4810	0.4447	0.0364
10	1.0538	0.1402	0.5076	0.4446	0.0630
11	1.0853	0.1480	0.5324	0.4434	0.0890
12	1.1167	0.1555	0.5556	0.4412	0.1144
13	1.1481	0.1627	0.5776	0.4380	0.1396
14	1.1795	0.1697	0.5983	0.4338	0.1645
15	1.2109	0.1764	0.6181	0.4288	0.1894
16	1.2423	0.1829	0.6370	0.4228	0.2142
17	1.2737	0.1892	0.6551	0.4160	0.2391
18	1.3052	0.1953	0.6725	0.4083	0.2641

3.4.1 Flow Chart of the Proposed State Plane Trajectory Algorithm

The technique discussed above is used for the out-of-step relay algorithm. The flow chart describing the proposed algorithm is shown in Figure 3.13. The relay keeps on monitoring voltages at the sending and receiving end, and current from the generator at every sample, and calculates real power and the power angle. As soon as the fault is detected in the

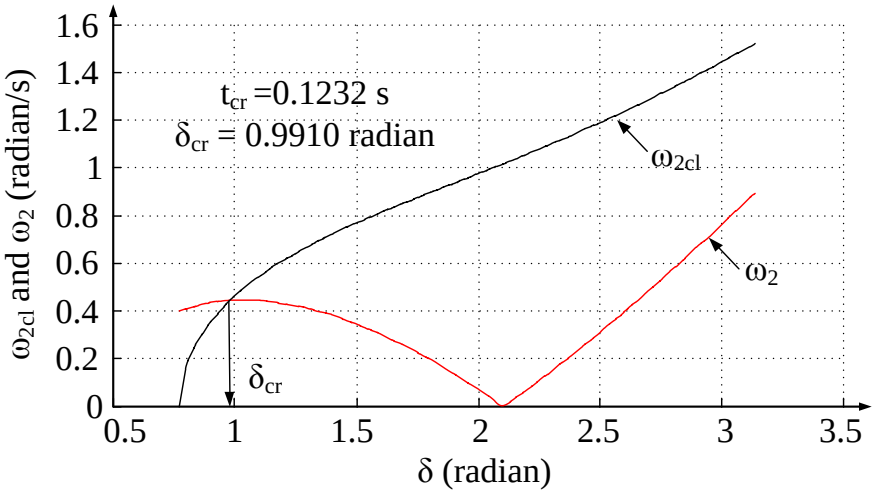

Figure 3.12: State plane trajectories to find CCA and CCT for test case E

system and, based on the fault location, the relay finds the power-angle characteristics for "during fault condition". The fault in the line is identified by detecting the sudden drop in electrical power by more than 20%. The first two steps (Step-I and Step-II) as explained in Section 3.4 are then computed by the relay. After the fault is cleared, the measurements take a small while to reach to the after fault values, so a small time lag of (0.04 s) is used. After getting the post-fault measurements, the algorithm predicts the post fault power-angle characteristics, and the next two steps (Step-III and Step-IV) are computed. Finally, the decision (stable/unstable) is made using the decision logic explained in Step-IV. It is assumed in the analysis that the mechanical power input remains the same, damping is zero, and the voltage behind transient reactance is constant.

3.5 Case Studies: Single Machine Infinite Bus System

A power system as shown in Figure 3.2 is used to test the proposed out-of-step relay algorithm. The power system model for SMIB system is developed in PSCAD/EMTDC^{TM} [1] which is shown in Appendix B.1. The relay is placed at the generator terminal. Three phase fault is applied at the middle of the transmission line II and is removed by opening the

[1]PSCAD/EMTDC^{TM} are the registered trademark of Manitoba HVDC Research Centre Inc., Winnipeg, Canada

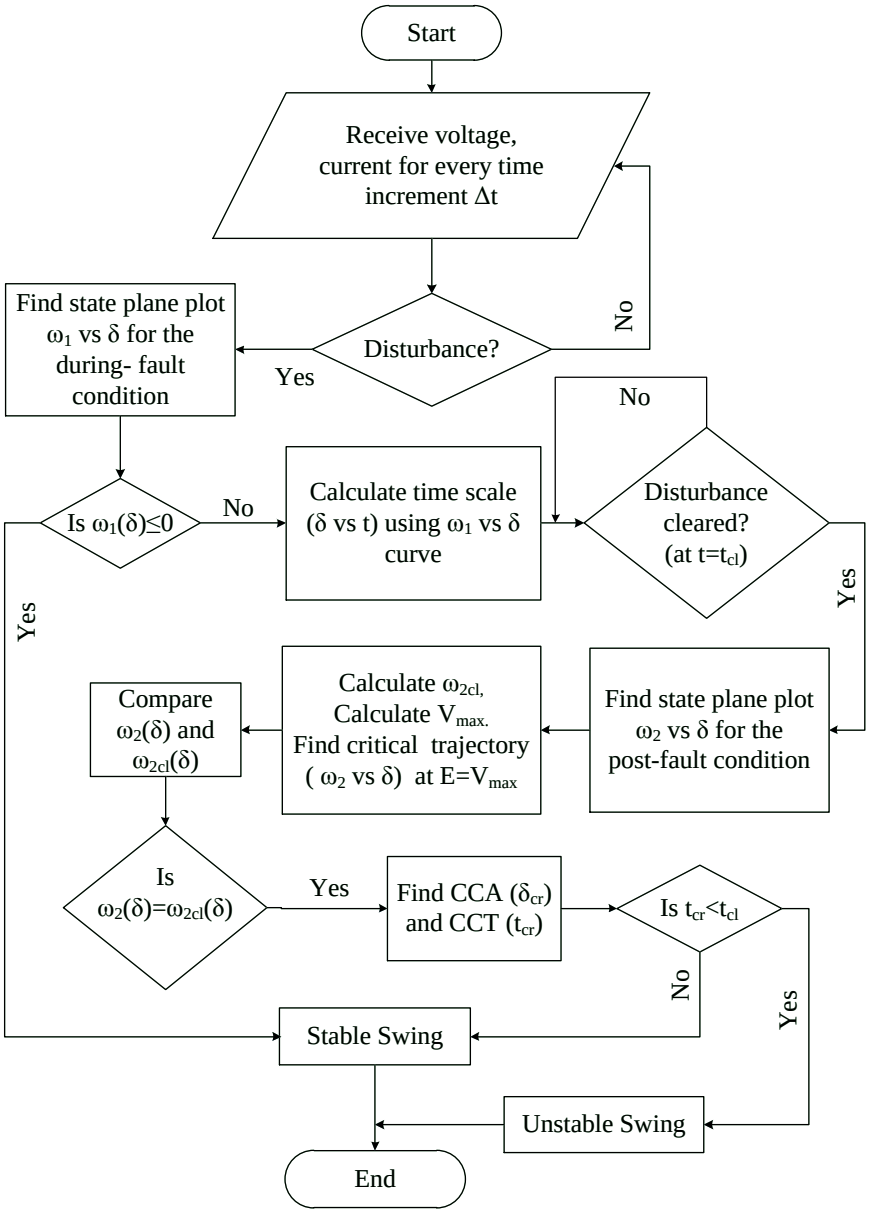

Figure 3.13: Flow chart of the proposed state plane trajectory algorithm

breakers $Brk1$ and $Brk2$ simultaneously. The operating conditions and the fault durations are varied. The operating conditions are varied by changing the power angle at the generator bus (δ_t) from 25^o to 35^o at the interval of 5^o and the fault duration is varied from 3 cycles to 26 cycles to get various possible swings. Fault is applied at 2 s, and the detection time is measured from the time of fault inception. The test results are divided into stable and unstable cases and are discussed in Section 3.5.1 and 3.5.2.

3.5.1 Stable Swings

For the initial operating points explained in Section 3.5, six different stable test scenarios are generated with fault durations varying from 3 to 18 cycles. Initially, the generator is loaded at 77% of its rated value, i.e., the generator bus angle δ_t is set to 25^o. Figure 3.14 shows a power swing with a pre-fault $\delta_t = 25^o$, and fault duration of 18 cycles(0.3 s). The CCT calculated by the algorithm is 0.3703 s. Since the fault duration is less than the CCT, swing is detected to be a stable swing at 0.3400 s. The detection is made at a power angle of 76.2030^o. Figure 3.15 shows the corresponding rotor angle swing. Figure 3.16 shows the power swing with pre-fault $\delta_t = 25^o$ and fault duration of 20 cycles (0.3330 s). The swing is detected as a stable swing at 0.3730 s and the decision is made at a power angle of 82.2500^o. Now the generator loading is increased to 94.86% by changing δ_t to 30^o. Figure 3.17 shows

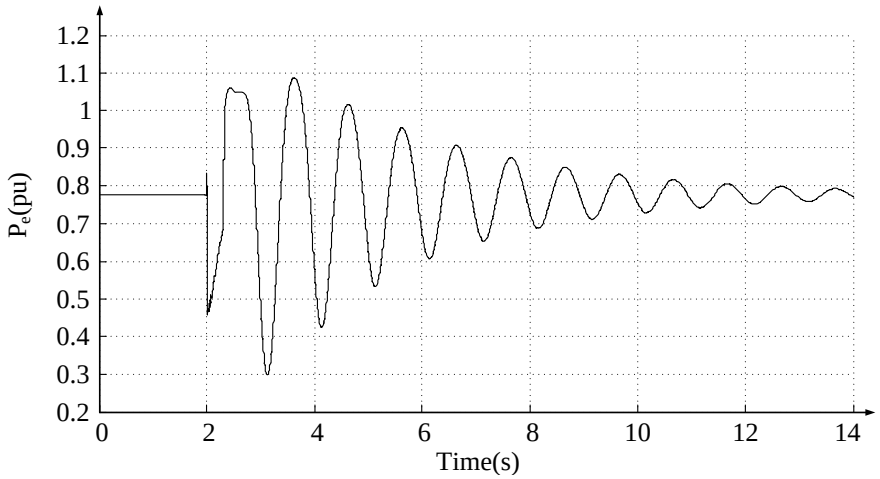

Figure 3.14: Power swing curve for an initial $\delta_t = 25^o$, fault cleared after 18 cycles

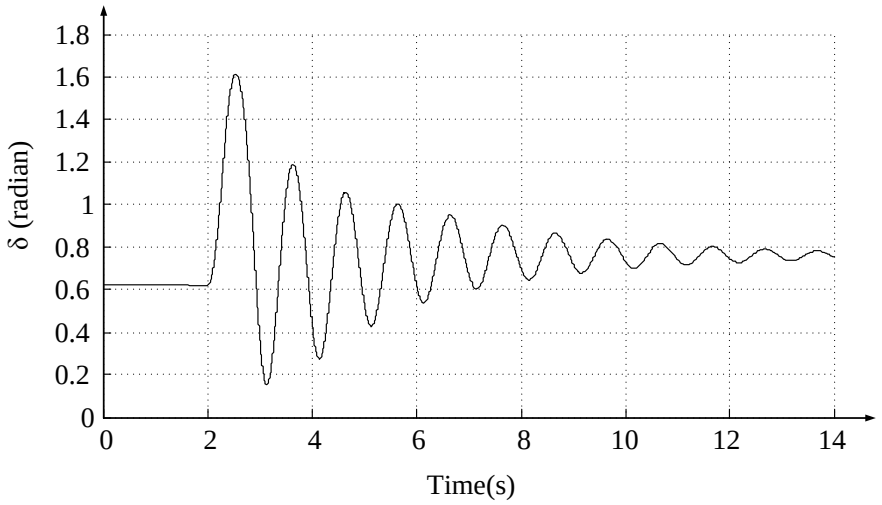

Figure 3.15: Power angle plot for an initial $\delta_t = 25^o$, fault cleared after 18 cycles

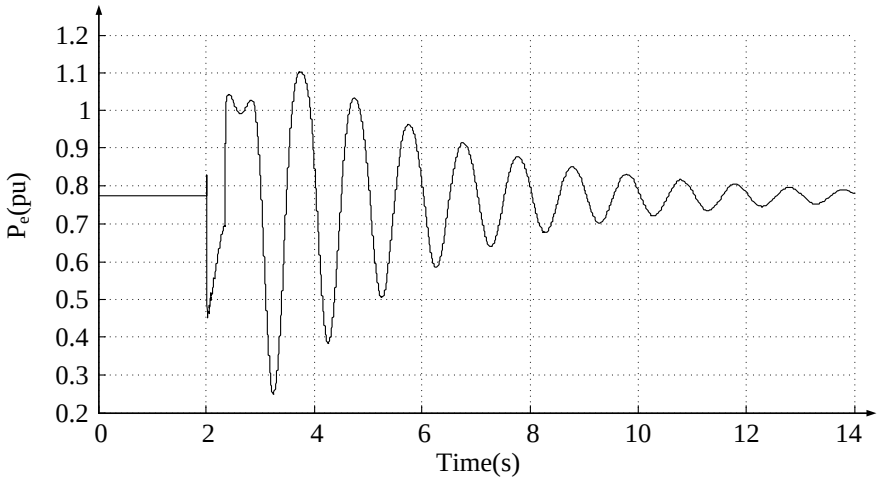

Figure 3.16: Power swing curve for an initial $\delta_t = 25^o$, fault cleared after 20 cycles

the power swing for the fault duration of 6 cycles (0.1 s) . The CCT calculated by the algorithm is 0.1512 s. Since the fault duration is less than the CCT, the swing is detected as a stable swing at 0.1400 s and at a power angle of 54.86^o. Further, the fault duration is increased to 8 cycles (0.1330 s). The power swing is stable and is shown in Figure 3.18. The detection is made at 0.1730 s and at a power angle of 60.31^o. To observe the effectiveness of the algorithm during nearly fully loaded condition, the loading is increased to 98.28% by increasing δ_t to 35^o. Figure 3.19 shows power swing for fault duration of 3 cycles (0.05 s). The CCT calculated is 0.1312 s. The swing is detected as a stable swing at 0.09 s and at a power angle of 48.6200^o. Similarly, Figure 3.20 shows the stable swing for the fault duration

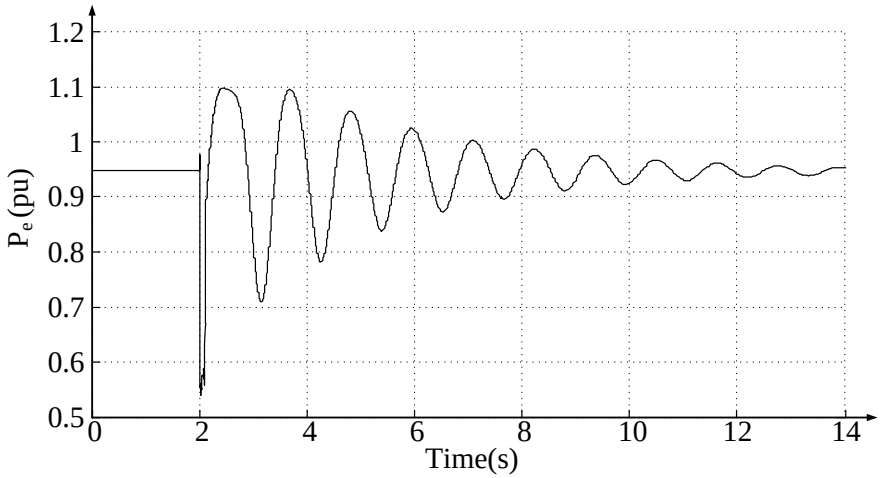

Figure 3.17: Power swing curve for an initial $\delta_t = 30^o$, fault cleared after 6 cycles

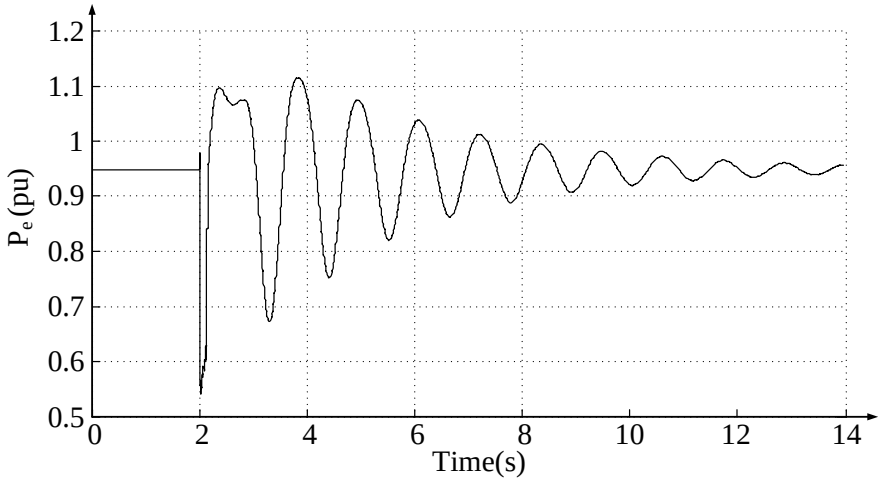

Figure 3.18: Power swing curve for an initial $\delta_t = 30^o$, fault cleared after 8 cycles

of 6 cycles (0.1 s). The relay is also tested with fault duration of 7.86 cycles (0.1310 s) which is a critically stable case. Figure 3.21 shows the power swing for fault duration of 0.1310 s. The swing is detected to be a stable swing at 0.1710 s and at a power angle of 60.4500^o.

3.5.2 Unstable Swings

Power system is subjected to longer duration faults to create unstable swings. Test results for $\delta_t = 30^o$ with fault duration of 10 and 12 cycles is discussed here. Figure 3.22

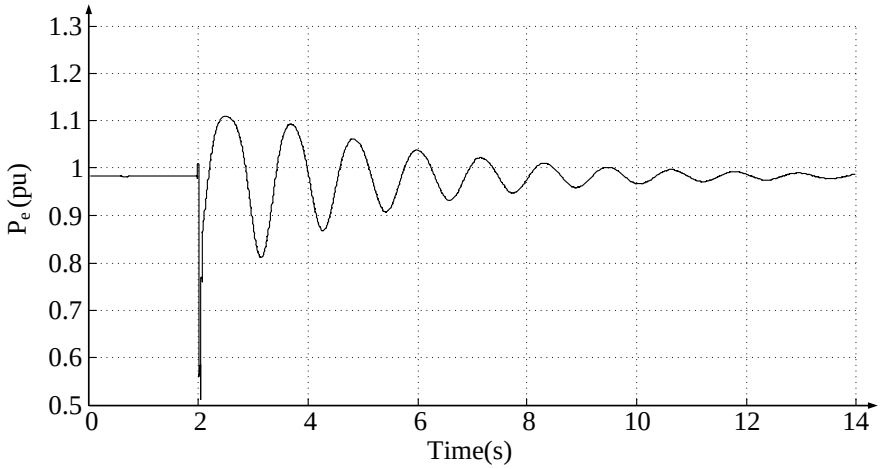

Figure 3.19: Power swing curve for an initial $\delta_t = 35^o$, fault cleared after 3 cycles

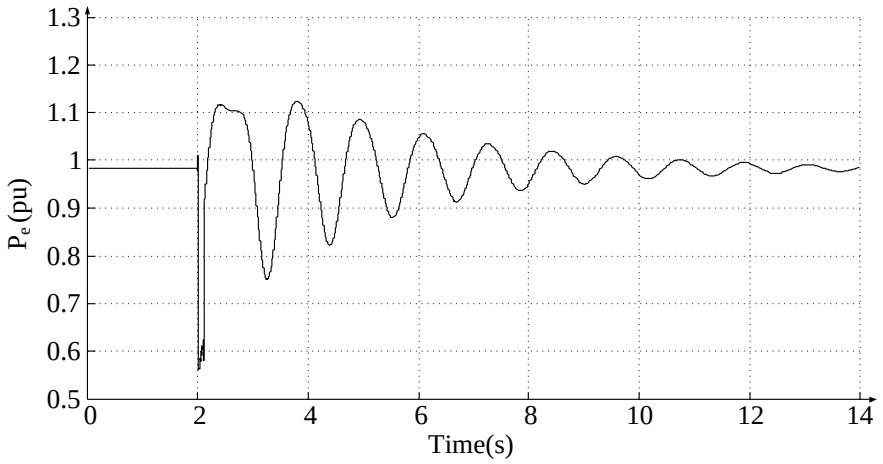

Figure 3.20: Power swing curve for an initial $\delta_t = 35^o$, fault cleared after 6 cycles

Table 3.3: Summary of simulation results for stable swings

Power angle (δ_t), degrees	25^o		30^o		35^o	
CCT(t_{cr},s)	0.3703		0.1512		0.1312	
Fault duration(cycles)	18	20	4	8	3	6
Fault duration(s)	0.3000	0.3330	0.0660	0.1330	0.0500	0.1000
Decision time(s)	0.3400	0.3730	0.1060	0.1730	0.0900	0.1400
Decision angle(degrees)	76.2030	82.2590	50.4400	60.3100	48.6300	55.1300

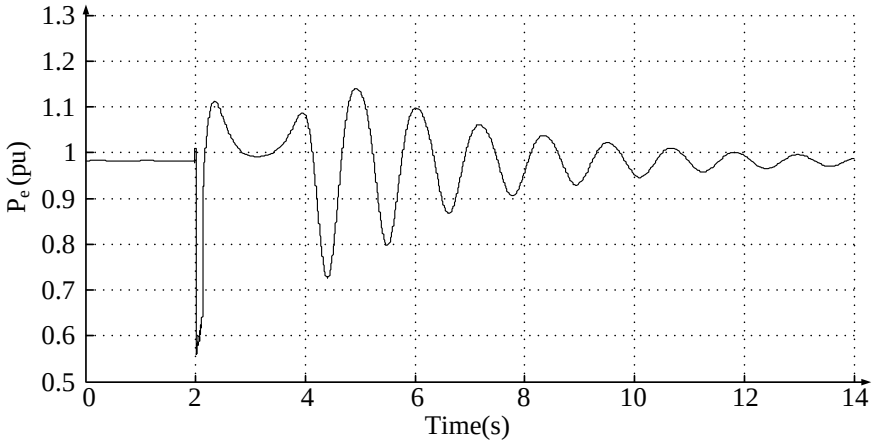

Figure 3.21: Power swing curve for an initial $\delta_t = 35^o$, fault cleared after 7.86 cycles

shows the electrical power swing for fault duration of 10 cycles (0.1660 s). The power-angle characteristics predicted by the relay and the actual electrical power versus delta plot are shown in Figure 3.23, where the predicted characteristics closely follow the actual one.

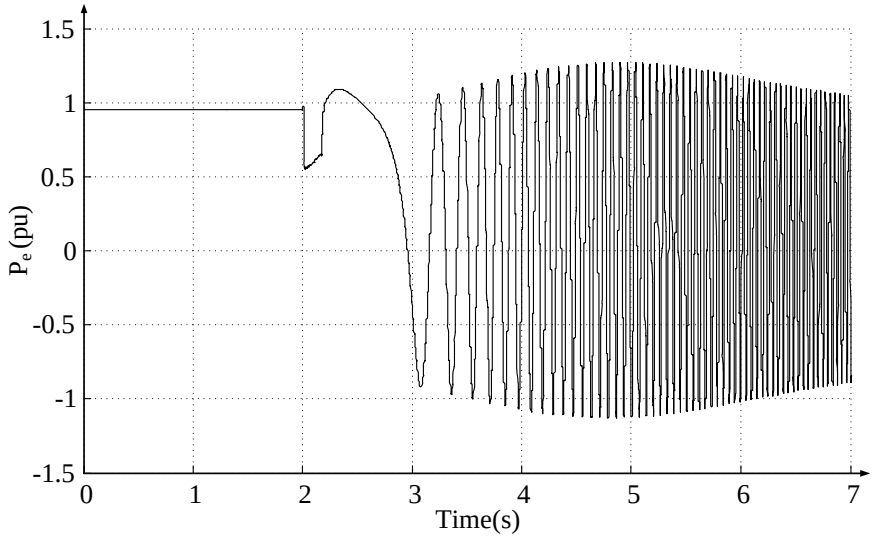

Figure 3.22: Power swing curve for an initial $\delta_t = 30^o$, fault cleared after 10 cycles

Figure 3.24 shows the plot of ω_{2cl} and ω_2 versus δ and time scale versus δ, that is calculated by algorithm to calculate the critical clearing angle and time. The CCT calculated is 0.1512 s which is less than the fault clearing time. The swing is therefore detected to be unstable at 0.2060 s. The power angle at the time of detection is 66.70^o. The fault duration is further increased to 12 cycles (0.2 s). The electrical power response is shown in Figure 3.25. Since

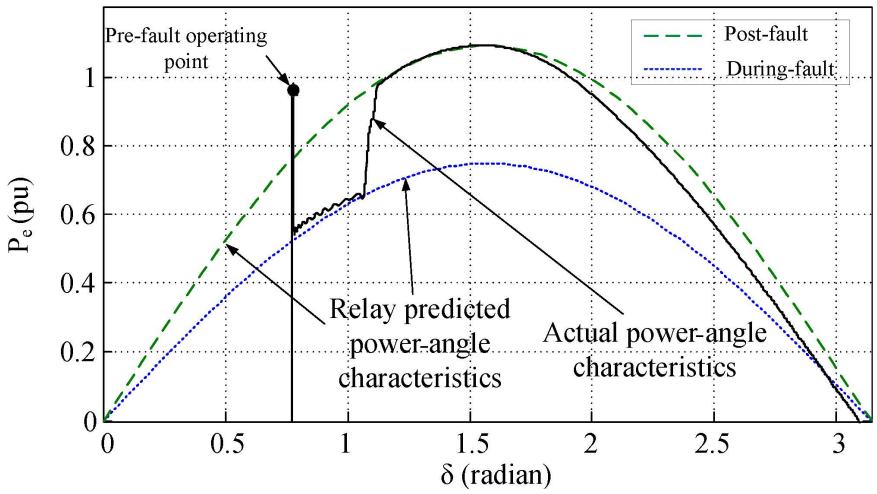

Figure 3.23: Comparison between relay predicted and actual P_e vs δ characteristics for $\delta_t = 30^o$

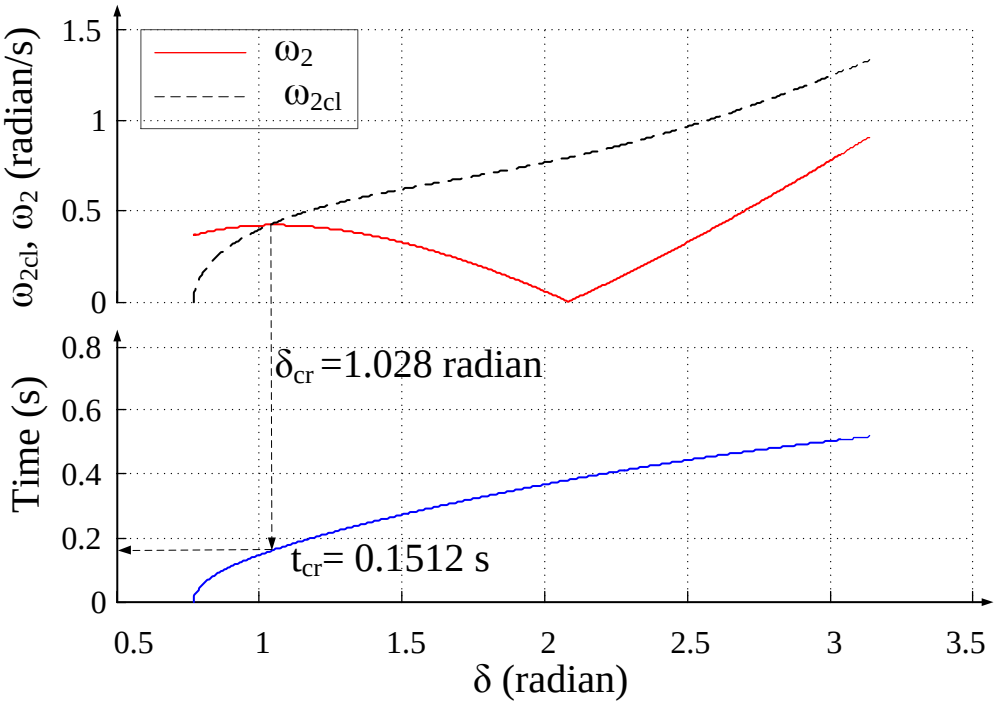

Figure 3.24: Plot of ω_{2cl}, ω_2 and time to calculate CCT for an initial $\delta_t = 30^0$

the fault duration is greater than the CCT, the swing is detected as an unstable swing. Again, the generator loading is increased to 98.28% by increasing δ_t to 35^o. Fault durations of 8, 10 and 12 cycles are used for generating unstable scenarios. Figure 3.26 shows the electrical power swing for fault duration of 8 cycles (0.133 s). The predicted power-angle

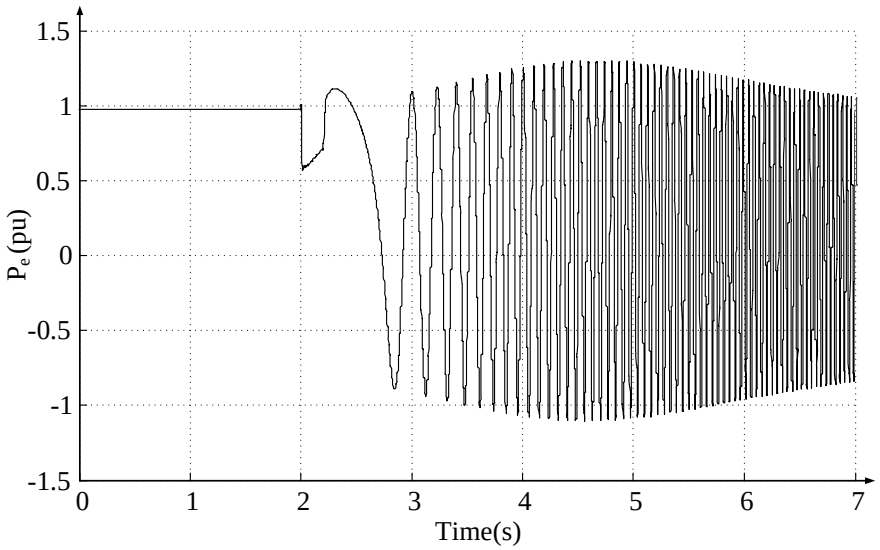

Figure 3.25: Power swing curve for an initial $\delta_t = 30^o$ and fault cleared after 12 cycles

characteristics and the actual characteristics are shown in Figure 3.27, where the predicted characteristics follows the actual characteristics obtained from simulation closely. Figure

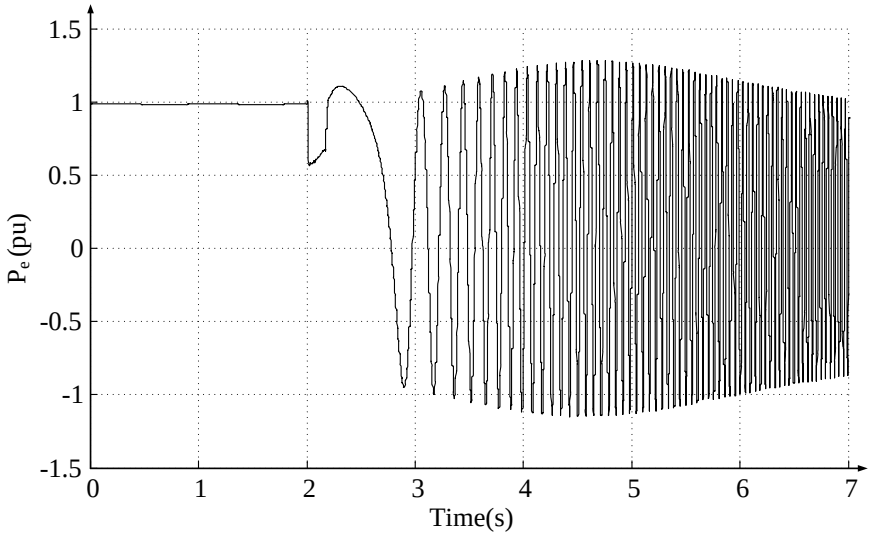

Figure 3.26: Power swing curve for an initial $\delta_t = 35^o$, fault cleared after 8 cycles

3.28 shows the plot of ω_{2cl} and ω_2 versus δ and time scale versus δ, which is used by the algorithm to calculate the critical clearing angle and time. As can be seen from the Figure 3.28, CCT calculated is 0.1312 s and is less than fault duration. The swing is hence classified as an unstable swing at 0.1730 s and at a power angle of 48.23^o. Similarly, Figure 3.29

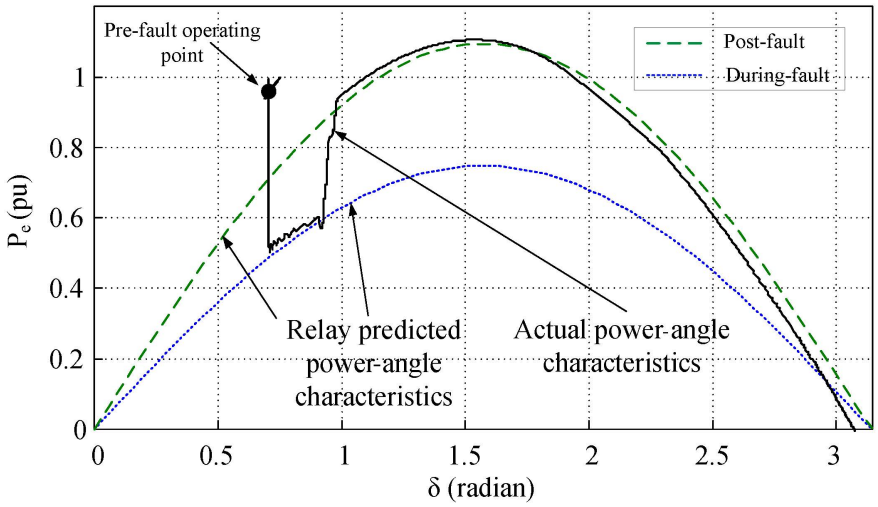

Figure 3.27: Comparison between relay predicted and actual P_e vs δ characteristics for $\delta_t = 35^o$

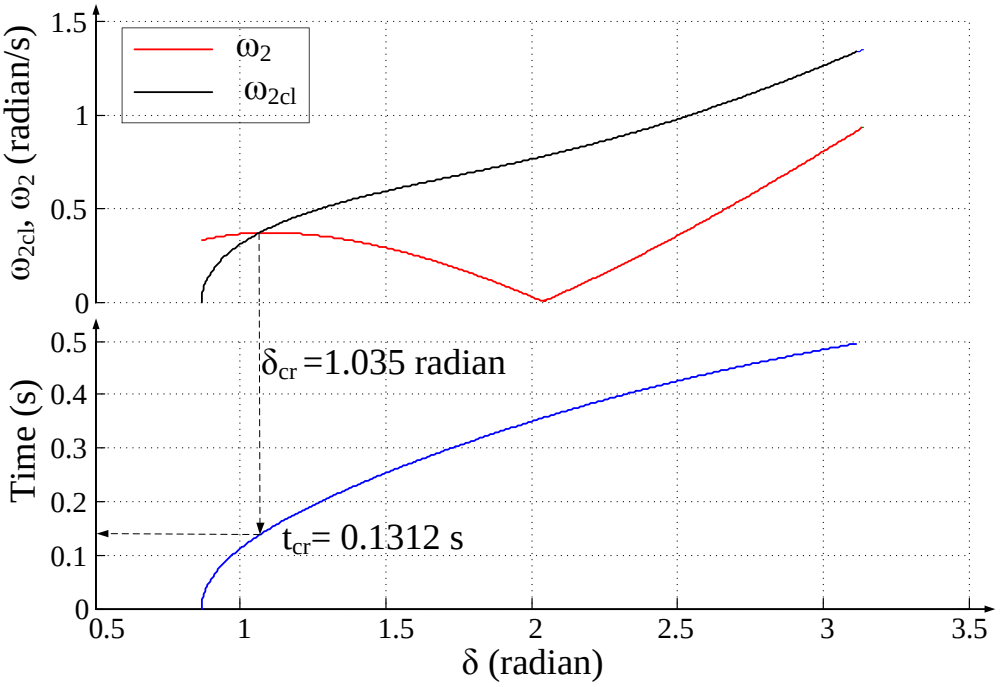

Figure 3.28: Plot of ω_{2cl}, ω_2 and time to calculate CCT for an initial $\delta_t = 35^o$

shows the power swing for fault duration of 10 cycles (0.1660 s). The swing is detected as an unstable swing at 0.2060 s and at a power angle of 53.54^o. Power swing for fault duration of 7.92 cycles (0.1320 s) is a critically unstable case and is shown in Figure 3.30. The swing is accurately detected as an unstable swing at time 0.1720 s. The detection angle is 60.56^o

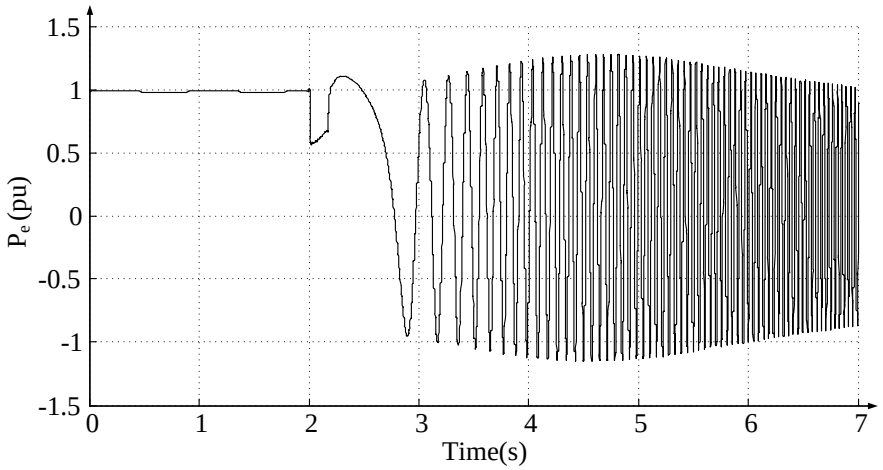

Figure 3.29: Power swing curve for an initial $\delta_t = 35^o$, fault cleared after 10 cycles

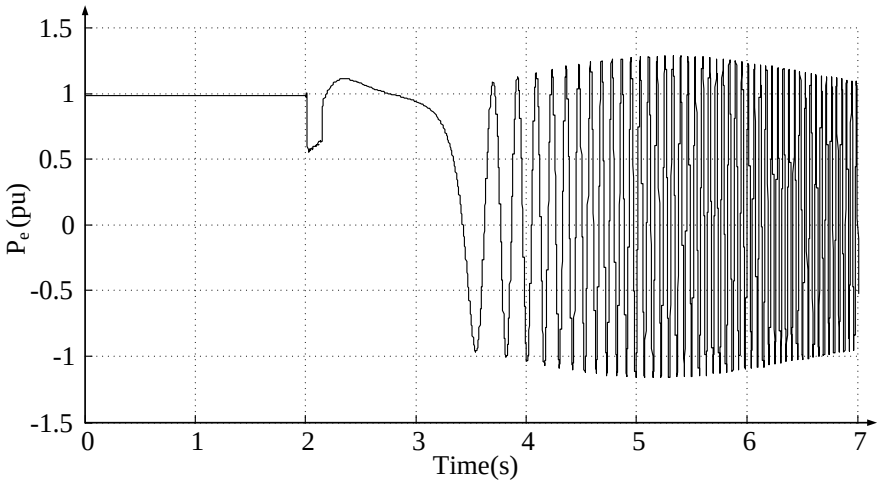

Figure 3.30: Power swing curve for an initial $\delta_t = 35^o$, fault cleared after 7.92 cycles

. The results for the unstable cases are shown in Table 3.4.

3.5.3 Comparision with the Blinder Scheme

In most of the power industries, the distance relays for major lines are designed to respond to power swing and out-of-step conditions. The distance relay has a power swing blocking and an out-of-step tripping element to prevent undesired tripping or to allow intentional opening of transmission line [16]. The blinder scheme is the most popularly used technique for power swing and out-of-step detection. It is useful to compare the new relay logic

Table 3.4: Summary of simulation results for unstable swing cases

Power angle (δ_t), degrees	25^o		30^o		35^o	
CCT(t_{cr},s)	0.3703		0.1512		0.1312	
Fault duration(cycles)	23	24	10	12	8	10
Fault duration(s)	0.3830	0.4000	0.1660	0.2000	0.1330	0.1660
Decision time(s)	0.4230	0.4400	0.2060	0.2400	0.1730	0.2060
Decision angle(degrees)	93.8500	96.9300	66.7000	74.1600	60.8100	67.4900
Breaker angle(degrees)	74.3280	77.7500	51.6700	57.6300	48.2200	53.5500

with one of the standard practices being used in an industry. The performance of the proposed algorithm is hence compared with blinder scheme (Two Blinders Scheme)discussed in Section 2.6.1. Figure 3.31 shows the two blinder scheme where the two blinder elements are indicated by either RRO and RRI or LRO and LRI . Whenever there is fault in the line, impedance immediately jumps from the operating point to short circuit impedance inside the distance relay characteristics. However, during power swing, the impedance vector exhibits a steady progression and its rate of change corresponds to the power swing frequency of the system [33]. The scheme measures the time taken by the impedance trajectory to traverse outer and inner blinders, and compares with a pre-set time to discriminate between a power swing and fault. If the measured time is less than the pre-set time, then the disturbance is a fault. If the trajectory enters the outer blinder and stays inside the two blinders for more than a pre-set time, then it is a power swing. Now if the trajectory crosses the inner blinder in more than a pre-set time, then it is an out-of-step condition. If the trajectory crosses the outer blinder but does not cross the inner blinder, then the swing is a stable swing [6].

In order to test the performance, an impedance relay with a two blinder scheme is located at one end of the TL-I (Figure 3.2)to protect 80% of the line. A three phase fault is applied at the middle of the TL-II followed by opening the Brk1 and Brk2, simultaneously. Reference [6] provides a detailed description on how to set the blinder elements. A brief explanation on the procedure is given in Appendix D.

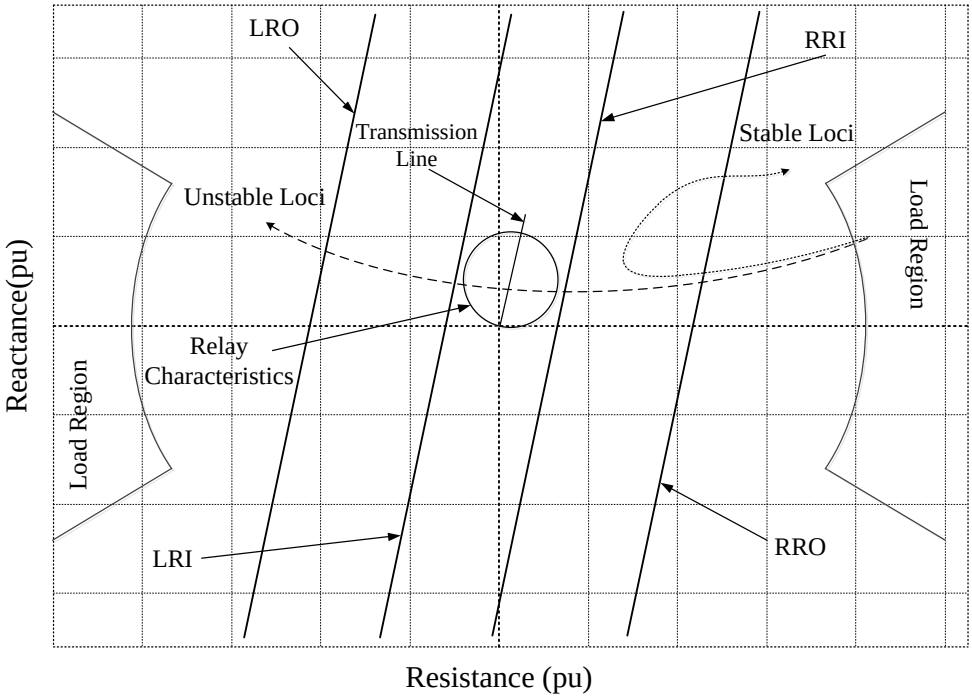

Figure 3.31: A two Blinder Scheme

After multiple stability studies for different initial operating state and fault durations, the two blinder elements are set as follows,

Right Resistance-Inner (RRI) =0.3 pu

Right Resistance-Outer (RRO) =1.0 pu

Left Resistance-Outer (LRI) =-0.3 pu

Left Resistance-Inner (LRO) =-1.0 pu

Using above settings, power swing blocking time delay (PSBD) is calculated using Equation (D.1), which is 2.152 cycles.

3.5.3.1 Test Cases

Different simulations are carried out to compare the proposed technique with the two blinder scheme. Test cases for pre-fault δ_t=30^o (fault duration 8 and 12 cycles) and 35^o (0.1310 s and 10 cycles) are discussed, and the rest of the simulation results are shown in Table 3.5.

Figure 3.32 shows the impedance locus for pre-fault δ_t=30^o, and a fault duration of 8 cycles (0.1330 s). The impedance locus enters the region between the two blinders and comes out of the outer blinder at 1.1542 s. Therefore, it takes 1.1542 s to detect the swing as a stable swing, whereas the proposed scheme takes only 0.1730 s for the same swing detection. The times indicated in Figure 3.32 are measured from the instant when the fault occurs in the system. To simulate an unstable case, fault duration is set for 12 cycles (0.2 s) for

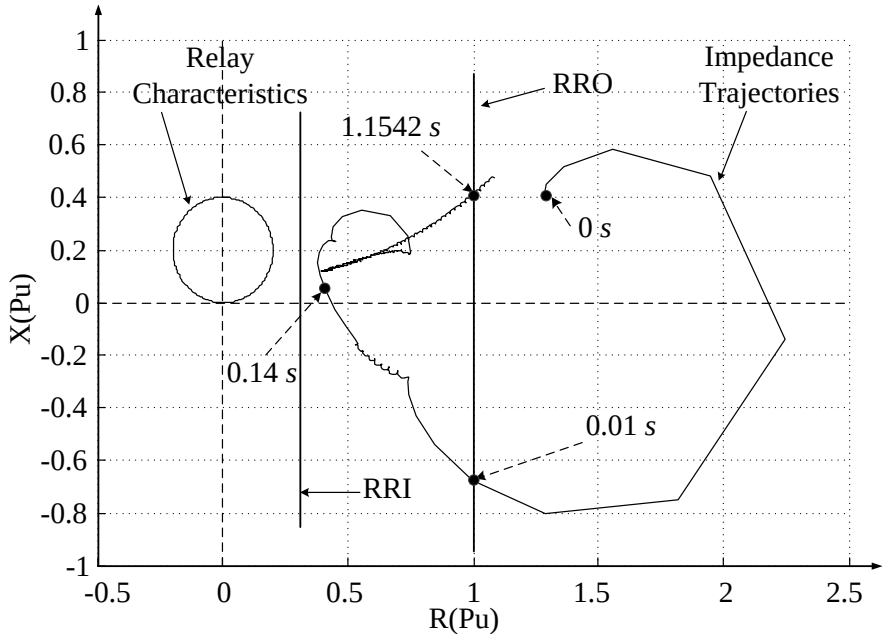

Figure 3.32: Impedance locus for an initial $\delta_t = 30^o$, fault cleared after 8 cycles

the same pre-fault power angle. Figure 3.33 shows the impedance locus. It crosses both blinders, which means the swing is going to be unstable. The impedance trajectory enters the inner blinder at 0.4810 s. The scheme hence detects the swing as an unstable swing at 0.4810 s, whereas the proposed scheme detects the instability at 0.2060 s. The pre-fault power angle δ_t is increased to 35^o, and tested for fault duration of 7.86 cycles (0.1310 s.) Figure 3.34 shows the impedance locus during and after fault condition. The locus enters the outer blinder and swings back before reaching the inner blinder. The swing is detected as a stable swing at 2.2740 s, whereas the proposed scheme detects the swing at 0.1710 s. Now an unstable case simulated with the fault duration of 10 cycles (0.1660 s). Figure 3.35 shows the impedance locus for the fault duration of 10 cycles. The swing is detected as an unstable swing at 0.5050 s, whereas the proposed technique takes only 0.2060 s for detection.

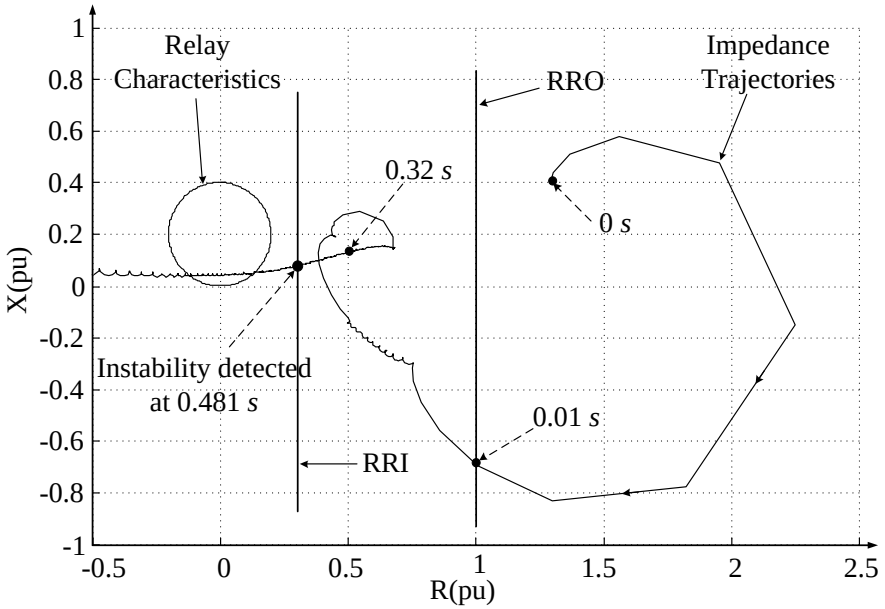

Figure 3.33: Impedance locus for an initial $\delta_t = 30^o$, fault cleared after 12 cycles

The two blinders scheme works well for most of the swings. However, for a fault duration

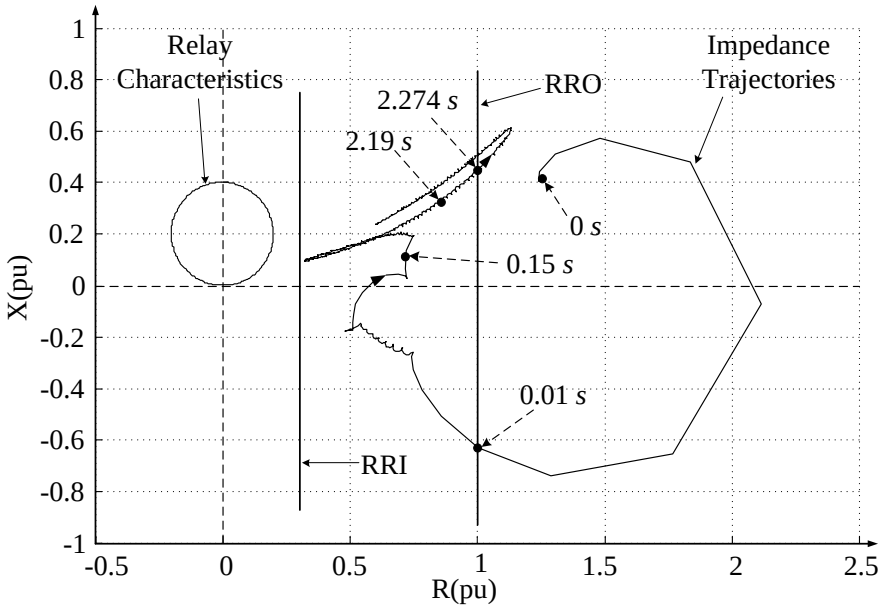

Figure 3.34: Impedance locus for an initial $\delta_t = 35^o$, fault cleared after 7.86 cycles

of 7.92 cycles (0.1320 s) with δ_t=35^o, the blinders set for scheme tends to misclassify the swing initially. The impedance locus for this case is shown in Figure 3.36. The impedance locus enters the outer blinder, oscillates back and crosses the outer blinder again. The swing

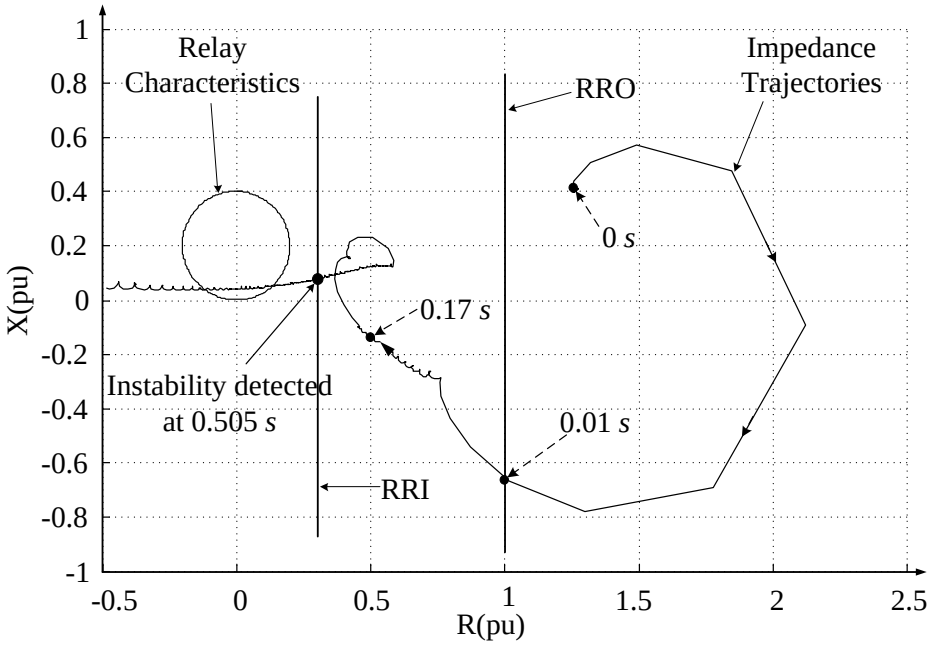

Figure 3.35: Impedance locus for an initial $\delta_t = 35^o$ and fault cleared after 10 cycles

is detected to be stable at the moment when it crosses the outer blinder. However, when the swing locus re-enters the outer blinder and passes through the inner blinder as well, the swing becomes an unstable swing. The instability is detected at 0.9596 s. This shows that the blinder set for most of the swing conditions may not work for some other kind of swings. The blinders settings should therefore be revisited. The proposed technique detects the instability at 0.1720 s. The results above show that the proposed scheme is accurate and much faster than the two blinder scheme. For stable cases, the detection by blinder scheme is much slower than the proposed scheme because of the impedance locus moving slowly. The detection near CCT for example at δ_t=35^o and t_{cl}=0.1310 s, two blinder scheme took 2.2740 s to detect the swing as a stable swing. For a longer duration of a fault, which causes the system to becomes unstable, the detection time of the blinder scheme improves because of the faster swing rate because of the severe fault. However, the detection is still slower than the proposed scheme. The detection time for δ_t=35^o and for fault duration of 0.1320 s and 0.1330 s decreases from 0.9596 s to 0.7910 s, but the detection times using the proposed scheme are 0.1720 s and 0.1730 s for the same cases which are much faster than the blinder scheme.

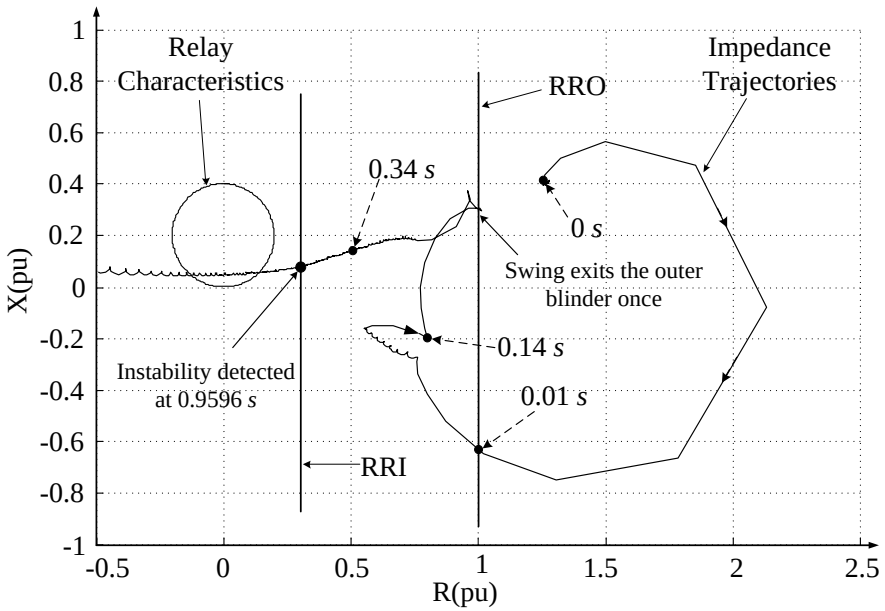

Figure 3.36: Impedance locus for an initial $\delta_t = 35^o$ and fault cleared after 7.92 cycles

Table 3.5: Summary of results using a two blinder scheme

Power angle (δ_t), degrees	Fault duration (cycles)	Fault duration (s)	Decision time (s)	Decision
25^o	18	0.300	0.8880	Stable
	20	0.3330	1.0210	Stable
	23	0.3830	0.5510	Unstable
	24	0.4000	0.5320	Unstable
30^o	4	0.0660	0.9814	Stable
	8	0.1330	1.1542	Stable
	10	0.1660	0.6120	Unstable
	12	0.2000	0.4810	Unstable
35^o	3	0.0500	1.0908	Stable
	7.86	0.1310	2.2740	Stable
	7.92	0.1320	0.9596	Unstable
	8	0.1330	0.7910	Unstable
	10	0.1660	0.5050	Unstable

3.5.4 Comparison with the State Deviation Approach

A short description of the state deviation approach was given in Section 2.6.6. This approach is based on observing the state (i.e., speed) of the machine at the saddle point, where the machine goes from deceleration to acceleration. At this point, if the speed of the machine is lower than the rated speed, then the machine becomes stable, and if the speed is greater than the rated speed, then the machine becomes unstable. The proposed scheme using SPA is compared with this approach for a number of test cases. Figure 3.37

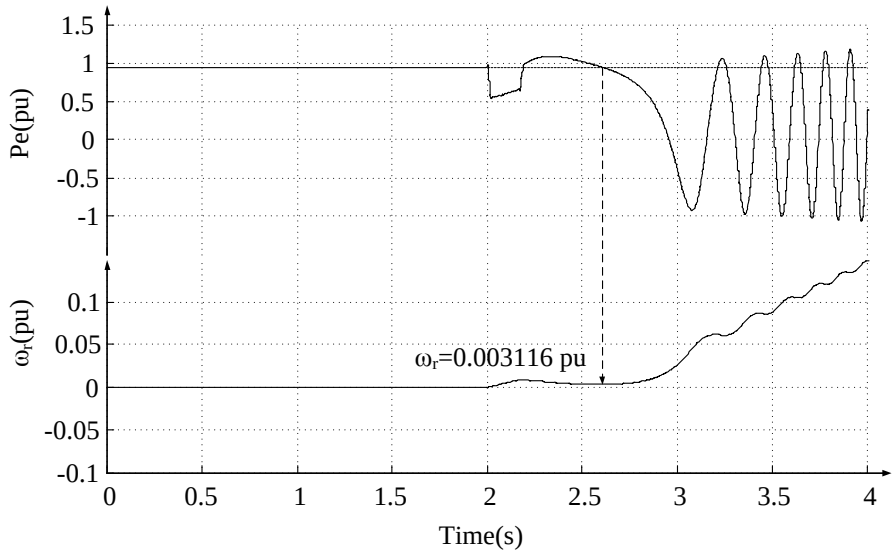

Figure 3.37: Plots of electrical power and relative speed for an initial $\delta_t = 30^o$, fault cleared after 12 cycles

shows the electrical power output and the relative speed (ω_r) of the machine for δ_t=30^o and fault cleared after 12 cycles. The relative speed of the machine observed at the saddle point is positive (i.e., 0.003116 pu). The approach hence detects the swing as an unstable swing at 0.4782 s. For the same test case, the proposed scheme using SPA detects it as an unstable swing at 0.24 s. Further, the state deviation approach is tested with δ_t=35^o and fault duration of 7.86 cycles (0.131 s). Figure 3.38 shows electrical power and relative speed of the machine. The relative speed measured at the saddle point is negative (i.e., -0.006339).

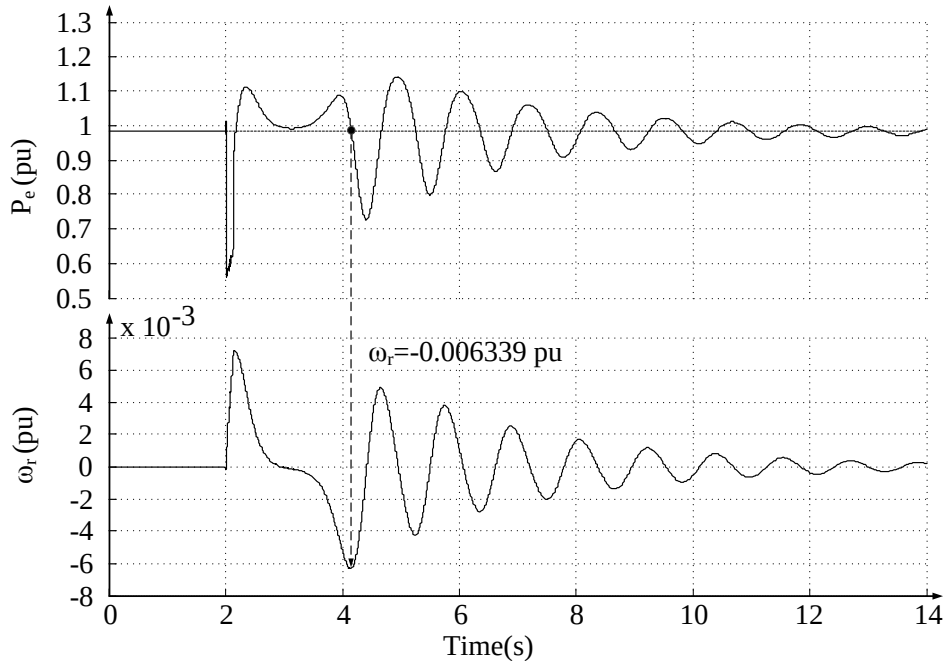

Figure 3.38: Plots of electrical power and relative speed for an initial $\delta_t = 35^o$, fault cleared after 7.86 cycles

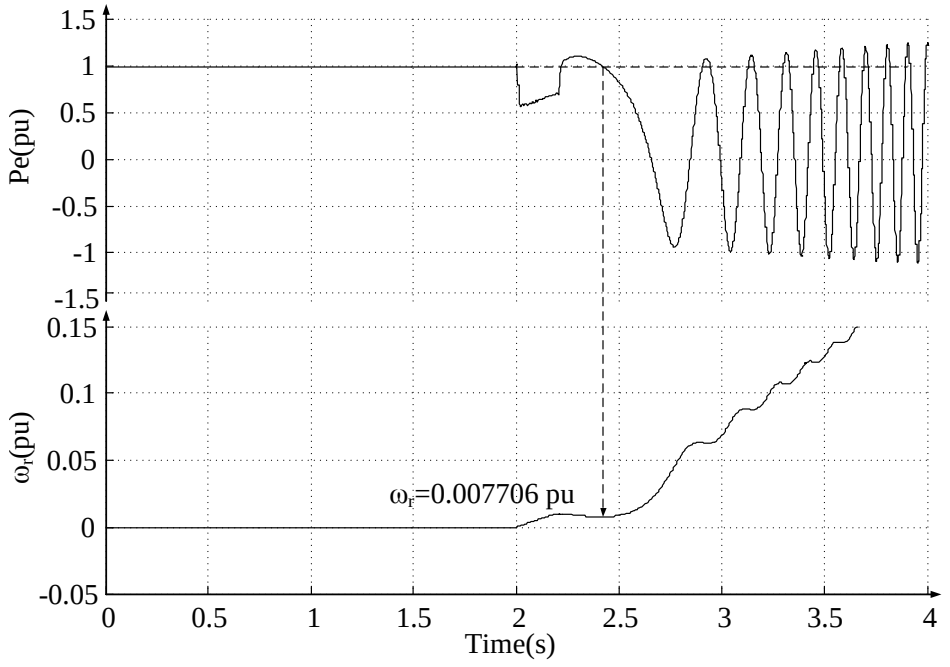

Figure 3.39: Plots of electrical power and relative speed for an initial $\delta_t = 35^o$ and fault cleared after 10 cycles

The swing is detected as a stable swing at 2.1532 s, whereas the proposed scheme using SPA detects it at 0.1710 s. Similarly, Figure 3.39 shows the unstable swing, which is detected at 0.4970 s using state deviation approach for δ_t=35^o, and fault duration of 10 cycles (0.1660 s).

Test results for initial conditions (δ_t=25^o, 30^o and 35^o) and for different fault durations are shown in Table 3.6.

Table 3.6: Summary of results using the proposed state deviation approach

Power angle (δ_t), degrees	Fault duration (cycles)	Fault duration (s)	Decision time (s)	Decision
25^o	18	0.3000	0.9000	Stable
	20	0.3330	1.0210	Stable
	23	0.3830	0.6710	Unstable
	24	0.4000	0.6230	Unstable
30^o	4	0.0660	0.8564	Stable
	8	0.1330	1.0594	Stable
	10	0.1660	0.6042	Unstable
	12	0.2000	0.4782	Unstable
35^o	3	0.0500	0.8960	Stable
	6	0.1000	1.0050	Stable
	7.86	0.1310	2.1532	Stable
	7.92	0.1320	0.8428	Stable
	8	0.1330	0.7230	Unstable
	10	0.1660	0.4970	Unstable

3.6 Case Studies: Two Area System

In an electrical power network, two areas are interconnected through tie lines. The network should hold synchronism during both steady state and transient conditions. Transient instability in an area might lead to an angular separation between the interconnected areas, causing loss of synchronism. To study the out-of-step conditions in an interconnected power system due to transient conditions, a two area power system model consisting of a machine with finite inertia in each area is considered for the transient stability study. Figure 3.40 shows the power system configuration. Parameters of generators and transmission line of the system are given in Appendix A.2. The two area system studies are considered under different fault locations and fault durations to achieve various power swing conditions. The system goes through stable and unstable power swing conditions. The effectiveness of the proposed technique to predict such phenomena is studied and reported in this section. The test results of the proposed scheme are compared with the conventional two blinder scheme. In addition, studies on multi-swing instability in this system are carried out and a combined prediction scheme using state plane analysis and state deviation technique is proposed. The test results for multi-swing instability prediction are then discussed and reported in this section.

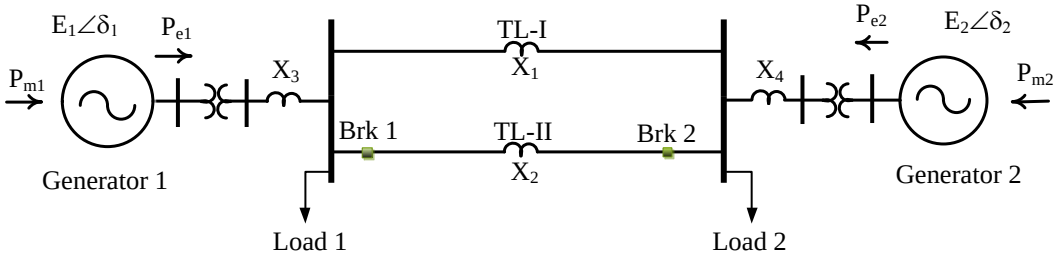

Figure 3.40: A two machine system

3.6.1 Test Procedure

The two machines under disturbed conditions form two groups oscillating with each other. The separation between two areas can be identified by measuring angular deviation

between the two machines. The identification of groups of machines is discussed in Section 5.2.1 which is known as coherency analysis. The two area system can now be transformed into a SMIB equivalent using the procedure explained later in Section 5.2.2. The procedure predicts the power-angle characteristics of the SMIB equivalent system for during-fault and post-fault condition. Transient stability analysis using state plane analysis is then performed on the SMIB equivalent system to calculate CCT. The calculated CCT gives the stability boundary for the two area system. The decision is hence made based on the decision criterion explained in Section 3.4. The power system as shown in Figure 3.40 is modeled in the PSCAD/EMTDC^{TM} environment. A number of time domain simulations are performed to produce various stable, unstable and multi-swing unstable scenarios.

3.6.2 Multi-swing Instability Prediction

In a power system, transient instability usually appears in the form of aperiodic angular separation, causing first swing instability. Even though the first swing instability is the most common phenomenon, it is not necessary that the system will remain stable for subsequent swings. The superposition of slow inertia swing mode and a local plant mode might cause rotor angle instability beyond first swing [1]. In a multi-swing instability condition, the trajectory oscillates for several cycles and becomes unbounded. The real power system usually experiences multi-swing instability because of its complicated dynamic behaviour [34]. It is necessary to identify multi-swing instability in time before the system starts pole slipping. Figure 3.41 shows electrical power signal of the two area system experiencing multi-swing instability where DYP_1, DYP_2 and DYP_3 are the dynamic saddle points (DYP). The DYPs are the points where $(P_m - P_e)$ goes negative to positive. The system seems to be stable for first two swings, but it becomes unstable after the third swing.

To facilitate the multi-swing instability prediction, the proposed relay algorithm was modified and consisted of SPA for first swing instability followed by state deviation approach using the generator speeds to find the instability at the later swings.

A multi-swing can either be a stable or multi-swing unstable case. After every stable

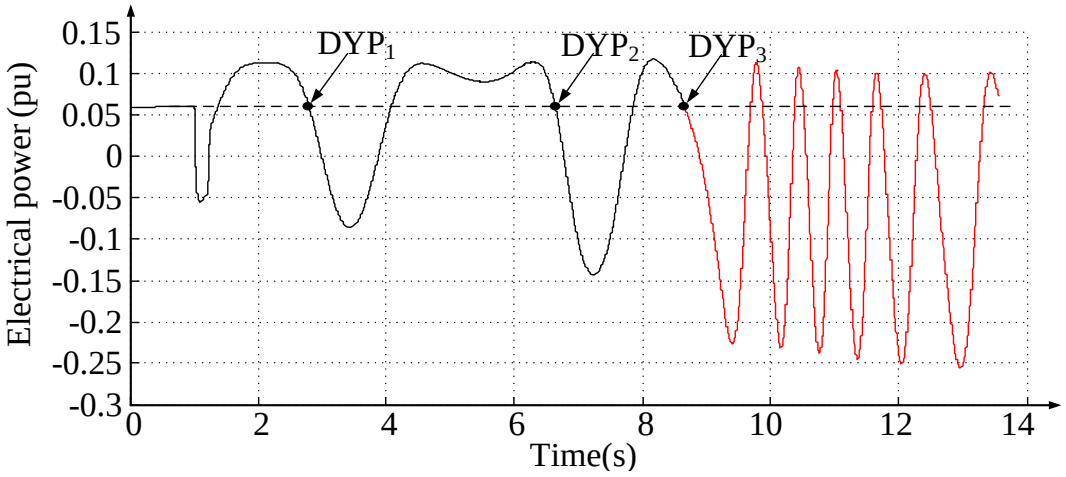

Figure 3.41: Electrical power plot of a system undergoing multi-swing instability

prediction of the swing using SPA, state deviation approach is started to monitor the SMIB equivalent speed of the generators at every DYPs. The proposed technique for multi-swing instability first uses SPA to distinguish between stable and unstable swing. If the swing is detected as a stable swing, it starts the state deviation approach to examine the multi-swing instability in the system. The approach uses the online measurements of generator speed and electrical power signals which are eventually transformed into SMIB equivalent parameters as explained in Section 5.4. Equivalent speed of the system represented by ω, is monitored at every DYP and the instability is predicted based on decision criterion explained in Section 2.6.6.

3.6.3 Test Cases

The two area system is tested for various fault durations and two different fault locations. Case 1: a three phase fault is applied on the transmission line TL-II which is 50 km away from the bus 4[2], and the fault is cleared by opening the breakers Brk1 and Brk2. For fault duration varied from 6 cycle to 20 cycles, stable, unstable and multi-swing unstable cases are observed. Case 2: a three phase fault is applied on transmission line TL-II which is 75 km away from the bus 4 and is cleared by opening breakers Brk1 and Brk2. Fault duration is

[2]Refer to Appendix B.2 for the figure

varied from 8 cycles to 26 cycles to develop stable, unstable and multi-swing unstable cases. In all test cases, the detection time is calculated from the time of fault inception.

3.6.3.1 Stable Swings

Two stable cases are discussed here. For Case 1, a three phase fault is applied for 6 cycles (0.1 s). Angular separation of the two generator buses is shown in Figure 3.42. When the post-fault rotor angles separates more than 5 degrees from the initial post-fault value, relay starts the SMIB equivalent procedure for the two area system. The system information, i.e.,

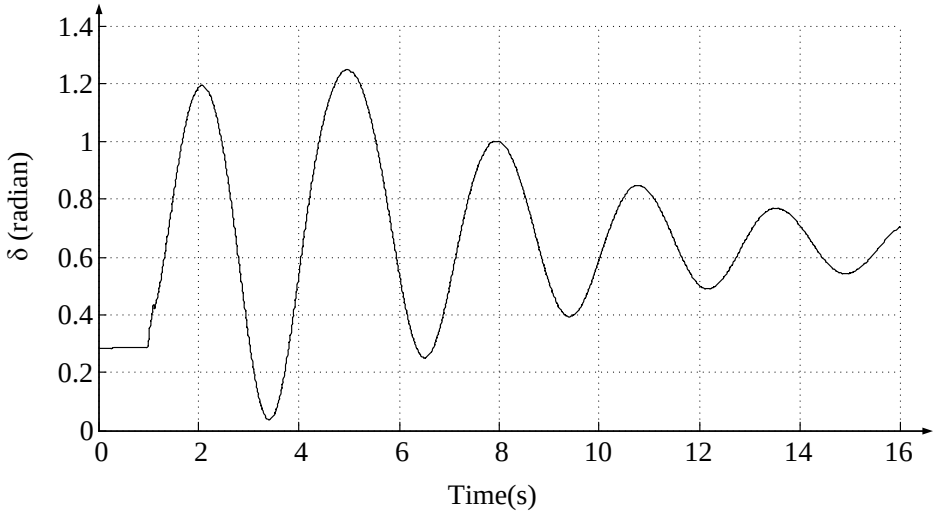

Figure 3.42: SMIB equivalent power angle plot, fault duration of 6 cycles (Case 1)

fault location and breaker status during and after fault, are communicated to the relay. The power-angle characteristics for during and post fault predicted by the relay for Case 1 are shown in Figure 3.43. The values for parameters in Figure 3.43 are given in Table 3.7.

Using the predicted values of the parameters as shown in Table 3.7, the relay calculates CCT of the system. Figure 3.44 shows the state plane plot and the time scale generated by relay to calculate CCT. The CCT calculated for this case is 0.2704 s. Since the fault clearing time (i.e., 0.1 s) is less than the CCT calculated, the swing is detected to be stable and the detection time is 0.2400 s. The SMIB equivalent electrical power obtained from the simulation is shown in Figure 3.45. For Case 2, a three phase fault is applied for 8 cycles

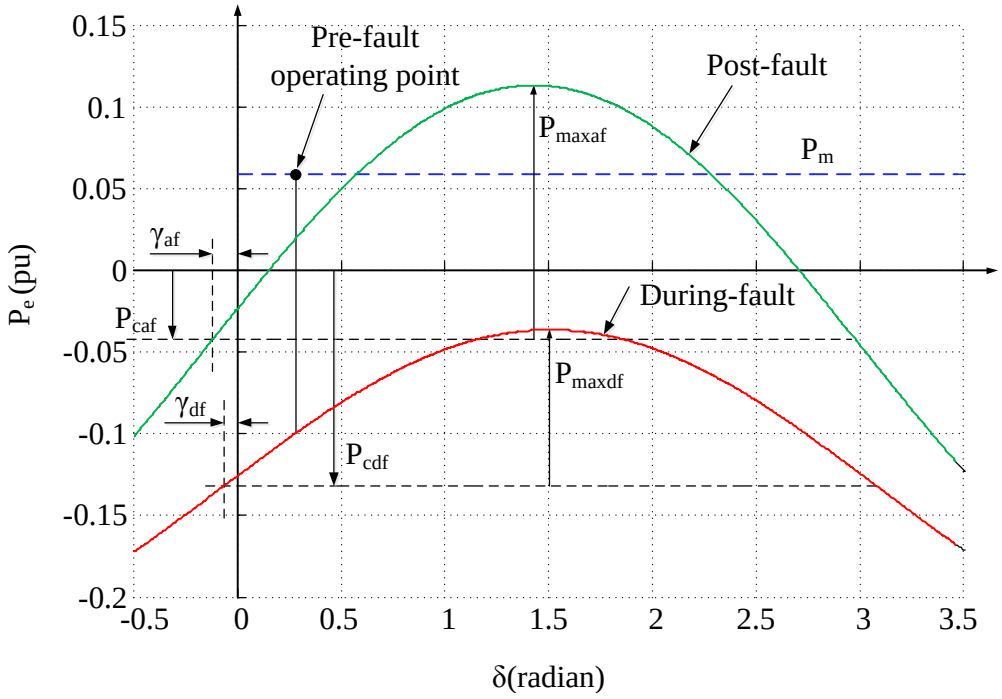

Figure 3.43: Power-angle characteristics of SMIB equivalent (Case 1)

Table 3.7: Power-angle characteristics values for Case 1

During-fault		Post-fault	
$P_{cdf}(pu)$	-0.1318	$P_{caf}(pu)$	-0.0458
$P_{maxdf}(pu)$	0.0954	$P_{maxaf}(pu)$	0.1591
$\gamma_{df}(radian)$	0.0584	$\gamma_{af}(radian)$	0.1383
CCT(s)		0.2704	

(0.1330 s). The two machines oscillate with each other in response to the disturbance as shown in Figure 3.46. As soon as the the generator bus angles separation exceeds 5 degrees during the post fault period, relay starts the SMIB equivalent procedure. The power-angle characteristics predicted by the relay for during fault and post fault condition of the network are shown in Figure 3.47. The values of parameters in Figure 3.47 are given in Table 3.8.

Using the predicted values of the parameters as shown in Table 3.8, the relay calculates CCT of the system. The CCT calculated for this case is 0.3679 s. Since the fault clearing time (i.e., 0.1330 s) is less than the CCT calculated, the swing is detected to be stable and

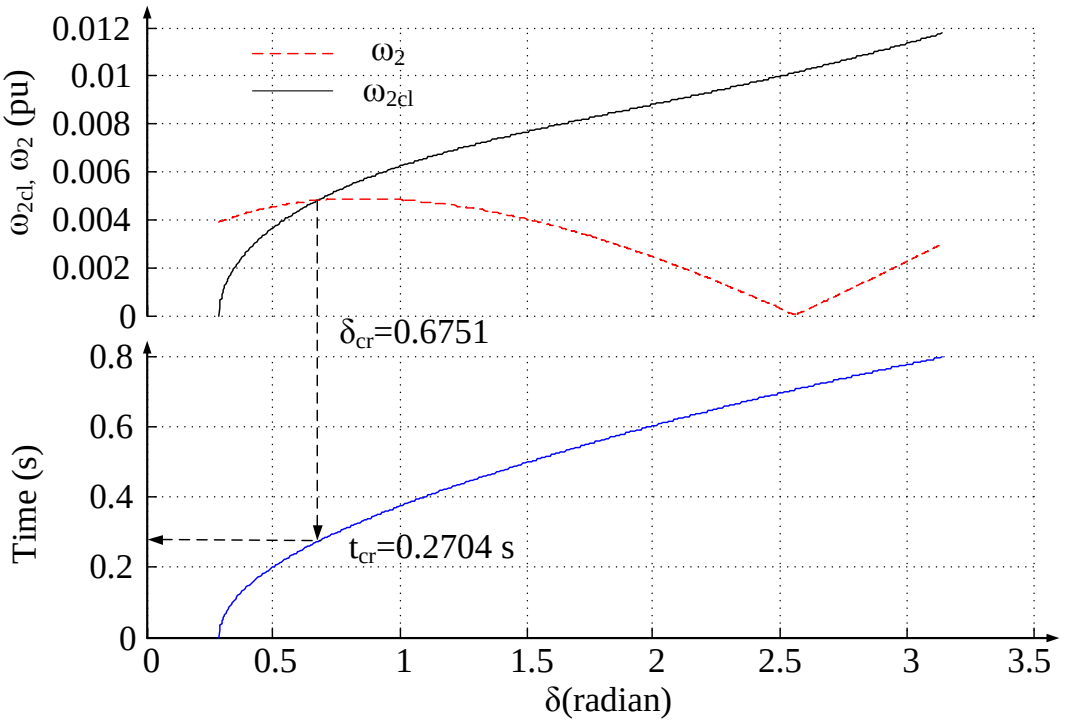

Figure 3.44: State plane and time scale plots to calculate CCT for Case 1

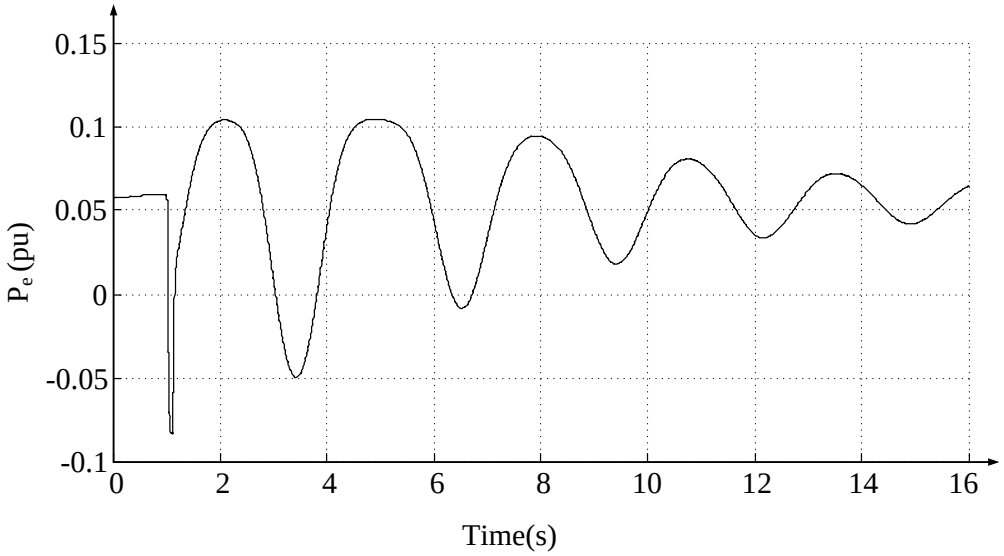

Figure 3.45: SMIB equivalent electrical power plot for Case 1, fault duration of 6 cycles

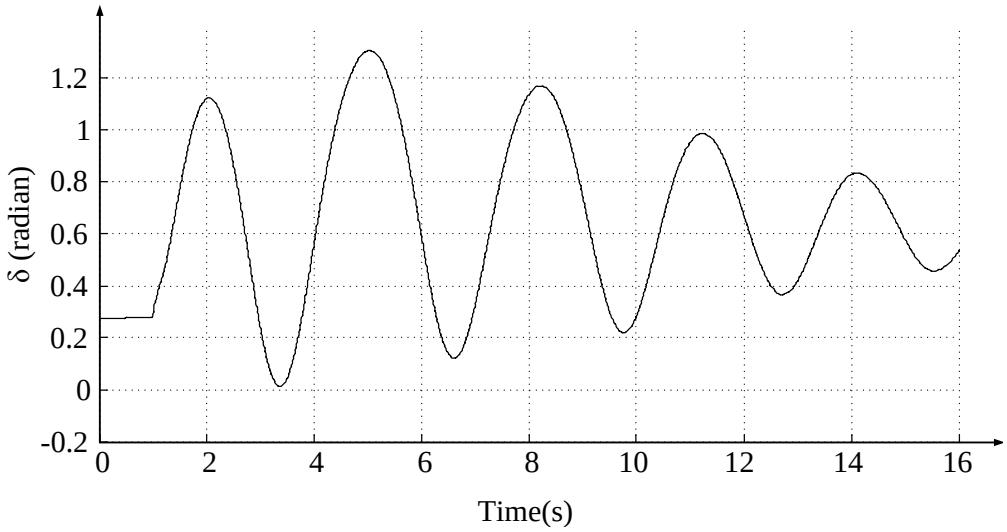

Figure 3.46: SMIB equivalent power angle plot for Case 2, fault duration of 8 cycles

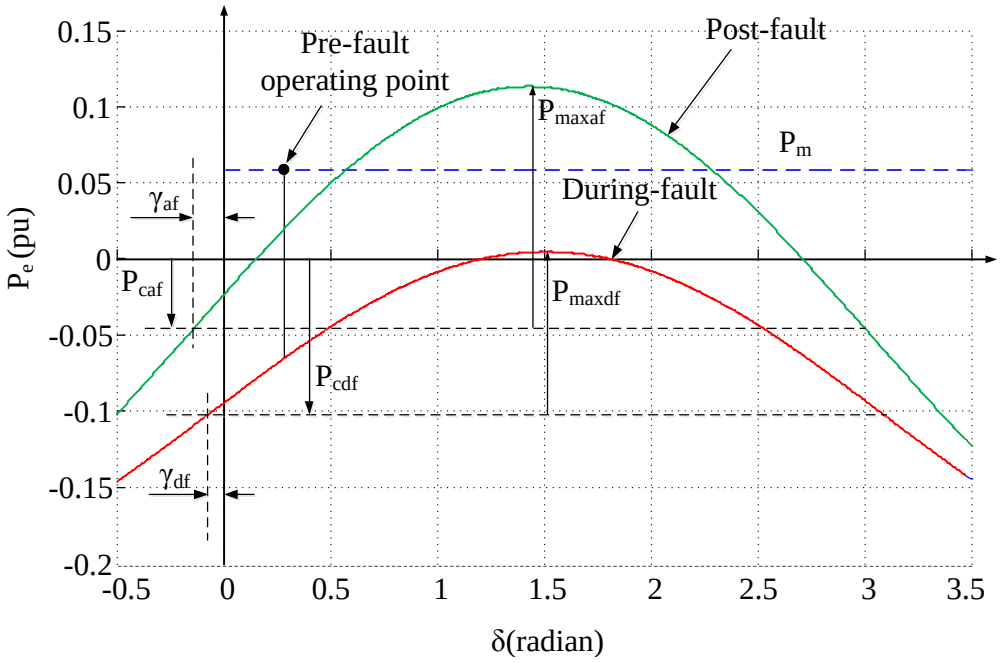

Figure 3.47: Power-angle characteristics of SMIB equivalent (Case 2)

the detection time is 0.2600 s. The SMIB equivalent electrical power obtained from the simulation is shown in Figure 3.48. It shows that it is a stable power swing.

Table 3.8: Power-angle characteristics values for Case 2

During-fault		Post-fault	
$P_{cdf}(pu)$	-0.1012	$P_{caf}(pu)$	-0.0458
$P_{maxdf}(pu)$	0.1059	$P_{maxaf}(pu)$	0.1591
$\gamma_{df}(radian)$	0.0601	$\gamma_{af}(radian)$	0.1383
CCT(s)		0.3679	

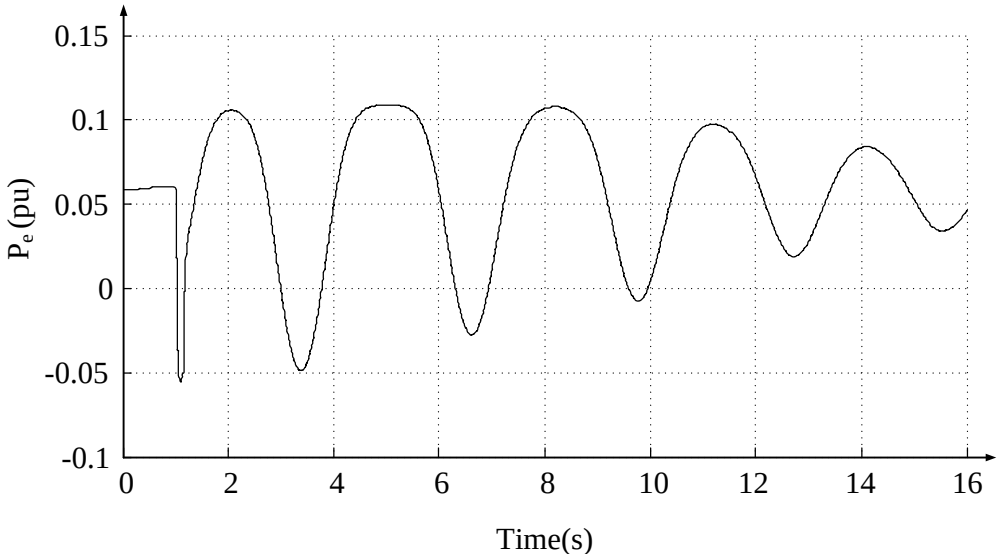

Figure 3.48: SMIB equivalent electrical power plot for Case 2, fault duration of 8 cycles

3.6.3.2 Unstable Swings

To get an unstable swing, a longer fault duration is used. Four unstable cases are discussed here. For case 1, fault duration of 18 cycles (0.3 s) and 20 cycles (0.3330 s) are taken.

When the fault is applied at 1 s and cleared after 18 cycles, the two areas starts separating. Figure 3.49 shows the rotor angle separation of the generators. As soon as the angle separation exceeds 5 degrees, relay starts calculating SMIB equivalent parameters. The parameters calculated for Case 1 will be same as that shown in Table 3.7. The CCT calculated is 0.2704 s. Since the fault clearing time (0.3 s) is greater then the CCT calculated, relay detects the swing as an unstable swing at 0.3700 s. The SMIB equivalent electrical power

swing as shown in Figure 3.50 also confirms the prediction from the proposed algorithm using SPA.

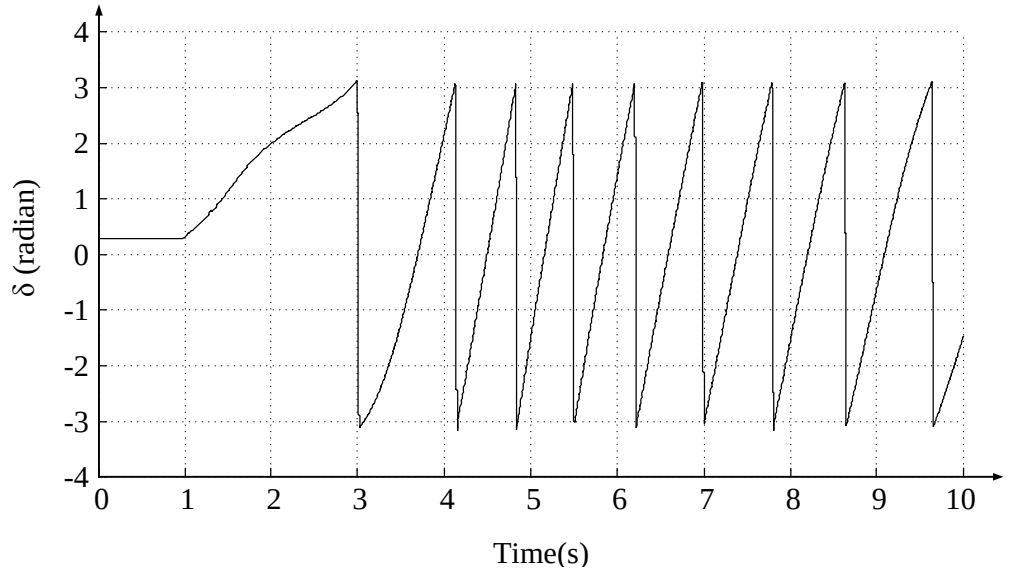

Figure 3.49: SMIB equivalent power angle plot for Case 1, fault duration of 18 cycles

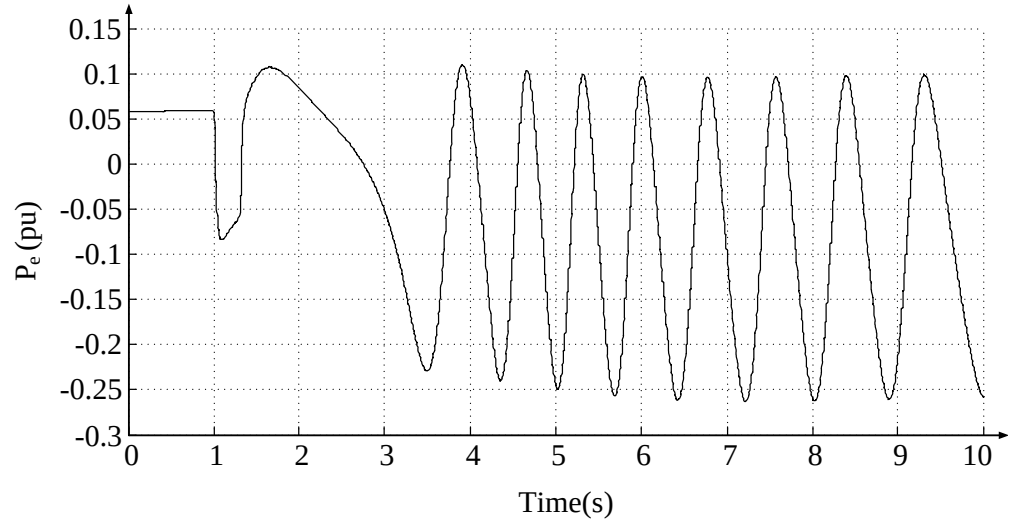

Figure 3.50: SMIB equivalent electrical power plot for Case 1, fault duration of 18 cycles

Similarly, for fault duration of 20 cycles (0.3330 s), relay follows the same procedure and detects the swing as an unstable swing at 0.3950 s. Figure 3.51 shows the unstable SMIB equivalent electrical power oscillation after the fault is cleared. For Case 2, unstable cases are created by applying fault for 24 cycles (0.4 s) and 26 cycles (0.4330 s). Figure 3.52 shows

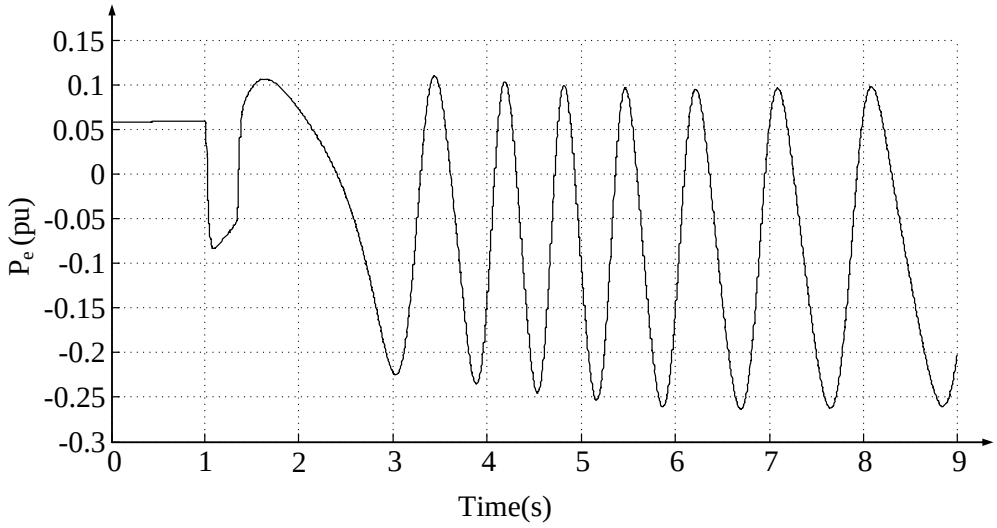

Figure 3.51: SMIB equivalent electrical power plot for Case 1, fault duration of 20 cycles

the rotor angle separation between generators for fault duration of 24 cycles. The predicted parameters of power-angle characteristics are shown in Table 3.8. The CCT calculated using SPA is 0.3679 s. The fault is cleared beyond the CCT, hence the system becomes unstable. The instability is detected at 0.4700 s. Figure 3.53 shows the unstable SMIB equivalent electrical power oscillation. Using the similar procedure for fault duration of 26 cycles, the

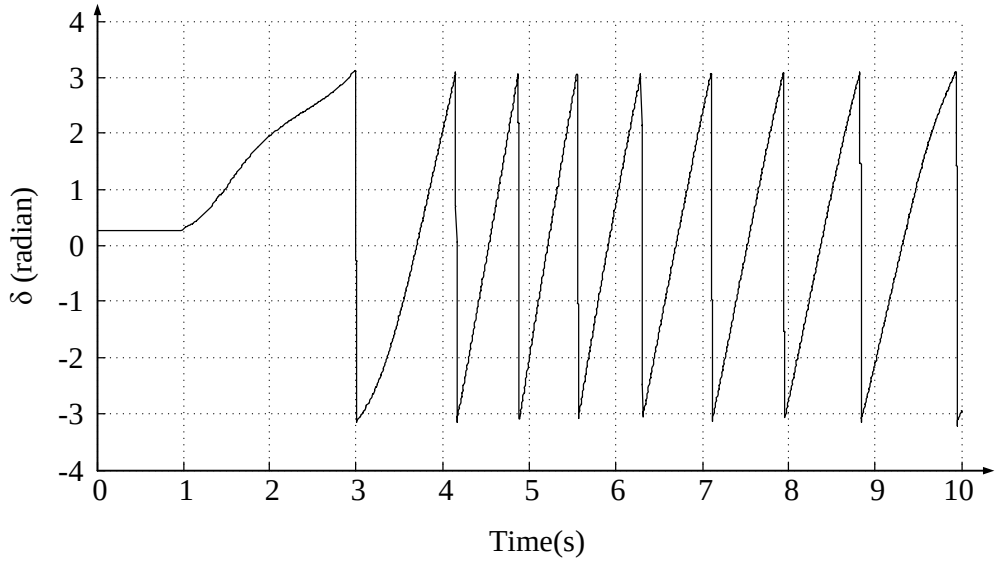

Figure 3.52: SMIB equivalent power angle plot for Case 2, fault duration of 24 cycles

swing is detected to be unstable at 0.5040 s. The unstable SMIB equivalent electrical power

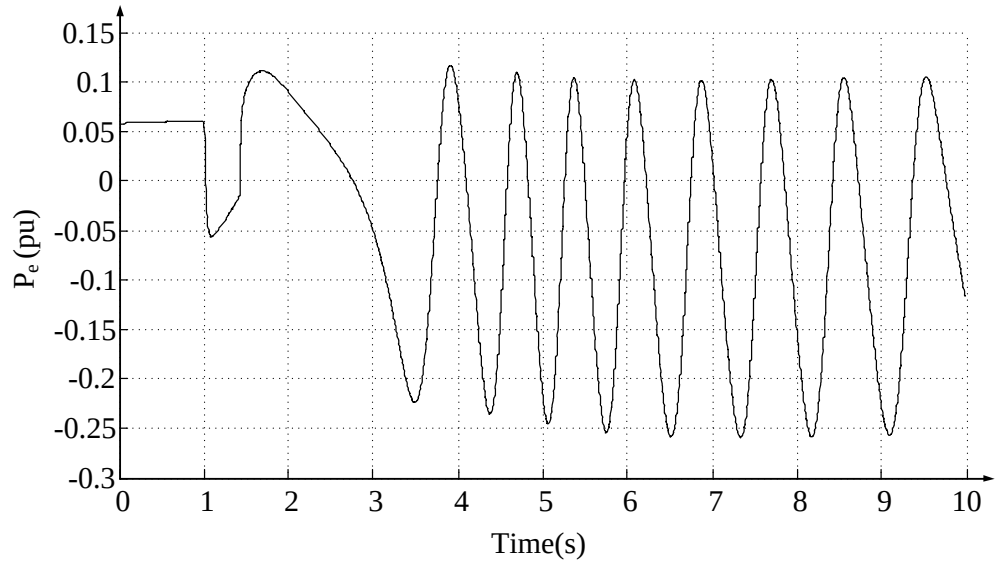

Figure 3.53: SMIB equivalent electrical power plot for Case 2, fault duration of 24 cycles

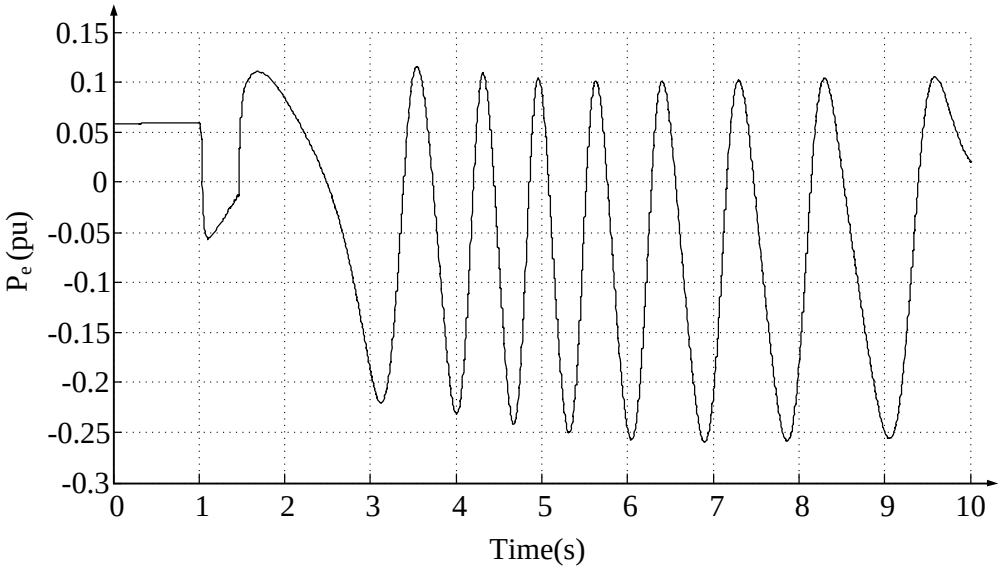

Figure 3.54: SMIB equivalent electrical power plot for Case 2, fault duration of 26 cycles

swing in this case is shown in Figure 3.54. Table 3.9 shows the summary of the results for stable and unstable swings detected using proposed technique based on SPA.

Table 3.9: Summary of stable and unstable swing detection results using the proposed state plane technique for a two area system

Case No.	Fault duration (cycle)	Fault duration (s)	Detection time (s)	Decision
Case 1	6	0.1000	0.2400	Stable
	8	0.1330	0.2650	Stable
	18	0.3000	0.3700	Unstable
	20	0.3330	0.3950	Unstable
Case 2	8	0.1330	0.2600	Stable
	24	0.4000	0.4700	Unstable
	26	0.4330	0.5040	Unstable

3.6.3.3 Multi-Swing Instability Cases

The two area system undergoes multi-swing instability for both cases (Case 1 and Case 2) for different fault durations.

Two multi-swing instability cases for Case 1 with fault duration of 10 cycles (0.1660 s) and 14 cycles (0.2330 s) are discussed here. For the fault duration of 10 cycles, as soon as the rotor angle separation exceeds 5^o, relay predicts the power-angle characteristics and calculates CCT which is given in Table 3.7. Figure 3.55 shows the SMIB equivalent power angle. Since the fault clearing time (0.1660 s) is less than CCT, the first swing is detected to be stable. The algorithm based on state deviation is then enabled to check multi-swing instability. At each DYP, it checks the value of SMIB equivalent speed deviation. Figure 3.56 shows the SMIB equivalent electrical power and speed deviation, where, the system at first two DYPs (DYP_1 and DYP_1) is found to be stable. At DYP_1 and DYP_2, the state (ω) deviation is less then zero. At DYP_3, the system is detected as unstable as the value of ω deviation is greater than zero. The detection is made at 7.6350 s which is measured from the instant when fault occurs in the system. For the fault duration of 14 cycle, rotor angle oscillation between the two generators is shown in Figure 3.57. Figure 3.58 shows the SMIB

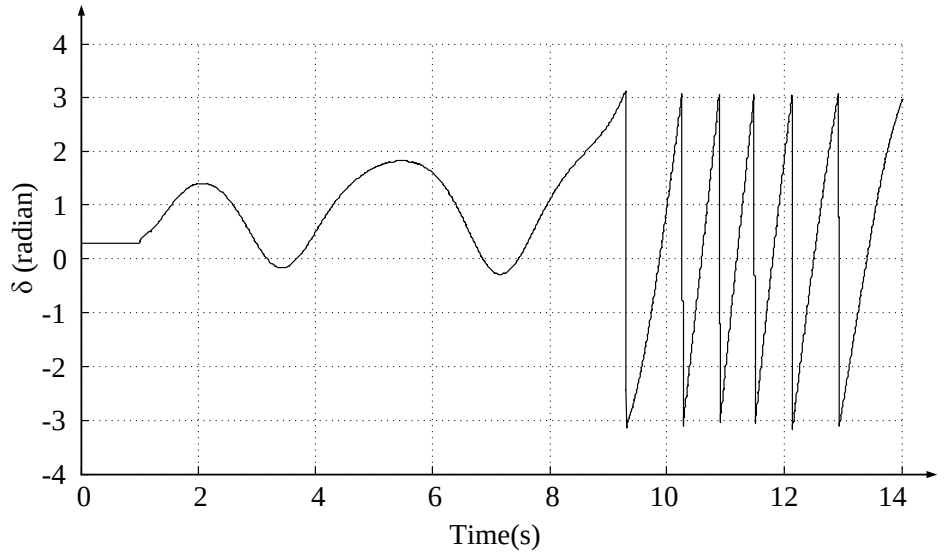

Figure 3.55: SMIB equivalent power angle plot for Case 1, fault duration of 10 cycles

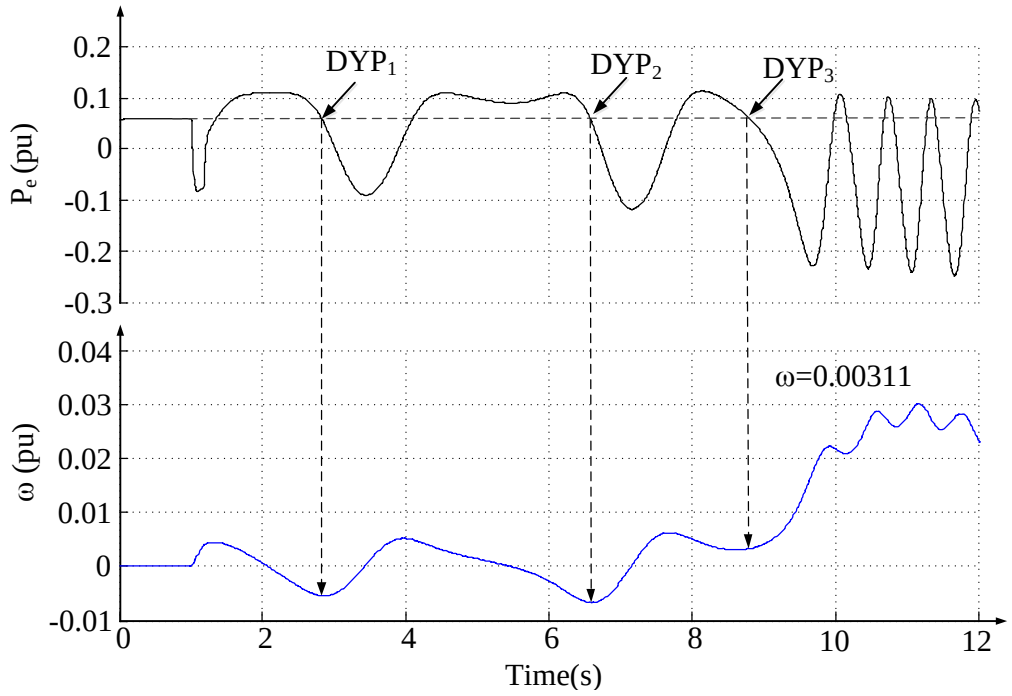

Figure 3.56: SMIB equivalent electrical power and speed deviation plots for Case 1, fault duration of 10 cycles

equivalent electrical power and speed deviation plot. The first swing is detected to be stable at 0.3200 s using SPA. Then, the swing is checked for multi-swing instability at each DYPs. At DYP_2, the algorithm based on state deviation detects that the system is going to become

unstable. The detection time is 4.1450 s.

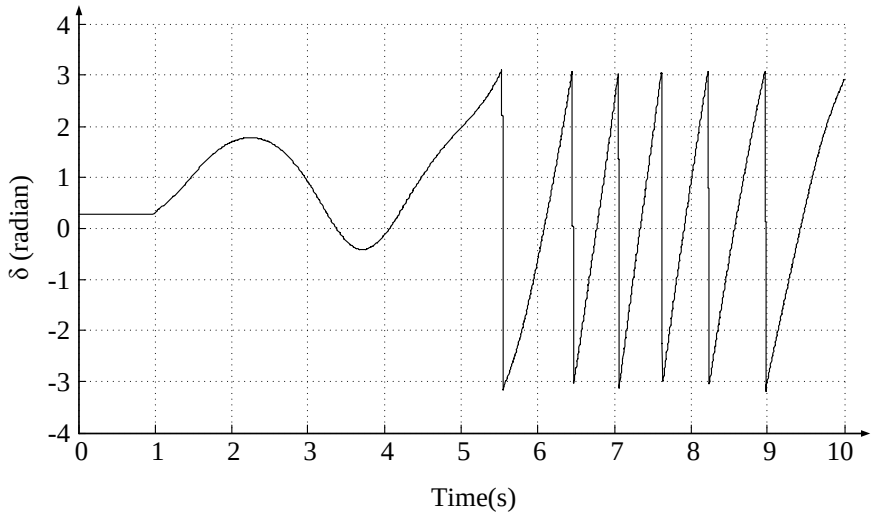

Figure 3.57: SMIB equivalent power angle plot for Case 1, fault duration of 14 cycles

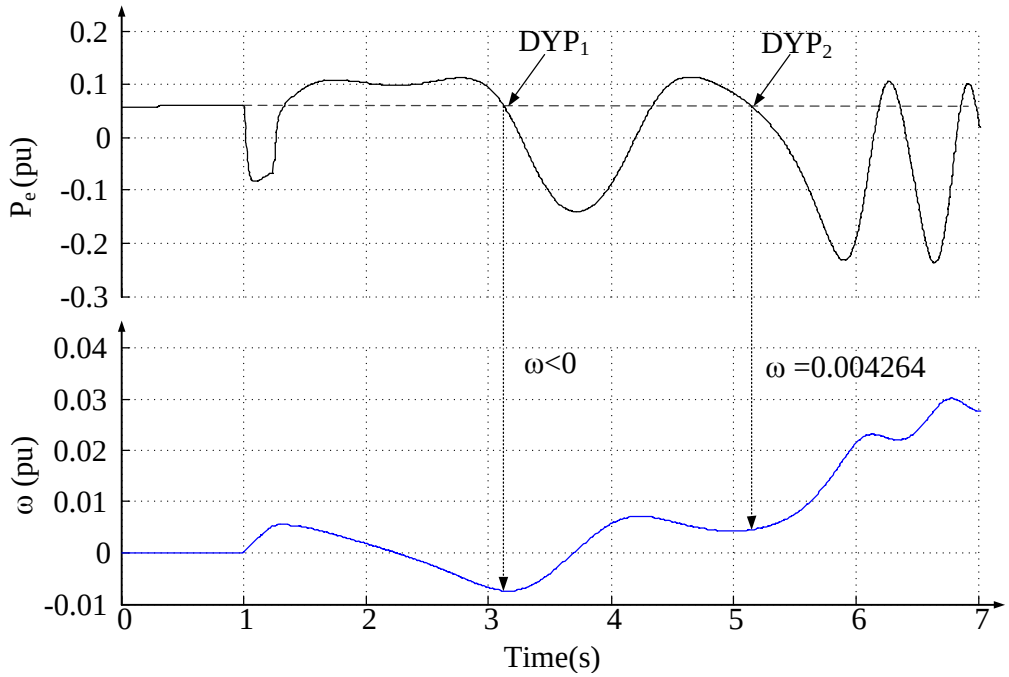

Figure 3.58: SMIB equivalent electrical power and speed deviation plots for Case 1, fault duration of 14 cycles

For case 2, fault duration of 10 cycles(0.1330 s) and 22 cycles (0.3660 s) are used to create multi-swing unstable scenarios. For the fault duration of 10 cycles, Figure 3.59 shows the

rotor angle separation between generators. The first swing is detected to be stable at 0.2800 s using SPA. The system is then checked for multi-swing instability using state deviation technique. At DYP_1 and DYP_2 the algorithm confirms the system to be stable, but the algorithm detects the system becoming unstable at DYP_3. The detection time is 7.6600 s. Figure 3.60 describes the detection procedure of state deviation technique. Similarly, for

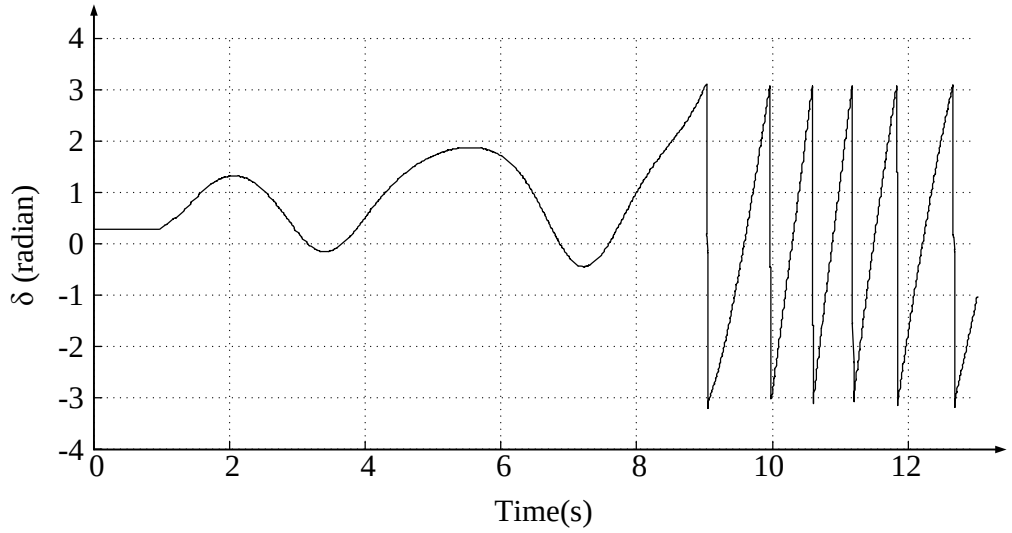

Figure 3.59: SMIB equivalent power angle plot for Case 2, fault duration of 10 cycles

the fault duration of 22 cycles, the first swing is detected as a stable swing using SPA at 0.4300 s. The state deviation technique detects the system becoming unstable at DYP_2, at time 2.5370 s. Figure 3.61 and 3.62 shows the SMIB equivalent power angle, electrical power and speed oscillation.

Table 3.10 shows the results for multi-swing instability detections using proposed scheme.

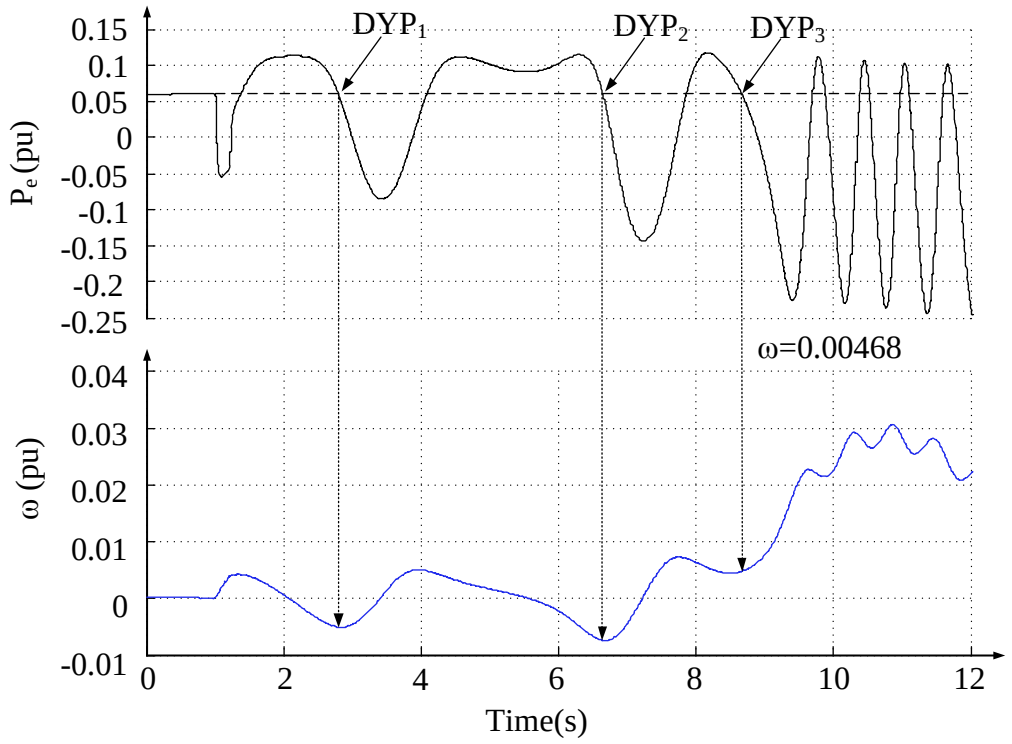

Figure 3.60: SMIB equivalent electrical power and speed deviation plots for Case 2, fault duration of 10 cycles

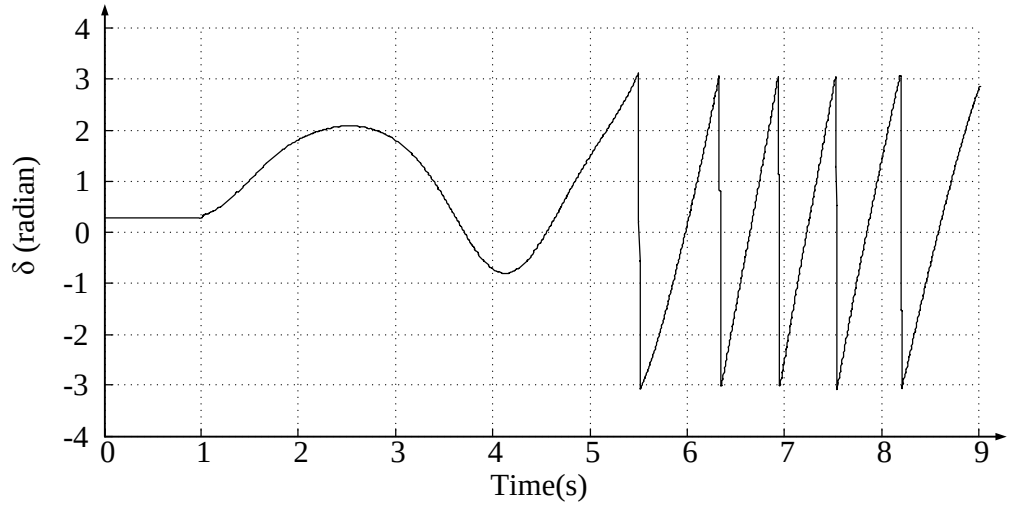

Figure 3.61: SMIB equivalent power angle plot for Case 2, fault duration of 22 cycles

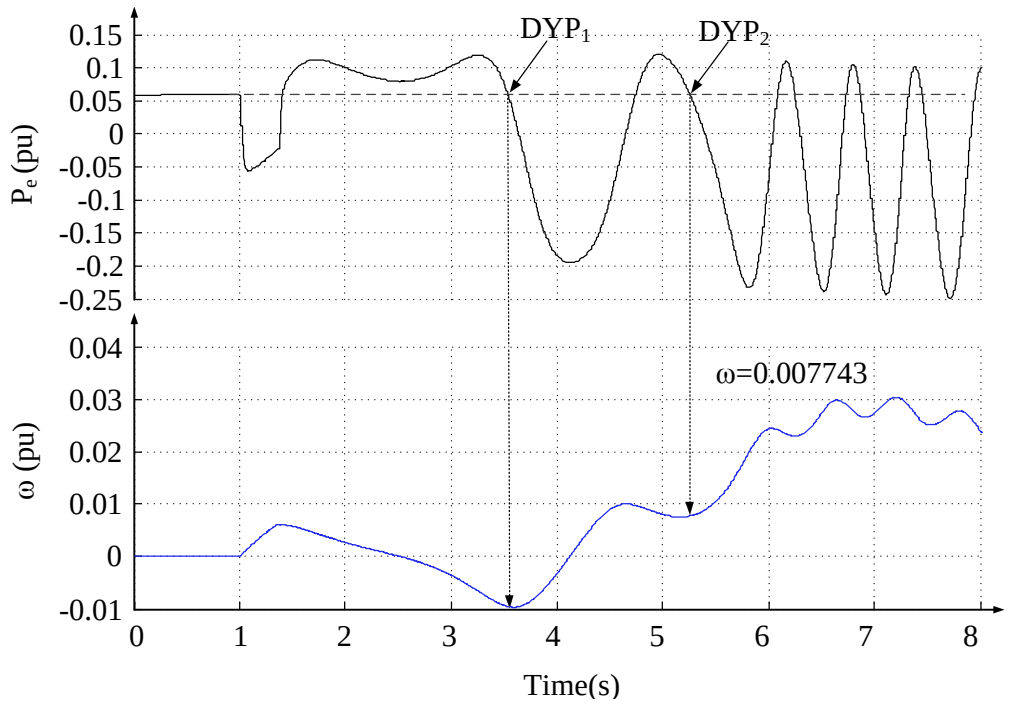

Figure 3.62: SMIB equivalent electrical power and speed deviation plots for Case 2, fault duration of 22 cycles

Table 3.10: Summary of multi-swing instability detection results using proposed combined scheme in a two area system

Case No.	Fault duration (cycle)	Fault duration (s)	Detection time (s)	DYP at detection
1	10	0.1660	7.6350	3^{rd}
	14	0.2330	4.1450	2^{nd}
2	10	0.1660	7.6660	3^{rd}
	18	0.3000	4.1313	2^{nd}
	22	0.3660	4.2500	2^{nd}

3.6.4 Comparison with the Two Blinder Scheme

The prediction of stable and unstable swings based on SPA is compared with conventional two blinder technique. A distance relay with two blinder scheme is placed at transmission line TL-I near bus 5. The relay protects 80% of the line. The inner blinder is set at 0.85 pu and the outer blinder is set at 4 pu. The power swing blocking time delay is taken as 2.5 cycles as recommended by [6]. For each test case (Case 1 and Case 2), one stable and one unstable case is discussed here.

For Case 1 and fault applied for 6 cycles, the apparent impedance seen by the distance relay is shown in Figure 3.63. Since the impedance locus does not enter the inner blinder, the swing is a stable swing and is detected at 1.9320 s, whereas the detection time for SPA is only 0.2400 s. For Case 1 and fault applied for 18 cycles, the apparent impedance seen

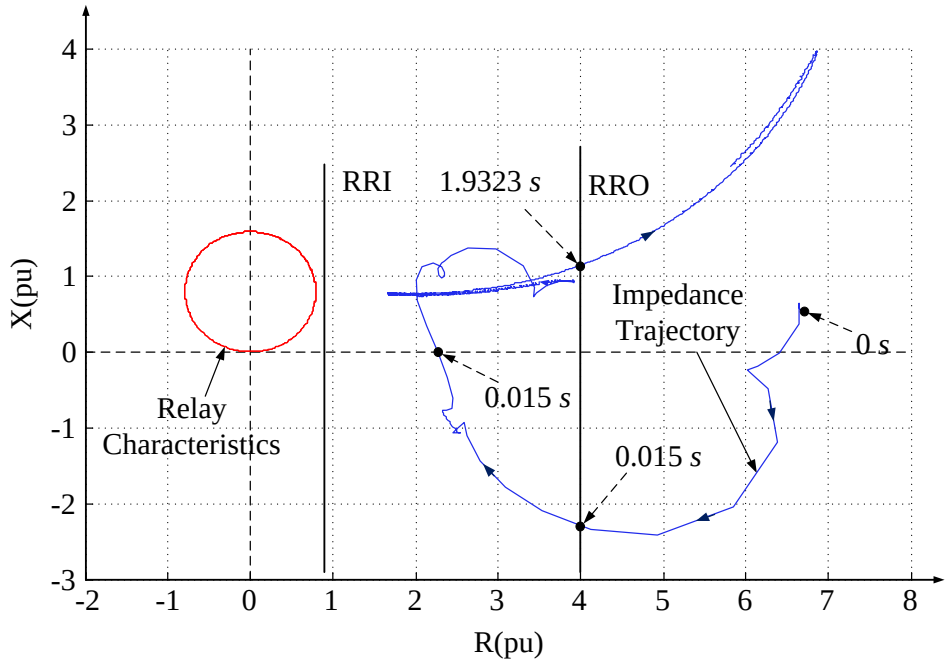

Figure 3.63: Impedance trajectory for Case 1 and fault duration of 6 cycles

by the distance relay is shown in Figure 3.64. Since the impedance locus enters the inner blinder, the swing is a unstable swing and is detected as an unstable swing at 0.9470 s. Whereas the detection time for SPA is only 0.3700 s.

For Case 2, fault is applied for 8 cycles (0.1330 s). The impedance trajectory seen by

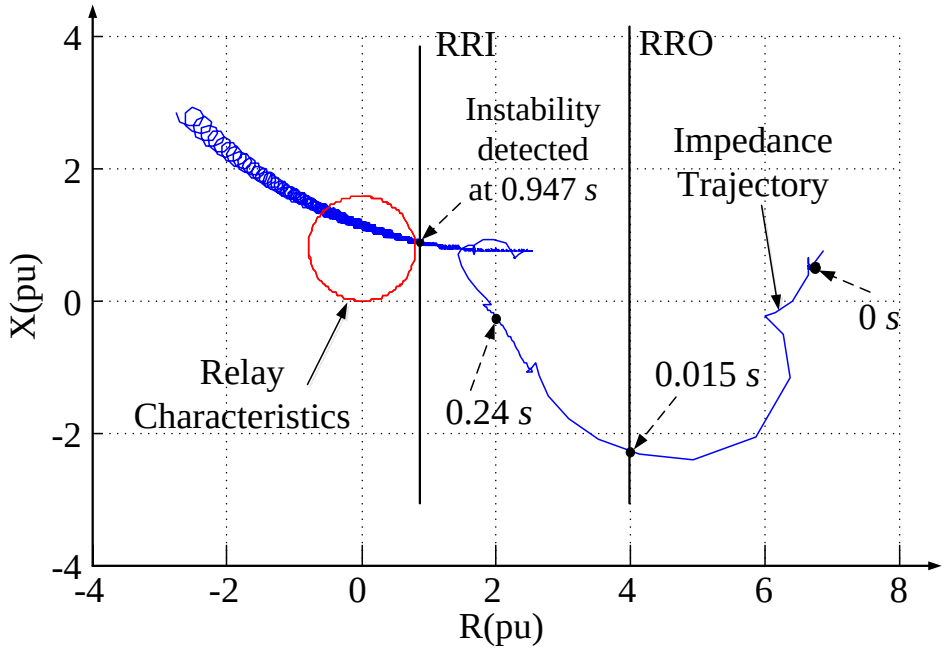

Figure 3.64: Impedance trajectory for Case 1 and fault duration of 18 cycles

relay is shown in Figure 3.65. The swing is detected as a stable swing at 1.8610 s whereas algorithm based on SPA detects it at 0.2600 s. Similarly, for Case 2 and fault duration

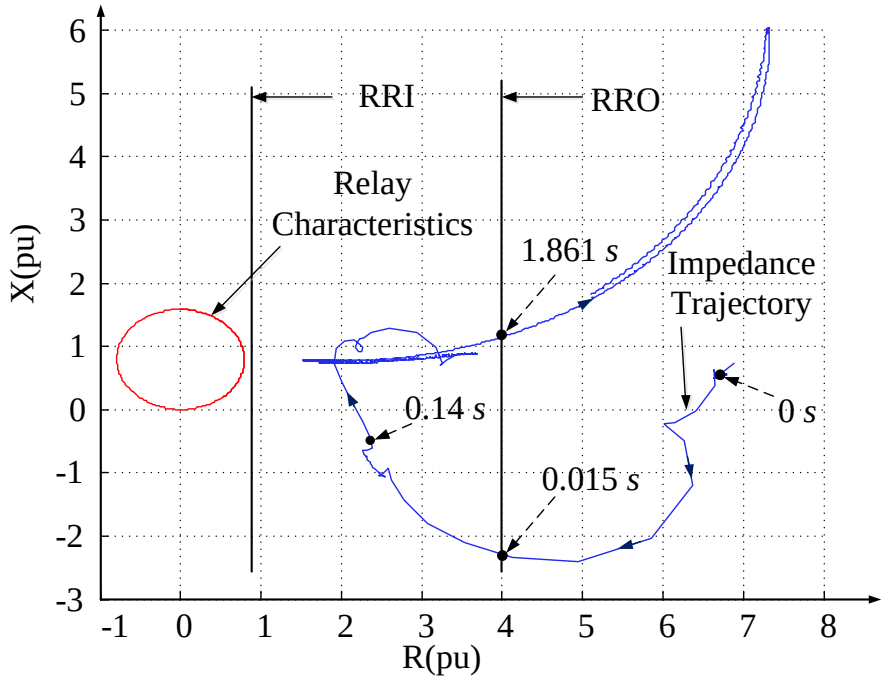

Figure 3.65: Impedance trajectory for Case 2 and fault duration of 8 cycles

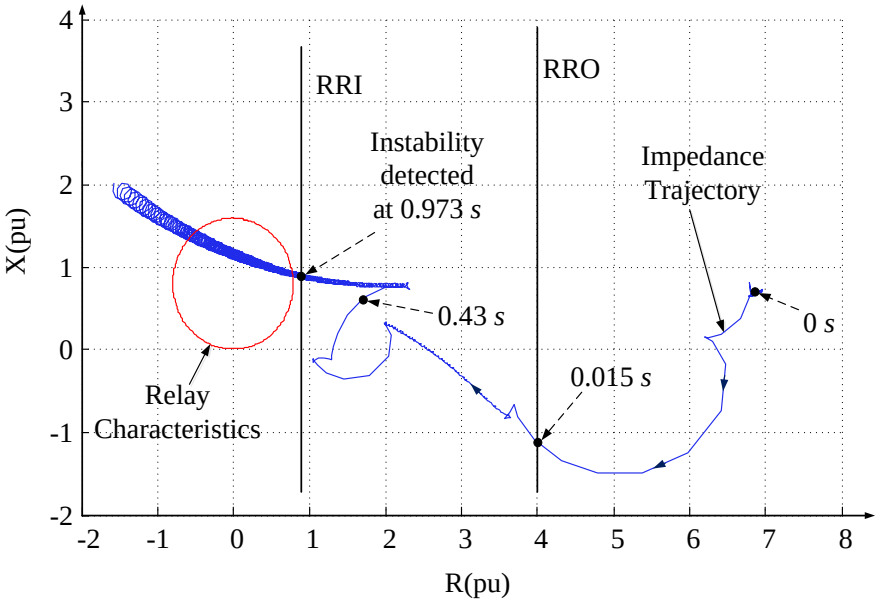

Figure 3.66: Impedance trajectory for case 2 and fault duration of 24 cycles

of 24 cycles, impedance seen by the distance relay is shown in Figure 3.66. The impedance locus crosses the inner blinder at time 25.9730 s and hence detected as an unstable swing at time 0.9730 s.

Table 3.11 shows the test results for stable and unstable swings using two blinder scheme.

Table 3.11: Summary of results using the two blinder technique for a two area system

Case No.	Fault duration (cycle)	Fault duration (s)	Detection time (s)	Decision
1	6	0.1000	1.9323	Stable
	8	0.1330	1.9010	Stable
	18	0.3000	0.9470	Unstable
	20	0.3330	0.8600	Unstable
2	8	0.1330	1.8610	Stable
	24	0.4000	0.9730	Unstable
	26	0.4330	0.9120	Unstable

3.6.5 Comparison with the State Deviation Technique

The stable and unstable cases, studied using the proposed algorithm using SPA, are also compared with the proposed state deviation technique. Figure 3.67 shows the SMIB equivalent electrical power and speed plot for Case 1 and fault duration of 18 cycles (0.3 s). The SMIB equivalent speed of the system is found to be 0.002374 pu at the saddle point. Hence, the system is detected to be unstable at 1.2563 s. The proposed technique based on SPA detects the same instability condition in 0.3700 s. Electromagnetic transient simulations are performed for many other test cases using different fault durations for Case 1 and Case 2. The swing detection time and decision for different fault durations are listed in

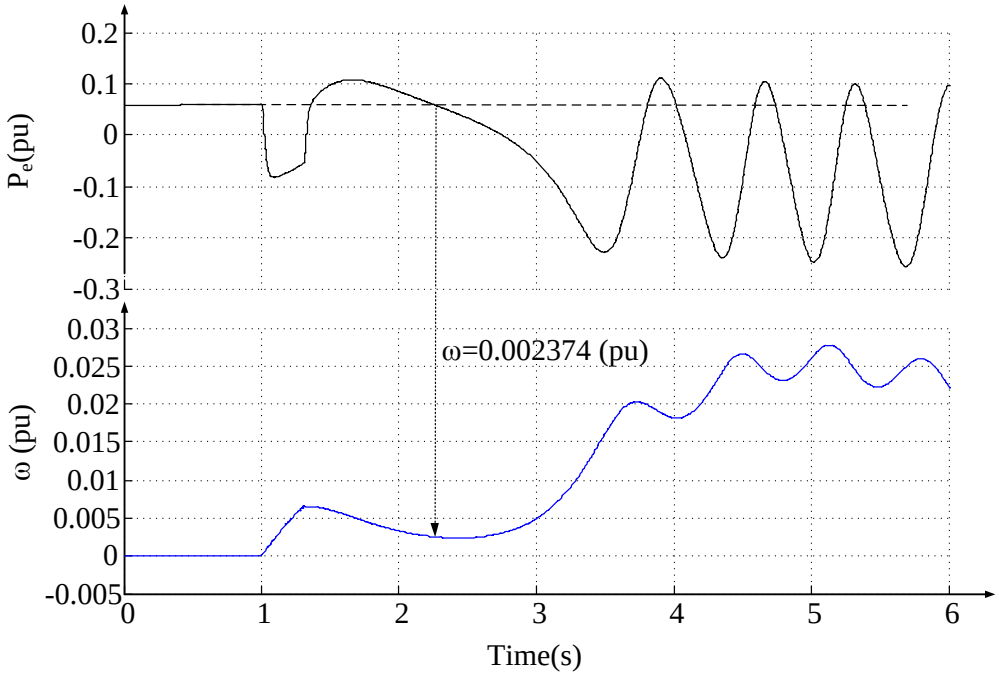

Figure 3.67: SMIB equivalent electrical power and speed plots for Case 1, fault duration of 18 cycles

Table 3.12. By comparing the detection times for same cases in Table 3.9, it can be seen that the detection using proposed algorithm is much faster than the state deviation technique.

Table 3.12: Summary of results for a two area system using the proposed state deviation technique

Case No.	Fault duration (cycle)	Fault duration (s)	Detection time (s)	Decision
1	6	0.1000	1.8240	Stable
	8	0.1330	1.7640	Stable
	18	0.3000	1.2563	Unstable
	20	0.3330	1.0896	Unstable
2	8	0.1330	1.7200	Stable
	24	0.4000	1.3000	Unstable
	26	0.4330	1.1625	Unstable

3.7 Summary

In this chapter, a relay algorithm based on SPA was developed. The algorithm was tested on a SMIB test system and a two area test system. The results were compared with the conventional technique using two blinders and with another technique using generator state deviation. The test results for stable and unstable cases as seen from the Tables 3.3 and 3.4, using proposed algorithm based on SPA, were compared with the results obtained using two blinder scheme shown in Table 3.5. The comparisons showed that the proposed technique is much faster than the two blinder scheme and the breaker angles at the time of detection were also smaller. The results were also compared with the results obtained using generator state deviation technique (Table 3.6). The comparisons on detection time showed that the proposed technique detects faster than the state deviation technique.

Test results for stable and unstable cases for the two area system were shown in Table 3.9 and was compared with the results obtained using two blinder scheme (Table 3.11). The results again showed that the proposed technique detects the power swing faster than the two blinder scheme. The power swing detection for two area system was also studied using the state deviation technique and the detection times were shown in Table 3.12. The multi-

swing instability studies carried out for two area test system were shown in Table 3.10. The proposed technique combined with the state deviation technique was successful to detect the multi-swing instability conditions accurately.

Chapter 4

Hardware Implementation and Testing Using a Real Time Digital Simulator

4.1 Introduction

In Chapter 3, the proposed algorithm was tested using computer simulations for a single machine and two machine system to verify the capabilities of the proposed algorithm. Once the relay algorithms are verified using computer simulations, it is also necessary to verify their behavior using experimental studies. Therefore a prototype of the relay was also developed in this research, using a Digital Signal Processing (DSP) board and tested with a real-time simulator (RTDS^{TM})[1]. A real-time simulator is a dedicated computer hardware on which a power system network can be modeled in detail. It performs electromagnetic transient power system simulations with very small steps (typically 50 microseconds). All the nonlinear equations representing the complex power system are computed in this very small time step. This kind of simulator is very often used by power utilities and equipment manufactures for experimental verification of the relays and hardware in the loop testing [35].

This chapter describes the implementation and testing of the proposed algorithms using RTDS^{TM} and the other necessary hardwares. The power system is modeled in RSCAD^{TM} [2]. The power system model developed in RSCAD^{TM} is simulated in RTDS^{TM}, and the signals from the RTDS^{TM} are fed to the relay model. The decision from the relay model is then fed back to RTDS^{TM}, forming a closed loop testing system. The results obtained from these

[1]RTDS^{TM} is the registered trade mark of RTDS Technologies Inc., Winnipeg, Canada

[2]RSCAD^{TM} is the registered trade mark of RTDS Technologies Inc., Winnipeg, Canada

closed loop testing are discussed in this chapter.

4.2 Brief Description of Hardware/Software

The project uses two main hardwares : RTDS^{TM} and ADSP $-$ BF533^{TM}[3]. A brief introduction to each of them is provided in Sections 4.2.1 and 4.2.2.

4.2.1 RTDS^{TM}/RSCAD^{TM}

RTDS^{TM} is a fully digital power system simulator which is capable of performing electromagnetic simulation in real time. The simulation is done in a fixed simulation time step of 50 μs using a combination of advanced computer hardware and custom software [36], [35]. The main components associated with the simulator are Workstation Interface Cards (GTWIF and WIF), Triple Processor Card (3PC) , GIGA Processor Card (GPC) and a user friendly software RSCAD^{TM}. The simulator hardwares are assembled in a modular unit called a rack. Each rack is provided with processing units such as 3PC or GPC and communication units. The workstation interface card in a rack is a backplane mounted to facilitate computer workstation communication, multi-rack case synchronization, inter-rack data communication paths, backplane communication and rack diagnostic. The 3PC is used to run software which represents the user's power and control circuits in real time. One GPC per rack is mainly dedicated to network solution. More than one GPC can be used to compute other power system components in parallel.

Each 3PC card consists of the following major features [37],

- ADSP-21062 SHARC PROCESSOR
- Instruction cycle time: 25 ns (=40 MIPS)
- Floating Point computation rate: 40-120 MFLOPs

[3]ADSP $-$ BF533^{TM} is the registered trade mark of Analog Devices, Inc.

- Floating Point Numeric Format: IEEE 40 bit (8 bit exponent, 32 bit mantissa)
- Link Port communication channels: 6
- Link Port communication rate: 40 Megabytes/s
- On-Chip Memory: 2 Megabit static ram

Each GPC card consists of the following major components [37],

- Two IBM PPC750GX PowerPC processors
- Core frequency: 1 GHz
- Floating Point computation rate: 1.0 GFLOPs
- Floating Point Numeric Format: IEEE-754 64 bit
- L1 Cache: 32 Kilobyte instruction, 32 Kilobyte data
- L2 Cahce: 1.0 Megabyte
- On-Chip Memory: 2 Megabit static ram

RSCAD^{TM} is a graphical user interface of RTDS^{TM} hardware. It consists of two sections: Draft and Runtime. In the draft section, circuits are built with custom power system and control components, parameters of the components are entered and the processor for the components is assigned. The runtime section is used to control the hardware. The control actions, such as starting and stopping simulation, applying disturbance, closing and opening of breakers, etc., are done in runtime section. RSCAD^{TM} communicates with the RTDS^{TM} hardware through either 10 Mbit/s or 100 Mbit/s ethernet connection. GTWIF works as a communication interface between RSCAD^{TM} and RTDS^{TM} processors.

4.2.2 ADSP – BF533™/Visual DSP++

In addition to RTDS™, ADSP – BF533™ EZ-kit lite board is used to model the proposed relay. A short list of features of the board are given below,

- One ADSP – BF533™ Blackfin®
- Clock Speed MHz (Max): 600MHz
- 32MB (16M x 16 bit) SDRAM
- 2 MB (512 K x 16 bit x 2) FLASH memory
- AD 1836 96 KHz audio codec with input and output RCA jacks

Detail on the board can be found in [38]. The DSP board is controlled through an user interface software called Visual DSP++. The Visual DSP++ communicates with the DSP board via an USB cable [39].

4.3 Test Procedure

The test procedure includes two distinct steps: a) modeling a power system and simulating it in real time, b) modeling out-of-step relay in DSP board and hardware in the loop testing. Figure 4.1 shows a block diagram of the process involved in closed loop testing of the proposed algorithm. The two parts of the test procedure is explained in Section 4.3.1 and 4.3.2.

4.3.1 Power System Modeling and Real Time Simulation

As explained in previous sections, the power system and control circuit design is done in RSCAD™. RSCAD™ provides custom library for power system and control components. The components are used to build two test cases: a) SMIB test system, and b)two area system. The two systems build in RSCAD™ are shown in Figures B.2 and B.3.

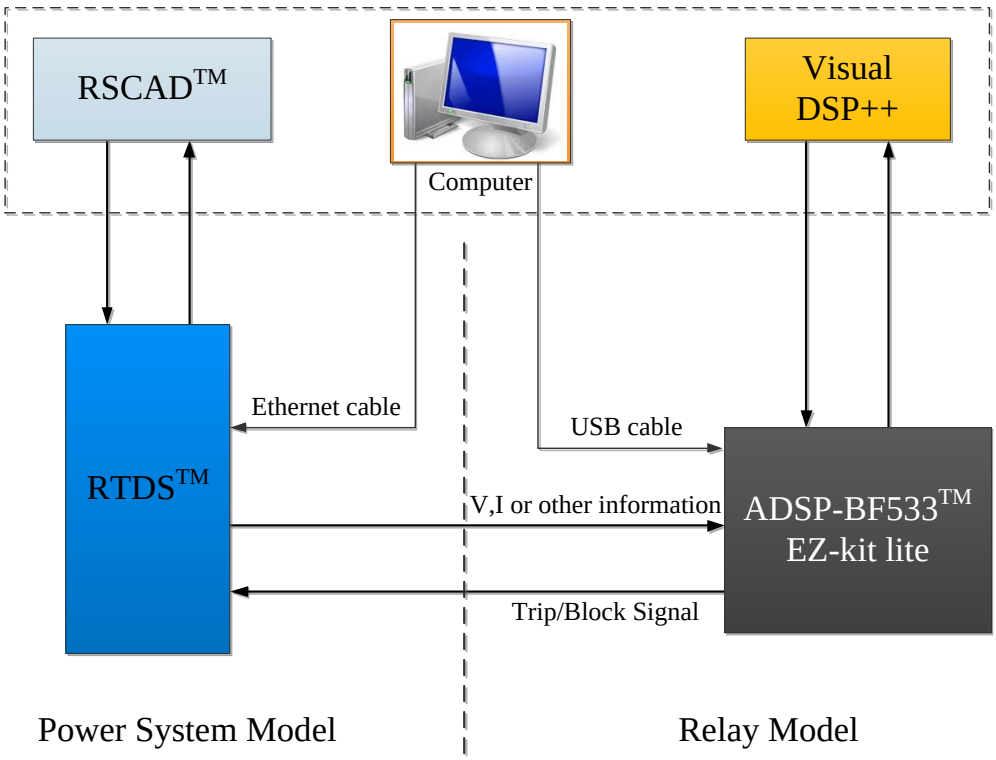

Figure 4.1: Block Diagram of the closed loop testing environment using the RTDS™

In a SMIB test system, a three phase to ground fault in the transmission line TL-II (refer Figure 3.2) is applied for a certain fault duration and is removed by opening the two breakers at the ends of the line. The control circuit built for this purpose is shown in Figure 4.2. The control signals generated by the circuit are shown in Figure 4.3. The fault is applied using a switch. Initially, when there is no fault, the output of the switch is 0, i.e. the fault signal and s_1 will be 0. Since the input to the square wave generator (SQW) is 0, s_2 will also be 0. Both inputs to the XNOR gate are 0, the output (i.e. BRK signal) will be 1. This means the breaker remains closed. The XNOR truth table is given in Figure 4.3. Whenever fault is applied by turning the switch on, signal s_1 becomes 1. Since the input to SQW is 1, it triggers the output which is a square wave. The width of the square wave is controlled by the value assigned on the dial. The value represents the fault duration. With the two input values equal to 1, output of XNOR gate(BRK) will be 1, i.e., the breaker is still closed. When the the fault duration is over, s_2 resets to 0. Now, with s_1 equals to 1, and s_2 equals to 0, signal BRK also resets to 0, which opens the breaker. The same circuit is used for two

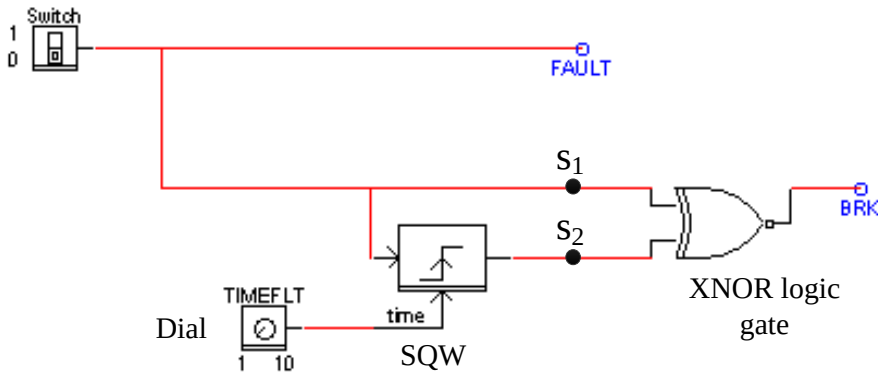

Figure 4.2: Control block to control the fault duration and breaker operation

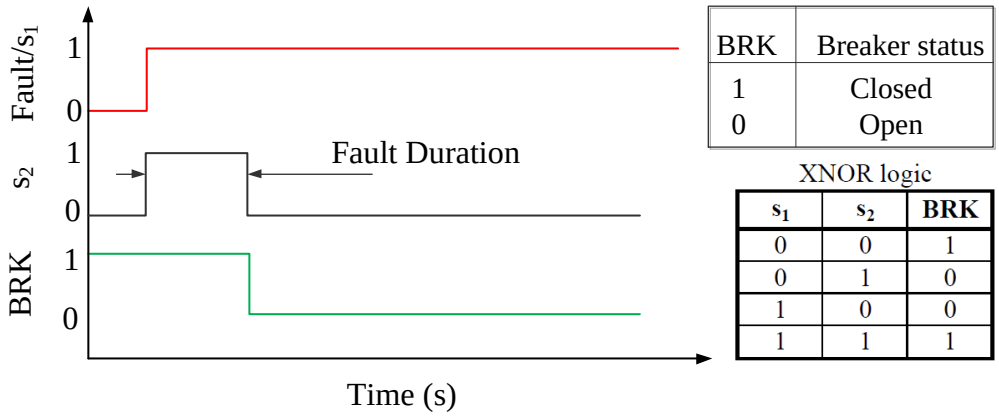

BRK	Breaker status
1	Closed
0	Open

XNOR logic

s_1	s_2	BRK
0	0	1
0	1	0
1	0	0
1	1	1

Figure 4.3: Control signal to control the fault duration and breaker operation

area system to control fault duration and breakers. The necessary signals from the power system model in a real time simulator are sent to the DSP board using RTDS^{TM} analog output ports.

4.3.2 Out-of-Step Relay Model in DSP

In SMIB system, voltage and current from the sending end and the voltage at the receiving end are communicated to the ADSP $-$ BF533^{TM}. The relay model developed consists of four blocks: Filtering, Down-sampling, Phasor Estimation and Out-of-step Algorithm using SPA. Figure 4.4 shows the block diagram of the relay model.

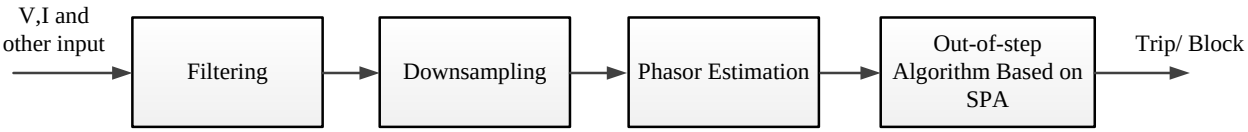

Figure 4.4: Block diagram of the relay model

4.3.2.1 Filtering

A Butterworth filter of fifth order is used to filter out the frequencies other than 60 Hz. The filter is a low pass filter with a cutoff frequency of 65 Hz. Transfer function of the filter is given by Equation 4.1.

$$H(z) = \frac{b_0 + b_1 z^{-1} + b_2 z^{-2} + b_3 z^{-3} + b_4 z^{-4} + b_5 z^{-5}}{a_0 + a_1 z^{-1} + a_2 z^{-2} + a_3 z^{-3} + a_4 z^{-4} + a_5 z^{-5}} \tag{4.1}$$

where, b's and a's are the filter coefficients which are listed in Table 4.1. The frequency response of the filter is shown in Figure 4.5.

Table 4.1: Filter coefficients of the low pass Butterworth filter

a coefficients	value	b coefficients	value
a_0	1.0	b_0	1.374456104486 e-12
a_1	-4.9724660423435	b_1	6.87228052243 e-12
a_2	9.89024269671581	b_2	13.744561044859 e-12
a_3	-9.83592884998049	b_3	13.744561044859 e-12
a_4	4.89099364358940	b_4	6.87228052243 e-12
a_5	-0.97284148604639	b_5	1.374456104486 e-12

4.3.2.2 Down-sampling

The DSP board samples the input signal at 48000 samples per second. The sampling frequency of 48 kHz for a power signal is not necessary. This study uses 32 samples per cycle. Since the power frequency is of 60 Hz, the signal should be sampled at 1920 samples per second. This means that the input signal is downsampled by 48000/1920=25 times.

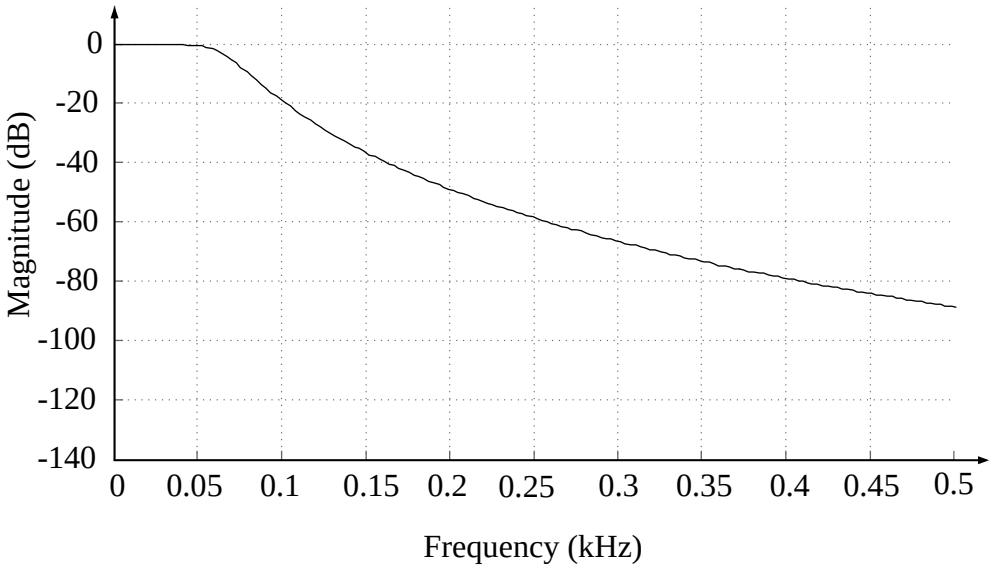

Figure 4.5: Magnitude response of low pass Butterworth filter

4.3.2.3 Phasor Estimation

Phasor estimation based on Discrete Fourier Transform (DFT) is used to estimate the voltage and current phasor. Consider a periodic input signal given by Equation 4.2 having fundamental frequency ω_0.

$$v(t) = V_p \sin(\omega_0 t + \phi) \tag{4.2}$$

The signal can be represented with a phasor consisting of two orthogonal components. The DFT technique uses two orthogonal signals, sine and cosine to estimate the phasor of the input signal. In this project, it uses a full cycle (i.e., 32 samples) data and estimates the real and imaginary parts of the input signal using the relations given by Equation 4.3.

$$\begin{aligned} Re(v) = V_p \cos\phi &= \frac{2}{N} \sum_{k=0}^{N-1} v_k \sin(k\omega_0 \Delta T) \\ Im(v) = V_p \sin\phi &= \frac{2}{N} \sum_{k=0}^{N-1} v_k \cos(k\omega_0 \Delta T) \end{aligned} \tag{4.3}$$

where k is the sample number, N represents the total number of samples in a cycle, and ΔT is sampling period. The two orthogonal signals $\sin(k\omega_0 \Delta T)$ and $\cos(k\omega_0 \Delta T)$ have same frequency as the input signal and are sampled with same sampling rate of ΔT. The 32 values

of the orthogonal signals are listed in Table 4.2. The kth orthogonal component is multiplied with kth input sample [40].

Table 4.2: Coefficients of the two orthogonal signals

k	$\sin(k\omega_0\Delta T)$	$\cos(k\omega_0\Delta T)$	k	$\sin(k\omega_0\Delta T)$	$\cos(k\omega_0\Delta T)$
0	0	1	16	0	-1
1	0.19509032201	0.9807852804	17	-0.19509032201	-0.9807852804
2	0.3826834323	0.92387953251	18	-0.3826834323	-0.92387953251
3	0.55557023301	0.83146961230	19	-0.55557023301	-0.83146961230
4	0.70710678118	0.70710678118	20	-0.70710678118	-0.70710678118
5	0.83146961230	0.55557023301	21	-0.83146961230	-0.55557023301
6	0.92387953251	0.3826834323	22	-0.92387953251	-0.3826834323
7	0.9807852804	0.19509032201	23	-0.9807852804	-0.19509032201
8	1	0	24	-1	0
9	0.9807852804	-0.19509032201	25	-0.9807852804	0.19509032201
10	0.92387953251	-0.3826834323	26	-0.92387953251	0.3826834323
11	0.83146961230	-0.55557023301	27	-0.83146961230	0.55557023301
12	0.70710678118	-0.70710678118	28	-0.70710678118	0.70710678118
13	0.55557023301	-0.83146961230	29	-0.55557023301	0.83146961230
14	0.3826834323	-0.92387953251	30	-0.3826834323	0.92387953251
15	0.19509032201	-0.9807852804	31	-0.19509032201	0.9807852804

With a power frequency of 60 Hz and the number of samples per cycle N=32, the sampling time is given by,

$\Delta T = \dfrac{1}{60 * 32} = 5.20833 * 10^{-4} s$

4.3.2.4 Algorithm based on SPA

Using the phasor estimation of the sending and receiving end voltage and current at the sending end, three phase power output from the generator and the power angle at the sending end is calculated using Equations (4.4) and (4.5) respectively.

$$P_e = 3 * V^j_{rms} * I^j_{rms} * cos(\theta^j_1 - \theta^j_2) \tag{4.4}$$

$$\delta^j = \delta^j_s - \delta^j_r \tag{4.5}$$

where V^j_{rms} and I^j_{rms} are single phase rms voltage and current at sending end respectively, θ^j_1 and θ^j_2 are phase angles of voltage and current at the sending end respectively, δ^j represents power angle, δ^j_s and δ^j_r represent phase angles of sending and receiving end respectively calculated at jth sample.

The execution time available between each interrupts in ADSP $-$ BF533$^{\text{TM}}$ is limited by its sampling frequency. With sampling frequency of 48 kHz, the execution time available between two consecutive interrupts is 20.833 μs. Since the execution time required for the algorithm is more than 20.833 μs , the algorithm is divided among different interrupts. The fault in the line is identified by detecting the decrease in power flow in the line. If the electrical power calculated decreases more than 20% of the pre-fault value, the fault is detected. The power-angle characteristic for the during-fault condition is calculated using the faulted network. The during-fault calculation of the algorithm is started after the fault inception is identified. The during-fault calculations require 16 sampling intervals (i.e., 0.333 milliseconds). After the fault is removed, the post-fault power-angle characteristics is calculated. The algorithm requires 14 sampling intervals (i.e., 0.291 milliseconds) for the post-fault calculations. The CCT is calculated and the decision on instability is made by using the decision criterion explained in Section 3.4 and a decision signal is sent back to RTDS$^{\text{TM}}$. The decision signal is either 0 (block the breaker operation) or 1 (trip the breaker). Figure 4.6 shows the decision signals generated by the relay. The test results for the SMIB and two area system are discussed in Sections 4.4 and 4.5

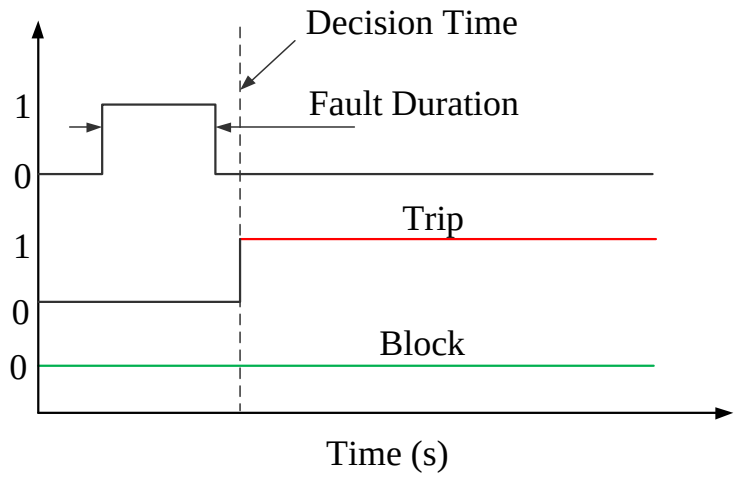

Figure 4.6: Decision signal from the out-of-step relay

4.4 Case Studies:Single Machine Infinite Bus System

The SMIB system described in Section 4.3.1 is considered as a test system to test the proposed algorithm under various swing conditions. Power swing conditions in the power system are created using a three phase to ground fault at different locations of the transmission line TL-II. Initial operating point and the fault duration is varied to achieve varieties of swing conditions. Initial operating point (δ_t) chosen for the study are 25^o and 30^o. Three test cases are discussed here.

Case i Initial δ_t=25^o, and the fault is applied at the middle of TL-II

Case ii Initial δ_t=25^o, and the fault is applied at $1/4^{th}$ of TL-II

Case iii Initial δ_t=30^o, and the fault is applied at the middle of TL-II

The swings obtained during testing are divided into two categories: stable and unstable swings, which are discussed below.

4.4.1 Stable Cases

Stable scenarios for Case i are simulated using fault durations of 14 to 20 cycles. Figure 4.8 shows the power oscillation for the fault applied at 1.0 s and cleared after 14 cycles (0.233

s). For the δ_t=25^o and the fault at the middle of the TL-II, power-angle characteristics predicted by the relay are shown in Figure 4.7a. Using the power- angle characteristics, the proposed algorithm using SPA calculates the CCT using the state plane plots as shown in Figure 4.7b. The CCT calculated is 0.3703 s. Since the fault clearing time is less than the critical clearing time calculated by the proposed algorithm, the swing is detected as a stable swing. The detection is made at 0.234 s.

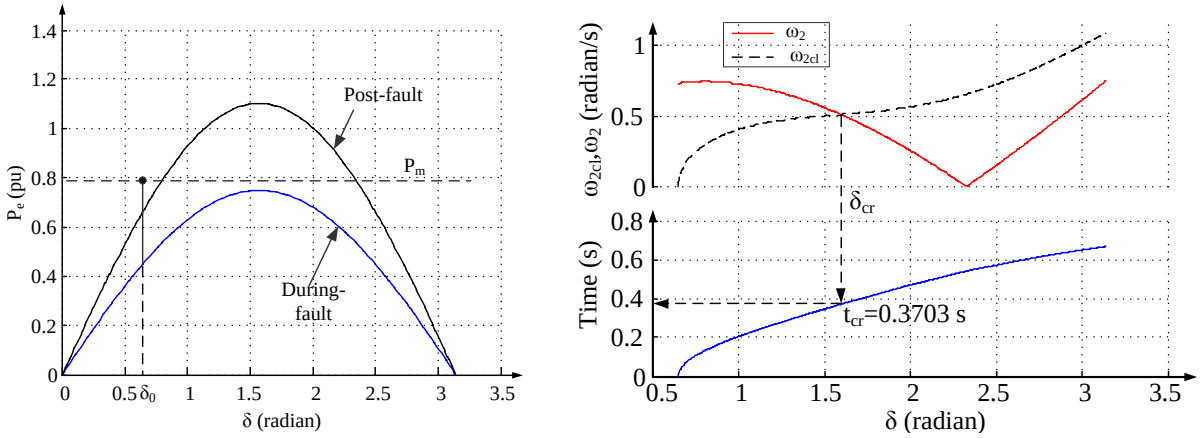

(a) Power-angle characteristics

(b) State plane plot and time scale

Figure 4.7: Calculation of CCT for Case i

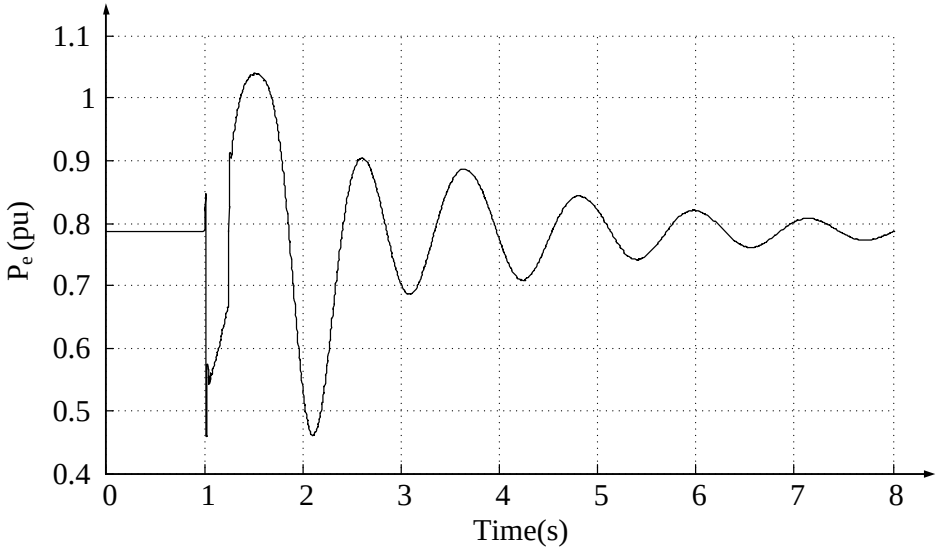

Figure 4.8: Power swing plot for Case i, fault duration of 14 cycles

Similarly, for Case ii, fault is applied at 1 s and cleared after 10 cycles(0.167 s). For this

initial operating point and the fault at one fourth of the TL-II, the power-angle characteristics predicted by relay are shown in Figure 4.9a. Using power-angle characteristics, the algorithm calculates CCT using state plane trajectories as shown in Figure 4.9b. The CCT calculated is 0.2454 s. The decision criterion detects the swing as a stable swing at 0.16733 s. Figure 4.10 shows the electrical power swing observed from the real time simulation, which verifies the stable nature of the swing.

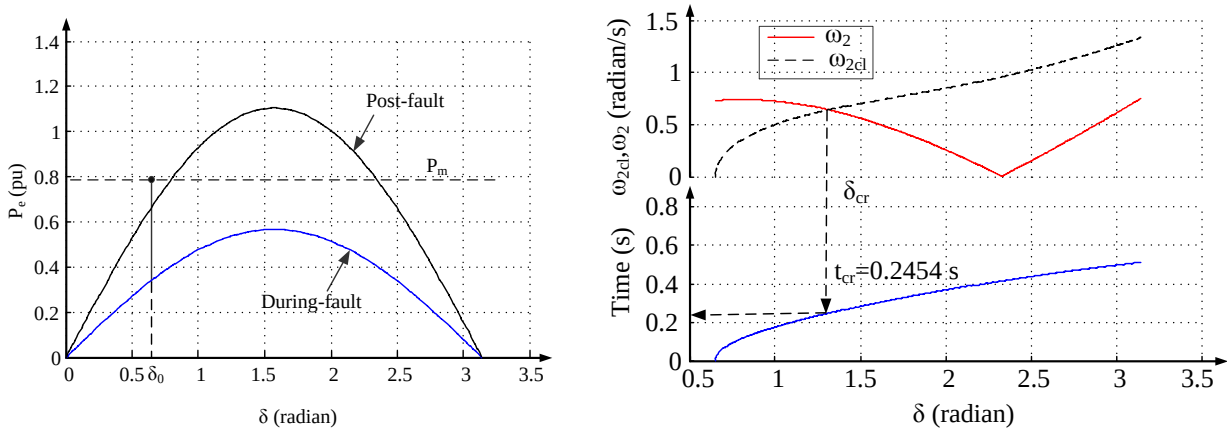

(a) Power-angle characteristics

(b) State plane plot and time scale

Figure 4.9: Calculation of CCT for Case ii

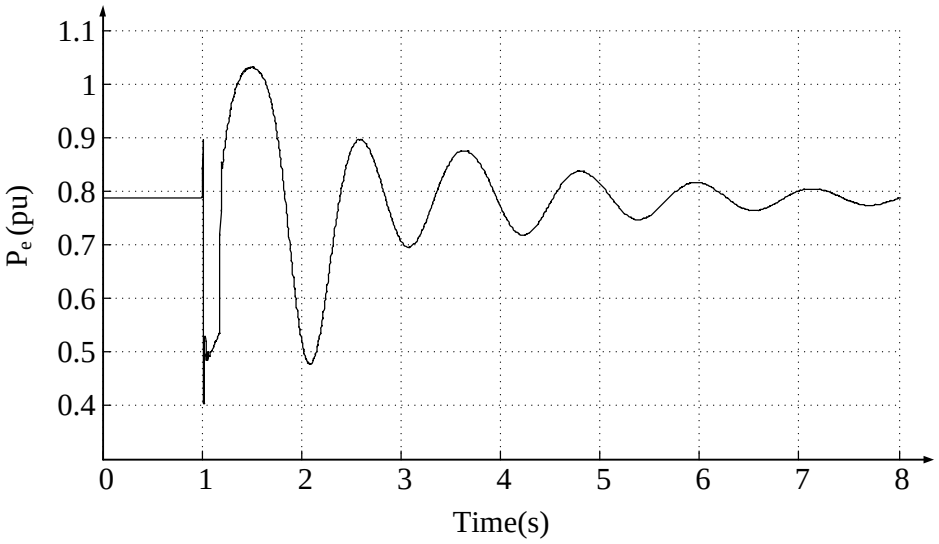

Figure 4.10: Power swing plot for Case ii and fault duration of 10 cycles

Similarly, for Case iii, fault is applied at 1.0 s and is cleared after 8 cycles (0.133 s).

The power-angle characteristics predicted by the relay is shown in Figure 4.11a. The relay algorithm finds the state plane trajectories and calculates the CCT, using the power-angle characteristics which are shown in Figure4.11b. The CCT calculated is 0.1512 s. The swing is detected as a stable swing at 0.134 s. Figure 4.12 shows the electrical power swing plot obtained from the simulation which is stable and verifies the detection.

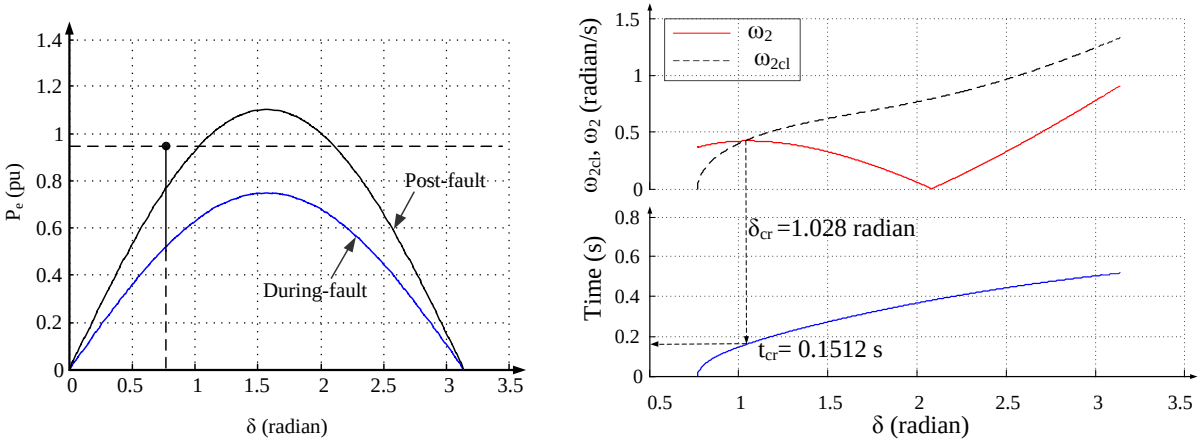

(a) Power-angle characteristics

(b) State plane plot and time scale

Figure 4.11: Calculation of CCT for Case iii

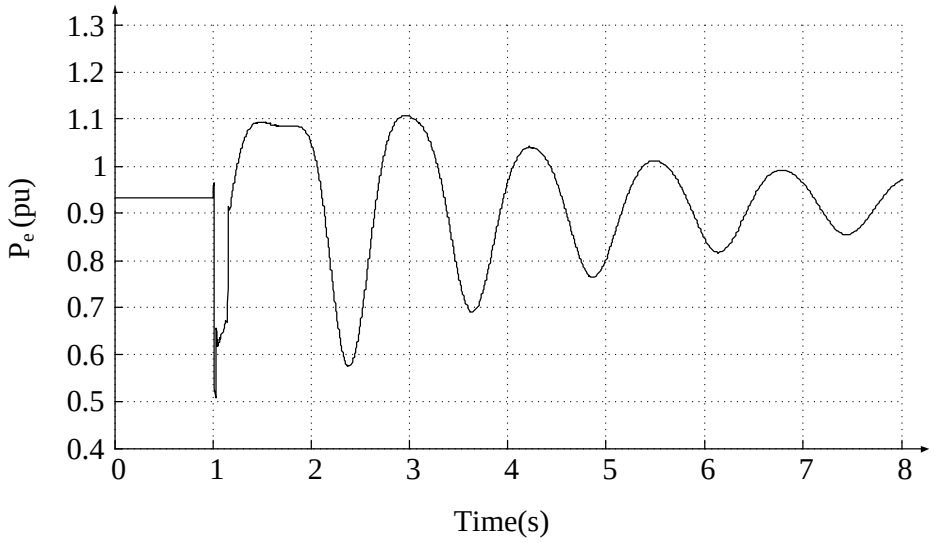

Figure 4.12: Power swing plot for Case iii and fault duration of 8 cycles

Table 4.3 shows the results for stable cases detection for SMIB using the proposed algorithm based on SPA. The table shows the results for the cases explained above as well as for

other fault durations. The algorithm is able to detect stable swings between 0.292 to 1.333 milliseconds after the fault is cleared.

Table 4.3: Summary of experimental test results for SMIB stable cases

Case No.	Fault duration (cycles)	Fault duration (s)	Decision time (s)	Decision
i	14	0.233	0.2340	Stable
	18	0.30	0.3013	Stable
	20	0.333	0.3340	Stable
ii	8	0.133	0.1343	Stable
	10	0.166	0.1673	Stable
	12	0.20	0.2013	Stable
iii	4	0.066	0.0673	Stable
	6	0.10	0.1013	Stable
	8	0.133	0.1343	Stable

4.4.2 Unstable Cases

Unstable cases for the SMIB test case are simulated by applying a fault for a longer time duration. For Case i, fault duration is varied from 23 to 26 cycles. For Case ii, the fault duration is varied from 16 to 20 cycles. Similarly for Case iii, the fault duration is varied from 10 to 14 cycles.

Figure 4.13 shows the power oscillations for Case i and fault duration of 23 cycles (0.383 s). The critical clearing angle calculated by algorithm for this case is 0.3703 s. The proposed algorithm detects the swing as an unstable swing at 0.3842 s. Figure 4.14 shows the voltage angle oscillation at the out-of-step breaker location. The voltage angle at the breaker location at the time of detection is 63.35^o which is a favourable angle to operate the out-of-step breaker. The breaker will experience only 103% of the rated voltage during its operation.

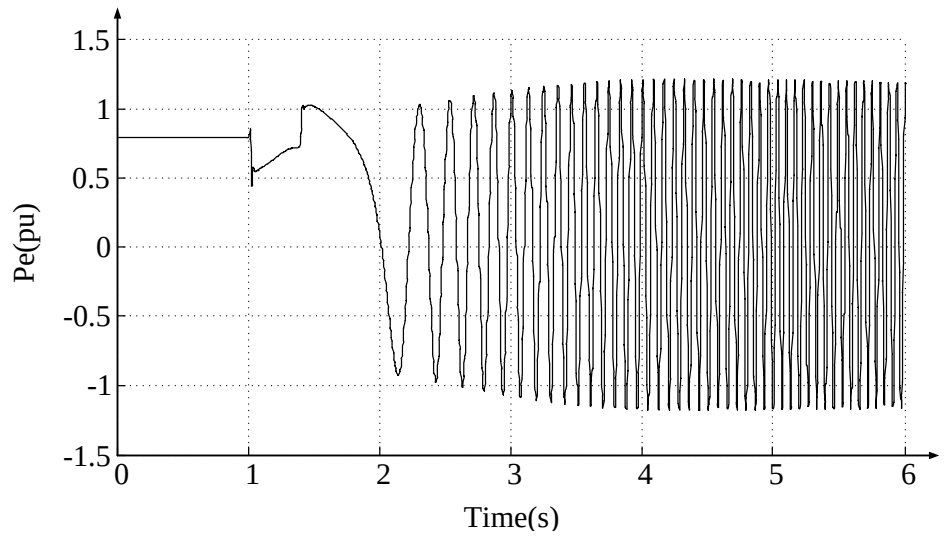

Figure 4.13: Electrical power plot for Case i and fault duration of 23 cycles

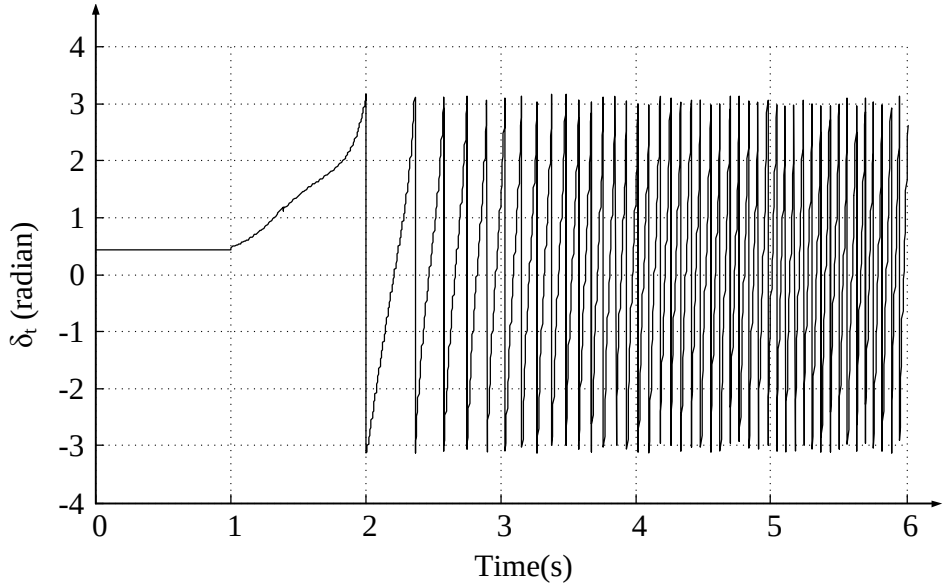

Figure 4.14: Power angle plot for Case i and fault duration of 23 cycles

For Case ii, fault is applied at 1.0 s and is cleared after 18 cycles (0.267 s). The CCT calculated by algorithm for this case is 0.2454 s. The swing is detected as an unstable swing at 0.2684 s. Figure 4.15 shows an unstable power oscillation for the given fault duration, which verifies the correctness of the detection made by the relay. The power angle at the breaker location is shown in Figure 4.16. The breaker angle separation at the time of detection is 58.32^o, which means that the voltage across the breaker during tripping is only 93% of the

rated value.

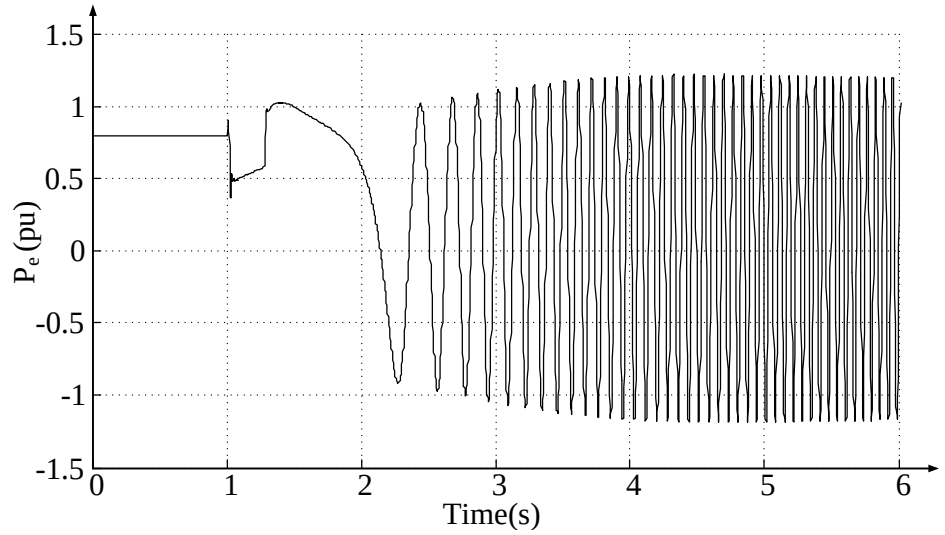

Figure 4.15: Electrical power plot for Case ii and fault duration of 16 cycles

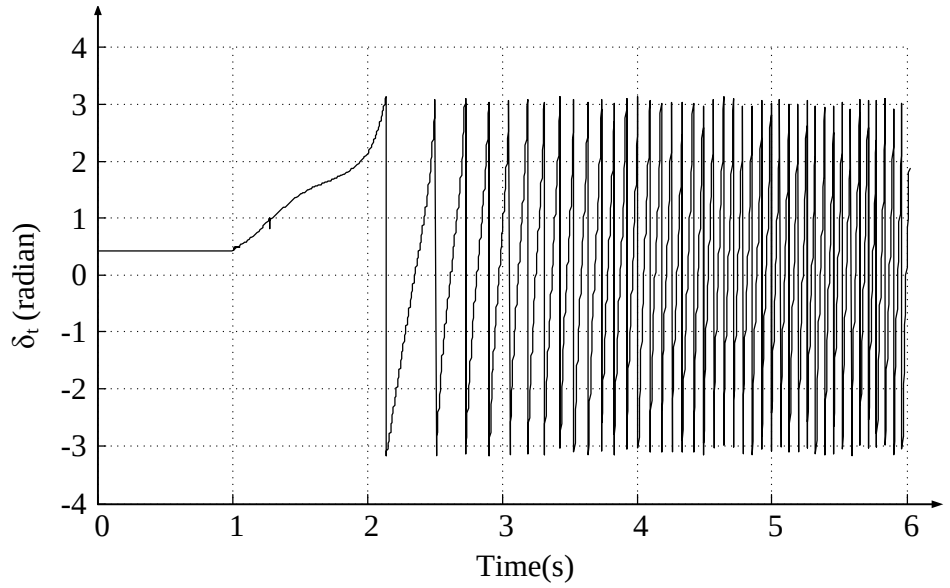

Figure 4.16: Power angle plot for Case ii and fault duration of 16 cycles

Similarly, for Case iii, fault is applied at 1.0 s and is cleared after 10 cycles (0.167 s). The CCT calculated by algorithm for this case is 0.1512 s. The swing is detected as an unstable swing at 0.168 s. Figure 4.17 shows an unstable power oscillation for the given fault duration, which again verifies the correctness of the detection made by the relay. The power angle at the breaker location is shown in Figure 4.18. The breaker angle separation at

the time of detection is 47.73^o, meaning that the voltage across the breaker during tripping is only 77.5% of the rated value.

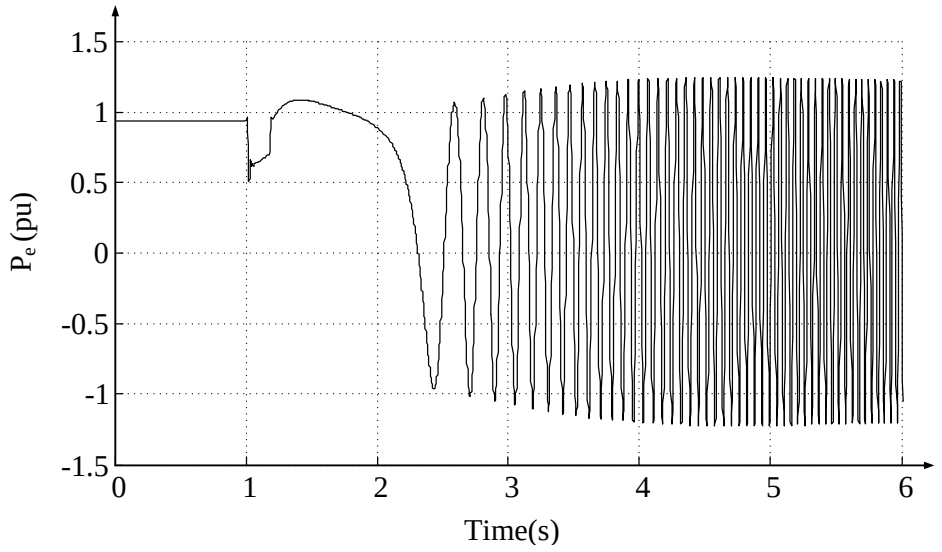

Figure 4.17: Electrical power plot for Case iii and fault duration of 10 cycles

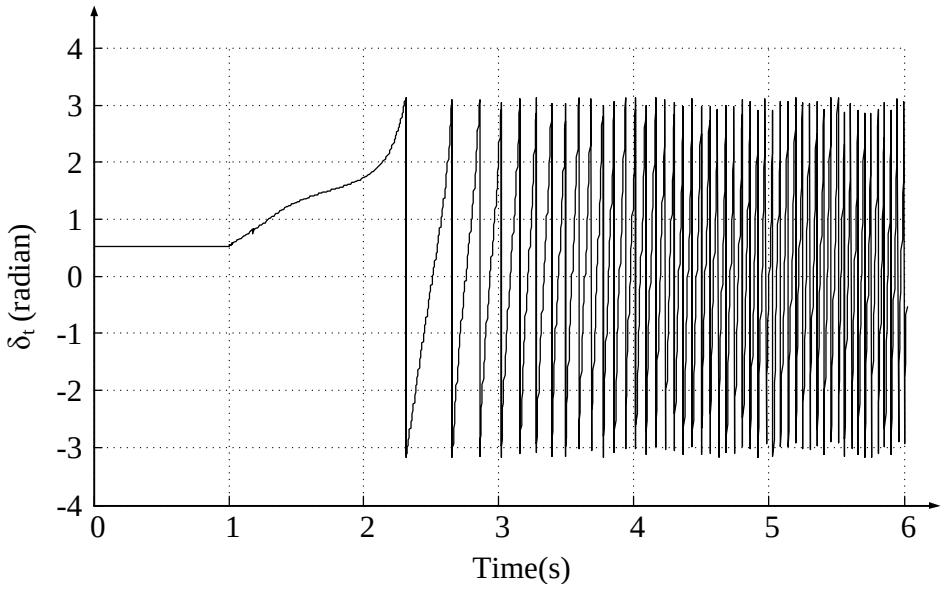

Figure 4.18: Power angle plot for Case iii and fault duration of 10 cycles

Table 4.4: Summary of experimental test results for SMIB unstable cases

Case No.	Fault duration (cycles)	Fault duration (s)	Decision time (s)	Decision	Breaker angle (^{o})
i	23	0.383	0.384	Unstable	65.35
	24	0.40	0.4013	Unstable	70.57
	26	0.433	0.4343	Unstable	77.07
ii	16	0.267	0.268	Unstable	58.32
	18	0.3	0.3013	Unstable	65.25
	20	0.333	0.334	Unstable	72.90
iii	10	0.167	0.168	Unstable	47.73
	12	0.20	0.2013	Unstable	51.61
	14	0.233	0.234	Unstable	56.90

4.4.3 Comparison with State Deviation Technique

The performance of the proposed algorithm is compared with the state deviation approach. The state deviation approach requires the measurement of electrical power and the speed of the generator. The electrical power is calculated in a similar manner as explained in Section 4.3.2.4. The speed of the generator is a low frequency signal which cannot be directly communicated to the relay module developed in ADSP-BF533$^{\text{TM}}$. An amplitude modulation technique based on Double Side Band-Suppressed Carrier (DSB-SC) is used to modulate the low frequency speed signal. The modulation technique is explained in Section 4.4.3.1. The modulated signal is then passed to the relay module and demodulated to retrieve the actual speed signal needed for the instability detection.

4.4.3.1 Double Side Band Suppressed Carrier Modulation

Modulation is a technique which facilitates the transmission of signal through some medium. One of the modulation techniques mostly used for low frequency signal is Ampli-

tude Modulation (AM) . In AM, the signal to be transmitted is multiplied with the carrier signal. The carrier signal is a sinusoid with higher frequency which carries the signal to be transmitted. The magnitude of the modulated signal varies in relation to the amplitude of the signal to be transmitted. DSB-SC is one of the AM technique where the carrier is suppressed during transmission as the information lies only in side bands. Figure 4.19 shows the block diagram of modulation and demodulation process where the m(t) represents the signal to be transmitted. The signal is modulated by multiplying it with carrier signal. The modulated signal is s(t), which is given by Equation (4.6).

$$s(t) = m(t) \times A_c \cos(2\pi f_c t) \tag{4.6}$$

The modulated signal is then sent to relay. Inside the relay, the modulated signal is demod-

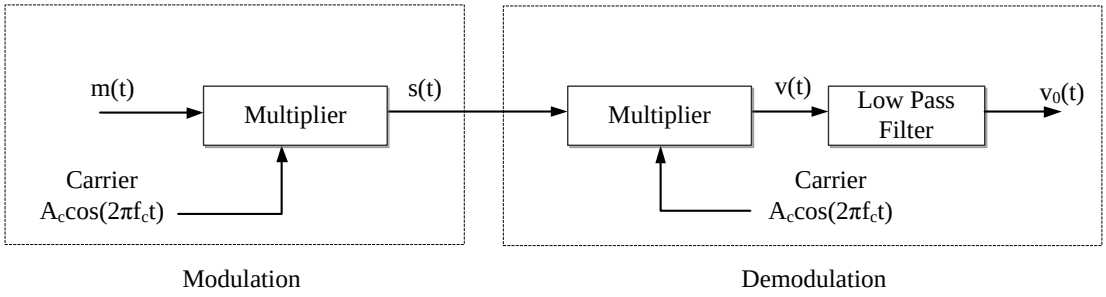

Figure 4.19: Block diagram illustration of the modulation and demodulation process

ulated. First, the signal is multiplied with the same carrier signal. Equation (4.7) gives the resulting signal $v(t)$. The first part of $v(t)$ contains the desired signal and some constants, and the second part of $v(t)$ contains a signal with high frequency. When $v(t)$ is passed through a low pass filter, the second part is filtered out and resulting signal $v_0(t)$ contains only the first part of $v(t)$. The signal $v_0(t)$ can be appropriately scaled to get the required signal $m(t)$.

$$\begin{aligned} v(t) =& s(t) \times A_c \cos(2\pi f_c t) && \text{(4.7a)} \\ =& m(t) \times {A_c}^2 \cos^2(2\pi f_c t) && \text{(4.7b)} \\ =& \frac{m(t) \times {A_c}^2}{2}(1 + \cos 2\pi(2f_c)t) && \text{(4.7c)} \\ =& \frac{m(t) \times {A_c}^2}{2} + \frac{m(t) \times {A_c}^2}{2} \cos 2\pi(2f_c)t && \text{(4.7d)} \end{aligned}$$

$$v_0(t) = \frac{m(t) \times {A_c}^2}{2} \tag{4.8}$$

An example of the modulation and demodulation is shown in Figure 4.20(a)-(d), where (a) represents the signal to be modulated, (b) represents the carrier signal ($c(t)$), (c) represents the modulated signal ($s(t)$), and (d) represents the the signal $v(t)$. After passing the signal $v(t)$ through low pass filter and scaling, the original signal can be obtained. The low pass filter used in this case is a fifth order Butterworth filter with cut-off frequency of 65 Hz. The coefficients of the filter are given in Table 4.1.

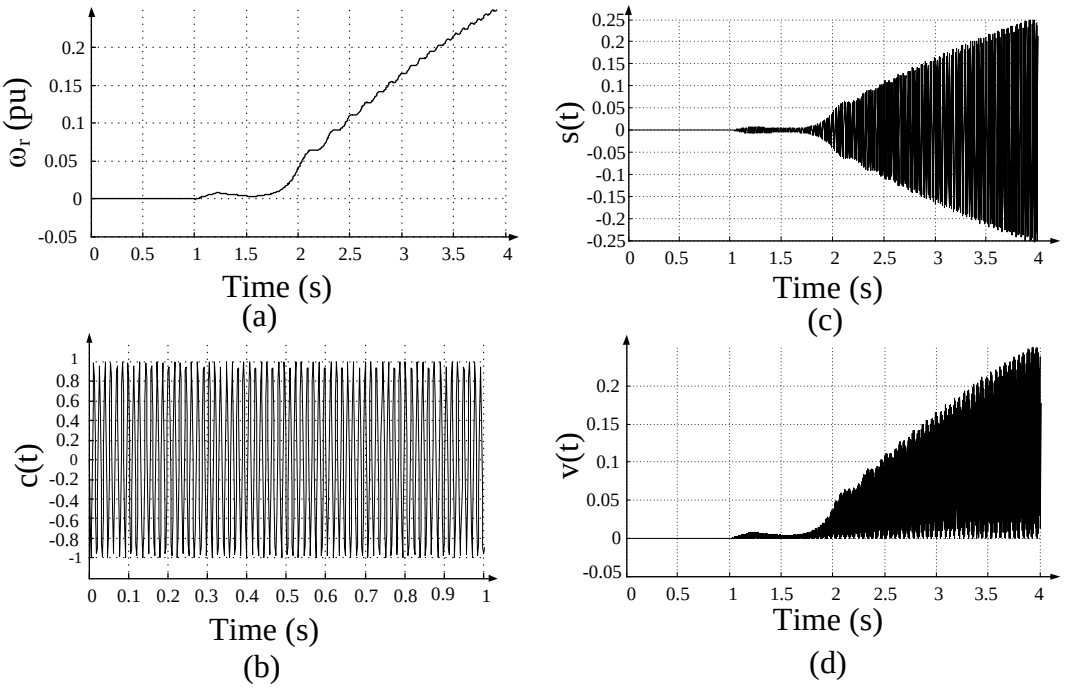

Figure 4.20: An example illustrating modulation and demodulation of a generator speed signal

The demodulated signal is a digital signal of 48000 samples per second. The number of samples are not required for processing electrical power and generator speed signals with frequency of 0.5 to 10 Hz. The signal is therefore downsampled 240 times so that the signal will have 200 samples per second. This facilitates a wider time interval between two consecutive downsampled signals, which can be utilized to perform calculations required by the algorithm.

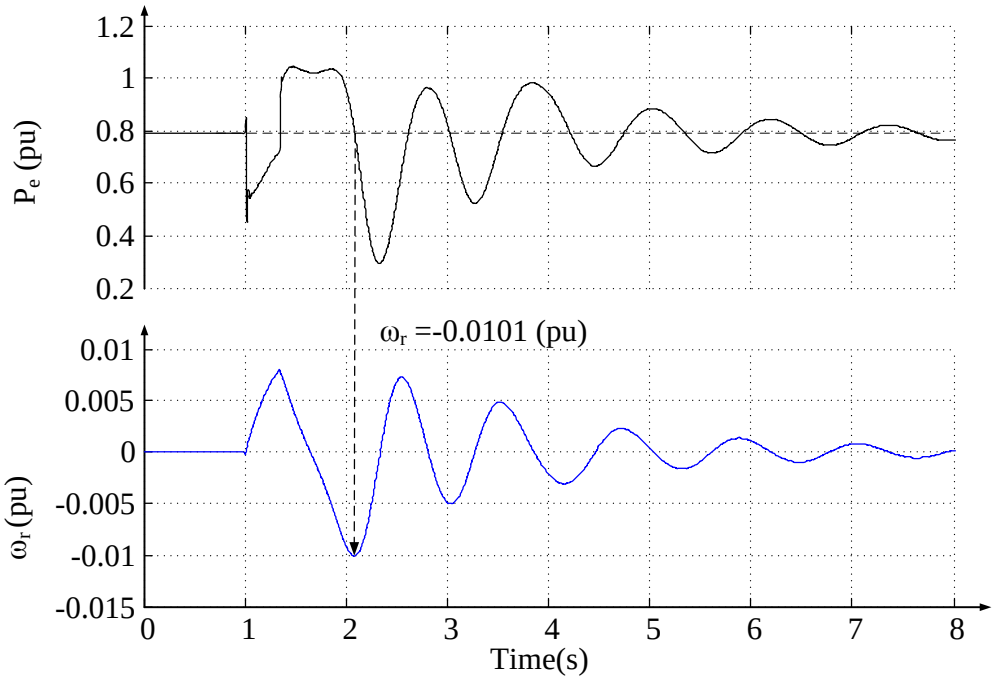

Figure 4.21: Electrical power and speed deviation plots for Case i, fault duration of 20 cycles

4.4.3.2 Test Results

For the test cases generated in Section 4.4, the state deviation approach is also used to make a comparison with the results obtained using the proposed technique. For Case i, Case ii and Case iii, fault durations are varied to get different swing conditions. Some of the test results with state deviation approach are discussed here.

Figure 4.21 shows the electrical power and the speed deviation plot for Case(i) and fault duration of 20 cycles. The speed of the generator at the saddle point of the system is observed to be -0.0101 pu, i.e., machine has relative speed less than the rated speed when it goes from deceleration to acceleration. Hence the swing is detected as a stable swing. The time of detection is 1.0892 s. For the same test case scenario, proposed technique detects the swing as a stable swing at 0.3340 s which is much faster than state deviation approach.

Now the fault duration is increased to 23 cycles. Figure 4.22 shows electrical power and speed deviation where the relative speed of the generator at the saddle point is 0.003899 pu. The swing is therefore detected to be an unstable swing at 0.7540 s. Breaker angle at the

time of detection is 104.40^o. The proposed algorithm detects the swing as an unstable swing at 0.384 s and a lower breaker angle i.e., 65.35^o, which is going to create significantly less stress on the breaker during the current interruption.

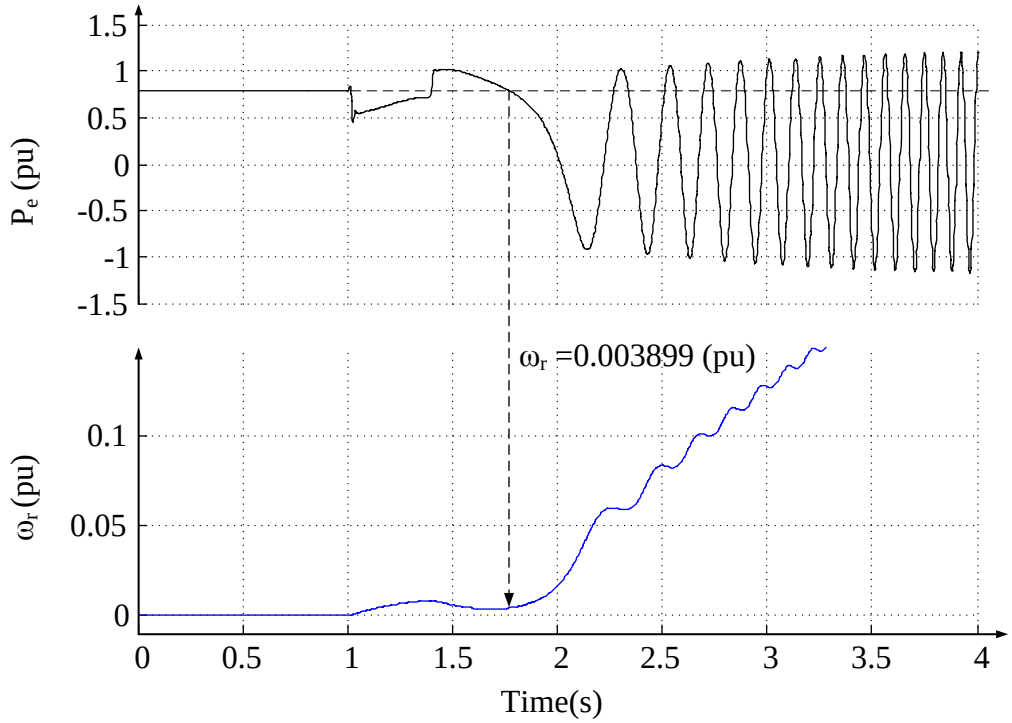

Figure 4.22: Electrical power and speed deviation plots for Case i, fault duration of 23 cycles

Similarly, Figure 4.23 shows the electrical power and speed deviation for Case(ii) and fault duration of 14 cycles. The speed of the machine observed at saddle point is negative (i.e., -0.008993). The swing is therefore detected as a stable swing. The time of detection is 1.0163 s, whereas the detection time for proposed technique is 0.2340 s.

Figure 4.24 shows the electrical power and the relative speed of generator for Case ii and fault duration of 16 cycles. The speed of the generator at the saddle point is found to be 0.001635 pu. The swing is therefore detected to be an unstable swing and the detection time is 0.8729 s. Breaker angle at the time of detection is 106^o. The proposed algorithm detects the swing as an unstable swing at 0.2680 s and at breaker angle of 58.32^o.

At an increased loading condition in Case iii, a fault duration of 8 cycles produces an electrical power and a speed oscillation as shown in Figure 4.25. At the saddle point, the

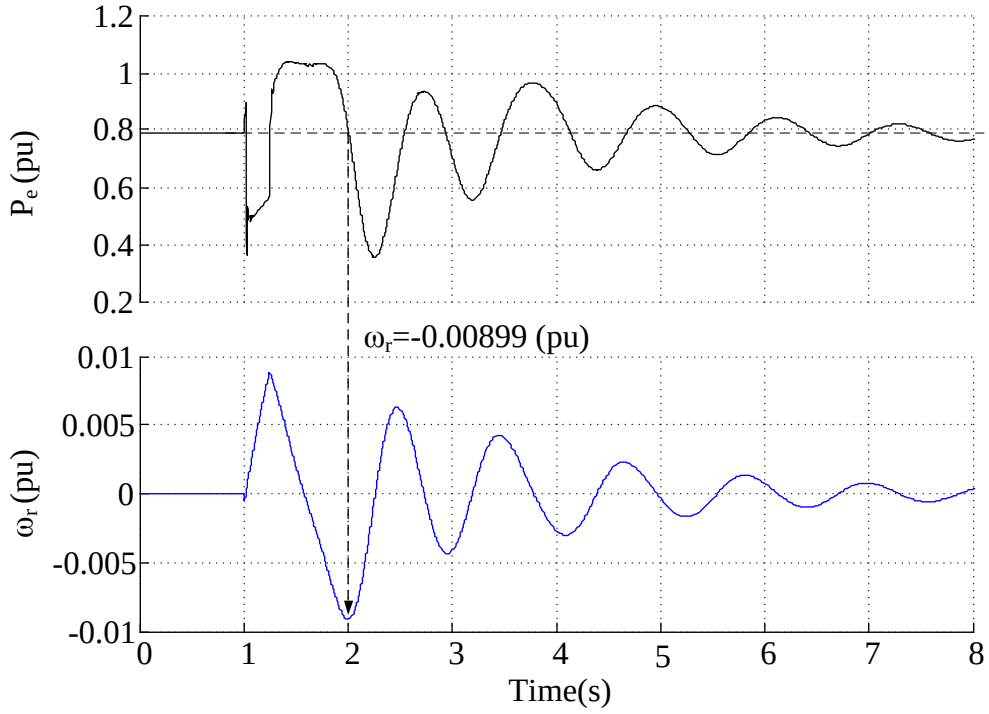

Figure 4.23: Electrical power and speed deviation plot for Case ii, fault duration of 14 cycles

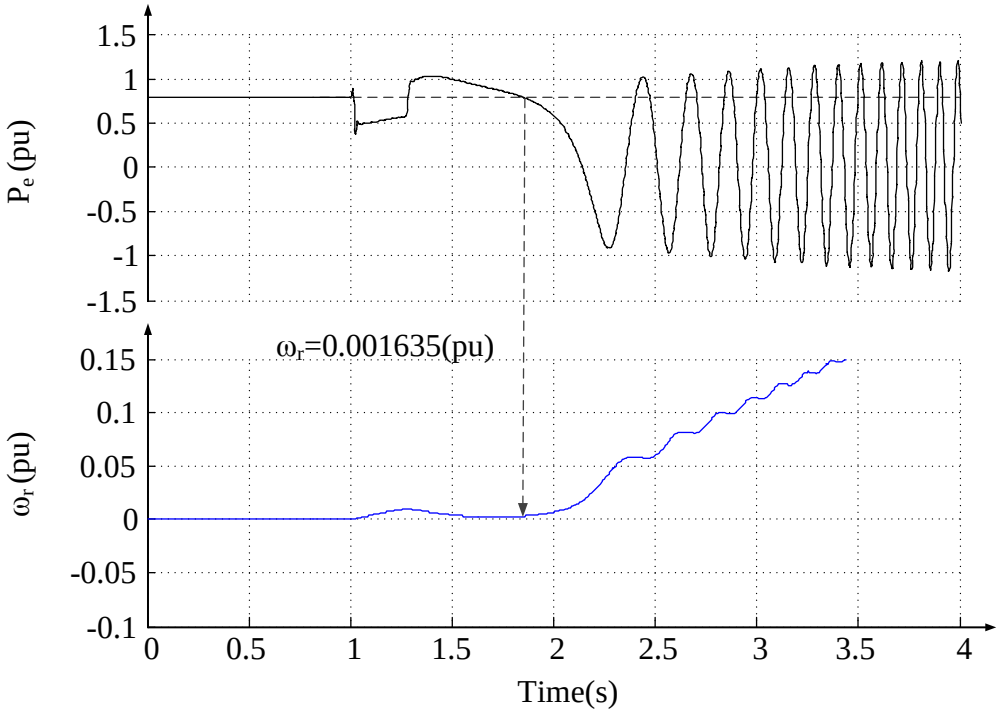

Figure 4.24: Electrical power and speed deviation plot for Case ii, fault duration of 16 cycles

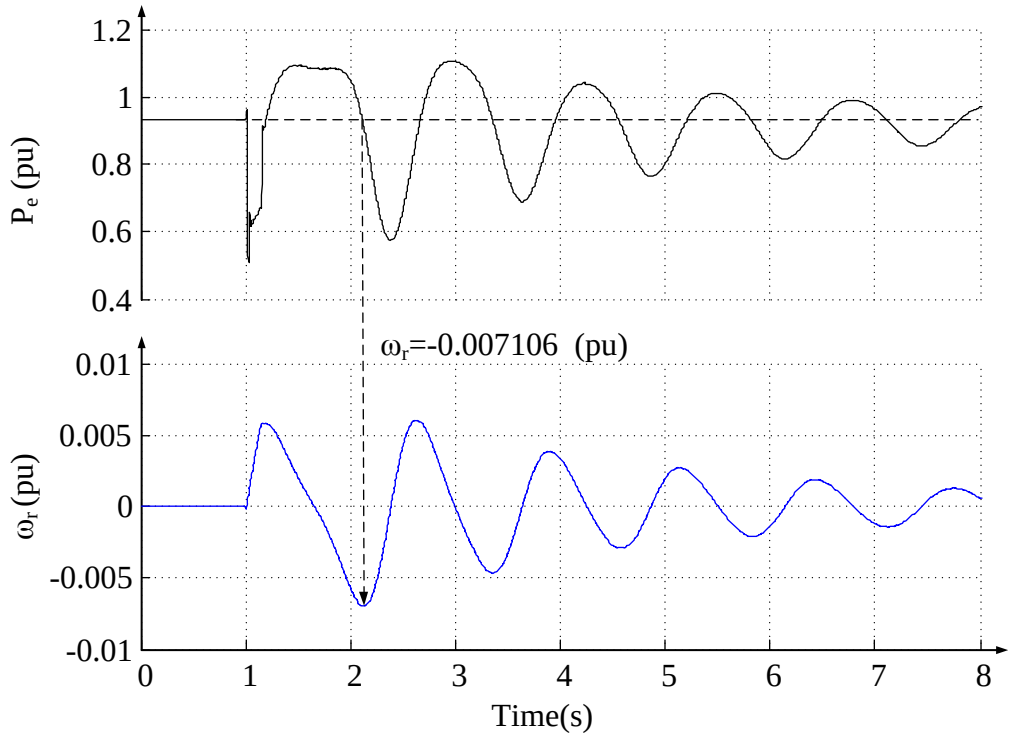

Figure 4.25: Electrical power and speed deviation plot for Case iii, fault duration of 8 cycles

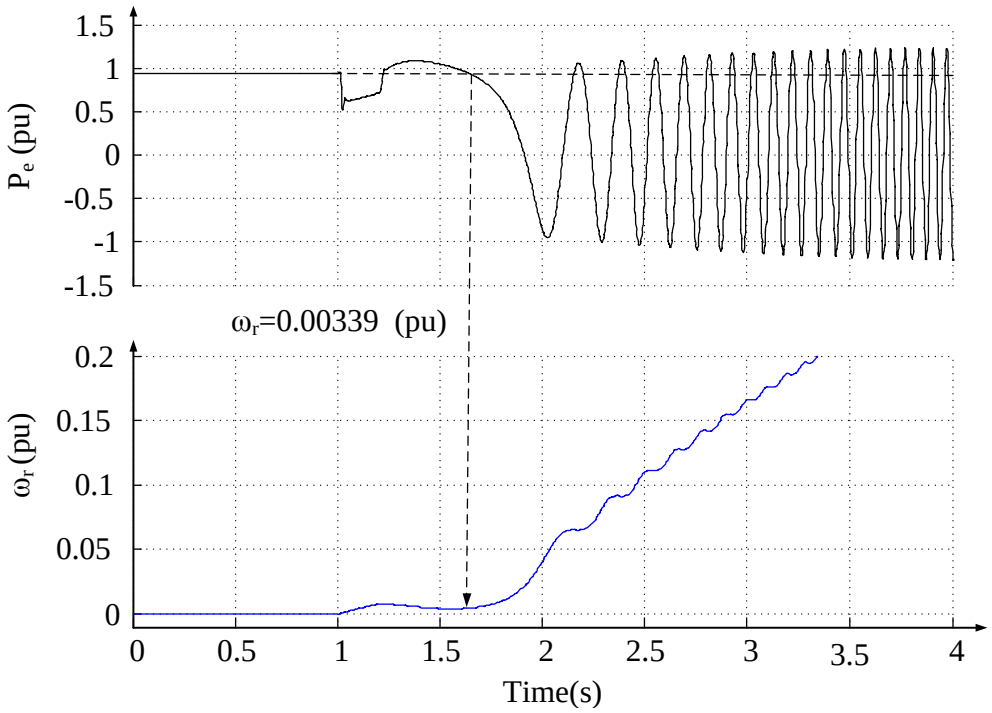

Figure 4.26: Electrical power and speed deviation plot for Case iii, fault duration of 12 cycles

speed of the generator is negative(i.e., -0.007106). Hence the swing is detected as a stable swing. The detection time is 1.1056 s, whereas the proposed scheme detects it at 0.134 s. An unstable scenario, as shown in Figure 4.26, is created using a fault duration of 12 cycles. The state deviation technique detects the swing to be an unstable swing at 0.6067 s, whereas the proposed technique detects it as an unstable swing at 0.2013s.

The test results with the state deviation technique are summarised in Table 4.5.

Table 4.5: Summary of experimental test results for SMIB using state deviation approach

Case No.	Fault duration (cycles)	Fault duration (s)	Decision time (s)	Decision	Breaker angle (^{o})
i	14	0.233	0.8597	Stable	-
	18	0.30	0.9730	Stable	-
	20	0.333	1.0892	Stable	-
	23	0.383	0.7537	Unstable	104.30
	24	0.40	0.7075	Unstable	107.90
	26	0.433	0.6349	Unstable	108.10
ii	8	0.133	0.809	Stable	-
	10	0.166	0.8350	Stable	-
	12	0.20	0.9040	Stable	-
	14	0.233	1.0163	Stable	-
	16	0.267	0.8729	Unstable	106.00
	18	0.3	0.5835	Unstable	107.10
	20	0.333	0.5210	Unstable	108.20
iii	4	0.066	0.9862	Stable	-
	6	0.10	1.024	Stable	-
	8	0.133	1.1056	Stable	-
	10	0.167	0.965	Stable	97.28
	12	0.20	0.6067	Stable	92.18
	14	0.233	0.537	Stable	96.62

4.5 Case Studies: Two Area System

A two area power system consisting of a finite machine in each area (similar to the PSCAD/EMTDC^{TM} two area case study) is modeled using RSCAD^{TM}. The system is simulated for different transient conditions using three phase to ground fault in a line between bus 4 and bus 5. Fault duration is varied to achieve different swing conditions. The system is analysed for three types of swing conditions: stable swing, unstable swing, and multi-swing unstable cases. The first swing stable and unstable swings are detected using the proposed technique based on SPA. The multi-swing unstable cases are detected using a combined algorithm consisting of SPA for finding the first swing instability followed by an additional logic using the state deviation technique (as explained in Section 3.6.2) to find instability during later swings. The test procedure is also explained in Section 3.6.1.

A relay module based on the above explained logics is developed in ADSP-BF533 ^{TM}. The signals required by the relay are electrical power, generator speed and angular separation between two areas, which are communicated to the relay using DSB-SC modulation technique as explained in Section 4.4.3.1. The carrier signal is a cosine wave of 500 Hz with magnitude equal to 0.5. The carrier signal is communicated to the DSP board and is used to demodulate the signals in relay module.

As soon as the two areas start separating beyond 5 degrees after the fault is cleared, the network data stored in the relay are used to reduce the network between two internal generator buses and the SMIB equivalent is carried out to predict the power-angle characteristics. Then, the proposed algorithm based on SPA is used to detect the type of power swing. The procedure takes 56 interrupts (i.e., 1.1667 milliseconds) to detect the power swing after the separation between the generators is detected.

For the proposed algorithm based on state deviation technique, the demodulated SMIB equivalent power signal signal and the SMIB equivalent generator speed are used. The DYP is identified at a sample when $P_m - P_e$ is less than 0 at the previous sample and is greater than 0 at the present sample. Where, P_m in this case is the SMIB equivalent mechanical power. Since the signals are downsampled by 240, the prediction from this technique might

have a maximum error of 5 milliseconds in its detection time.

Two test cases are considered and reported in this thesis. Case 1: Three phase to ground fault applied which is 50 km away from bus 4 [4] on TL-II and the fault is cleared by opening the breakers Brk1 and Brk2. Case 2: Three phase to ground fault applied at 75 km away from the bus 4 and the fault is cleared by opening the breakers Brk1 and Brk2. The test results for different fault durations are discussed in following sections.

4.5.1 Test Results: Stable and Unstable Swings

For test Case 1, fault duration is varied from 4 cycles to 20 cycles. For the fault duration of 6 cycles, the two areas oscillate with each other as shown in Figure 4.27, which shows the voltage angle separation of generator buses. During post fault condition, as soon as the angular separation exceeds 5 degrees from the initial post fault value, SMIB equivalent procedure is carried out. Using SMIB equivalent parameters, CCT of the system is calculated. The SMIB equivalent parameters calculated for the Case 1 are shown in Section 3.6.3. Using the parameters, algorithm based on SPA calculates the CCT which is 0.2704 s. The relay detects the swing as a stable swing and sends the block signal to breakers at 0.2672 s. Figure 4.28 shows the stable SMIB equivalent electrical power oscillation for the fault duration of 6 cycles.

Similarly for Case 2, fault is cleared at 8 cycles (0.133 s). Figure 4.29 shows the angular separation between generator buses due to this fault. The calculation for SMIB equivalent is started when the angular separation exceeds 5 degrees. The details of SMIB equivalent parameters calculation is given in Section 3.6.3. The CCT calculated for this case is 0.3679 s. Comparing the fault clearing time and CCT, the proposed algorithm detects the swing as a stable swing and sends a block signal to the breakers at 0.2540 s. The SMIB equivalent electrical power oscillation observed from the electromagnetic transient simulation is shown in Figure 4.30.

For Case 1, out-of-step conditions are observed with the fault durations of 18 and 20

[4]Refer to Appendix B.2 for the figure

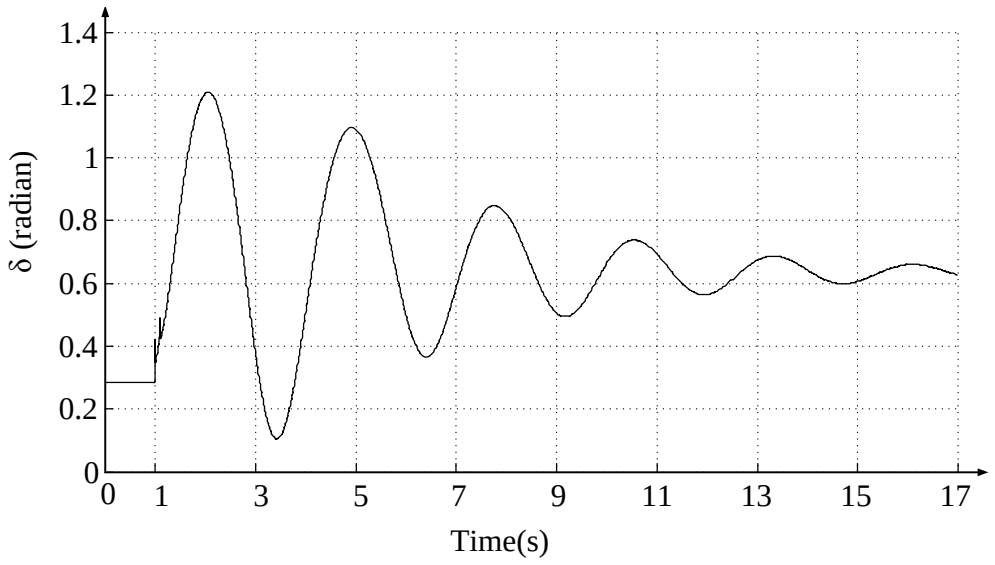

Figure 4.27: SMIB equivalent power angle plot for Case 1 and fault duration of 6 cycles

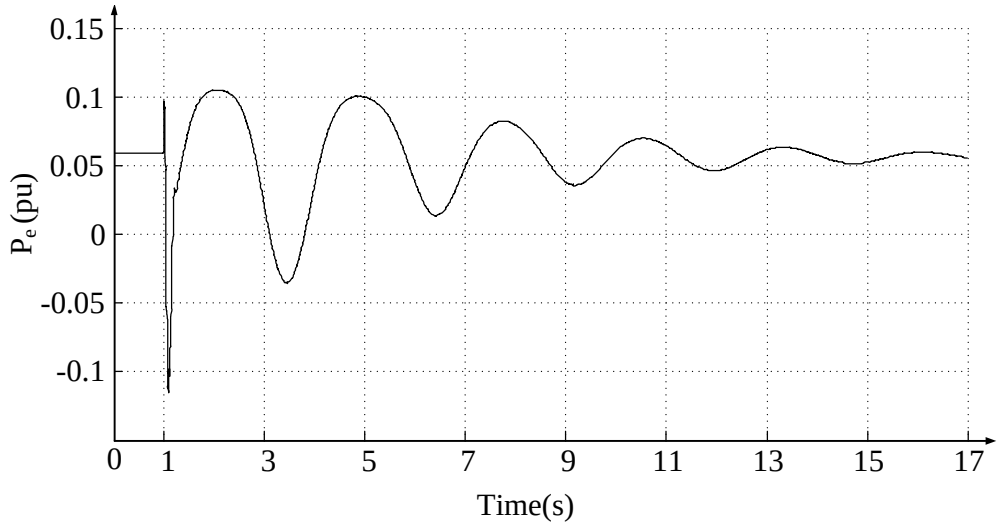

Figure 4.28: SMIB equivalent electrical power plot of for Case 1, fault duration of 6 cycles

cycles. The angular separation between the generator buses for fault duration of 18 cycles is shown in Figure 4.31. A similar procedure, as explained for the stable cases, is used to calculate the CCT. In this case the fault clearing time is greater than CCT (i.e., 0.2704 s), and the proposed algorithm detects it as an out-of-step condition. We can see from the angles between generator buses that it starts slipping between 180 and -180 degrees, showing an unstable scenario. The detection is made at 0.4032 s. The angle at the time of detection is 54.9630 degrees. The unstable SMIB equivalent power oscillation observed from simulation

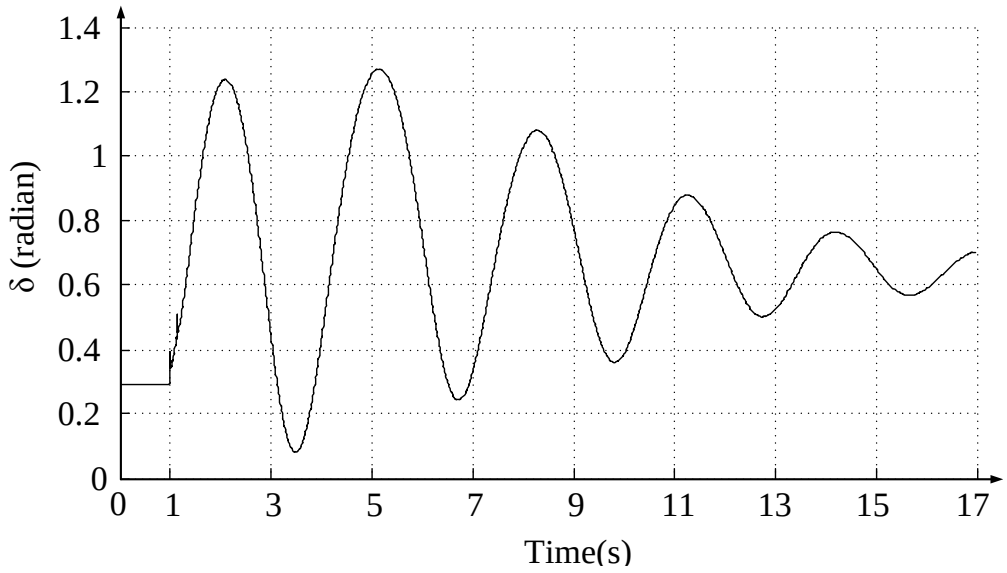

Figure 4.29: SMIB equivalent power angle plot for Case 2, fault duration of 8 cycles

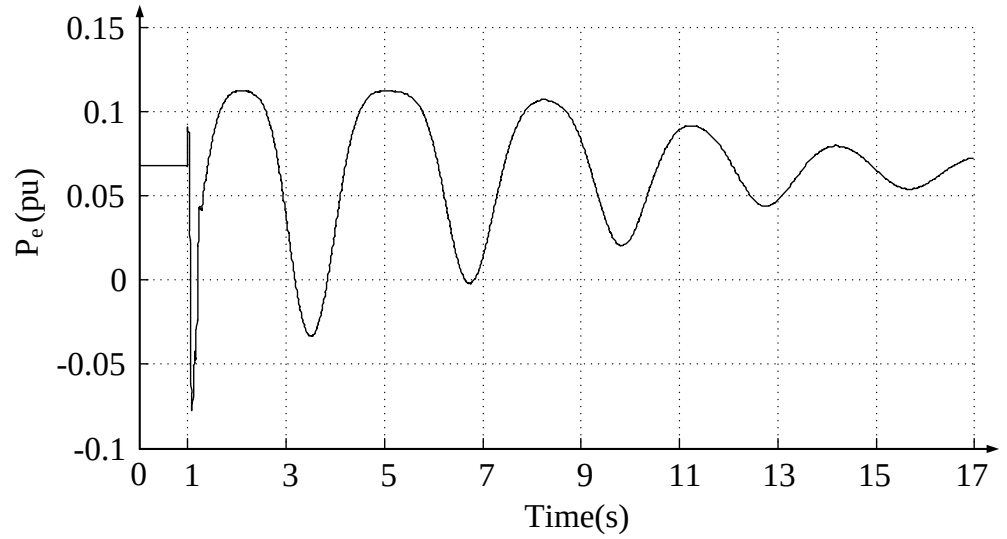

Figure 4.30: SMIB equivalent electrical power plot, Case 2 and fault duration of 8 cycles

for the test case is shown in Figure 4.32.

Similarly, out-of-step conditions for Case 2 are simulated with the fault durations of 24 and 26 cycles. Figure 4.33 shows the angular separation between two generator buses for the fault duration of 24 cycles (0.4 s). The CCT calculated by the proposed technique is 0.3679 s. The fault clearing time is greater than the CCT, hence the relay sends the trip signal to the breakers. The angle of separation at the time of detection is 91.5010 degrees. The

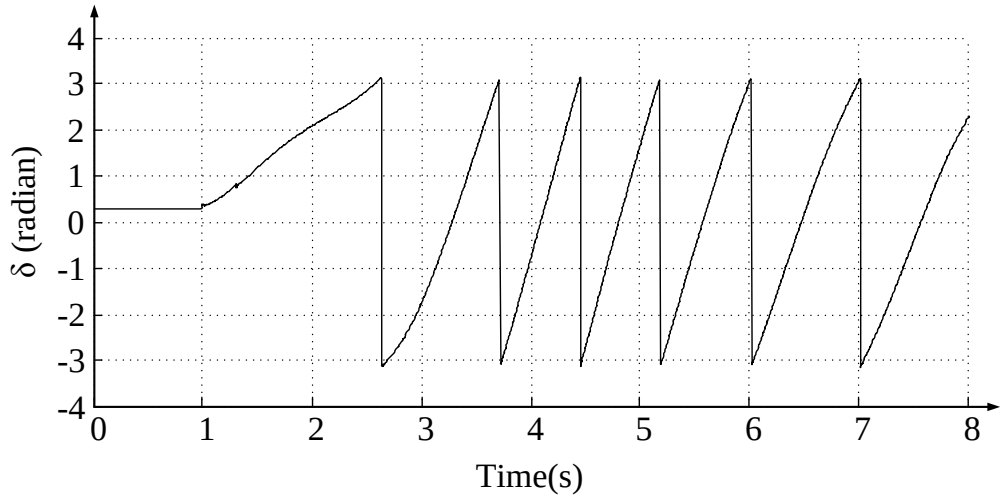

Figure 4.31: SMIB equivalent power angle plot for Case 1, fault duration of 18 cycles

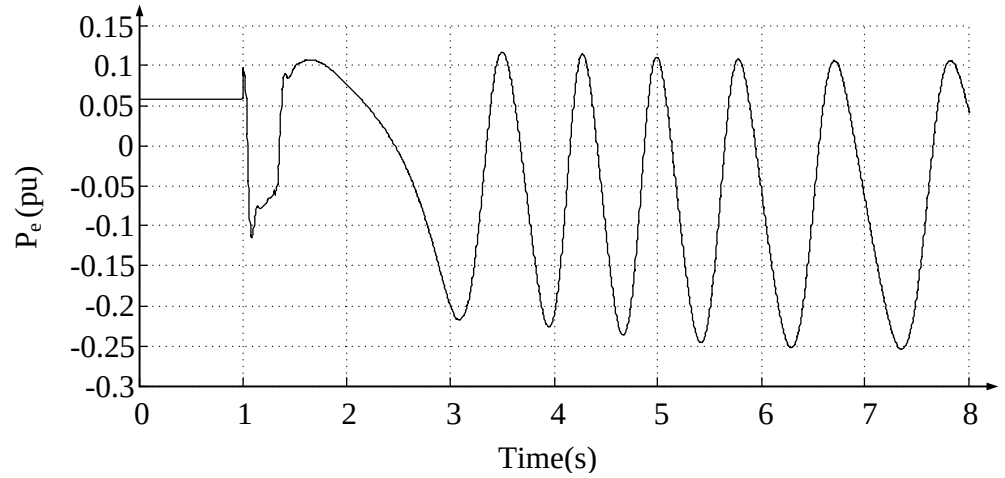

Figure 4.32: SMIB equivalent electrical power plot for Case 1, fault duration of 18 cycles

SMIB equivalent electrical power oscillation is shown in Figure 4.34 which actually verifies the correct detection made with the proposed technique.

The power swings are also detected using the proposed state deviation technique. The test results for the stable and unstable cases using algorithm based on SPA and state deviation technique are shown in Table 4.6.

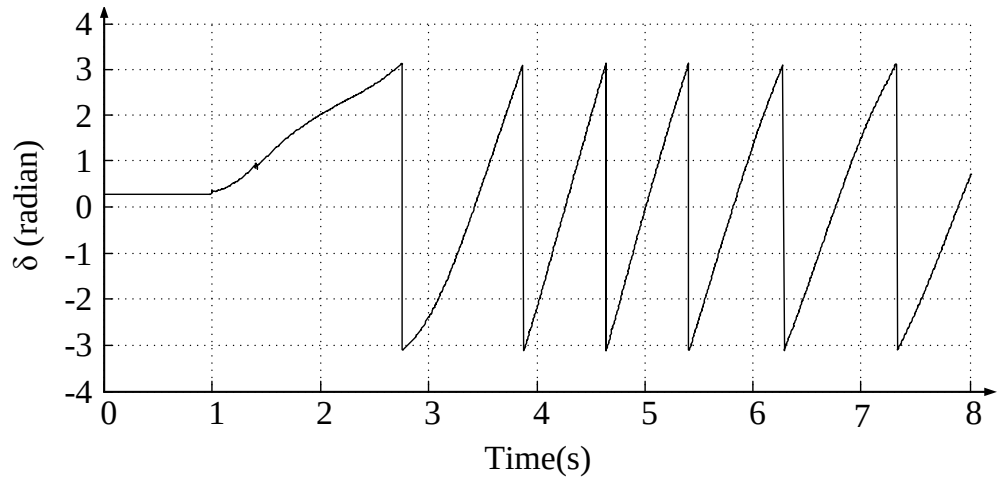

Figure 4.33: SMIB equivalent power angle plot for Case 2, fault duration of 24 cycles

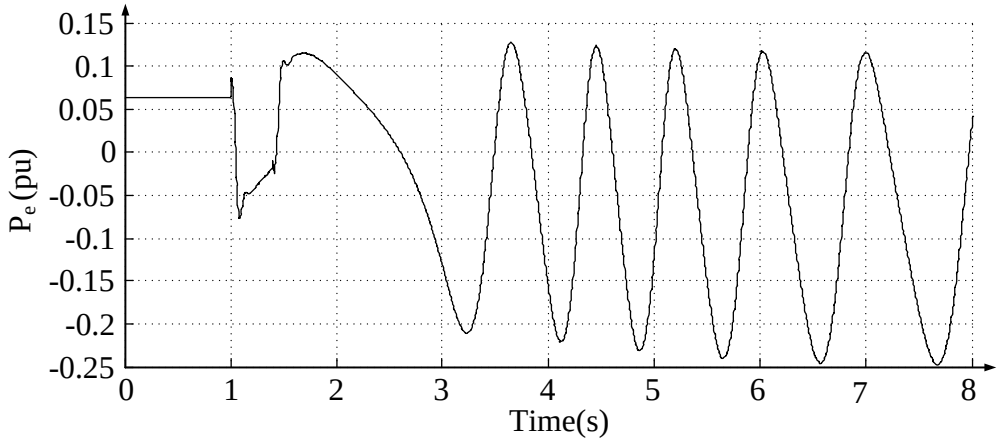

Figure 4.34: SMIB equivalent electrical power plot for Case 2, fault duration of 24 cycles

4.5.2 Test Results: Multi-swing Instability

For Case 1, multi-swing instability cases are observed for the fault durations of 12 cycles, 14 cycles and 15.6 cycles. Figure 4.35 shows the SMIB equivalent electrical power and the generator speed for fault duration of 12 cycles (0.2 s). The algorithm based on SPA detects the swing as a stable swing at 0.316 s. Then, the additional logic based on state deviation technique starts monitoring the speed of SMIB equivalent at every DYPs. In this case, SMIB equivalent speed at DYP_1 and DYP_2 are found to be negative. This shows that the system is stable for first two swings. However, at DYP_3, the speed measured is 0.003917 pu which is positive. This indicates the system is going out-of-step. The detection is made at 8.19 s and

Table 4.6: Summary of experimental test results for stable and unstable cases in a two area system using proposed algorithm based on SPA

Case No.	Fault duration	SPA		SDT***		Decision
	(cycles)	T_d^*	δ_d^{**}	T_d	δ_d	
Case 1	4	0.2320	-	1.806	-	Stable
	6	0.2672	-	1.838	-	Stable
	18	0.4032	54.96	1.165	132.52	Out-of-step
	20	0.4160	58.15	1.027	131.09	Out-of-step
Case 2	6	0.2768	-	1.9040	-	Stable
	8	0.2540	-	1.8620	-	Stable
	24	0.4751	54.96	1.208	130.35	Out-of-step
	26	0.4920	60.82	1.104	131.95	Out-of-step

*T_d: Time of detection in seconds, **δ_d: Angle of detection in degrees

***SDT: State Deviation Technique

the detection angle is 113.44 degrees. The ω signal modulation and demodulation process is shown in Figure 4.36. Test results for other fault durations are presented in Table 4.7.

Similarly, multi-swing instability conditions for Case 2 are observed for fault durations of 12 cycles, 18 cycles and 21.6 cycles. Figure 4.37 shows the SMIB equivalent electrical power and the generator speed for fault duration of 21.6 cycles (0.36 s). The algorithm based on SPA detects the swing as a stable swing at 0.456 s. Then, the additional logic based on state deviation technique starts monitoring the SMIB equivalent speed at every DYPs. In this case, SMIB equivalent speed at DYP_1 is found to be negative (i.e., -0.009475 pu). This shows that the system is stable for first swing. At DYP_2, the SMIB equivalent speed is 0.006935 pu which is positive and indicates the system is going out-of-step. The detection is made at 4.578 s and the detection angle is 126.10 degrees.

Test results for other fault durations are presented in Table 4.7.

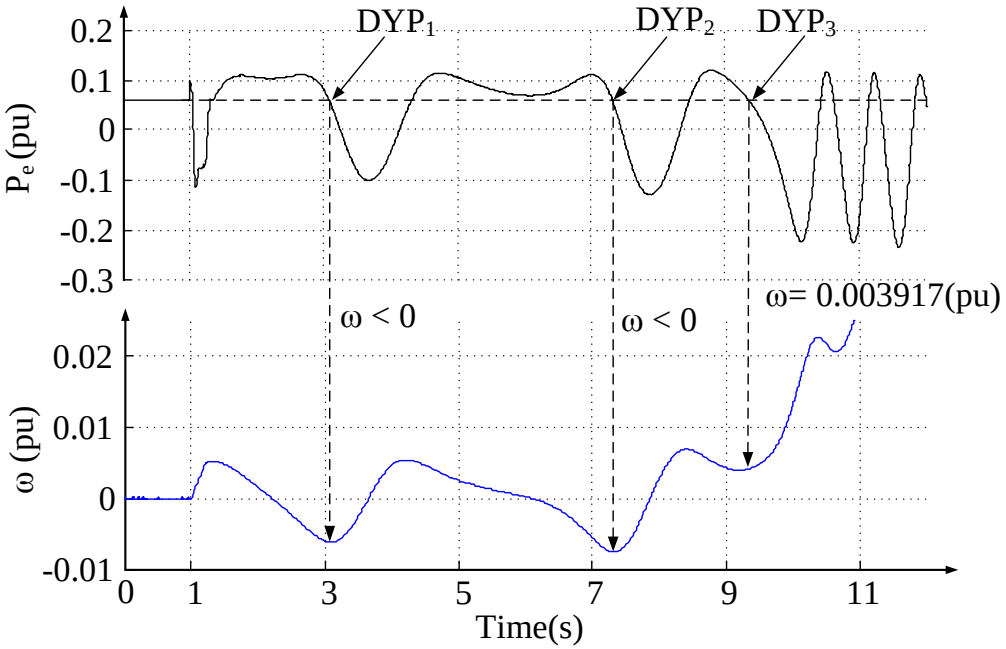

Figure 4.35: SMIB equivalent electrical power and speed plot for Case 1, fault duration of 12 cycles

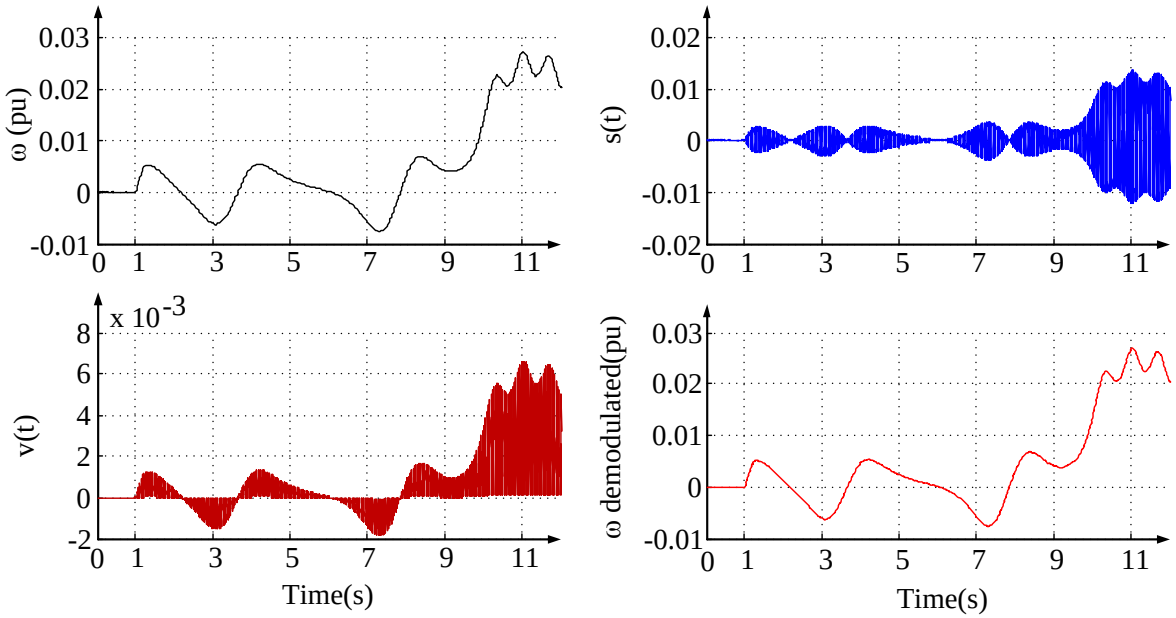

Figure 4.36: Modulation and Demodulation of ω signal for Case 1, fault duration of 12 cycles

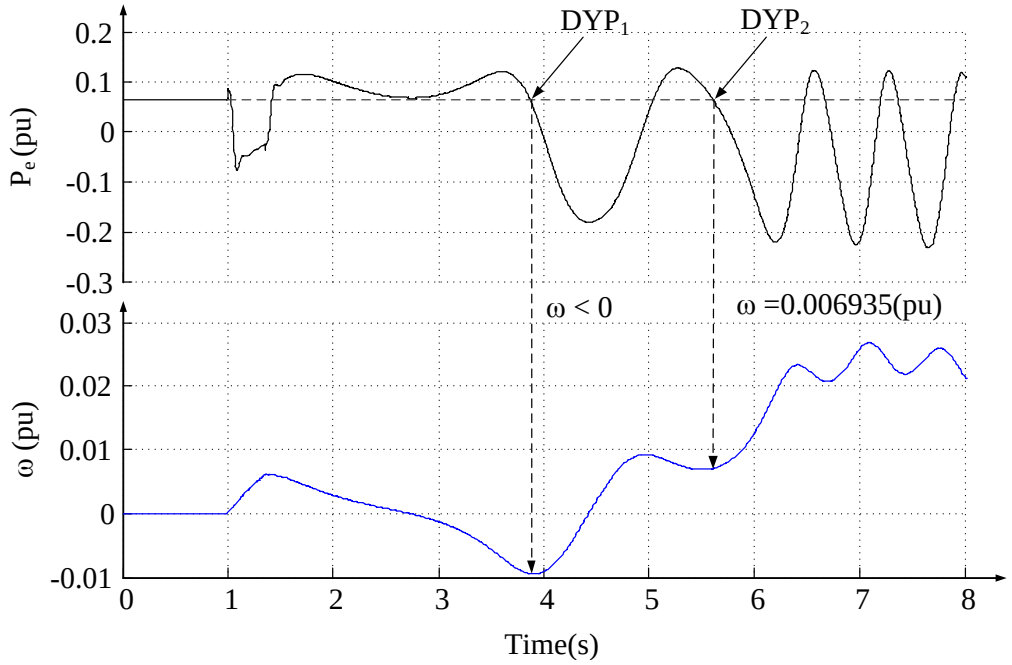

Figure 4.37: SMIB equivalent electrical power speed plots for Case 2, fault duration of 21.6 cycles

Table 4.7: Summary of experimental test results for multi-swing instability detections in a two area system

Case No.	Fault duration (s)	Detection time (s)	Detection angle (deg)	ω (pu)	DYP at detection
(1)	12	8.19	113.44	0.003917	3^{rd}
	14	4.5010	127.71	0.003947	2^{nd}
	15.6	4.6100	131.15	0.005845	2^{nd}
(2)	12	8.16	129.08	0.002108	3^{rd}
	18	4.427	127.02	0.003488	2^{nd}
	21.6	4.578	126.10	0.006935	2^{nd}

4.6 Summary

The out-of-step relay using state plane analysis and state deviation technique were modeled in a digital signal processing board (ADSP BE533), and closed loop testing was performed using the real-time simulator RTDS^{TM}. A SMIB system and two area power system configuration was used for the experimental verification studies. The detection of the stable and unstable swings in real time for the SMIB test system, using algorithm based on SPA was shown in Table 4.3 and 4.4. The relay took only 0.291 ms to decide the stability after the fault clearing information is received. Table 4.5 shows the detection of power swing using state deviation technique for SMIB test system. A comparison between the two techniques based on SPA and state deviation technique shows that the proposed technique using SPA detects the power swing much faster than the later one. Similarly the relay is tested for a two area system and the real time detection of the power swings are reported in Table 4.6. Multi-swing instability conditions were detected using a combined relay algorithm consisting of SPA and state deviation approach. Since first swing type of instabilities are the most common type in power system compared to multiswing instabilites, the SPA technique was used first for the first swing instability to ensure faster prediction. If the instability happened at a subsequent swing, the relay resorted to the state deviation approach to find the later condition. Obviously the state deviation solution is not going to be as fast as for the first swing, but this combined logic facilitated a straightforward and effective way for finding multi-swing instabilities. Multi-swing instability results for two area system using real time simulation studies are reported in Table 4.7

Chapter 5

Out-of-Step Prediction in Large Multi-Machine Power Systems

5.1 Introduction

This chapter first discusses the current practices for out-of-step detection in a multi-machine power system and the difficulties associated with the techniques. Then the extension of the proposed algorithm for multi-machine system is presented. An IEEE 39-bus test system (New England test system) is modeled in PSCAD/EMTDC^{TM}, and the proposed algorithm is tested by creating various transient scenarios. In addition, the other two techniques discussed in this thesis for out-of-step detection namely – state deviation technique (Section 2.6.6) and time domain energy equilibrium criterion – (Appendix F, [41]) are also used for comparison.

5.2 Out-of-Step Protection in Multi-Machine Power System

Power systems have grown in size and complexity with significantly large distances between generating plants and load areas. The different generating plants are interconnected so that the entire system operates in a more reliable fashion, i.e., there is more than one generation source available to meet the load demand in case of a failure of one of the generators. When such large multi-machine systems are subjected to a disturbance, interarea oscillation occurs in the transmission lines interconnecting the different areas of the system, i.e.,

a large group of generators in one area oscillate with respect to a large group of generators in another area. If the disturbance is severe, it may lead to a loss of synchronism condition in the system with different areas separating from each other [42]. Protection against loss of synchronism is therefore of paramount importance in large power systems, as such loss may cause widespread blackouts. As discussed before, out-of-step protection is often done by distance relays and the natural tripping of the distance element is allowed during out-of-step conditions. The tripping may be at a non-optimal angle and location which might cause unwanted outage of the other lines and generators from the system [16]. Application of the conventional blinder based technique in a large power system involves transient stability studies covering many possible stressed operating conditions, and the determination of optimal location of the out-of-step relay would be another big challenge.

Literature review shows that a number of methods have been proposed to find instability conditions in a multi-machine system. A recent paper [24] found the instability condition based on the classification of post-disturbance voltage trajectories. The method estimates the similarity of the post-disturbance voltage trajectories of the generator buses after the disturbance to some pre-identified templates. The instability prediction is done by a classifier which uses as inputs the similarity values calculated for different generator bus voltages. The method needs several offline contingency analysis runs to find stable and unstable cases and then an extensive training to obtain the required classification. Reference [43] introduced an online detection technique for loss of synchronism based on the energy function criterion using local measurements of voltage and currents. The technique has been successful to detect instability but requires detailed evaluation of energy functions for the system. The detection is based on local measurements on the lines where the swing rate is relatively slower and hence the detection time is longer. Conventional blinder schemes and SCV techniques explained in [6], [15] and [16] are only applicable for two machine equivalent system. Devising a blinder scheme for a multi-machine system is not clear cut. Extended equal area criterion (EEAC) is one of the most popular techniques to study the stability of the multi-machine system. Reference [19] describes the EEAC, which assumes the power system as a two-machine model, where one area (machine) oscillates against the rest of the system. The

critical group of machines is found by forming a list of candidate critical machines from the initial acceleration values and then computing CCTs for each of the candidate machines. Among these lists of candidates, the ones which give the smallest CCT are identified as the critical group of machines. The main difficulty associated with EEAC is that as the system size increases, the number of CCT calculations will also increase, requiring a huge computational effort.

The proposed SPA algorithm is applied to the multi-machine system with the assumption that the machines will separate into two groups. This is a fairly valid assumption, because whenever a disturbance occurs in a power system, a group of generators tends to oscillate with another group of generators, forming two coherent groups. The separation of machines is found by real time coherency analysis, which will be discussed later in Section 5.2.1. Each group is represented with an equivalent machine, thereby reducing the two groups of machines into a simple two machine system. The inertia of the equivalent machines is equal to the respective sum of inertias of all machines in the group, and the angle is equal to the center of angle (COA) of all the machines in the group. The two machine system is simplified further as a single machine infinite bus system. The formulation of SMIB equivalent is discussed later in Section 5.2.2. The proposed SPA algorithm is then used to find the CCT of the equivalent single machine system. This CCT value is compared to the fault duration value to predict the instability in the large system. The out-of-step tripping is then done on pre-selected lines to restore the stability of the system.

5.2.1 Real Time Coherency Determination

The generators in a coherent group oscillate together. A coherent group of generators can be identified by looking at the individual generator swing curves. Reference [44] described a technique based on direct comparison of rotor angle deviation at post fault unstable equilibrium point with pre-fault and during fault rotor angles to determine the coherency in early stages of the disturbance. The authors determine the coherency of the generators in the later part of the disturbance by checking the transfer admittance distance between generators. Reference [45] and [46] proposed coherency analysis using generator swing curves. The

literature review shows that the comparison of generator swings curves are popularly used to determine the coherency among the generators. A real time coherency study uses an online measurement of generator bus voltage angles to determine the coherency in the early part of the post fault condition. The coherency in later part of the disturbance is determined using generator internal voltage swing curves.

In this research, a time domain simulation is run for the system under investigation (IEEE 39-bus test system), and the generator bus voltage angle separation from a reference generator bus is measured at every simulation time step. The reference generator forms a group and the criterion to check whether the generator being compared falls in the same group is given by Equation (5.1). Any generator violating the criterion forms a new group.

$$\Delta\theta_i - \Delta\theta_r < \epsilon \tag{5.1}$$

where ϵ is the specified tolerance in degrees, i represents the machine being clustered, and r represents the reference generator. A tolerance of 5 degrees is selected for this study. Some examples of real time coherency determination in IEEE 39-bus test system are discussed below.

For a three phase fault applied at bus 5 for a fault duration of 110 ms, the generator bus voltage swing curves with respect to the reference generator bus (generator 1 at bus 39) are shown in Figure 5.1. The generators at buses 30 to 38 start separating from the reference generator bus during post fault condition and as soon as all the generators bus voltage angles separate beyond 5 degrees, the coherency between the generators at buses 30 to 38 is identified. The coherency between the generators is also confirmed using the internal voltage angle deviation of the generator groups with respect to the reference generator and is shown in Figure 5.2. Similarly, for the fault at bus 27 and fault cleared after 110 ms, the generator bus voltage angle with respect to the reference generator bus is shown in figure 5.3. The generators (at bus 30 to 38) separate from the reference generator bus at bus 39. The coherency among generators from 30 to 38 is detected at 0.203 s. The coherency between the generators at bus 30 to 39 can also be seen from the generator internal voltage angles separation, which is shown in Figure 5.4. As soon as all the generators bus voltage angles separate from the reference generator bus voltage angle beyond 5 degrees and by also

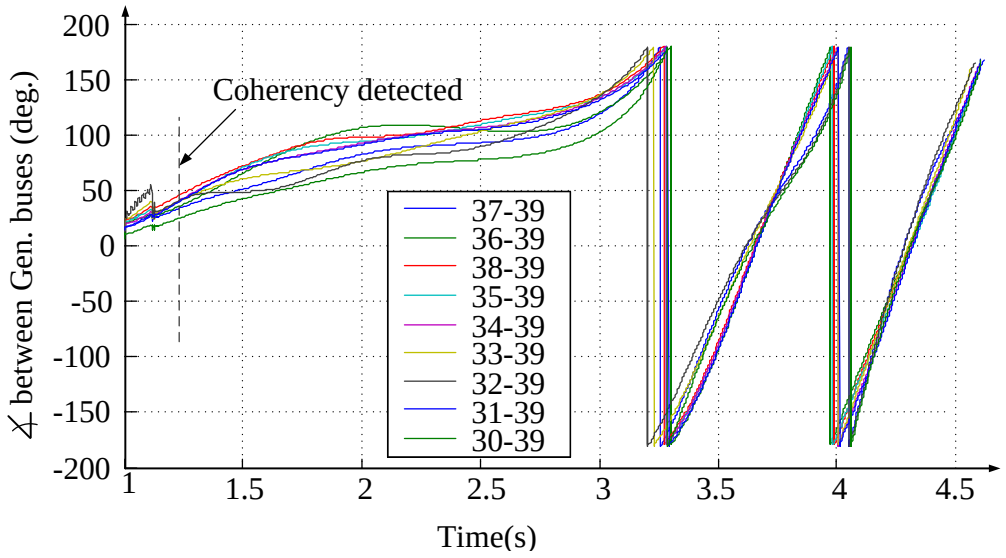

Figure 5.1: Generator bus voltage angle difference for three phase fault at bus 5 and fault duration of 110 ms

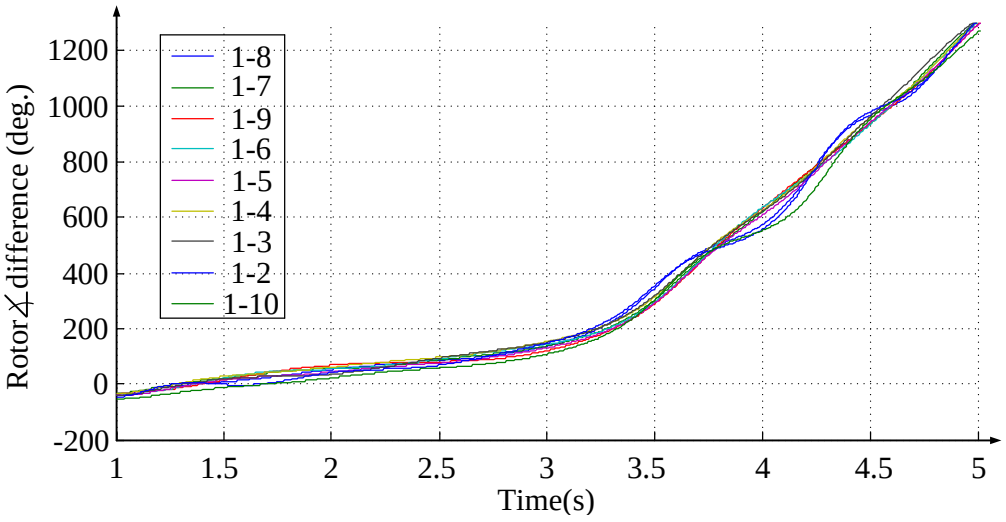

Figure 5.2: Rotor angle differences for the same three phase fault at bus 5 and fault duration of 110 ms

observing the internal voltage angles, coherency between the generators at bus 30 to 38 is identified.

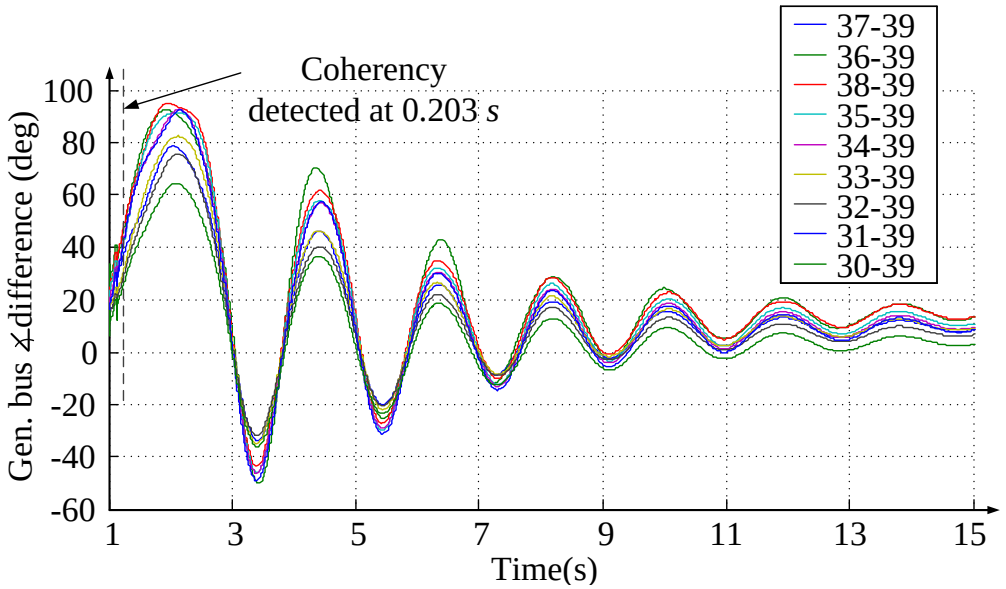

Figure 5.3: Generator bus voltage angle difference for the fault at bus 27 and fault duration of 110 ms

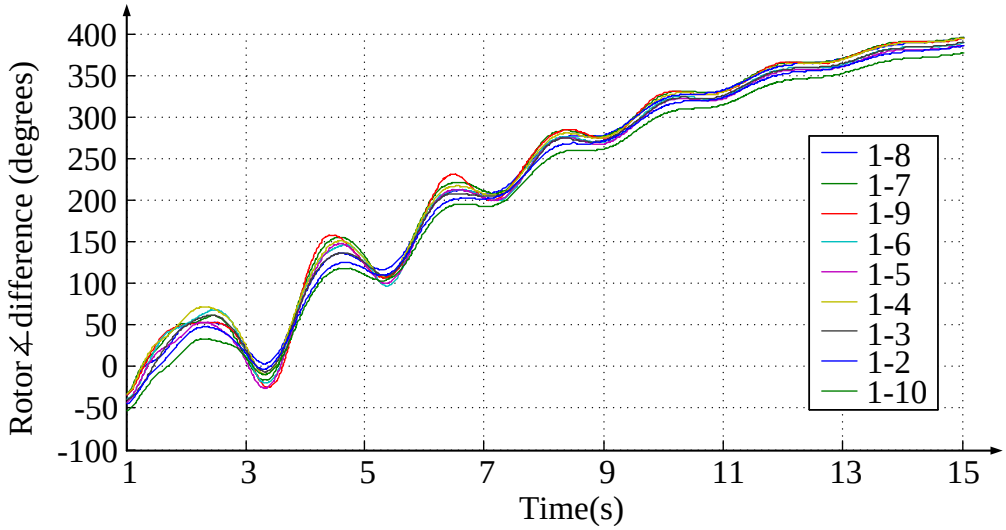

Figure 5.4: Rotor angle difference for the fault at bus 27 and fault duration of 110 ms

5.2.2 Formulation of SMIB Equivalent

The proposed relay uses the technique explained in [19] to obtain SMIB equivalent of multi-machine system. It approximates the multi-machine power system with the classical model, where each generator is represented with a constant voltage source behind the transient reactance and each load as a constant impedance. With the classical model, the

generator dynamics are described by Equation (5.2) [19].

$$\dot{\delta}_i = \omega_i, \qquad M_i \frac{d\omega_i}{dt} = P_{mi} - P_{ei} \tag{5.2}$$

where,

$$P_{ei} = E_i^2 Y_{ii} \cos\theta_{ii} + \sum_{\substack{j=1 \\ j\neq 1}}^{n} E_i E_j Y_{ij} \cos(\delta_i - \delta_j - \theta_{ij}) \tag{5.3}$$

M_i	inertia constant of i^{th} generator
δ_i	internal voltage angle of the i^{th} generator
ω_i	rotor speed of i^{th} generator
$P_{mi}(P_{ei})$	mechanical input (Electrical output)power of i^{th} generator
E_i, E_j	voltage behind transient reactance
Y	admittance matrix reduced at the internal generator node
$Y_{ij}(\theta_{ij})$	modulus (argument) of the ij^{th} element of Y

Using the assumption made by [19] that the disturbed multi-machine system separates in two groups, let us define the two groups of machines as an Area A and Area B as shown in Figure 5.5.

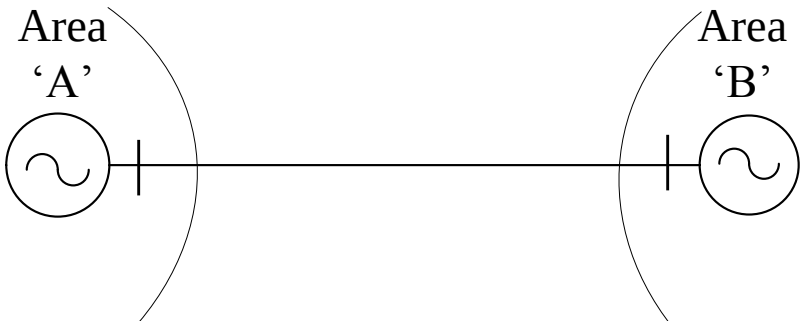

Figure 5.5: Two machine representation

The partial COA of Area A and that of Area B are given by Equation 5.4.

$$\delta_a = \sum_{i \in A} \frac{M_i \delta_i}{M_a} \tag{5.4a}$$

$$M_a = \sum_{i \in A} M_i \tag{5.4b}$$

$$\delta_b = \sum_{j \in B} \frac{M_j \delta_j}{M_b} \tag{5.4c}$$

$$M_b = \sum_{j \in B} M_j \tag{5.4d}$$

where, δ_a is the COA of the generators in Area A, M_a is the sum of the inertia constants of the generators in Area A, δ_b is the COA of the generators in Area B, M_b is the sum of the inertia constants of the generators in Area B. The COA of a group is assumed to be equal to the rotor angles of the generators in that group, i.e., :

$$\delta_a = \delta_i \qquad \forall i \epsilon A \tag{5.5a}$$

$$\delta_b = \delta_j \qquad \forall j \epsilon B \tag{5.5b}$$

Using above formulations, two groups of generators can be transformed into two machine system running in its own partial center of angles (PCOA). The motion of PCOAs of Group A and B in two machine system are described by the Equations (5.6).

$$M_a \ddot{\delta_a} = \sum_{i \in A} (P_{mi} - P_{ei}) \tag{5.6a}$$

$$M_b \ddot{\delta_b} = \sum_{j \in S} (P_{mj} - P_{ej}) \tag{5.6b}$$

where,

$$P_{ei} = E_i^2 Y_{ii} \cos\theta_{ii} + E_i E_j Y_{ij} \cos(\delta_a - \delta_b - \theta_{ij}) + \sum_{\substack{i \in A \\ i \neq j}} E_i E_j Y_{ij} \cos\theta_{ij} \tag{5.7a}$$

$$P_{ej} = E_j^2 Y_{jj} \cos\theta_{jj} + E_j E_i Y_{ji} \cos(\delta_b - \delta_a - \theta_{ji}) + \sum_{\substack{j \in B \\ j \neq i}} E_j E_i Y_{ji} \cos\theta_{ji} \tag{5.7b}$$

The two machine system can further be reduced to a SMIB equivalent system with single machine parameters $\delta, \omega, M, P_m, P_e$. The motion of the resulting SMIB equivalent system can be described using Equation (5.8).

$$M\ddot{\delta} = P_m - (P_c + P_{max}\sin(\delta - \gamma)) \tag{5.8}$$

where,

$$\delta = \delta_b - \delta_a \tag{5.9a}$$

$$M = \frac{M_b M_a}{M_T} \tag{5.9b}$$

$$M_T = \sum_{i=1}^{n} M_i \tag{5.9c}$$

$$P_m = (M_a \sum_{j\in B} P_{mj} - M_b \sum_{i\in A} P_{mi}){M_T}^{-1} \tag{5.9d}$$

$$P_c = (M_a \sum_{j,k\in B} E_j E_k G_{jk} - M_b \sum_{i,l\in A} E_i E_l G_{il}){M_T}^{-1} \tag{5.9e}$$

$$P_{max} = \sqrt{C^2 + D^2} \tag{5.9f}$$

$$\gamma = -\arctan(C/D) \tag{5.9g}$$

$$C = (M_a - M_b){M_T}^{-1} \sum_{i\in A, j\in B} E_i E_j G_{ij} \tag{5.9h}$$

$$D = \sum_{i\in A, j\in B} E_i E_j B_{ij} \tag{5.9i}$$

where, δ and M are the rotor angle and inertia constant of the SMIB equivalent respectively, M_T is the sum of the inertia constants of n generators, n represents the total number of generators, P_m and P_e are the mechanical input power and electrical output power of SMIB equivalent respectively, and B and G are the susceptance and conductance of the network respectively.

5.3 State Plane Analysis Applied to a Multi-Machine System

The proposed algorithm based on state plane analysis is used in a multi-machine system after the multi-machine system is represented with a SMIB equivalent system. Equation

(5.8) representing SMIB equivalent can be written in a form given by Equation (5.10), where $P_{mc} = P_m - P_c$ and $\beta = \delta - \gamma$.

$$M\ddot{\delta} = P_{mc} - P_{max} \sin \beta \tag{5.10}$$

Figure 5.6 shows the power-angle characteristics of the during-fault and post-fault conditions for SMIB equivalent system.

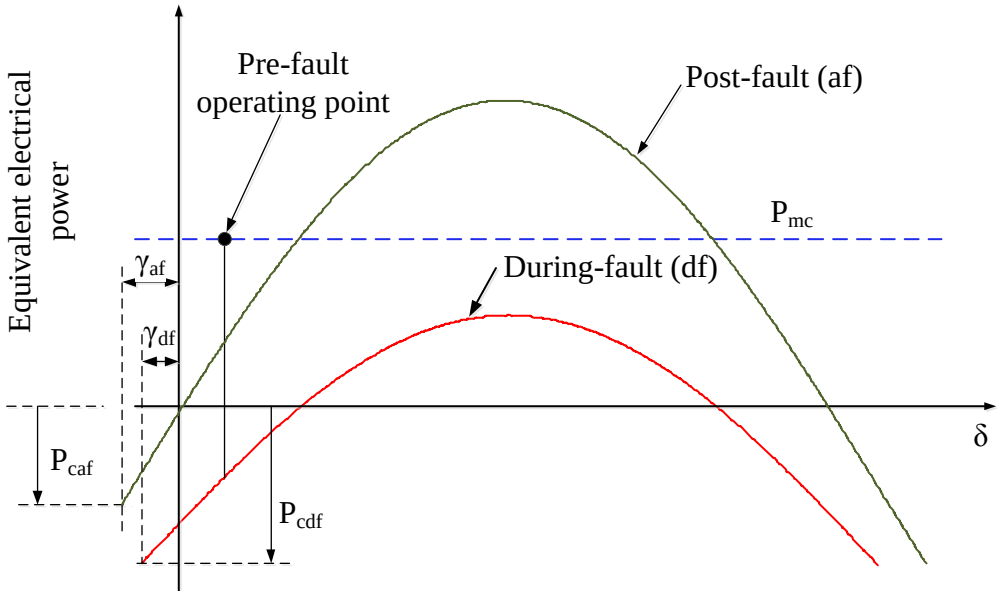

Figure 5.6: Power-angle characteristics of SMIB equivalent system

The SMIB equivalent technique uses the reduced bus admittance matrix of during and after fault condition to calculate the SIMB equivalent parameters as explained in Section 5.2.2. The network is reduced between the internal generator buses. The procedure of network admittance matrix reduction is described in Appendix E.

SPA, as explained in Section 3.4, is used for the SMIB equivalent system to evaluate the CCT of the system. The out-of-step condition is decided based on the criterion presented in Section 3.4.

5.3.1 Testing Methodology

Whenever a fault occurs at a bus in a power system[1], the faulted bus information is communicated to the relay, and network reduction is carried out for the during-fault condition. As soon as the fault is cleared from the bus, the network reduction is carried out for post-fault condition and is done in the same time interval when the coherent machines are being identified.

The coherent groups of machines are found using real time coherency analysis as explained in Section 5.2.1. As soon as the generator bus voltage angles (measured from the initial post fault value) deviates from the reference generator bus voltage angle beyond a certain value (5 degrees were used for the studies), the associated machines are assumed to separate from the reference generator. The reference generator chosen in this study is the generator 1 connected at bus 39. When the generators separate from the reference generator, SMIB equivalent process is carried out using the during-fault and post-fault network equivalents to calculate the during-fault and post-fault power-angle characteristics. The CCT is calculated using SPA, and the instability is detected using the criterion explained in Section 3.4. The stable swing detection results in blocking all the distance relays, whereas in case of instability detected between the two areas, system separation can be decided in two ways. First, the weak lines through which the system separates can be found using either past data or from offline simulation studies, and the system can be separated at those lines. Second, a threshold value can be set for the bus voltage angle, and if the difference goes beyond the threshold value after the instability is detected, separation can be initiated on those lines. The study on forming islands of the power system after instability detection is out of scope of this research and hence is not discussed in detail.

[1]IEEE 39-Bus Test System

5.4 State Deviation Technique Applied to a Multi-Machine System

The state deviation technique, explained in Section 2.6.6, can also be extended for a multi-machine system, using the real time calculation of the SIMB equivalent parameters of the system. In the real time SMIB equivalent, electrical power output and speed are continuously measured at all generator locations. As soon as the two coherent groups of generators (i.e., Group A and Group B) are identified using real time coherency, the measured quantities and the inertia constants of the generators are used to find SMIB equivalent parameters such as P_e and ω using Equation (5.11), and Equation 5.12 respectively. The SMIB equivalent electrical power and speed deviation thus calculated are used by the state deviation technique (Section 2.6.6) to predict instability in the system.

$$P_e = (M_a \sum_{i \in B} P_{ei} - M_b \sum_{j \in A} P_{ej}) M_T^{-1} \tag{5.11}$$

$$\omega = \omega_s - \omega_a \tag{5.12}$$

where,

$$\omega_s = \frac{1}{M_b} \sum_{i \in B} M_i \omega_i \tag{5.13a}$$

$$\omega_a = \frac{1}{M_a} \sum_{j \in A} M_j \omega_j \tag{5.13b}$$

5.5 Case Studies: IEEE 39-Bus Test System

An IEEE 39-bus test system is simulated in PSCAD/EMTDC^{TM}. The system data are shown in Appendix A.3. Three phase fault is applied at different buses in the system and the instability is predicted using three different approaches: (i) proposed algorithm based on SPA (ii) proposed algorithm based on state deviation technique (iii) algorithm based on energy equilibrium criterion in time domain which is reported in [47]. A short description of the technique based on energy equilibrium in time domain is given in Appendix F.

Figure 5.7 shows the flow chart for detecting instability in a large system using the three algorithms. Some of the test cases are discussed in the following sections.

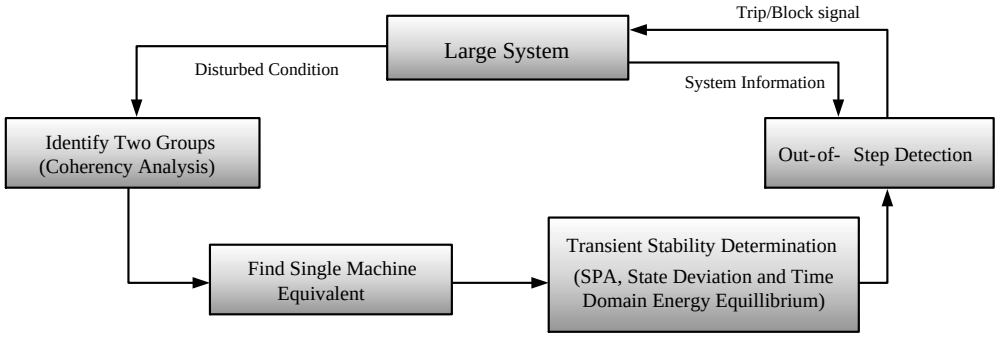

Figure 5.7: Flow chart explaining out-of-step prediction procedure

5.6 Test Cases: SPA

In this section, test results for 2 cases, each for stable and unstable scenario will be discussed. A three phase fault is applied at bus 3 for the first case and at bus 13 for the second case. The fault durations are varied to get stable and unstable cases.

For the fault at bus 3, the fault is applied at 1 s and is cleared after 80 ms. The voltage angle swing observed at different generator buses with respect to the reference generator bus are shown in Figure 5.8. At 0.19 s, all the machines (machine 2 to 10) separates from the reference machine. At this point, calculations are carried out to find SMIB equivalent power-angle characteristics. The predicted power-angle characteristics for during and post fault conditions are shown in Figure 5.9a. Then the relay performs SPA to calculate CCT which is shown in Figure 5.9b. The CCT calculated is equal to 0.0983 s. The fault duration is less than the CCT, i.e., the system is stable. Figure 5.10 shows the SMIB equivalent electrical power obtained from the simulation which also shows a stable swing. During post-fault condition, the voltage angle at the individual buses throughout the system may oscillate, but the voltage angle difference between series elements is going to be small. Figure 5.11 plots the voltage angle difference between series elements and confirms that the variation is minor.

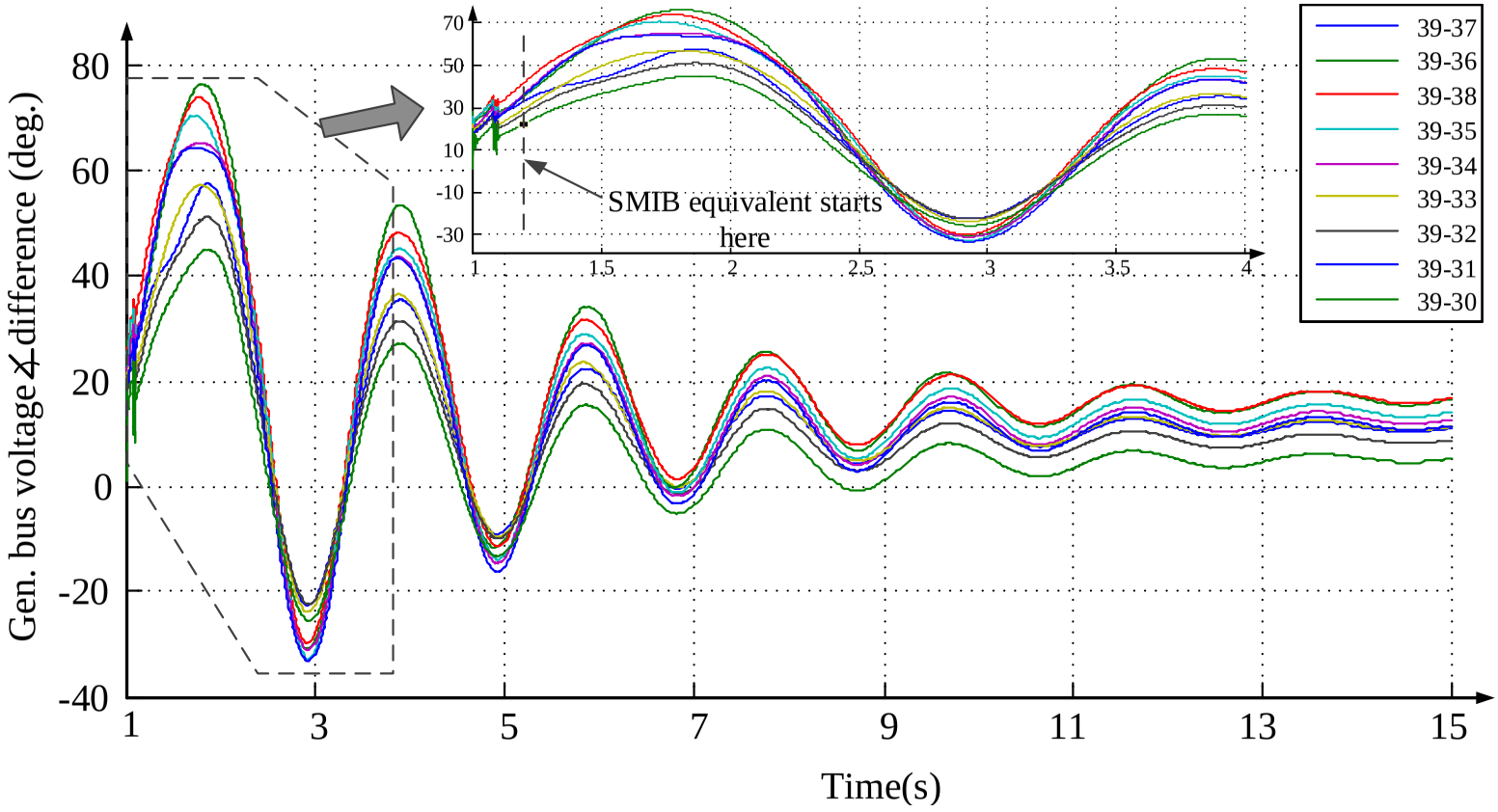

Figure 5.8: Generator bus voltage angles with respect to reference generator bus for the fault at bus 3 and fault cleared after 80 ms

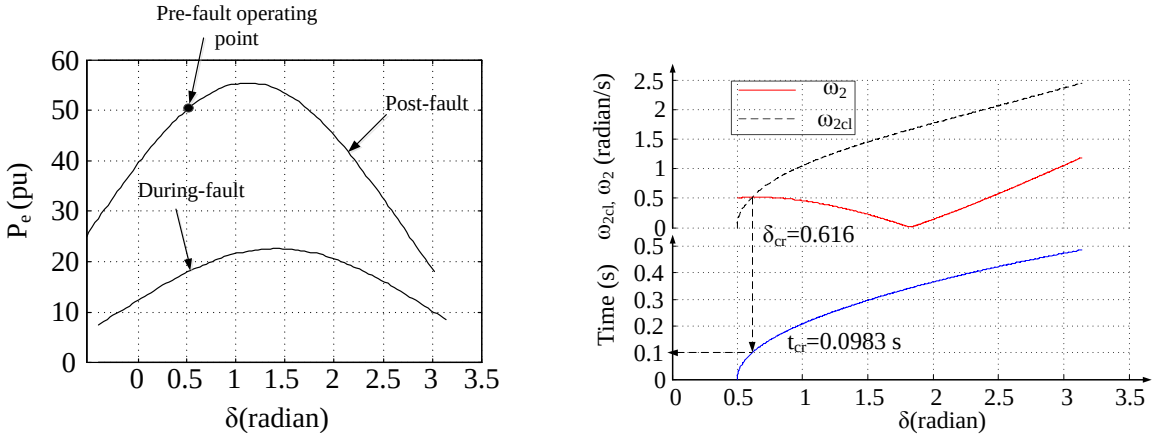

(a) Power-angle characteristics (b) Calculating CCT using state plane plots

Figure 5.9: Relay predicted characteristics and CCT calculation for fault at bus 3

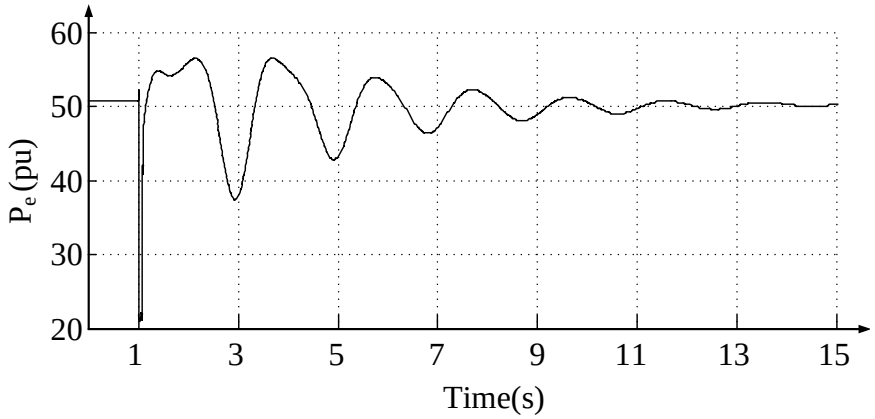

Figure 5.10: SMIB equivalent electrical power for the fault at bus 3 and fault cleared after 80 ms

Now the fault duration is increased to 100 ms for the fault at bus 3. The angular separation of the generator bus angles with respect to the reference generator bus angle is shown in Figure 5.13. All the other generator bus voltage angles deviate from the reference bus. The separation beyond 5 degrees is detected at 0.2 s and the SMIB equivalent procedure is started. The CCT calculation procedure is shown in Figure 5.9. Since the fault duration is greater than the CCT calculated, the system becomes unstable. The SMIB equivalent electrical power is shown in Figure 5.14.

Figure 5.12 shows the voltage angle difference between consecutive buses. From the figure

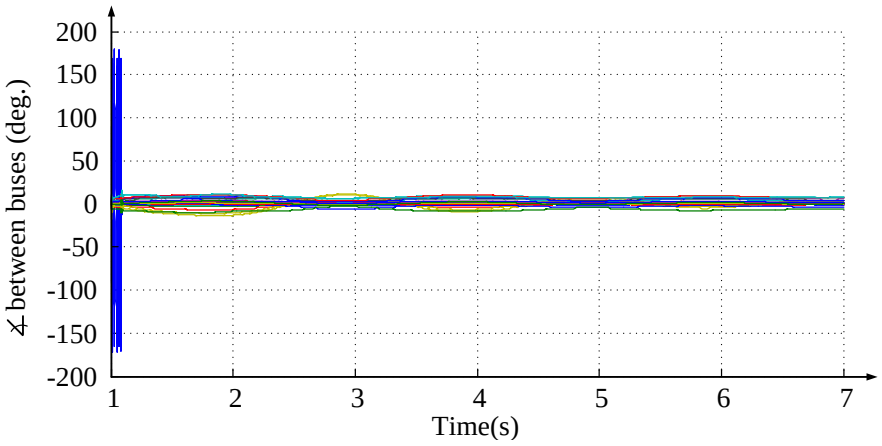

Figure 5.11: Voltage angle difference between series buses for the fault at bus 3 and cleared after 80 ms

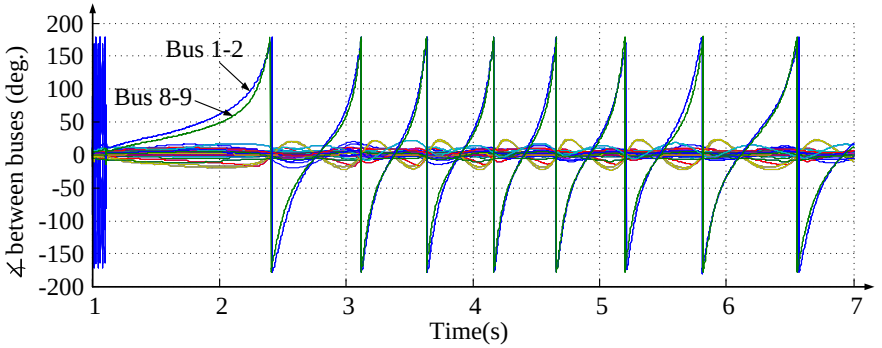

Figure 5.12: Voltage angle difference between series buses for the fault at bus 3 and cleared after 100 ms

it can be seen that the angles between buses 1-2 and 8-9 have become unbounded. It means that the two groups are going to separate at these two lines. Once the out-of-step prediction is made, the lines between 1-2 and 8-9 are tripped.

A similar study is performed with the three phase fault applied at bus 13 which is cleared after 0.115 s. The voltage angle swing, observed at different generator buses with respect to the reference generator bus, is shown in Figure 5.15. At 0.23 s, all the machines (machine 2 to 10) separate beyond 5 degrees from the reference machine. At this point, relay calculates SMIB equivalent power-angle characteristics. The relay predicted power-angle characteristics are shown in Figure 5.17a. Then the relay performs SPA to calculate CCT, which is shown

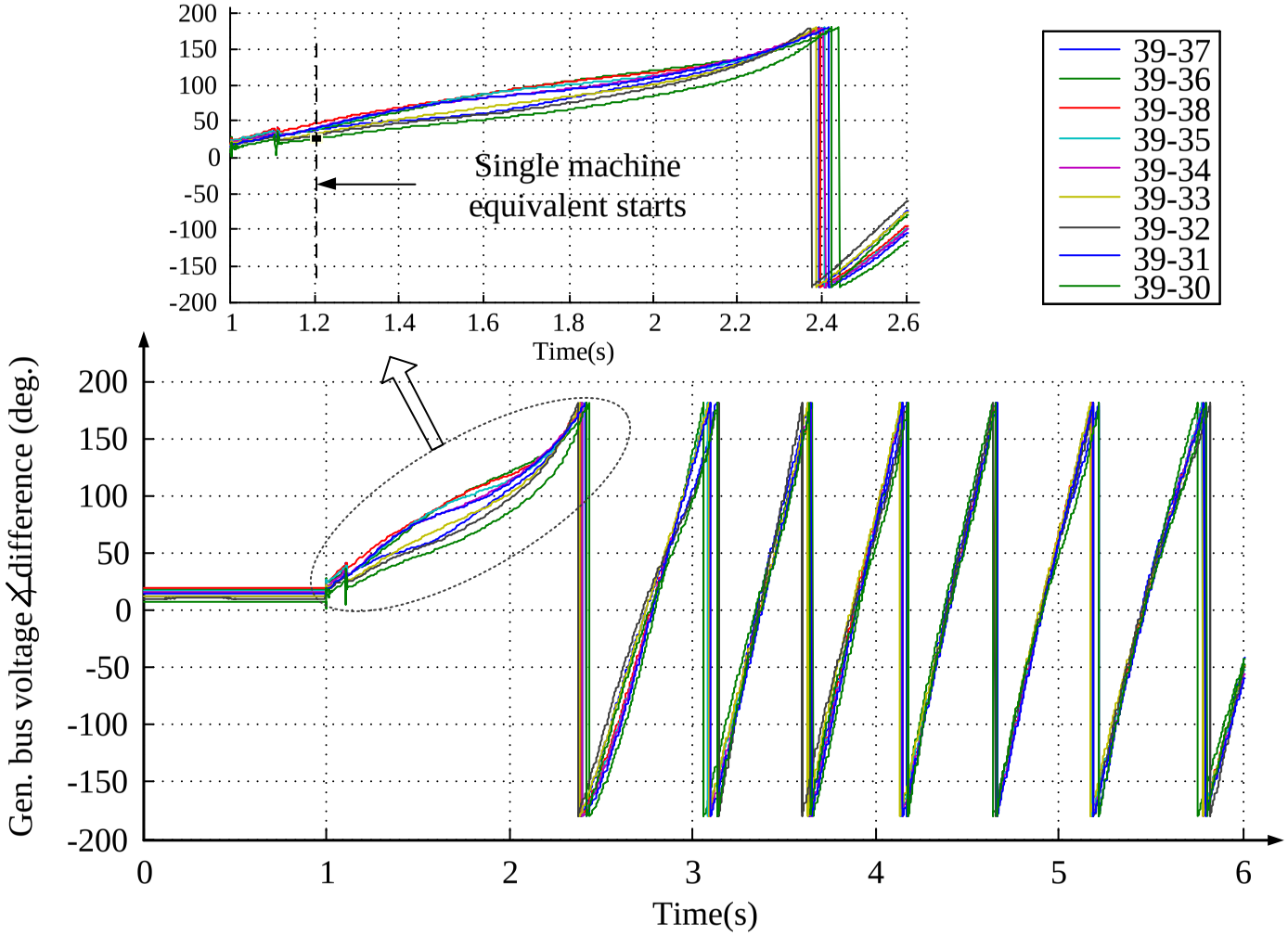

Figure 5.13: Generator bus voltage angles with respect to reference generator bus for the fault at bus 3 and fault cleared after 100 ms

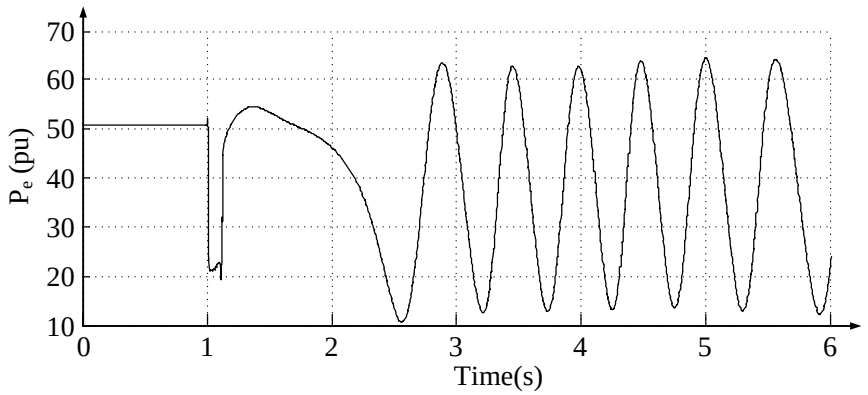

Figure 5.14: SMIB equivalent electrical power for the fault at bus 3 and fault cleared after 100 ms

in Figure 5.17b. The CCT calculated is equal to 0.1161 s. The fault duration is less than the CCT calculated. Therefore the relay detects the oscillation as stable. Figure 5.16 shows the SMIB equivalent electrical power obtained from the simulation. The power oscillation also shows a stable swing, which is in agreement with the CCT calculations made using SPA.

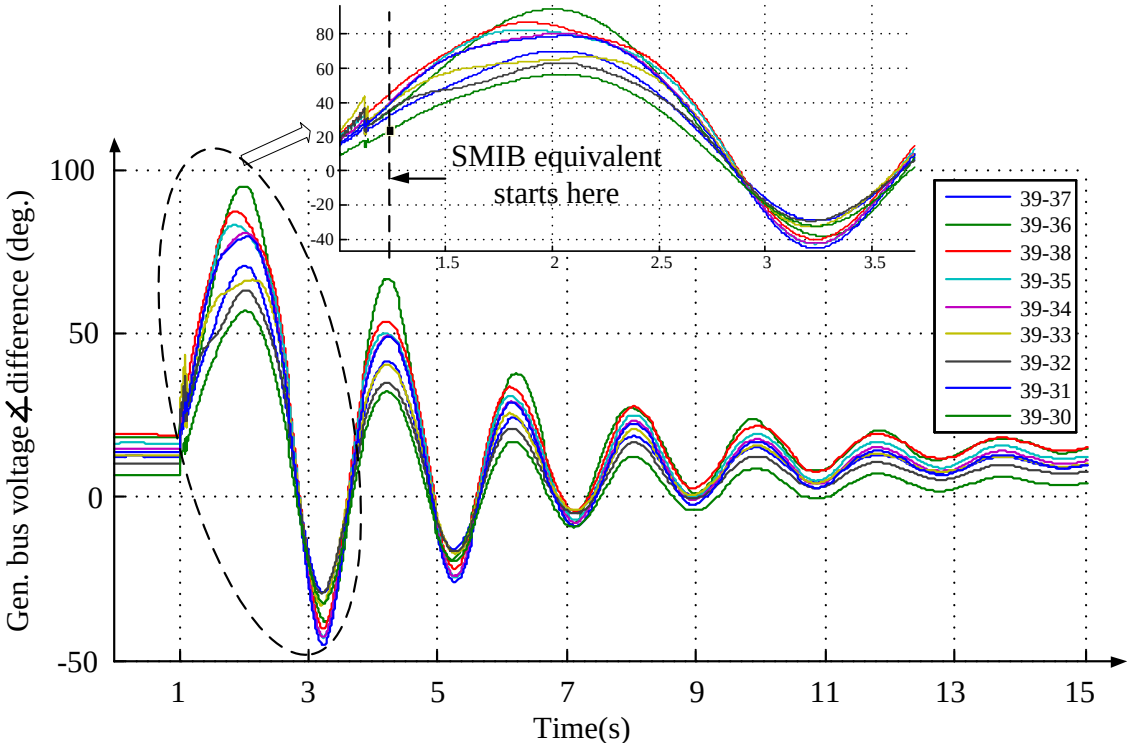

Figure 5.15: Generator bus voltage angles with respect to reference generator bus for the fault at bus 13 and fault cleared after 115 ms

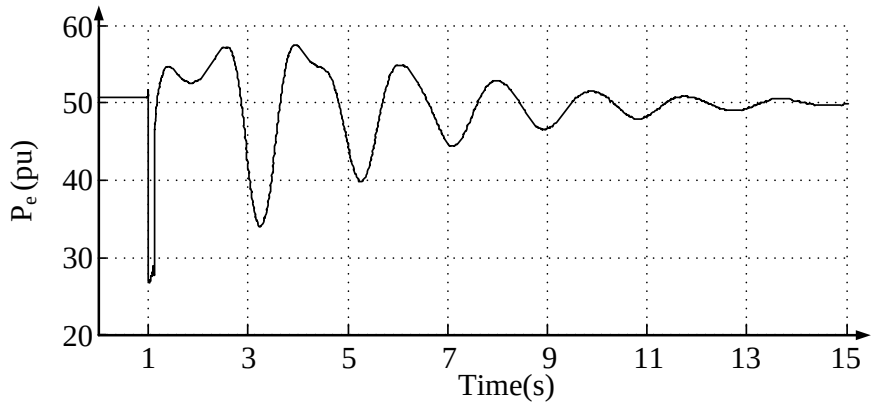

Figure 5.16: SMIB equivalent electrical power for the fault at bus 13 and fault cleared after 115 ms

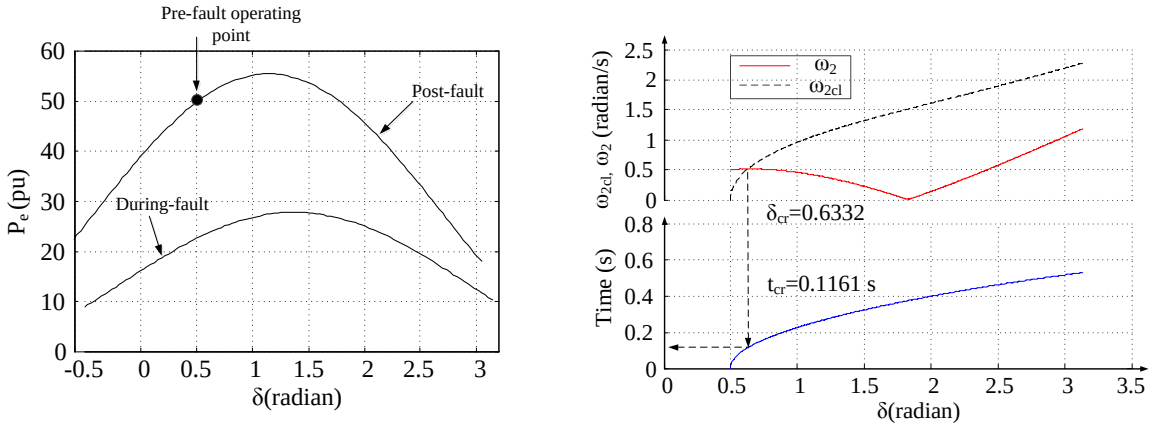

(a) Power-angle characteristics

(b) Calculating CCT using state plane plots

Figure 5.17: Relay predicted characteristics and CCT calculation for fault at bus 13

The voltage angle difference between two ends of the line can be seen in Figure 5.18. It shows that there is no large angular separation between the bus voltage angles throughout the system. This is in agreement with the stability detection made by the proposed algorithm.

For the same bus fault, fault duration is increased to 125 ms. The plot of generator bus voltage angles for this fault is shown in Figure 5.20. The power-angle characteristics and the calculation of CCT for the fault at bus 13 is discussed earlier using Figure 5.17. Since the fault clearing time is greater than the CCT obtained in this figure, the system is detected to be unstable and the time of detection is 0.2 s. The SMIB equivalent electrical

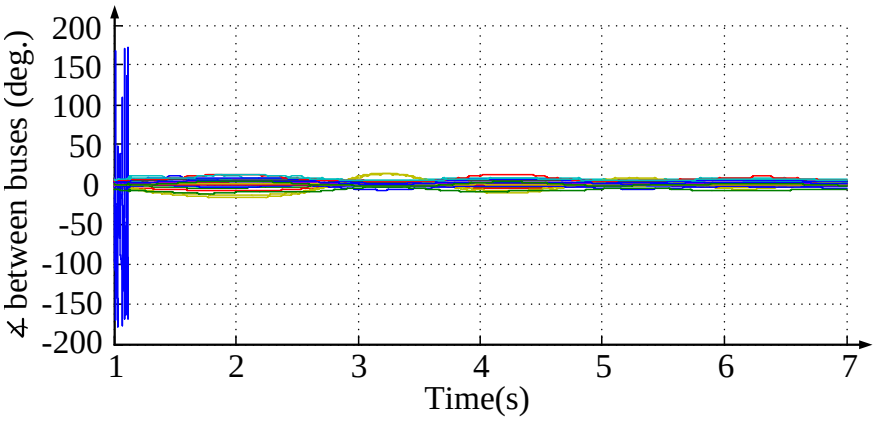

Figure 5.18: Voltage angle difference between series elements for the fault at bus 13 and cleared after 115 ms

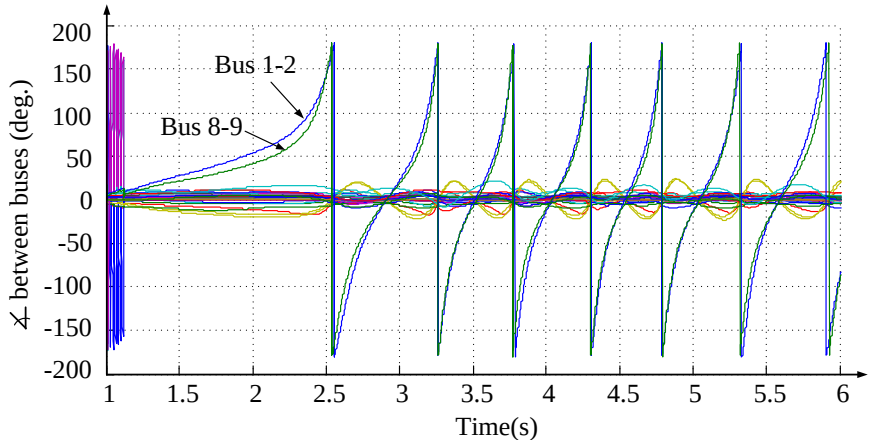

Figure 5.19: Voltage angle difference between series elements for the fault at bus 13 and cleared after 125 ms

power obtained from the simulation is shown in Figure 5.21. The power swing observed is an unstable power swing, as expected. The system separates between the two lines connecting buses 1-2 and 8-9 as shown in Figure 5.19.

Using a similar procedure, instability in the system is detected for the fault at other bus locations. The CCT calculated and the detection times for the corresponding cases are shown in Table 5.1

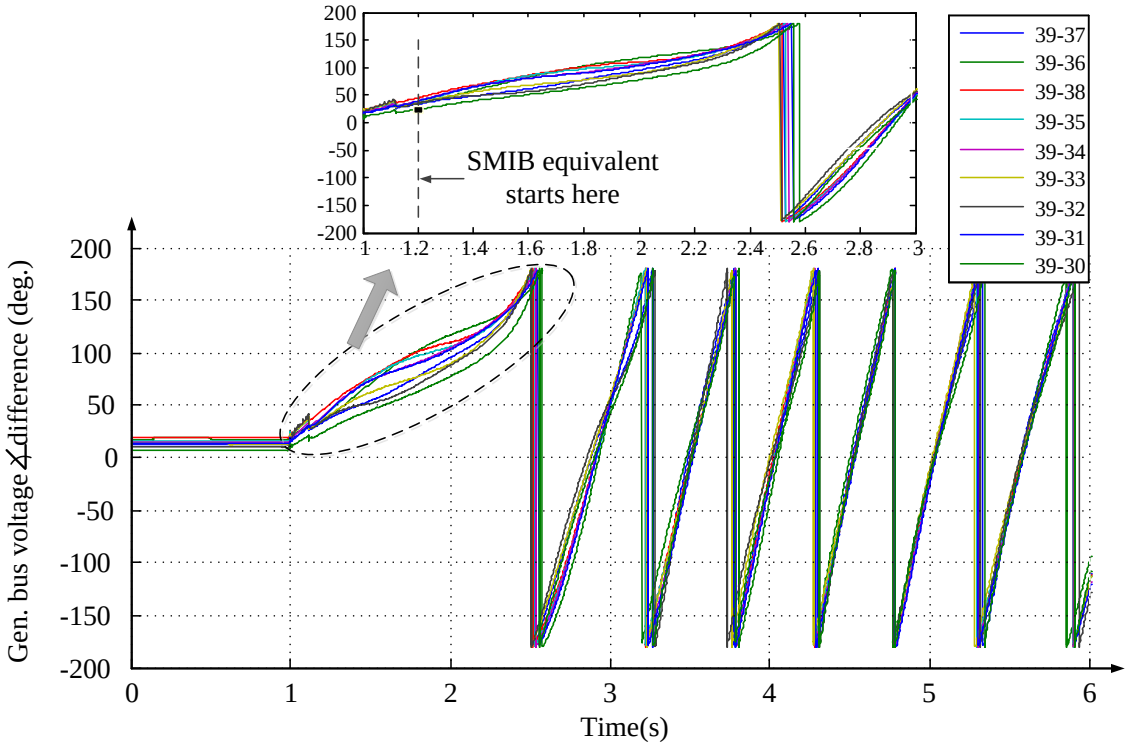

Figure 5.20: Generator bus voltage angles with respect to reference generator bus for the fault at bus 13 and fault cleared after 125ms

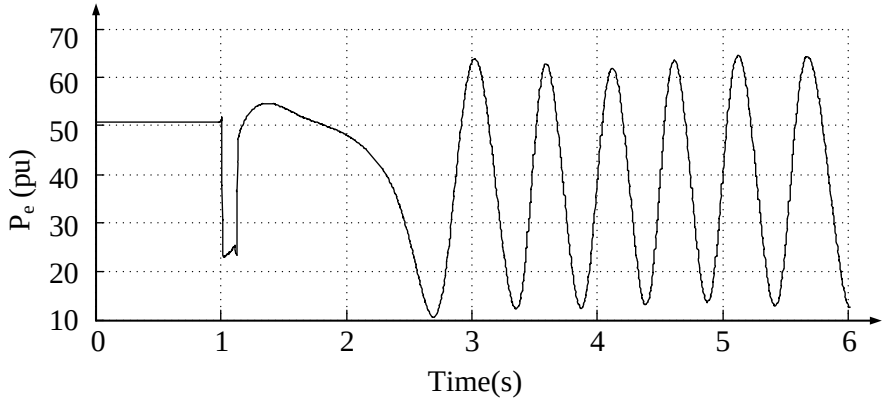

Figure 5.21: SMIB equivalent electrical power for the fault at bus 13 and fault cleared after 125 ms

5.7 Test Cases: State Deviation Technique

The extended state deviation technique is discussed in Section 5.4. The technique is used to predict instability in IEEE 39 bus New England Test system. The technique is based on

the assumption that the group of generators in each area remain coherent throughout the post fault condition. Continuous coherency between generators can be found by continuously calculating the rotor angle difference between the generators in that group. Out of the many simulation tests performed in the system, four test cases are discussed here.

Consider a three phase fault at bus 3 which is applied at 1 s and fault cleared after 80 ms. Because of the fault, the generators 2 to 10 (located at buses 38 to 30) separates from the generator 1 at bus 9. Figure 5.22 shows the rotor angle difference between the generators from 2 to 10 and generator 1. It is seen from the figure that the machines (2 to 10) form one coherent group. The SMIB equivalent electrical power and speed deviation obtained from the electromagnetic transient simulation is shown in Figure 5.23. The speed observed at the first equilibrium point at time 1.51 s is negative (-0.0063 pu). It shows that the system will be stable.

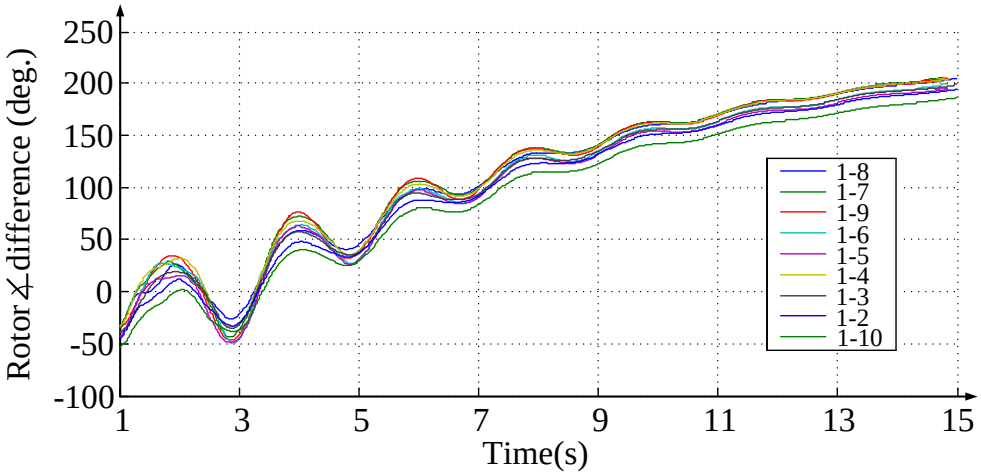

Figure 5.22: Generator rotor angles with respect to reference generator bus for the fault at bus 3 and fault cleared after 80 ms

The fault duration for the fault at bus 3 is increased to 100 ms to get an unstable scenario. The rotor angle separation between the groups of generators from 2-10 and generator 1 can be seen in Figure 5.24. The SMIB equivalent electrical power and speed deviation obtained from the simulation is shown in Figure 5.25. Since the speed observed at the saddle point is positive (0.003175 pu), instability is detected between the two groups. The detection time is

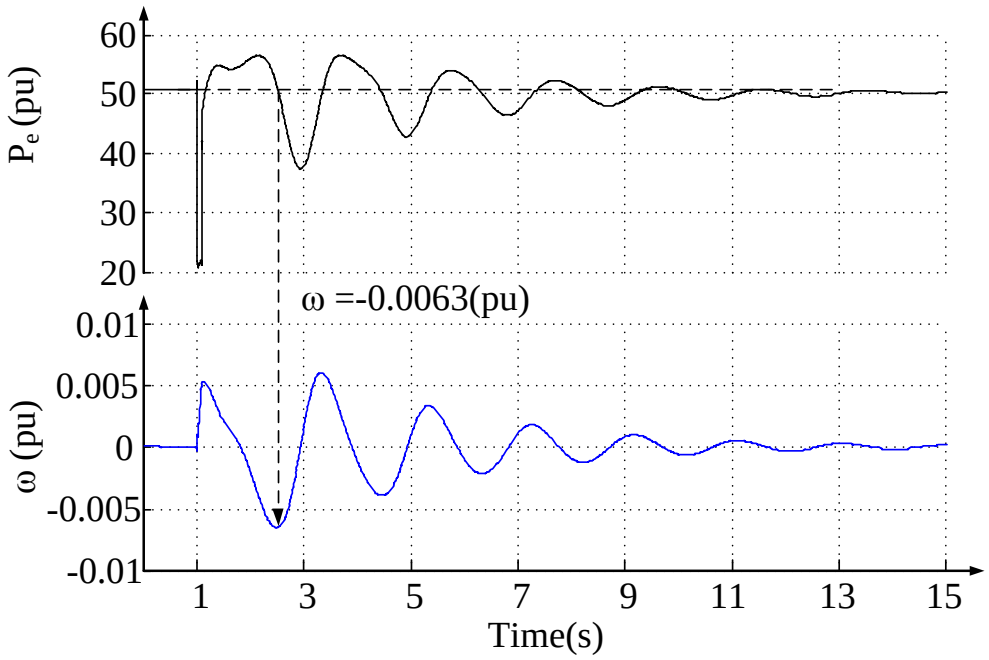

Figure 5.23: SMIB equivalent electrical power and speed deviation for the fault at bus 3 and fault cleared after 80 ms

0.7126 s. For the fault at bus 13, the SMIB equivalent electrical power and speed deviation

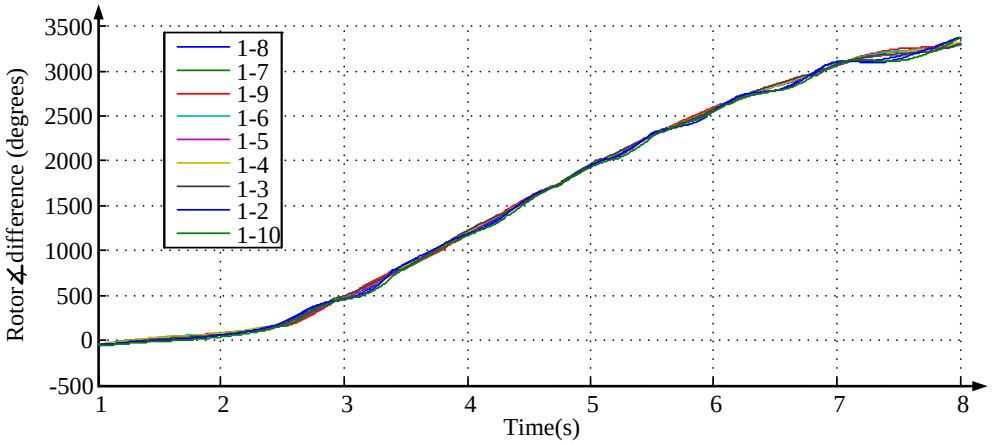

Figure 5.24: Generator rotor angles with respect to reference generator bus for the fault at bus 3 and fault cleared after 100 ms

obtained from simulation for fault durations of 115 ms and 125 ms are shown in Figure 5.26 and 5.27 respectively. The stable swing is detected at 1.8574 s and the instability is detected at 0.7542 s after the fault inception.

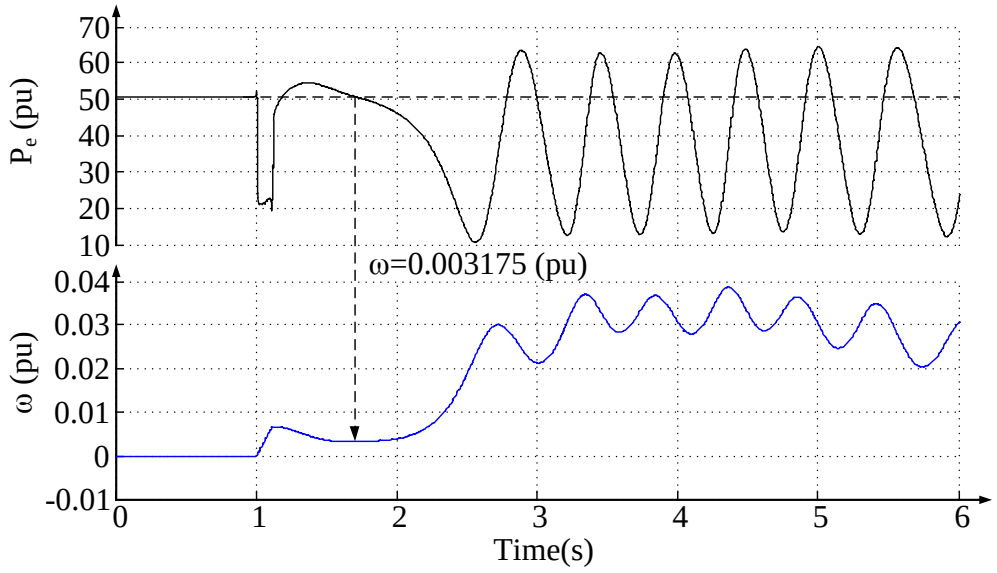

Figure 5.25: SMIB equivalent electrical power and speed deviation for the fault at bus 3 and fault cleared after 100 ms

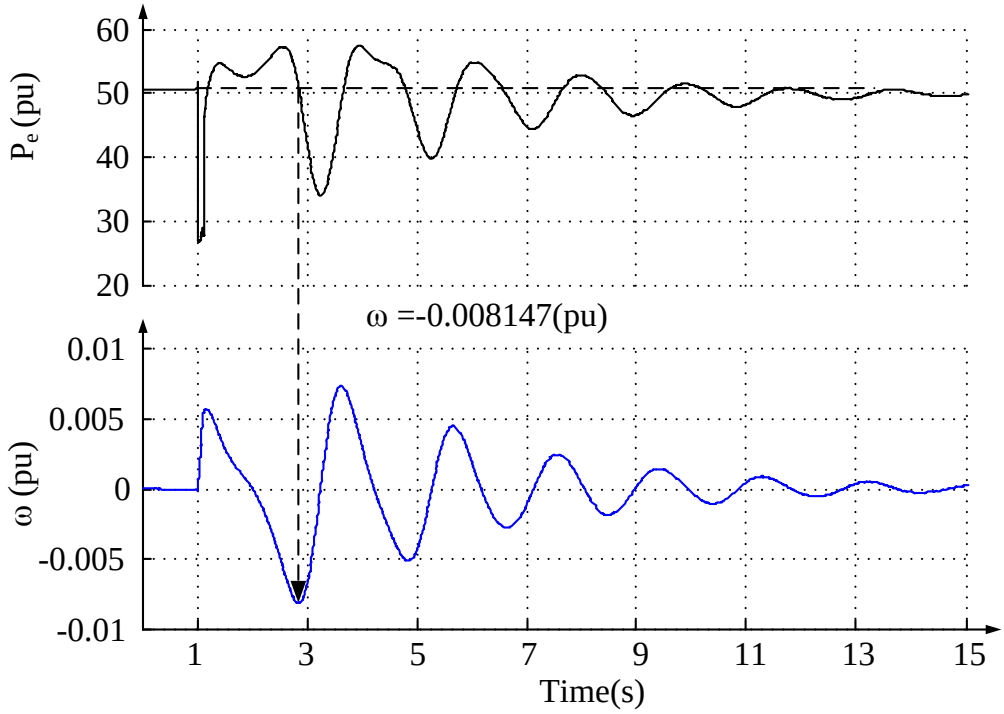

Figure 5.26: SMIB equivalent electrical power and speed deviation for the fault at bus 13 and fault cleared after 115 ms

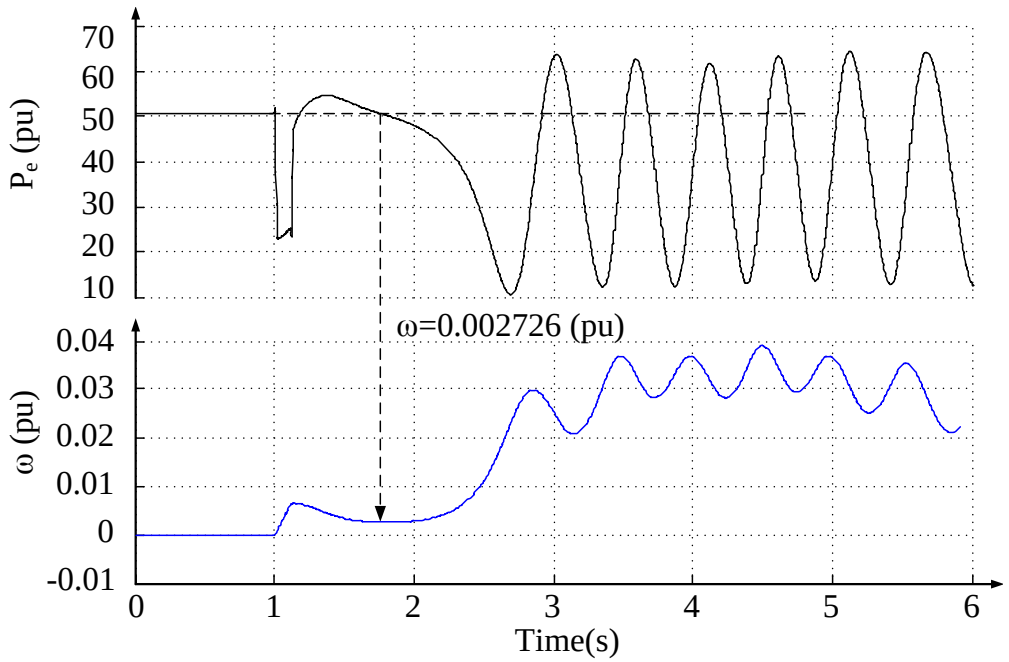

Figure 5.27: SMIB equivalent electrical power and speed deviation for the fault at bus 13 and fault cleared after 125 ms

The other test results and their detection time are listed in Table 5.1.

Table 5.1: Test results of instability detections using SPA and state deviation technique

Faulted bus	Fault duration(ms)	SPA		State Deviation Technique		Decision
		CCT	TOD	ω at TOD (pu)	TOD (s)	
3	80	0.09828	0.20	-0.00630	1.510	Stable
	100		0.19	0.003175	0.7126	Unstable
4	90	0.1010	0.21	-0.007149	1.702	Stable
	110		0.19	0.002460	0.7646	Unstable
5	100	0.1060	0.1912	-0.007446	1.740	Stable
	110		0.2112	0.000905	0.9896	Unstable
6	100	0.1061	0.1965	-0.007454	1.751	Stable
	120		0.2147	0.003632	0.6355	Unstable
11	115	0.1153	0.2102	-0.007854	1.807	Stable
	130		0.2132	0.002457	0.7396	Unstable
13	115	0.1161	0.2300	-0.008147	1.8574	Stable
	125		0.2000	0.002726	0.7542	Unstable
14	100	0.1047	0.1910	-0.008977	2.0371	Stable
	110		0.1927	0.002550	0.7896	Unstable
17	80	0.0942	0.1761	-0.009063	2.0320	Stable
	95		0.1820	0.004415	0.6063	Unstable
24	95	0.1083	0.1986	-0.009263	2.107	Stable
	110		0.1996	0.003876	0.6459	Unstable
27	110	0.1239	0.2037	-0.008796	2.0107	Stable
	125		0.21173	0.003702	0.7084	Unstable
TOD: Time of detection						

5.8 Test Cases: Time Domain Energy Equilibrium Method

The instability detection using time domain energy equilibrium is discussed in Appendix F. The application of this method in multi-machine systems is also based on the similar assumption of coherency between the generators in a group as mentioned in Section 5.7. The accelerating and decelerating energy is calculated using the SMIB equivalent electrical power. For the fault at bus 3 and fault duration of 80 ms, the SMIB equivalent electrical power from simulation is shown in Figure 5.28a. The accelerating energy is calculated continuously as shown in Figure 5.28b. The accelerating area calculated is 2.6460 $pu - s$. As soon as the system reaches the decelerating region, the accumulating decelerating energy is subtracted from the accumulated accelerating energy value. The total area (TA, i.e., accelerating energy minus decelerating energy) indicator is 1, when TA is greater than 0, and 0 when TA$\leq$0. If TA becomes $\leq$0, TA indicator drops to 0. At that moment, the system will be detected to be in a stable condition. If TA is always greater 0, then TA indicator remains 1, which indicates instability in the system. The area is measured up to $(\pi - \delta_1)$ (refer to Figure 3.8) in case if the TA indicator does not drop to 0 before this point. For this fault case, TA becomes 0 at 0.9098 s after the fault inception; hence the swing is detected as a stable swing. For the fault at bus 3 and fault duration of 100 ms, the accelerating area calculated is 3.2968 $pu - s$ whereas the decelerating area calculated is only 1.2219 $pu - s$. This shows that the system is going to be unstable. The instability is detected at 0.7126 s. Figure 5.29 explains the instability detection results obtained.

For the fault at bus 13 and fault duration of 115 ms and 125 ms, the calculation of accelerating area and decelerating area are shown in Figure 5.30 and 5.31 respectively. For fault duration of 115 ms, the accelerating area calculated is 2.8565 $pu-s$ and the total decelerating area available is 6.0899 $pu - s$. The decelerating area becomes equal to accelerating area at time 1.2216 s and hence the TA indicator goes zero. The swing is therefore detected as a stable swing. For the fault duration of 125 ms, the accelerating area calculated is 3.1471 $pu - s$ and the total decelerating area available is 1.3860 $pu - s$. The TA will always be

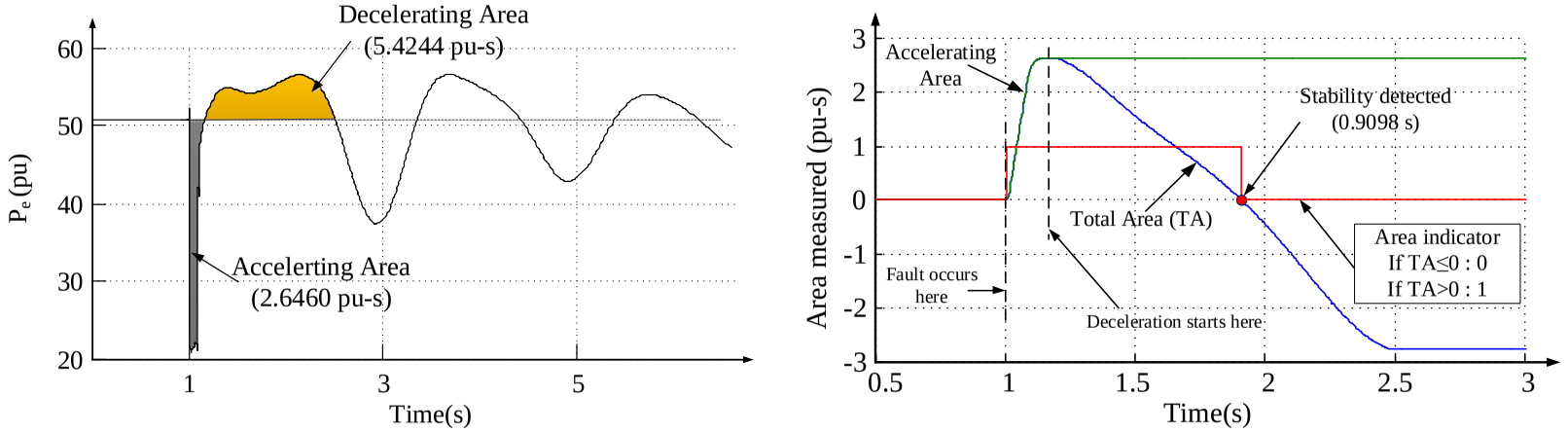

(a) SMIB equivalent electrical power for fault cleared after 80 ms

(b) Calculating accelerating and decelerating area

Figure 5.28: Using time domain energy equilibrium method for the fault at bus 3

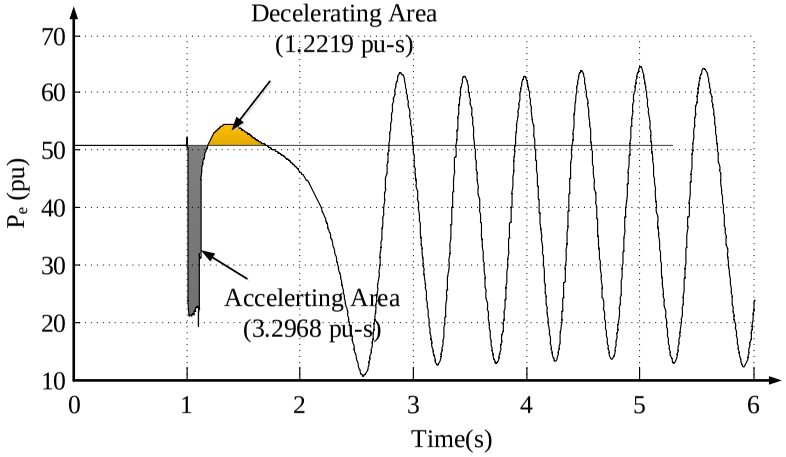

(a) SMIB equivalent electrical power for fault cleared after 100 ms

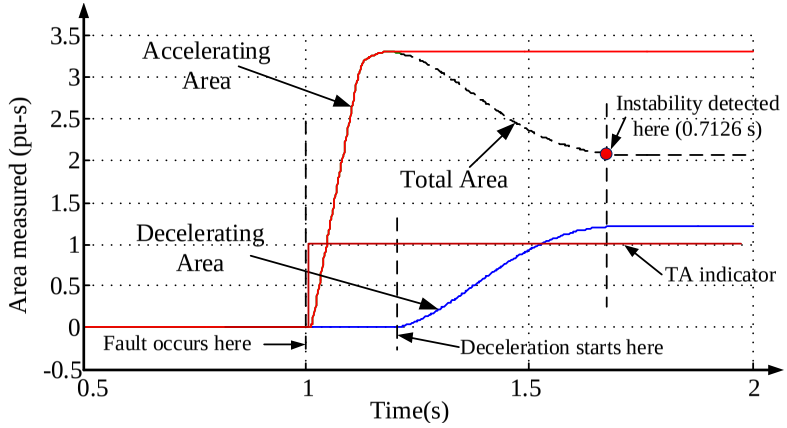

(b) Calculating accelerating and decelerating area

Figure 5.29: Using time domain energy equilibrium method for the fault at bus 3

greater than zero. The swing is therefore detected as an unstable swing at 0.7542 s.

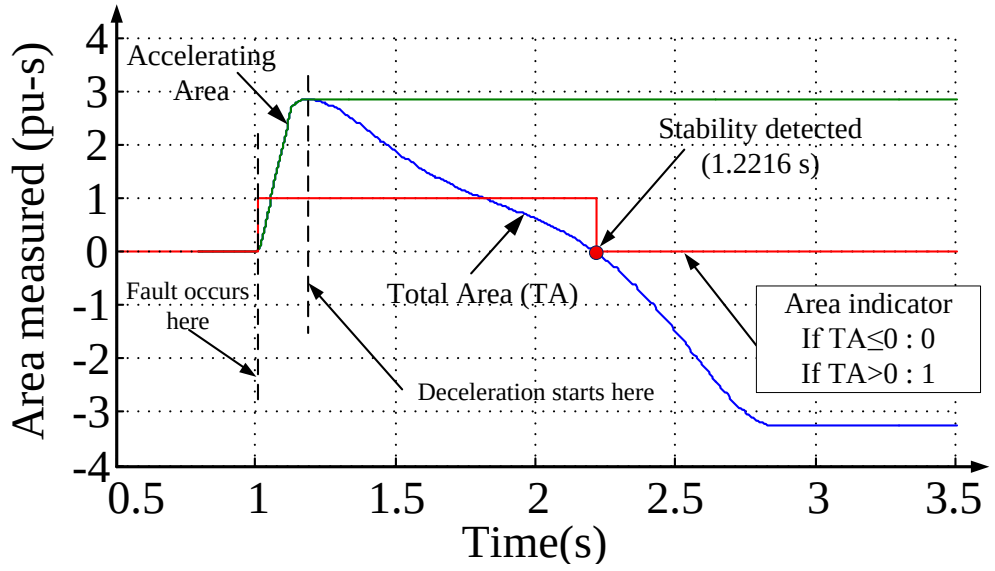

Figure 5.30: Calculating accelerating and decelerating area for the fault at bus 13 and fault cleared after 115 ms

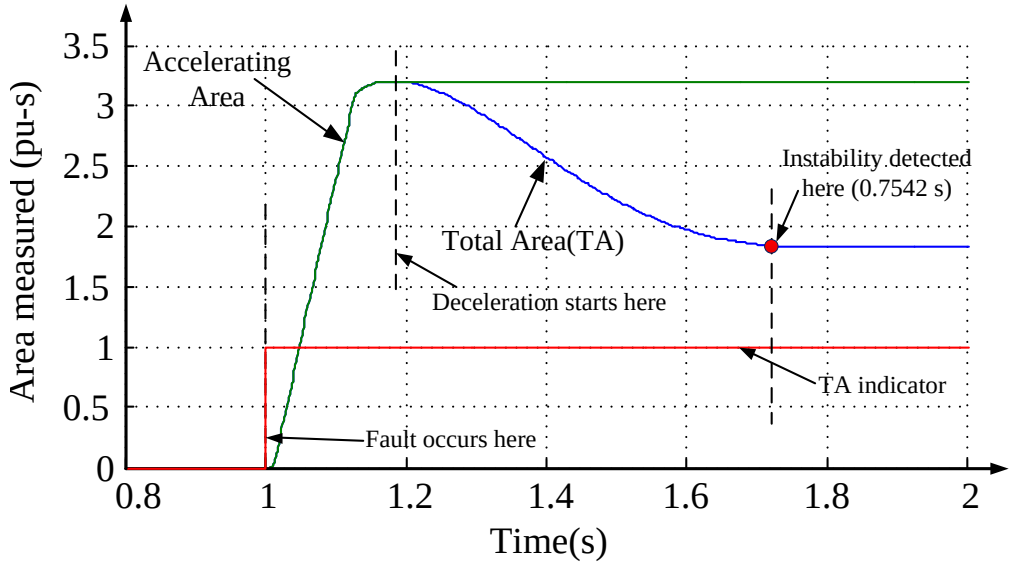

Figure 5.31: Calculating accelerating and decelerating area for the fault at bus 13 and fault cleared after 125 ms

The test results with the faults applied at other buses are listed in Table A.1.

Table 5.2: Test results of instability detection using time domain energy equilibrium

Faulted bus	Fault duration(ms)	Accelerating area ($pu-s$)	Decelerating area ($pu-s$)	Time of detection (s)	Decision
3	80	2.6460	5.4244	0.9098	Stable
	100	3.2968	1.2219	0.7126	Unstable
4	90	2.7963	5.7979	1.027	Stable
	110	3.20325	1.3739	0.7646	Unstable
5	100	2.86197	5.8514	1.1158	Stable
	110	3.0808	1.6134	0.9896	Unstable
6	100	2.8661	5.8400	1.1316	Stable
	120	3.4445	0.9747	0.6355	Unstable
11	115	2.8274	5.9760	1.1760	Stable
	130	3.1791	1.2395	0.7396	Unstable
13	115	2.8565	6.0899	1.2216	Stable
	125	3.1413	1.2808	0.7542	Unstable
14	100	2.9900	6.3059	1.4250	Stable
	110	3.1471	1.3860	0.7896	Unstable
17	80	2.9832	6.0950	1.5225	Stable
	95	3.4931	0.7122	0.6063	Unstable
24	95	2.7977	6.2661	1.4640	Stable
	110	3.1950	0.5217	0.6459	Unstable
27	110	2.9310	6.3166	1.3969	Stable
	125	3.2204	0.7084	0.7084	Unstable

5.9 Summary

This chapter explained the application of SPA when applied to a large system. The technique was based on the assumption that the system separates into two groups of machines. The proposed method used a real time coherency analysis, network reduction and the SMIB equivalent procedure. The network reduction for during-fault condition was carried out during the fault duration itself, and network reduction for after fault condition was carried out during the time interval between fault clearance and coherency detection. After the coherency of machine groups was found, the SMIB equivalent procedure was carried out, which involved simple mathematical calculations such as additions and multiplication of available data such as voltages, inertias and impedances as discussed in Section 5.2.2. The computational effort for these calculations was found to be very small. The real time processing of the algorithm using SPA will take less than 0.1 cycle using the digital signal processing board (ADSP-BF533). The proposed algorithm hence can be easily implemented as a numerical relay for the instability detection in large power systems in real time. The test results discussed in this chapter show that the proposed technique using SPA is fast and accurate in detecting instability in the system. The angle of separation in the critical line (1-2 and 8-9) at the time of detection was also less than 50 degrees. It means that the breakers would be subjected to less stress at the time of system separation at these lines.

This chapter also explained the generator state deviation applied to the larger system. The technique was also found to be very accurate, but the time taken for instability detection using the technique was found to be much greater than that from SPA. Similarly, the time domain energy equilibrium method gave the same detection time as that of the state deviation technique. These comparisons confirmed the superiority of the proposed SPA technique

Chapter 6

Conclusions

6.1 Summary

In an interconnected power system, a large system disturbance could result in instability, and the various parts of the system cease to operate together in synchronism. The resulting loss of synchronism required that the parts of the system be separated and stabilized using out-of-step relaying. Typically, as described in the thesis, the relaying function is implemented by analysing the impedance trajectories and how they enter the blinder characteristics [26], rate of change of impedance method or the rate of change of apparent resistance augmentation method [17], the Swing Center Voltage (SCV) technique [26], transient energy calculation method [18], the Equal Area Criterion (EAC) methods [20], or the frequency deviation calculation method from voltage signal [25]. The problem with the blinder scheme is that accurate settings of the blinders and timer settings are difficult, especially in large systems, because they need extensive a priori simulation studies. False tripping of the lines due to incorrect blinder settings is quite common. The rate of change of impedance method or the R-Rdot method also need extensive simulation studies and have similar demerits as the blinder scheme. The SCV technique estimates the rate of change of voltage, which is maximum at the electrical center. The detection is usually made at a voltage angle of separation closer to 180 degrees, which will cause twice the rated stress for the circuit breaker. Therefore, with the SCV technique, the operation of the circuit breaker is differed to a later instant when voltage angle separation is less. Transient energy method (using Lapunov's direct method) predicts loss of synchronism using local measurements. The technique was applied for only local generator protection and predicted out-of-step condition

at large voltage angles of separation. The EAC method finds accelerating and decelerating areas of the swing curves to find the instability condition. The method is directly applicable to a single machine infinite bus system. For large systems, extended EAC (EEAC) [19] was proposed when the system separates into two oscillation groups. A relay using EEAC approach was experimentally tested on the intertie between Georgia and Florida between 1993-1995 (there were close to a dozen significant swings during this period and three line faults). The instability condition with the EEAC approach was also found at a large voltage angle of separation. It also needs a step-by-step integration technique to calculate critical clearing time (CCT). In the frequency deviation of voltage method, the unstable condition is detected when the frequency, measured at the point, when acceleration changes its sign from negative to positive, is greater than zero. The technique is sound and the benefit of this technique is that it can detect not only the first swing instability but also the multi-swing instability. The deficiency of this approach is that the voltage transient behaviour during faults can cause accurate determination of frequency deviation to be difficult. Also, wide area system protection using the frequency deviation of voltage method has not been done so far.

This thesis proposed a novel technique based on state plane analysis (SPA) to detect first swing out-of-step conditions in large power system configurations. The technique proposed is computationally simple and fast compared to the current methods. The main advantage of the proposed technique is that it provides a fast prediction of loss of synchronism condition and provides enough time for decision making before the machines actually start slipping poles, thereby preventing loss of system generation and loads. It will also lessen circuit breaker wear and tear as the tripping can be done at a lower angle of voltage separation. Chapter 3 discussed the results for a single machine infinite bus (SMIB) and two-area system configurations.

This thesis presented another out-of-step prediction technique using generator state deviations to detect multi-swing instability conditions in a power system. The approach is an extension of the frequency deviation method from voltages [25], but instead used a more stable measurement (generator speed deviation) to detect instability. The technique was

applied in an interconnected system and used online measurement of electrical power and the generator speed as inputs (using wide-area measurements). The benefit of this approach is that it can predict both first swing and multi-swing instability conditions. The state plane method and state deviation method were also combined for finding multi-swing instability conditions in a two-area power system configuration.

With the current availability of Wide Area Measurement Systems (WAMS) and Phasor Measurement Units (PMUs) in power systems, the proposed relaying algorithms could be used on large power system configurations. The state plane and state deviation techniques were also tested on a large power system configuration (IEEE 39-bus test system) to find their accuracy and speed of computation on large systems. For the SPA, the instability detection is based on representing the multi-machine dynamical behaviour with a single machine infinite bus dynamical behaviour after the disturbance using coherency analysis and SMIB equivalent procedure. The first swing stability of the multi-machine system was found by finding the stability of the SMIB equivalent. Using the system wide informations, such as pre-fault voltages, fault location, breaker status and fault isolation, to identify the network status, the algorithm predicted CCT for the three phase to ground fault at different substations of the system. The test results showed that the algorithm accurately detects the stable/unstable conditions in very small time duration after the fault is cleared. The state deviation approach used online SMIB equivalent, and electrical power and generator speed calculations to detect instability. The test results showed that this approach also detects stable/unstable swings accurately. A comparison of the results showed that the state plane technique is much faster than the state deviation technique for finding first swing instability. Both the techniques detected the instability much sooner than when the system actually started slipping poles. The techniques hence are effective and could be implemented in a large power system configuration using wide area measurement signals.

Prototypes of the relays (using the SPA and state deviation technique's) were developed on a digital signal processing board ($ADSP - BF533^{TM}$). The relay was connected in a closed loop with $RTDS^{TM}$ to evaluate its performance in a SMIB and two-area power system. The test results using the proposed algorithm based on SPA for the SMIB and two-area system

were shown in this chapter. Moreover, the algorithm based on the state deviation technique was also implemented in the DSP board. The generator speed signal was communicated to a relay using the DSB-SC modulation technique. The results from the real time testing of the algorithm were also shown in Chapter 4. A multi-swing instability case in two-area system was also studied using a technique based on SPA and state deviation technique and the results were presented. The results from the real time testing showed that the proposed scheme using SPA is very fast to detect instability in power system. The scheme using generator state deviation also detects instability significantly sooner than the generators or the two areas start the first pole slipping.

6.2 Thesis Contributions

Followings are the thesis contributions:

- *Out-of-Step Prediction Using State Plane Trajectories Analysis:* This thesis proposed a new procedure using the analysis of omega versus delta curve for during fault and post fault conditions to predict whether the system is going to be stable or unstable. The critical clearing angle was found when the total energy of the system at the instant the fault is cleared becomes equal to the maximum potential energy of the system. The time corresponding to this delta value (i.e., critical clearing angle) was found directly from the omega versus delta solution curve unlike the EAC approach where the critical clearing angle is found first, and then the critical clearing time is found by a step-by-step integration. The simultaneous calculation of the critical clearing angle and the time made the proposed state plane approach much faster than the EAC or EEAC approaches (and also the other approaches) discussed in the literature. The proposed prediction scheme using the state plane trajectories was used to detect first swing out-of-step conditions in the SMIB system. The method was also extended to predict the out-of-step condition in larger power system configurations (two-area and IEEE 39-bus test systems).

  Overall, the proposed algorithm was found to be computationally efficient, and as can

be seen in the simulation studies, the technique is accurate and fast in detecting the instability in the power system.

- *Out-of-Step Prediction Using State Deviation Technique:* This thesis also proposed another new technique using the online measurements of the generator speed and the electrical power to detect instability conditions in a power system. The electrical power measurement was used to find the singular points during a power swing. The speed at the singular point was found to be greater or less than the rated value for an unstable and a stable swing, respectively. The technique was also extended to detect instability in large multi-machine power systems (two-area and IEEE 39-bus test systems).
  This technique, in addition to being simple and easy to implement, was also accurate. The test results showed that the out-of-step prediction time using the state deviation technique was greater than that from the SPA. However, the state deviation does not require network reduction (described in appendix E) unlike the SPA method for instability prediction.

- *Multi-Swing Instability Prediction:* The state deviation technique was found to be very effective for finding multiple swing instability conditions in the power system. This thesis proposed a combined out-of-step relaying algorithm, where the first swing instability was found using the faster state plane approach, and the instability in a later swing was found using the relatively slower state deviation technique.

6.3 Future Work

- Studying Effect of Recovery Voltage on Out-of-Step Breakers: During a normal short circuit, a circuit breaker can experience a recovery voltage up to the peak of rated voltage, whereas during an out-of-phase condition, the breakers experience much higher recovery voltage which could reach up to 2 times the rated voltage. In addition, the natural frequency because of the system inductance and capacitance causes additional transient rise in recovery voltage with a higher frequency. For these reasons, the out-of-step breaker should specially be designed to withstand the voltage level during an

out-of-step condition. The out-of-step detection using the proposed SPA technique ensured fast detection with lower breaking angles. However, a further detailed study is necessary to analyse the effect of recovery voltage on the breaker for out-of-step breaker design.

- Real Time Implementation of Proposed Techniques for Large Power Systems: A hardware-in-the-loop testing of the proposed algorithms was done for SMIB and two area test systems using RTDS^{TM}. In RTDS^{TM}, the power system is simulated in a fixed simulation time step of 50 μs which requires adequate processors to complete all the calculations within that time step. Hence, the size of power system that can be simulated in a real time environment depends on the processors available for the calculations. With the current processing capacity of the RTDS^{TM} available in power system research laboratory at University of Saskatchewan, it was only possible to simulate the SMIB and two area system. However, with the undergoing expansion of the RTDS^{TM} Simulator, it would soon be possible to simulate a large power system (such as an IEEE 39-bus test system) and use the WAMS technology. The proposed SPA and state deviation technique could be tested on the IEEE 39-bus test system using the new simulator.

- Out-of-Step Prediction in Power System Including Wind Generators: More renewable energy sources such as wind generators are being added to the electric utility grids. The wind generators are often induction type generators, which are asynchronous type of machines, and include number of fast acting power electronic components for fast voltage and frequency control. Out of step protection in power systems consisting of both synchronous and asynchronous machines is an important problem which needs further research. In particular, the accuracy of the single machine infinite bus equivalenting procedure needs to be established by comparing it with the detailed model simulations for this kind of power system configuration. Also, the accuracy of the state plane and state deviation methods for predicting instability conditions for such a configuration needs to be verified.

References

[1] P. Kundur, *Power System Stability and Control*. The EPRI Power System Engineering Series, New York: TATA McGraw-Hill, 2004.

[2] J. Casazza and F. Delea, *Understanding Electric Power Systems*. John Wiley & Sons, New York, 2003.

[3] W. D. Stevenson, *Elements of Power System Analysis*. McGraw-Hill, 1982.

[4] J. L. Blackburn and T. J. Domin, *Protective Relaying Principles and Applications*, 3rd ed. CRC Press, Taylor & Francis Group, 2007.

[5] S. H. Horowitz and A. G. Phadke, *Power System Relaying*, 3rd ed. John Wiley & Sons, New York, 2008.

[6] "Power swing and out-of-step considerations on transmission lines," *IEEE PERC WG D6*, June 2005.

[7] D. Novosel, G. Bartok, G. Henneberg, P. Mysore, D. Tziouvaras, and S. Ward, "IEEE PSRC Report on Performance of Relaying During Wide-Area Stressed Conditions," *IEEE Transactions on Power Delivery*, vol. 25, no. 1, pp. 3 –16, jan. 2010.

[8] A. G. Phadke and J. S. Thorp, *Computer Relaying for Power Systems*, 2nd ed. John Wiley & Sons, New York, 2009.

[9] M. G. Adamiak, A. P. Apostolov, M. M. Begovic, C. F. Henville, K. E. Martin, G. L. Michel, A. G. Phadke, and J. S. Thorp, "Wide area protection—technology and infrastructures," *IEEE Transactions on Power Delivery*, vol. 21, no. 2, pp. 601–609, 2006.

[10] P. Kundur, J. Paserba, V. Ajjarapu, G. Andersson, A. Bose, C. Canizares, N. Hatziargyriou, D. Hill, A. Stankovic, C. Taylor, T. Van Cutsem, and V. Vittal, "Definition and

classification of power system stability IEEE/CIGRE joint task force on stability terms and definitions," *IEEE Transactions on Power Systems*, vol. 19, no. 3, pp. 1387 – 1401, aug. 2004.

[11] W. A. Elmore, *Protective Relaying Theory and Applications*, 2nd ed. New York: Marcel Decker, Inc., 2004.

[12] V. Madani, D. Novosel, S. Horowitz, M. Adamiak, J. Amantegui, D. Karlsson, S. Imai, and A. Apostolov, "IEEE PSRC Report on Global Industry Experiences With System Integrity Protection Schemes (SIPS)," *IEEE Transactions on Power Delivery*, pp. pp. 2143–2155, 2010.

[13] *Network Protection and Automation Guide.* Areva, July,2002.

[14] *SEL-421 Relay Instruction manual, January 2005.*

[15] P. Mooney and N. Fischer, "Application guidelines for power swing detection on transmission systems," in *Protective Relay Engineers, 2006. 59th Annual Conference for*, 0-0 2006, p. 10 pp.

[16] F. Plumptre, S. Brettschneider, A. Hiebert, M. Thompson, and M. Mynam, "Validation of out-of-step protection with a real time digital simulator," in *proceedings of the 60th Annual Georgia Tech Protective Relaying Conferencee, Atlanta, GA*, May, 2006.

[17] C. Taylor, J. Haner, L. Hill, W. Mittelstadt, and R. Cresap, "A new out-of-step relay with rate of change of apparent resistance augmentation," *IEEE Transactions on Power Apparatus and Systems*, vol. PAS-102, no. 3, pp. 631 –639, march 1983.

[18] E. Farantatos, R. Huang, G. J. Cokkinides, and A. P. Meliopoulos, "A predictive out of step protection scheme based on pmu enabled dynamic state estimation," *IEEE PES General Meeting 2011*, 2011.

[19] Y. Xue, T. Van Custem, and M. Ribbens-Pavella, "Extended equal area criterion justifications, generalizations, applications," *IEEE Transactions on Power Systems*, vol. 4, no. 1, pp. 44–52, 1989.

[20] V. Centeno, A. Phadke, A. Edris, J. Benton, M. Gaudi, and G. Michel, "An adaptive out-of-step relay," *IEEE Transactions on Power Delivery*, vol. 12, no. 1, pp. 61 –71, 1997.

[21] M. Bozchalui and M. Sanaye-Pasand, "Out of step relaying using phasor measurement unit and equal area criterion," in *Power India Conference, 2006 IEEE*, 0-0 2006, p. 6 pp.

[22] W. Rebizant and K. Feser, "Fuzzy logic application to out-of-step protection of generators," in *Proc. IEEE Power Engineering Society Summer Meeting*, vol. 2, 2001, pp. 927–932.

[23] A. Abdelaziz, M. Irving, M. Mansour, A. El-Arabaty, and A. Nosseir, "Adaptive protection strategies for detecting power system out-of-step conditions using neural networks," *Generation, Transmission and Distribution, IEE Proceedings-*, vol. 145, no. 4, pp. 387 –394, jul 1998.

[24] A. D. Rajapakse, F. Gomez, K. Nanayakkara, P. A. Crossley, and V. V. Terzija, "Rotor angle instability prediction using post-disturbance voltage trajectories," *IEEE Transactions on Power Systems*, vol. 25, no. 2, pp. 947–956, 2010.

[25] K. H. So, J. Y. Heo, C. H. Kim, R. K. Aggarwal, and K. B. Song, "Out-of-step detection algorithm using frequency deviation of voltage," *IET Generation, Transmission & Distribution*, vol. 1, no. 1, pp. 119–126, 2007.

[26] D. A. Tziouvaras and D. Hou, "Out-of-step protection fundamentals and advancements," in *Proc. 57th Annual Conf Protective Relay Engineers for*, 2004, pp. 282–307.

[27] L. L. Grigsby, Ed., *Electric Power Engineering Handbook*. CRC Press, Taylor & Francis Group, 2007.

[28] *Application Manual REL 531*2.3*, ABB.

[29] J. Berdy, *Application of Out-of-Step Blocking and Tripping Relays*, General Electric Company.

[30] J. M. Haner, T. D. Laughlin, and C. W. Taylor, "Experience with the r-rdot out-of-step relay," *IEEE Power Engineering Review*, no. 4, pp. 28–29, 1986.

[31] D. Hou, G. Benmouyal, and D. Tziouvaras, "Zero-setting power-swing blocking protection," *IEE Conference Publications*, vol. 2005, no. CP508, pp. 249–254, 2005. [Online]. Available: http://link.aip.org/link/abstract/IEECPS/v2005/iCP508/p249/s1

[32] S. H. Zak, *System and Control*, A. S. SEDRA, Ed. Oxford University Press, Inc., 2003.

[33] G. Ziegler, *Numerical Distance Protection:Principles and Applications*, B. Siemens Aktiengesellschaft and Munchen, Eds. Publicis Corporate Publishing,Erlangen, 2008.

[34] C. C. Chu, "Multi-swing transient instability problems in electric power systems: a preliminary study," in *Proc. IEEE Int Circuits and Systems ISCAS '97. Symp*, vol. 2, 1997, pp. 805–808.

[35] P. Forsyth, T. Maguire, and R. Kuffel, "Real time digital simulation for control and protection system testing," in *Proc. IEEE 35th Annual Power Electronics Specialists Conf. PESC 04*, vol. 1, 2004, pp. 329–335.

[36] D. X. Du, Z. Q. Bo, Z. X. Zhou, A. Perks, L. Denning, and B. Smith, "An advanced real time digital simulator based test system for protection relays," in *Proc. 41st Int. Universities Power Engineering Conf. UPEC '06*, vol. 3, 2006, pp. 851–855.

[37] *RTDS Manuals*, RTDS Technologies Inc., Winnipeg , Canada.

[38] *ADSP-BF533 Blackfin Processor Hardware Reference*, Revision 3.3, September 2008.

[39] *ADSP-BF533 EZ-KIT Lite Evaluation System Manual*, Analog Devices Inc.

[40] *Advancement in Microprocessor based protection and Communication*, IEEE Tutorial Course, Sponsored by the Power Engineering Edication Committee and the Power System Relaying Committee of the IEEE Power Engineering Society, 97TP120-0.

[41] S. Paudyal, "Out-of-step protection using energy equillibrium criterion in the time domain," Master's thesis, University of Saskatchewan, 2008.

[42] A. A. Fouad and V. Vittal, *Power System Transient Stability Analysis Using Transient Energy Function Method*. Prentice-Hall, Inc., 1992.

[43] K. R. Padiyar and S. Krishna, "Online detection of loss of synchronism using energy function criterion," *IEEE Transactions on Power Delivery*, vol. 21, no. 1, pp. 46–55, 2006.

[44] M. Haque, "Identification of coherent generators for power system dynamic equivalents using unstable equilibrium point," *Generation, Transmission and Distribution, IEE Proceedings C*, vol. 138, no. 6, pp. 546 –552, nov 1991.

[45] E. Pires de Souza and A. Leite da Silva, "An efficient methodology for coherency-based dynamic equivalents [power system analysis]," *Generation, Transmission and Distribution, IEE Proceedings C*, vol. 139, no. 5, pp. 371 –382, sep 1992.

[46] R. Podmore, "Identification of coherent generators for dynamic equivalents," *IEEE Transactions on Power Apparatus and Systems*, no. 4, pp. 1344–1354, 1978.

[47] S. Paudyal, G. Ramakrishna, and M. Sachdev, "Out-of-step protection using the equal area criterion in time domain - smib and 3-machine case studies," in *TENCON 2008 - 2008 IEEE Region 10 Conference*, nov. 2008, pp. 1 –6.

[48] H. Saadat, *Power System Analysis*. WCB/McGraw-Hill, 1999.

[49] S. Paudyal, G. Ramakrishna, and M. S. Sachdev, "Application of equal area criterion conditions in the time domain for out-of-step protection," *IEEE Transactions on Power Delivery*, vol. 25, no. 2, pp. 600–609, 2010.

Appendix A

System data

A.1 SMIB

Base MVA=2220 MVA, Base kV=24 kV

Generator data:

$2220MVA$, $24kV$, $r_a = 0.00125p.u.$, $x_l = 0.163p.u.$, $x_d = 1.81p.u.$, $x_q = 1.76p.u.$, $x'_d = 0.3p.u.$, $x'_q = 0.65p.u.$, $x''_d = 0.23p.u.$, $x''_q = 0.25p.u.$, $T'_{d0} = 8s$, $T''_{d0} = 0.03s$, $T'_{q0} = 1s$, $T''_{q0} = 0.07s$, $InertiaConstant(H) = 3.5s$, $Frequency = 60Hz$

Impedances:

$X_T = j0.15p.u.$, $TL - I = j0.5p.u.$, $TL - II = j1.0p.u.$

Infinite Bus Voltage=$0.9p.u.$

A.2 Two Machine System

Table A.1: Machine and system data

Generator data	$900MVA$, $20kV$, $r_a = 0.00125p.u.$, $x_l = 0.2p.u.$, $x_d = 1.8p.u.$, $x_q = 1.76p.u.$, $x'_d = 0.3p.u.$, $x'_q = 0.65p.u.$, $x''_d = 0.25p.u.$, $x''_q = 0.25p.u.$, $T'_{d0} = 8s$, $T''_{d0} = 0.03s$, $T'_{q0} = 0.4s$, $T''_{q0} = 0.05s$, $H(Gen1) = 5.4s$, $H(Gen2) = 6.25s$.
Transmission line data	$X_L = 0.0529\Omega/Km$
Transformer data	$900MVA, 20/230kV, x_t = 0.15p.u.$

A.3 IEEE 39 Bus System

Table A.2: Generator data(Generator MVA base)

Gen. No.	T'_{do}	T'_{qo}	H	X_d	X_q	X'_d	X'_q	X_d"	X_l
1	3.797	0.438	5.8	2.134	2.049	0.319	0.478	0.224	0.185
2	3.826	0.5084	3.41	1.7241	1.6587	0.2586	0.4524	0.2029	0.145
3	6.7	0.41	6.05	1.87	1.74	0.37	0.467	0.2805	0.23
4	5.8	1.2	3.6	1.86	1.81	0.282	0.466	0.233	0.164
5	3.8260	0.5084	3.41	1.7241	1.6587	0.2586	0.4524	0.2029	0.145
6	5.3180	0.97	5.016	1.834	1.798	0.419	0.83	0.314	0.26
7	3.8	0.52	3.141	1.84	1.77	0.28	0.478	0.215	0.155
8	3.8	0.52	3.141	1.84	1.77	0.28	0.478	0.215	0.155
9	7.61	0.84	5.32	1.643	1.573	0.3169	0.4793	0.246	0.1922
10			500.00			0.0005			

Table A.3: Line data(100 MVA base)

Line Data					Transformer Tap	
From Bus	To Bus	R	X	B	Magnitude	Angle
1	2	0.0035	0.0411	0.6987	0.000	0.00
1	39	0.0010	0.0250	0.7500	0.000	0.00
2	3	0.0013	0.0151	0.2572	0.000	0.00
2	25	0.0070	0.0086	0.1460	0.000	0.00
3	4	0.0013	0.0213	0.2214	0.000	0.00
3	18	0.0011	0.0133	0.2138	0.000	0.00
4	5	0.0008	0.0128	0.1342	0.000	0.00
4	14	0.0008	0.0129	0.1382	0.000	0.00
5	6	0.0002	0.0026	0.0434	0.000	0.00
5	8	0.0008	0.0112	0.1476	0.000	0.00

6	7	0.0006	0.0092	0.1130	0.000	0.00
6	11	0.0007	0.0082	0.1389	0.000	0.00
7	8	0.0004	0.0046	0.0780	0.000	0.00
8	9	0.0023	.0363	0.3804	0.000	0.00
9	39	0.0010	0.0250	1.2000	0.000	0.00
10	11	0.0004	0.0043	0.0729	0.000	0.00
10	13	0.0004	0.0043	0.0729	.000	0.00
13	14	0.0009	0.0101	0.1723	0.000	0.00
14	15	0.0018	0.0217	0.3660	0.000	0.00
15	16	0.0009	0.0094	0.1710	0.000	0.00
16	17	0.0007	0.0089	0.1342	0.000	0.00
16	19	0.0016	0.0195	0.3040	0.000	0.00
16	21	0.0008	0.0135	0.2548	0.000	0.00
16	24	0.0003	0.0059	0.0680	0.000	0.00
17	18	0.0007	0.0082	0.1319	0.000	0.00
17	27	0.0013	0.0173	0.3216	0.000	0.00
21	22	0.0008	0.0140	0.2565	0.000	0.00
22	23	0.0006	0.0096	0.1846	0.000	0.00
23	24	0.0022	0.0350	0.3610	0.000	0.00
25	26	0.0032	0.0323	0.5130	0.000	0.00
26	27	0.0014	0.0147	0.2396	0.000	0.00
26	28	0.0043	0.0474	0.7802	0.000	0.00
26	29	0.0057	0.0625	1.0290	0.000	0.00
28	29	0.0014	0.0151	0.2490	0.000	0.00
12	11	0.0016	0.0435	0.0000	1.006	0.00
12	13	0.0016	0.0435	0.0000	1.006	0.00
6	31	0.0000	0.0250	0.0000	1.070	0.00
10	32	0.0000	0.0200	0.0000	1.070	0.00

19	33	0.0007	0.0142	0.0000	1.070	0.00
20	34	0.0009	0.0180	0.0000	1.009	0.00
22	35	0.0000	0.0143	0.0000	1.025	0.00
23	36	0.0005	0.0272	0.0000	1.000	0.00
25	37	0.0006	0.0232	0.0000	1.025	0.00
2	30	0.0000	0.0181	0.0000	1.025	0.00
29	38	0.0008	0.0156	0.0000	1.025	0.00
19	20	0.0007	0.0138	0.0000	1.060	0.00

Table A.4: Load flow data (100 MVA base)

Bus	Type	Voltage (p.u.)	Load		Generator		Unit No.
			MW	MVar	MW	MVar	
1	PQ	-	0.0	0.0	0.0	0.0	
2	PQ	-	0.0	0.0	0.0	0.0	
3	PQ	-	322.0	2.4	0.0	0.0	
4	PQ	-	500.0	184.0	0.0	0.0	
5	PQ	-	0.0	0.0	0.0	0.0	
6	PQ	-	0.0	0.0	0.0	0.0	
7	PQ	-	233.8	84.0	0.0	0.0	
8	PQ	-	522.0	176.0	0.0	0.0	
9	PQ	-	0.0	0.0	0.0	0.0	
10	PQ	-	0.0	0.0	0.0	0.0	
11	PQ	-	0.0	0.0	0.0	0.0	
12	PQ	-	7.5	88.0	0.0	0.01	
3	PQ	-	0.0	0.0	0.0	0.0	
14	PQ	-	0.0	0.0	0.0	0.0	
15	PQ	-	320.0	153.0	0.0	0.0	
16	PQ	-	329.0	32.3	0.0	0.0	
17	PQ	-	0.0	0.0	0.0	0.0	
18	PQ	-	158.0	30.0	0.0	0.0	
19	PQ	-	0.0	0.0	0.0	0.0	
20	PQ	-	628.0	103.0	0.0	0.0	
21	PQ	-	274.0	115.0	0.0	0.0	
22	PQ	-	0.0	0.0	0.0	0.0	
23	PQ	-	247.5	84.6	0.0	0.0	
24	PQ	-	308.6	-92.0	0.0	0.0	
25	PQ	-	224.0	47.2	0.0	0.0	

26	PQ	-	139.0	17.0	0.0	0.0	
27	PQ	-	281.0	75.5	0.0	0.0	
28	PQ	-	206.0	27.6	0.0	0.0	
29	PQ	-	283.5	26.9	0.0	0.0	
30	PV	1.0475	0.0	0.0	250.0	-	Gen10
31	PV	0.9820	9.2	4.6	-	-	Gen2
32	PV	0.9831	0.0	0.0	650.0	-	Gen3
33	PV	0.9972	0.0	0.0	632.0	-	Gen4
34	PV	1.0123	0.0	0.0	508.0	-	Gen5
35	PV	1.0493	0.0	0.0	650.0	-	Gen6
36	PV	1.0635	0.0	0.0	560.0	-	Gen7
37	PV	1.0278	0.0	0.0	540.0	-	Gen8
38	PV	1.0265	0.0	0.0	830.0	-	Gen9
39	PV	1.0300	1104.0	250.0	1000.0	-	Gen1

Appendix B

Test Systems

B.1 PSCAD^{TM} Model of a Single Machine Infinite Bus System

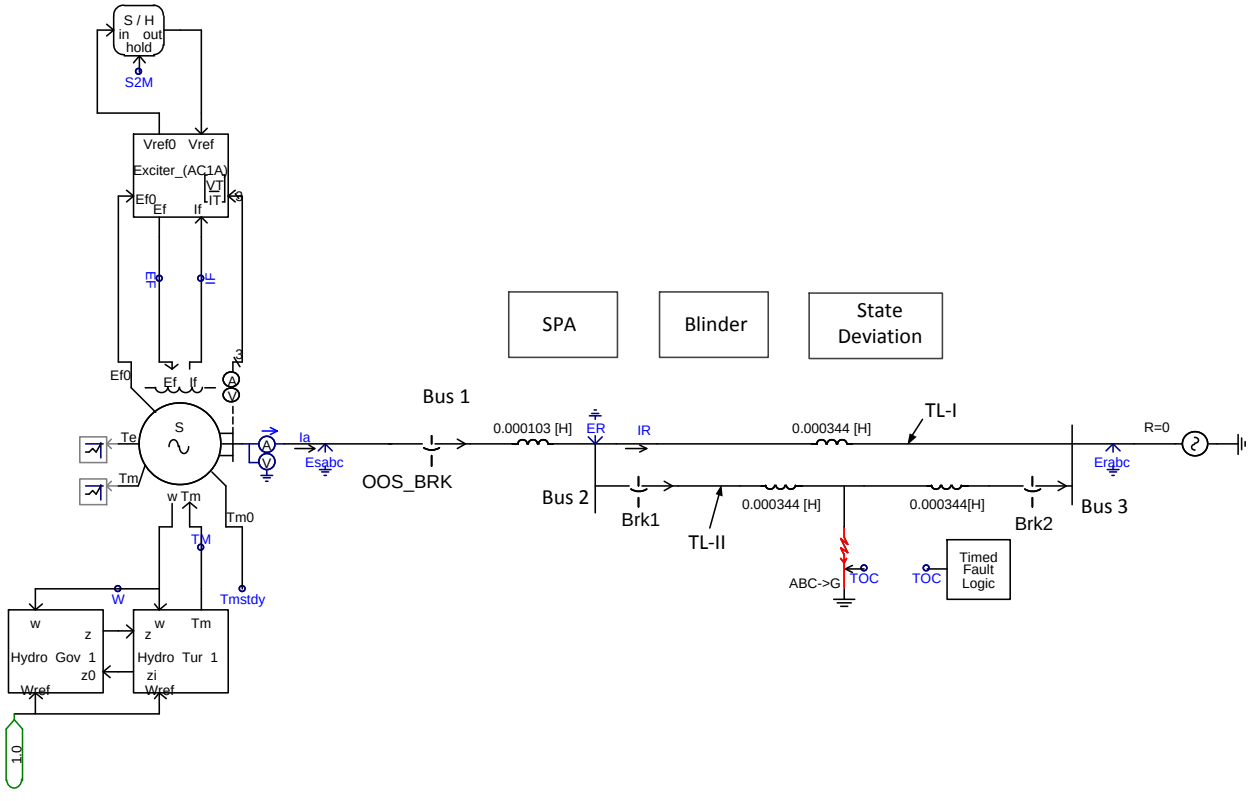

B.2 PSCAD^{TM} Model of a Two Area System

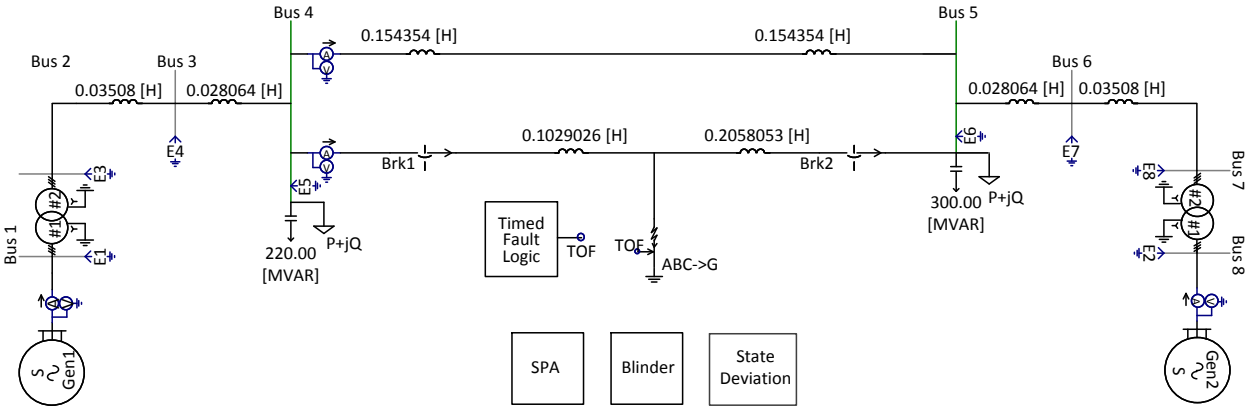

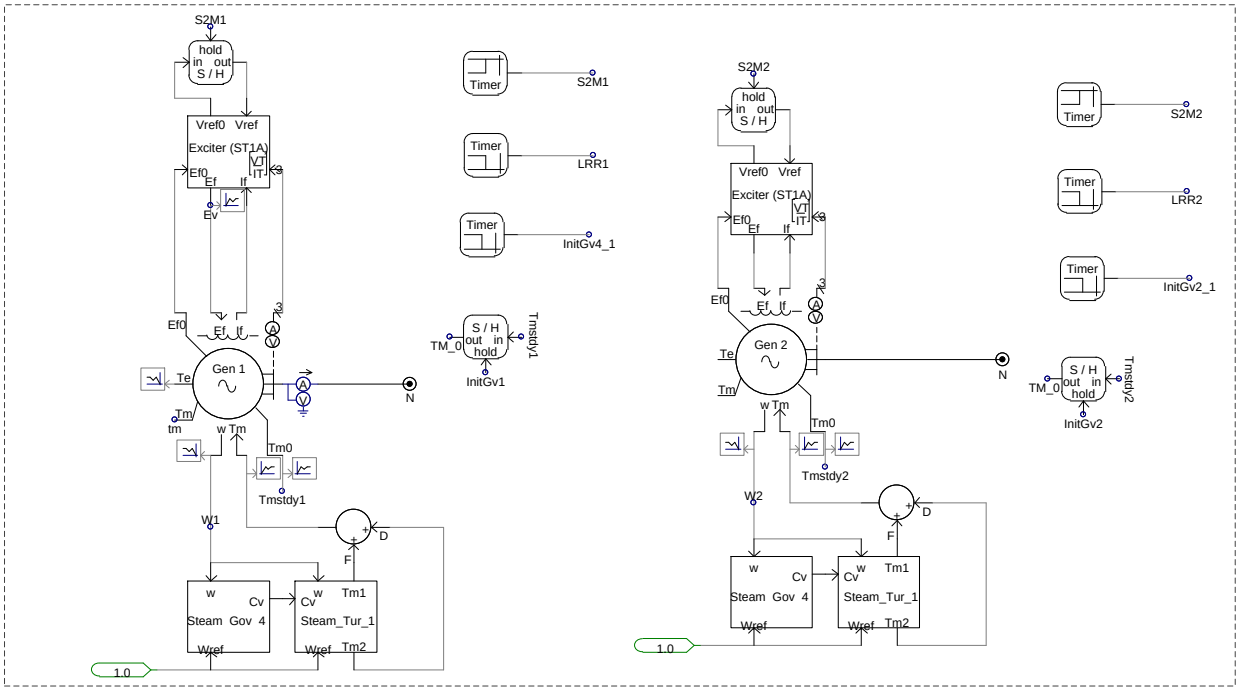

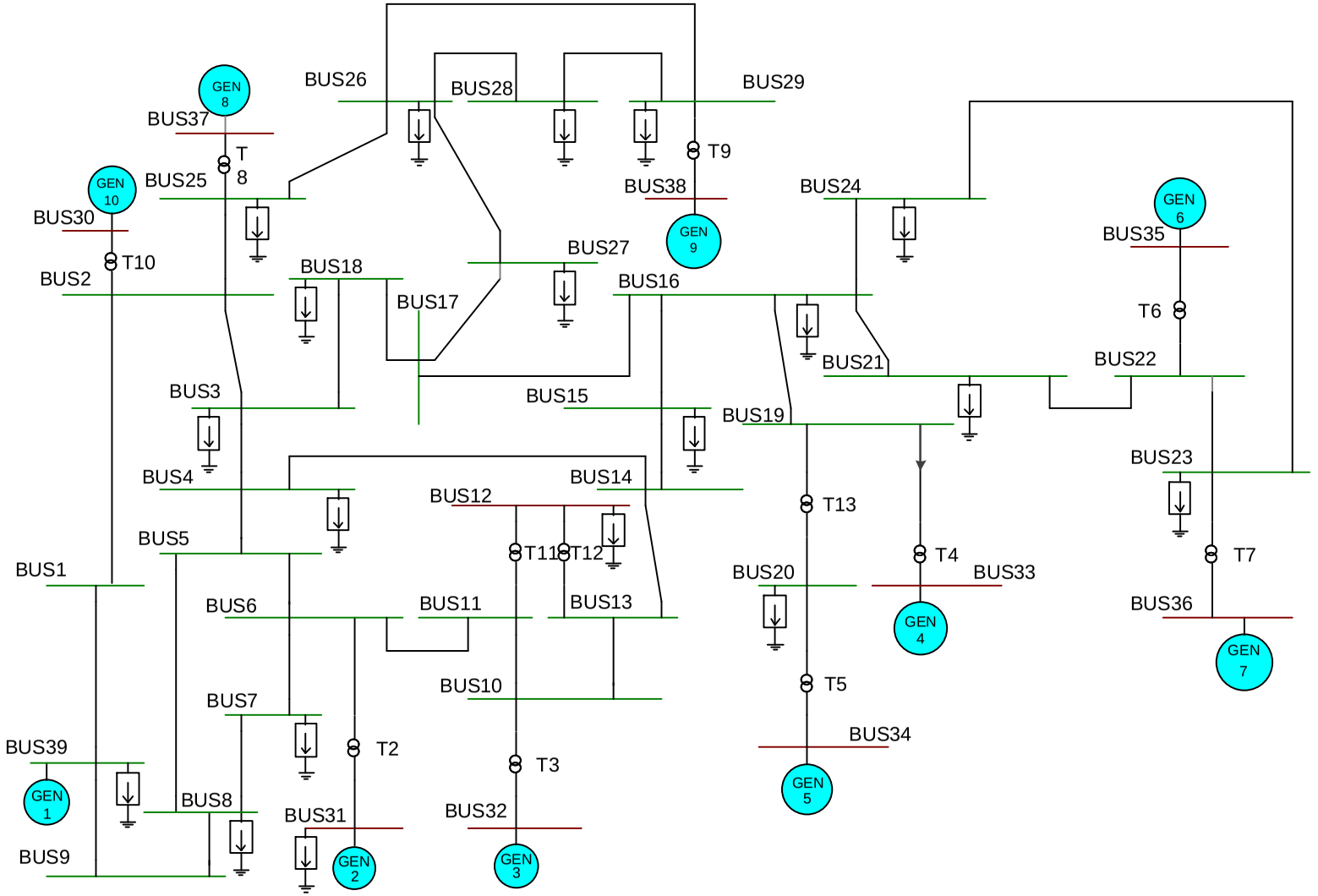

Figure B.1: IEEE 39 bus New England Test System

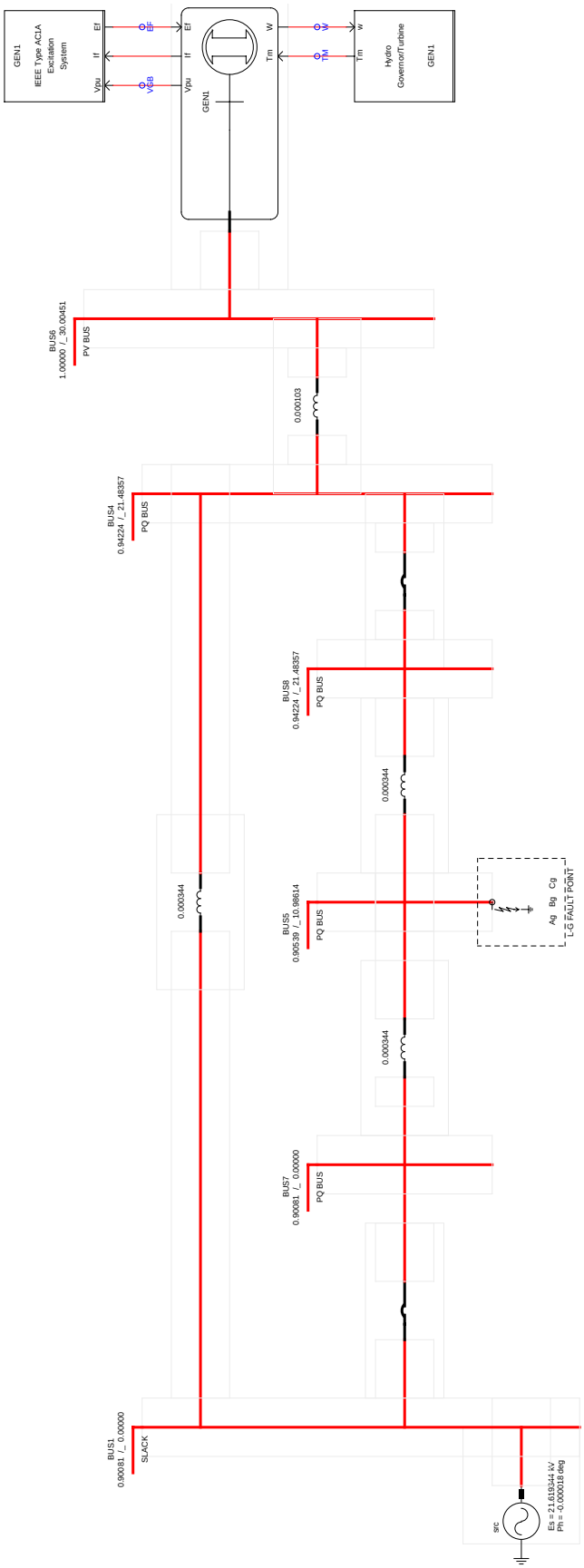

Figure B.2: SMIB test system in RSCAD^{TM}

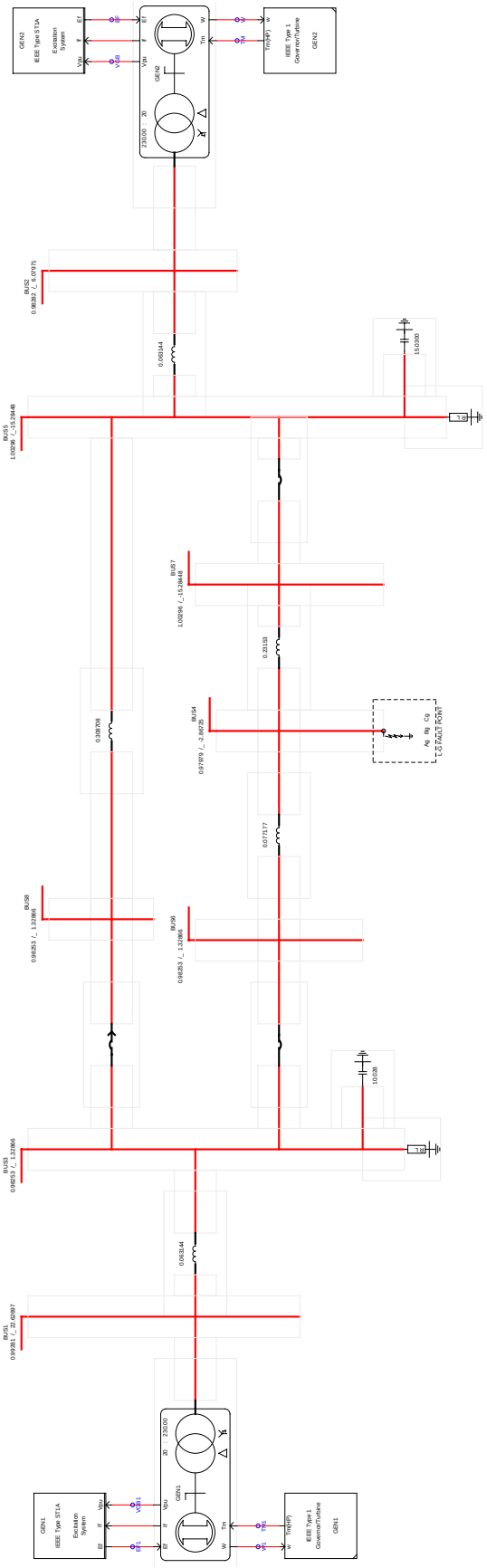

Figure B.3: Two area test system in RSCAD^{TM}

Appendix C

Checking Stability of the Singular Points

The stability study of the nonlinear system is usually done using a linearised system. The equilibrium point where the stability is to be tested is taken as an origin. A nonlinear system can be written in a simplified form of its state space representation as given by equation (C.1).

$$\dot{x} = f(x) \tag{C.1}$$

Using Taylor expansion theorem and expanding equation (C.1) around a singular point x_0, we get equation (C.2).

$$\frac{d}{dt}(x - x_0) = f(x_0) + \Delta f(x_0)(x - x_0) + \Delta^2 f(x_0)(x - x_0)^2 \tag{C.2}$$

$$\begin{aligned} &= \Delta f(x_0)(x - x_0) \\ &= A(x - x_0) \end{aligned} \tag{C.3}$$

Since $f(x_0) = 0$ and around $x = x_0$, the equation (C.2) almost behaves as a linear system which is given by equation (C.3). Where A is a Jacobian matrix. The stability of the nonlinear system at the singular point can then be evaluated by calculating eigenvalues of matrix A. The method is also called Lyapunov's indirect method for stability [32]. Real eigenvalues with opposite sign or both positive sign represent a saddle point and a real eigenvalues with negative signs represents a vortex point. A complex eigenvalues represents an oscillatory system with positive or negative damping. A more detailed explanation on lyapunov's indirect method is given in [32]. The saddle and vortex points are graphically shown in Figure C.1, where the trajectories converge towards the vortex point and the trajectories diverge away from the saddle point.

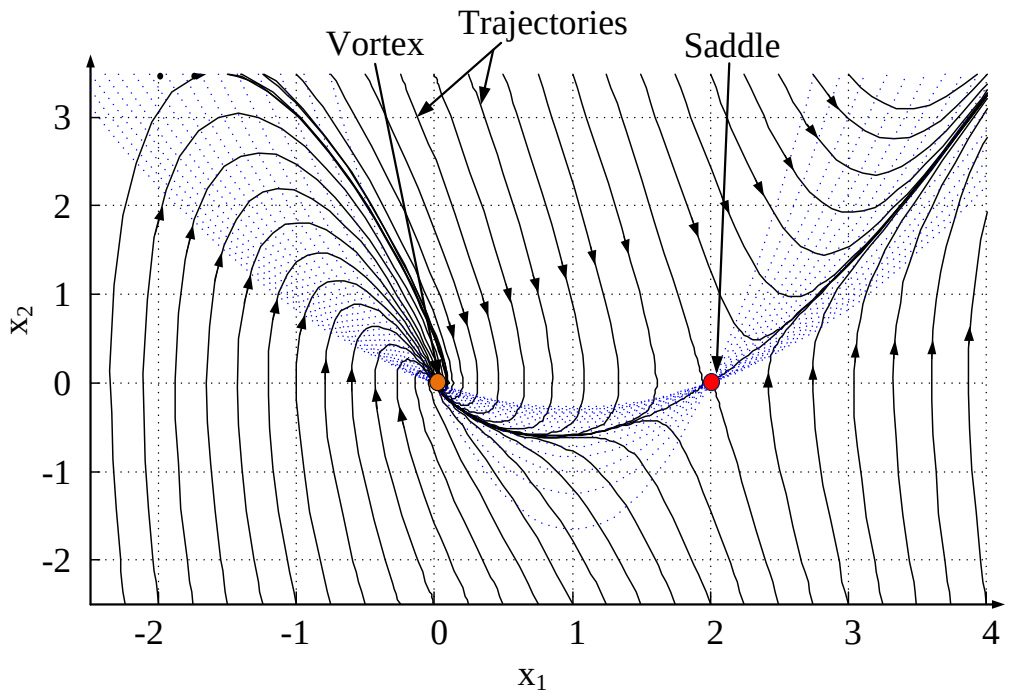

Figure C.1: State plane trajectories showing vortex and saddle point

Appendix D

Guidelines for Blinder Settings

Most of the blinder settings are implemented using the following guidelines:

* RRO: Set the outer resistive blinder inside the maximum possible load with some safety margin.

* RRI: Set the inner resistive blinder out side the most overreaching protective zone that is to be blocked when the power swing occurs. Some safety margin should be applied between the blinder and the outer most relay characteristics.

* LRO: Same as RRO but in negative direction.

* LRI: Same as RRI but in negative direction.

Based on the inner and outer blinders setting, power swing blocking time delay (PSBD) can be calculated using relation (D.1). PSBD is the time set to distinguish between power swing and fault. The distance relays equipped with this scheme is blocked for this time duration. If the swing is detected the blocking signal must be maintained until the impedance exits the outer blinder or until the a fixed time delay [33]. The PSBD should represent a reasonable time delay to ensure secure decision without impacting the operation of PSB element. A recommended range for PSBD is 1.5 to 2.5 cycles.

$$PSBD = \frac{(ANGIR - ANGOR) * F_{nom}}{360 * F_{slip}} \tag{D.1}$$

Where,

$ANGIR$: Machine angle at inner blinder

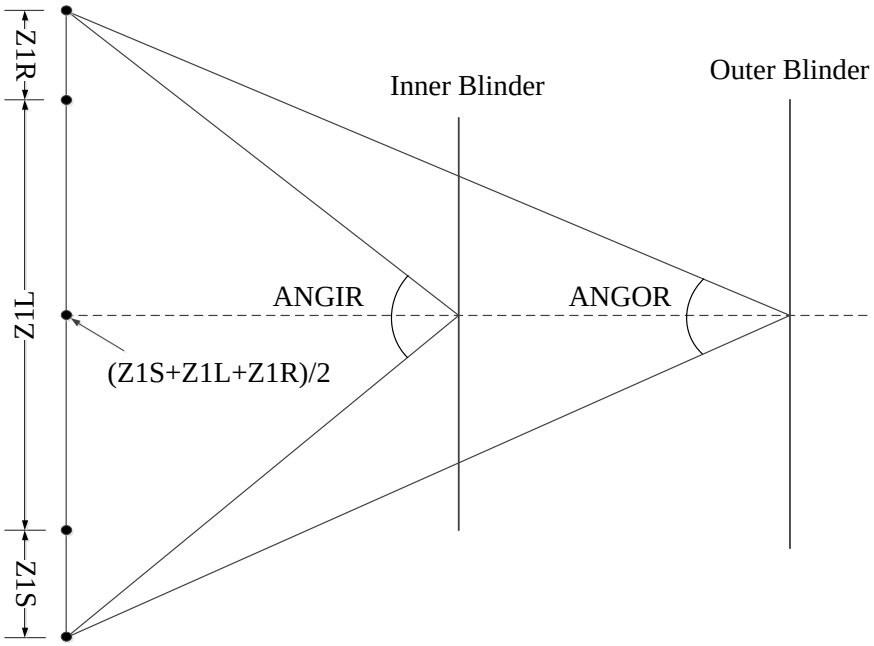

Figure D.1: Equivalent Source Angles During Power Swing

$ANGOR$: Machine angle at outer blinder

F_{nom}: System nominal frequency in Hz

F_{slip}: Power swing slip rate in Hz

Appendix E

Network Admittance Matrix Reduction

With the synchronous machine represented as a constant voltage source behind the transient reactance and the load modeled as a constant impedance, the power system network can be reduced between the genetator internal nodes. The n-bus nework is augmented to n+k-bus network to includes the transient reactances of k number of generators. Figure E.1 shows the equivalent network representation used for network reduction. The nodes

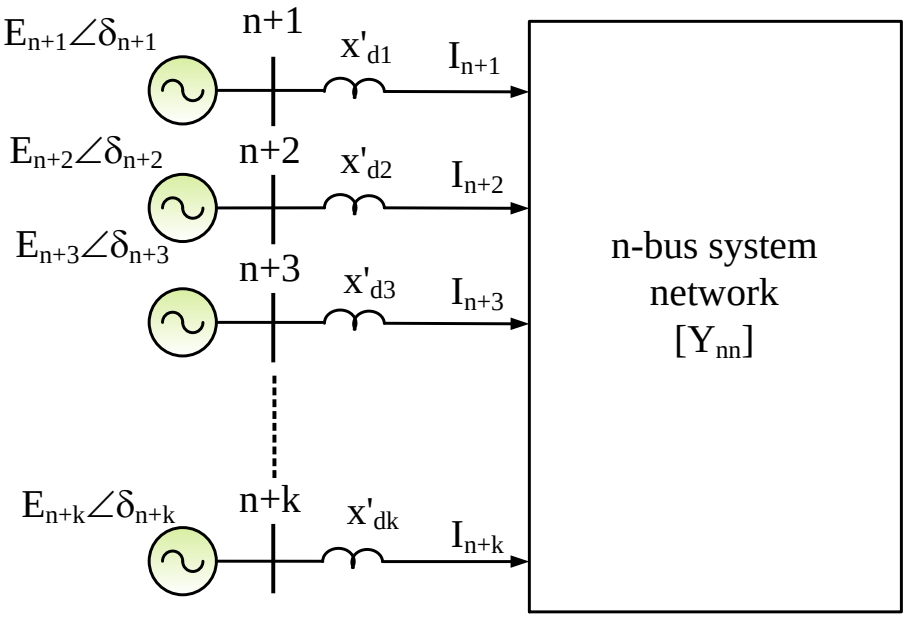

Figure E.1: Equivalent power system network representation

n+1, n+2, ...,n+k represents the internal machine buses. The node voltage equation for the augmented network is given by Equation (E.1)

$$\begin{bmatrix} I_1 \\ I_2 \\ I_3 \\ . \\ . \\ . \\ I_n \\ - \\ I_{n+1} \\ I_{n+2} \\ . \\ . \\ I_{n+k} \end{bmatrix} = \left[\begin{array}{ccc|ccc} Y_{11} & .... & Y_{1n} & Y_{1(n+1)} & .... & Y_{1(n+k)} \\ Y_{21} & .... & Y_{2n} & Y_{2(n+1)} & .... & Y_{2(n+k)} \\ Y_{31} & .... & Y_{3n} & Y_{3(n+1)} & .... & Y_{3(n+k)} \\ . & .... & . & . & .... & . \\ . & .... & . & . & .... & . \\ . & .... & . & . & .... & . \\ Y_{n1} & .... & Y_{nn} & Y_{n(n+1)} & .... & Y_{n(n+k)} \\ \hline Y_{(n+1)1} & .... & Y_{(n+1)n} & Y_{(n+1)(n+1)} & .... & Y_{(n+1)(n+k)} \\ Y_{(n+2)1} & .... & Y_{(n+2)n} & Y_{(n+2)(n+1)} & .... & Y_{(n+2)(n+k)} \\ . & .... & . & . & .... & . \\ . & .... & . & . & .... & . \\ Y_{(n+m)1} & .... & Y_{(n+m)n} & Y_{(n+m)(n+1)} & .... & Y_{(n+m)(n+k)} \end{array}\right] \begin{bmatrix} V_1 \\ V_2 \\ V_3 \\ . \\ . \\ . \\ V_n \\ - \\ E_{n+1} \\ E_{n+2} \\ . \\ . \\ E_{n+k} \end{bmatrix} \tag{E.1}$$

The buses other than the generator internal buses are eliminated by using Kron reduction formula. The buses to be removed are represented in upper n rows. Since no current enters or leaves the load buses, the currents in the n rows are set to zero. The generator currents are denoted by vector I_k and the generator and load voltages are denoted by E_k and V_n, respectively. The Equation (E.1) can be represented in the submatrix form as given by Equation (E.2).

$$\begin{bmatrix} 0 \\ I_k \end{bmatrix} = \begin{bmatrix} Y_{nn} & Y_{nk} \\ Y_{nk}^t & Y_{kk} \end{bmatrix} \begin{bmatrix} V_n \\ E_k \end{bmatrix} \tag{E.2}$$

Byeliminating V_n from the Equation (E.2), the expression for I_k is given by equation (E.3a).

$$I_k = [Y_{kk} - Y_{nk}^t Y_{nn}^{-1} Y_{nk}] E_k \tag{E.3a}$$

$$= Y_{bus}^{red} E_k \tag{E.3b}$$

where, $Y_{bus}^{red} = [Y_{kk} - Y_{nk}^t Y_{nn}^{-1} Y_{nk}]$ which is the reduced admittance matrix between the generator internal nodes [48].

Appendix F

Out-of-step Protection using Time Domain Energy Equilibrium

Reference [49] proposed an out-of-step detection technique using energy equilibrium in time domain. The accelerating and decelerating area in a power *vs* time curve is calculated in this approach. Accelerating and decelerating areas in P-t curve are given by Equation (F.1) and (F.2), respectively.

$$A_1 = \int_{t_0}^{t_{cl}} (P_m - P_e)dt \tag{F.1}$$

$$A_2 = \int_{t_{cl}}^{t_{max}} (P_m - P_e)dt \tag{F.2}$$

If total area A_2 becomes equal to area A_1 during the transient, the system becomes stable. If A_1 is greater than A_2, the system becomes unstable. Figure F.1 shows the P-t curve where area A_2 becomes equal to area A_1 at time t_{det}. The swing is hence detected as a stable swing. In figure F.2, Area A_1 is greater than area A_2 hence the swing is detected as an unstable swing at time t_{max}.

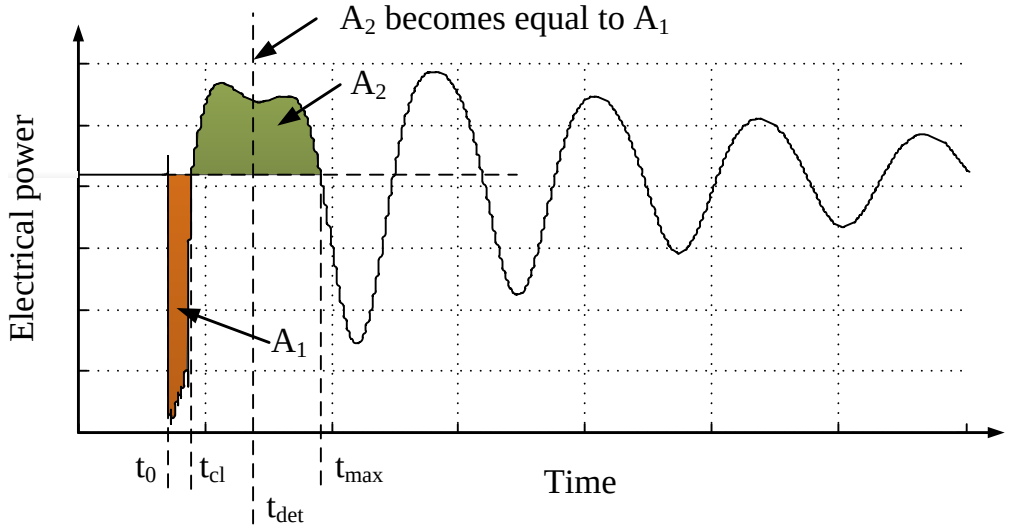

Figure F.1: Stable electrical power swing

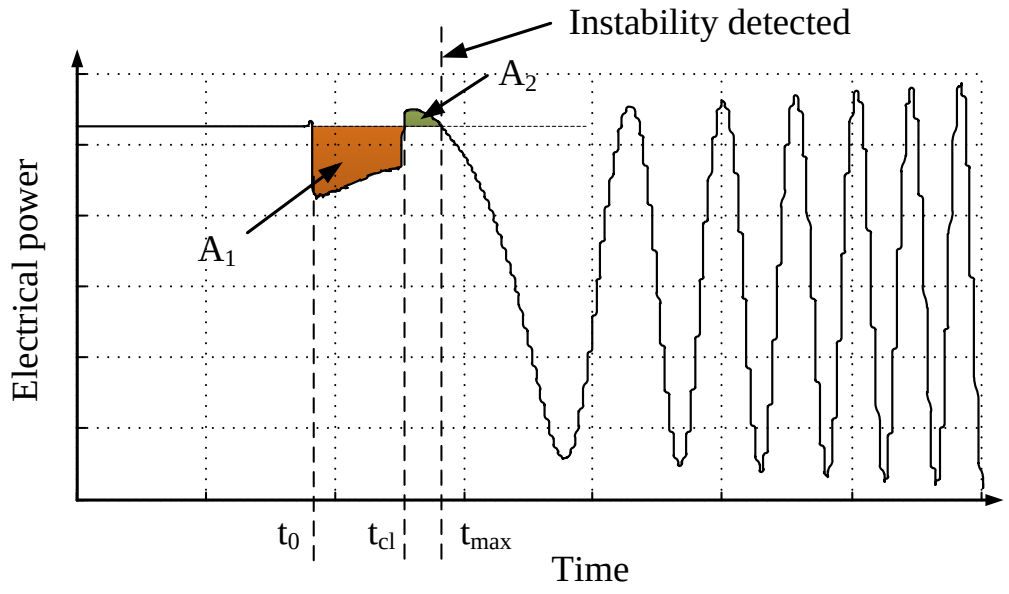

Figure F.2: Unstable electrical power swing